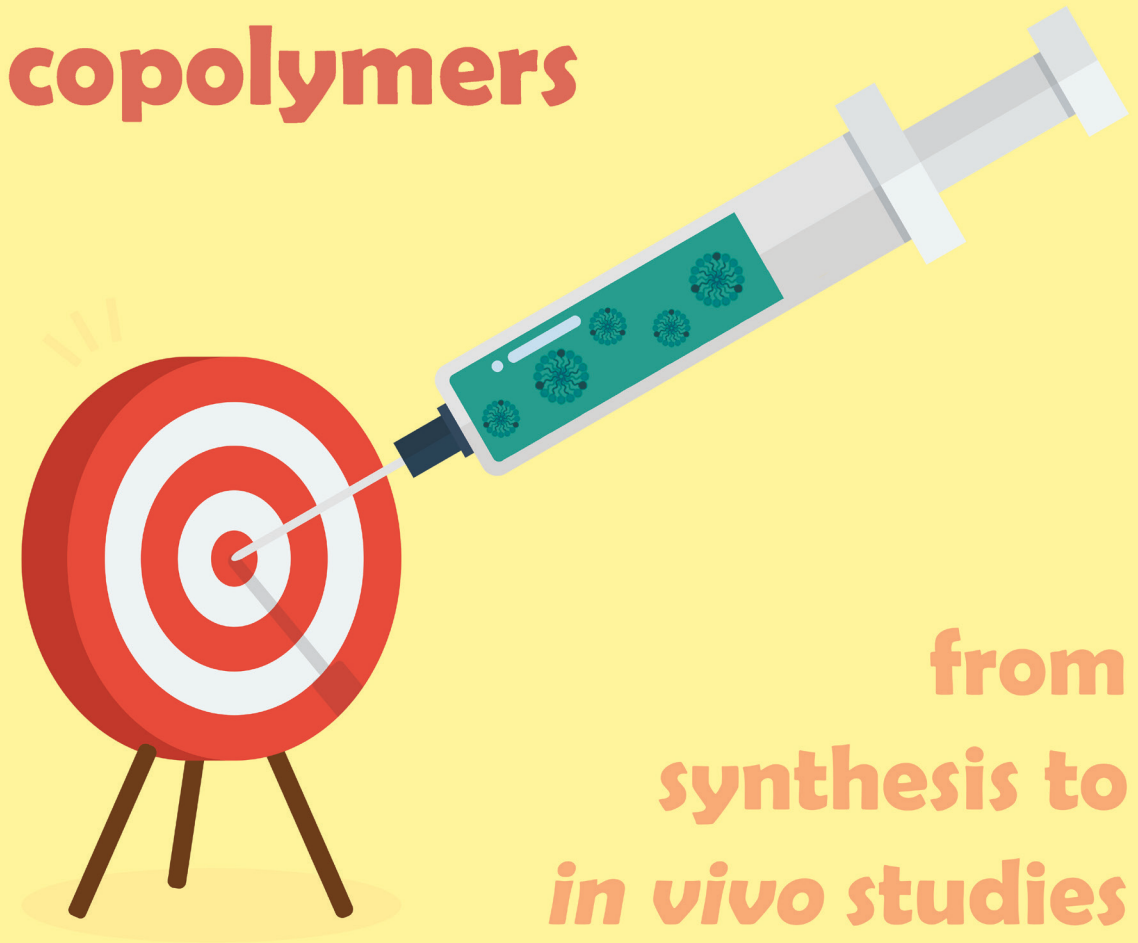# Biotinylated polymeric micelles

based on amphiphilic poly(HPMA) block copolymers

Yan Wang

from synthesis to *in vivo* studies

One step closer to curing cancer with targeted drug delivery, by Yan Wang

INVITATION

To attend the public defense of my PhD dissertation entitled:

Biotinylated polymeric micelles based on amphiphilic poly(HPMA) block copolymers:

From synthesis to in vivo studies

by
Yan Wang
y.wang3@uu.nl

On January 11th, 2023 at 16:15 pm

At
Utrecht University,
the Senate Hall of the Academiegebouw, 3512 JE Utrecht

Paranymphs:

Mahsa Bagheri
m.bagheri66@outlook.com

Marcel H. Fens
m.h.a.m.fens@uu.nl

Biotinylated polymeric micelles based on amphiphilic poly(HPMA) block copolymers:

From synthesis to *in vivo* studies

Yan Wang

2023

Biotinylated polymeric micelles based on amphiphilic poly(HPMA) block copolymers

From synthesis to *in vivo* studies

Gebiotinyleerde polymere micellen op basis van amfifiele poly(HPMA)-blokcopolymeren
Van synthese tot *in vivo* studies
(met een samenvatting in het Nederlands)

Proefschrift

ter verkrijging van de graad van doctor aan de
Universiteit Utrecht
op gezag van de
rector magnificus, prof.dr. H.R.B.M. Kummeling,
ingevolge het besluit van het college voor promoties
in het openbaar te verdedigen op

woensdag 11 januari 2023 des middags te 4.15 uur

door

Yan Wang

geboren op 4 november 1991
te Shandong, China

Promotor:
Prof. dr. W.E. Hennink

Copromotor:
Dr. C.F. Van Nostrum

Contents

1

General introduction

Nanomedicines for cancer treatment

Cancer is among the leading causes of death. According to worldwide statistics, cancer accounts for nearly 10 million death in 2020, or nearly one in six deaths [1]. Many different forms of cancers can be cured if diagnosed early and treated effectively and recently substantial progress has been made in the development of novel and improved modalities to treat cancer. Chemotherapy is the first-line systemic treatment usually in combination with surgery and radiotherapy. However, limitations of conventional chemotherapeutic agents including high systemic toxicity, drug resistance, and the lack of tumor selectivity cause severe adverse effects. Further, many drugs that are approved or under clinical development have low aqueous solubility and therefore excipients are required to prepare formulations that can be administered to patients. An effective solution to circumvent these limitations is to deliver anti-cancer agents to tumor sites by using a so-called 'magic bullet' [2,3].

The 'magic bullet' term was first proposed and envisioned about a century ago by Nobel Prize laureate Paul Ehrlich to refer to therapeutic compounds that selectively target a pathogen without affecting the host. Subsequently, this idea flourished not only for the treatment of infectious diseases but also in other pathological modalities, particularly cancer [4]. Nanomedicine is an advanced version of Paul Ehrlich's 'magic bullet' concept. Over the past decades, immense efforts have been devoted to developing nano-sized drug delivery systems to improve the therapeutic window and reduce the accompanying toxicity of anti-cancer drugs [5]. Since the first nano-based cancer drug liposomes-based doxorubicin formulation (Doxil) was approved in 1995 by the US food and drug administration (FDA), to date, 16 nanomedicines for cancer treatment have been approved by FDA whereas close to 75 nanoformulations are in clinical trials [6,7].

A key concept for the therapeutic efficacy of nanoformulations is the enhanced permeability and retention (EPR) effect [8,9]. This increased permeability is due to the unique pathophysiological nature of the tumor microenvironment compared to normal tissues [10]. Solid tumors have hypervascularization and leaky vasculature with gaps between endothelial cells to allow 10-300 nm diameter nanoparticles to extravasate and selectively accumulate in the tumor, often termed passive targeting [11]. The accumulation is further favored by the lack of lymphatic clearance contributing to prolonged retention of the deposited nanomedicines in tumor tissues for days to weeks [12]. Nevertheless, the anti-tumor efficacy of drug-loaded nanomedicines may not always benefit from passive accumulation in cancerous tissues through the EPR effect due to the heterogeneity and complexity of the tumor environment [13–15]. In this regard, using vascular mediators to enhance vascular permeability is a solution to augment blood flow in tumors and consequently improve the therapeutic efficacy of nanomedicines [16].

The efficacy of nanomedicines can be also enhanced by introducing targeting ligands on the surface of the nanoparticulate drug delivery system [17,18]. Targeting ligands can bind to cancer cell-selective receptors that are overexpressed compared to healthy cells, leading to prolonged retention in tumor tissues. The targeting ligands can further facilitate the internalization of the cell-bound nanomedicines through ligand-receptor interactions that induce receptor-mediated endocytosis and enhance drug release inside the cell [19]. This is crucial for drugs that are not able to spontaneously pass through cell membranes such as nucleic acid-based drugs, some pharmaceutical proteins, and therapeutic peptides and peptide antigens [20,21]. Targeting ligands investigated and exploited include among others folate, biotin, mannose, anti-epidermal growth factor receptor (EGFR) nanobodies and antibodies, and aptamers [22–27]. Conjugation of tumor-specific ligands to the nanoparticles requires surface chemistry and exploiting reactive functional groups [28,29].

Nanocarriers span diverse materials such as carbon nanotubes, gold nanoparticles, lipid-based nanoparticles, inorganic silica nanoparticles, and polymeric formulations that differ in size, surface charge, shape, loading capacity, stability, payload release, blood circulation, and clearance from the body [30–34]. In this thesis, biotin-decorated polymeric micelles were investigated as described in more detail below.

Polymeric micelles as next-generation of nanomedicines

Polymeric micelles are colloidal particles with a size below 100 nm, which are formed through spontaneous self-assembly of amphiphilic block copolymers in an aqueous solution [35–37]. The formation of micelles is a reversible process driven by solution thermodynamics, to minimize the interfacial free energy of block copolymers with a large solubility difference [38]. Depending on the block length ratio and composition of the amphiphilic block copolymers, the size and shape, the formed micelles obtained varies, including core-shell (spherical), rod-like, star-like, flower-like, vesicles, and so on [39–42]. For instance, shorter hydrophobic blocks yield smaller micelles, whereas larger micelles are formed by increasing the length of hydrophobic blocks. Core-shell structured polymeric micelles are considered to be one of the most prominent drug delivery systems in cancer therapy for several reasons: 1) The outer hydrophilic shell ensures their colloidal stability and provides long circulation in the blood circulation, whereas the hydrophobic core is highly

suitable for accommodating and solubilizing hydrophobic drugs; 2) Their small size leads to the efficient accumulation of the micelles in tumor site as a result of the EPR effect, and more importantly, facilitates tumor penetration and cellular uptake; 3) The versatility of the core-shell structure provides opportunities for the conjugation of targeting ligands as well as fine-tuning the colloidal carrier for optimal properties [35,43–47].

Formulation of polymeric micelles involves solvent extraction, dialysis, and tangential flow filtration [48–52]. The solvent extraction is driven by the 'ouzo effect' [50,51,53]. The ouzo effect occurs when the hydrophobic solute is rapidly brought into the metastable ouzo region between the miscibility-limit curve and stability-limit curve in a ternary phase diagram composed of hydrophobic solute, solvent, and non-solvent. Upon mixing solvent and non-solvent, local supersaturation leads to the spontaneous formation of nuclei that undergo growth with time [54]. The mixing method employed significantly influences the formulation quality [48]. Compared to conventional batch processes, continuous flow production methods, such as microfluidics, ensure a constant mixing time resulting in controlled size and other features, which in turn reduces the batch-to-batch variation of other preparation methods.

A crucial parameter for preparing polymeric micelles by a self-assembly process is the critical micelles concentration (CMC), above which polymeric micelles are spontaneously formed [55]. CMC values of polymeric micelles generally speaking depend on the hydrophobic/hydrophilic ratio of the amphiphilic block copolymer, temperature, ionic strength, and pH [56–58]. Three commonly applied methods for the determination of the CMC value are the fluorometric, conductivity, and surface tension methods [58–60].

Size and shape are among the most commonly reported characteristics of polymeric micelles that play critical roles in circulation, tumor disposition and penetration, and cellular uptake [38,46,61–63]. Polymeric micelles on one hand should be large enough for long circulation time and high tumor accumulation (>5.5 nm), but small enough for good tumor penetration (<100 nm) [13]. Except for electronic microscopy, the size and shape of polymeric micelles cannot be directly measured with routinely applied techniques including dynamic light scattering, multi-angle light scattering, ultracentrifugation, laser diffraction, and nanoparticle tracking method [64–66]. The data obtained are the so-called equivalent particle diameter in relation to the physical responses of particles such as light scattering intensity, weight, and volume. It is noted that different techniques have their strengths and limitations, and thus combined data analysis is required to obtain a good overview of the particle size and shape.

Surface charge is an important characteristic of the colloidal stability of polymeric micelles [67]. Moreover, the surface charge of micelles can affect clearance, tissue distribution, and cellular uptake. Further, the surface charge is an important feature that determines the formation of protein corona on the surface of the micelles also depends on the surface charge [68]. The surface charge and its tailoring is therefore an important step in the formulation development of nanomedicines. A typical measure of surface charge is given by the zeta potential ζ, which is defined as the electrical-potential difference between the stationary layer of charges surrounding the particle and solution potential [66,69]. Factors impacting the zeta potential of colloidal particles including nanomedicines are pH and ionic strength of the medium in which the colloidal particles are dispersed. PEGylation, the modification of colloidal particles by covalent conjugation with poly(ethylene glycol) (PEG), is known to increase their stability by reducing the zeta potential and importantly, by providing a steric barrier that prevents inter particle interactions [70].

Drug-loaded polymeric micelles are considered nano-Trojan horses by facilitating delivering of cytostatic agents into tumor cells. It is generally accepted that drug loading changes size of polymeric micelles and thus affects their *in vitro* and *in vivo* behavior [71,72]. Regarding the morphology of drug-loaded polymeric micelles, it is often assumed that hydrophobic drugs reside in the micellar core and do not affect the morphology and stability of nanoparticles. Moreover, higher drug loadings are preferred particularly when less potent therapeutics are formulated in polymeric micelles [73]. Indeed, many studies have shown that a higher drug loading capacity leads to favorable pharmacokinetics and improved performance [74]. However, commonly reported drug content of ~10%wt is sufficient to exert adequate therapeutic efficacy, such as FDA-approved liposomal medicine Doxil and protein-based medicine Abraxane, which means that a low drug loading is not an obstacle for clinical success. It has been reported that a higher drug loading can delay the release of the drug due to the interaction with co-loaded drugs, resulting in lower drug efficiency [75]. It is also possible that higher drug loading can alter the morphology of polymeric micelles because the hydrophobic drugs leach into the hydrophilic shell causing dehydration of the shell, leading to reduced cellular uptake [76–78].

PEG is the most used hydrophilic polymer for the design of long-circulating polymeric micelles [79,80]. PEG avoids adsorption of opsonins onto the surface of nanocarriers, which in turn reduces aspecific uptake of these particles by the mononuclear phagocyte system (MPS) [79,81]. The first micellar formulation Genexol-PM based on paclitaxel-loaded block copolymer mPEG-b-poly($_{D, L}$-lactic acid) was approved in 2007 in South Korea for the treatment of breast and non-small cell lung (NSCL) cancer [36]. Several formulations based on PEGylated micelles for anti-cancer therapy are currently under evaluation in clinical trials [3,35,37]. PEGylated surfaces

2

are considered bioinert by avoiding protein adsorption [82]. However, in recent years it has been shown that repeated injections of PEGylated nanoparticles can induce a phenomenon termed the accelerated blood clearance (ABC) effect. This causes rapid clearance of the second dose of PEGylated nanoparticles, which is mediated by the formation of anti-PEG immunoglobulin M antibodies (IgM) [83–85]. This ABC effect has been particularly investigated for PEGylated liposomes. However, it has also been reported that PEGylated polymeric micelles undergo this ABC effect and several studies showed that the induction of the ABC effect for PEGylated micelles is size-dependent [62,86]. Many efforts are devoted to the search for alternative polymers that do not result in the immune response but maintain long circulation properties also after repeated administration. A number of polymer coatings, such as poly(amino acid) (PAA), poly(hydroxyethyl L-asparagine) (PHEA), poly(vinylpyrrolidone) (PVP), poly(N-2-hydroxypropyl methacrylamide) (pHPMA), poly(N,N-dimethylacrylamide) (PDMA), poly(N-acryloyl morpholine) (PAcM), and polysarcosine (pSar), have all demonstrated the ability to prolong circulation times of liposomes and other nanoparticles upon repeated administration [38,87–91]. Particularly, pHPMA has favorable characteristics such as good hydrophilicity, good biocompatibility in many applications, possibilities for conjugation, and low protein binding [92–95]. HPMA copolymer-doxorubincin conjugates were rationally designed and developed as anticancer polymer therapeutics in the late 1970s and early 1980s by Kopecek and colleagues [96,97]. pHPMA was later used as micell-forming polymers of drug delivery system [92,98–100]. This thesis focuses on polymeric micelles composed of p(HPMAm)-block-poly(N-2-benzoyloxypropyl methacrylamide) (p(HPMAm)-b-p(HPMAm-Bz), Fig. 1) and explores the application and possible ABC effect after repeated administration. To simplify the name of the amphiphilic block copolymer, the term of 'fully pHPMA backbone' is used in this thesis to refer to the hydrophilic pHPMA blocks and hydrophobic pHPMA derivative blocks.
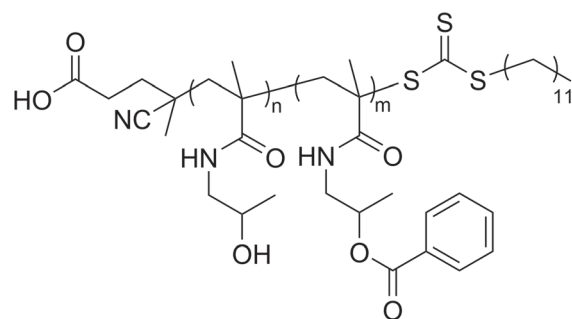

Fig. 1. Chemical structure of p(HPMAm)-b-p(HPMAm-Bz) block copolymer.

Biotinylated polymer-based nanoparticles as tumor-targeted drug delivery system

Biotin, also known as water-soluble vitamin B7, is essential for normal cellular functions, growth, and development, and serves as a coenzyme for carboxylase enzymes in glucose, fat, and amino acid metabolism [101]. As mammals are unable to biosynthesize biotin, these organisms must obtain biotin as a micronutrient from exogenous plant or bacterial sources from which it is taken up after oral administration, through the sodium-dependent multivitamin transporter (SMVT) system [102,103]. In 2004 Russell-Jones et al. compared the effectiveness of folate, vitamin B12, or biotin-functionalized poly(hydroxypropyl methacrylic acid) (pHPMAA) labeled with rhodamine as dynamic drug targeting agents to the tumor cells. Biotinylated polymers exhibited higher uptake in many aggressive cancer cells including leukemia, colon, mastocytoma, lung, renal, and breast cancer cell lines than folate or vitamin B12-functionalized polymers [104]. As a result, the anti-cancer efficacy of biotin-targeted doxorubicin-pHPMAA conjugate against colon carcinoma xenografts was efficiently enhanced *in vivo*, however, the same outcomes were not observed when either vitamin B12 or folate were used as targeting agents [105]. These findings suggest that the biotinylated polymers were more efficiently internalized than folate or vitamin B12-functionalized polymers. Therefore, biotin is considered and has been investigated as a remarkable active targeting ligand for the delivery of anti-cancer drugs [106–108].

Biotin (Fig. 2) has a valeric acid tail, through which it can be conjugated to other molecules to achieve biotinylation [106,109]. Biotin can be decorated on the surface of nanocarriers either through pre-conjugation of biotin to the polymers before their assembly into nanocarriers [110–112], or by attaching biotin onto the surface of nanocarriers after formation (post-conjugation) [113–116].
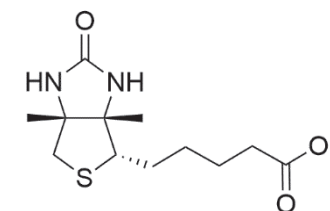

Fig. 2. Chemical structure of biotin.

The density of targeting ligand on the surface of nanocarriers has been demonstrated to influence targeting outcomes [117]. Therefore, screening of the ideal ratio of ligand conjugation is necessary for optimizing nanocarriers for high cellular internalization and deep penetration in diseased tissues. Doris et al. synthesized polydiacetylene micelles functionalized with controlled amounts of biotin, i.e. 0, 10, 25, and 50 mol%, using bioorthogonal click chemistry [113]. The micelles were loaded with a fluorescent dye to achieve selective cellular internalization by MCF-7 cells *in vitro*. The internalization kinetics differed significantly for the micelles with increasing biotin concentrations, suggesting that the efficiency of the cellular uptake was correlated to the density of grafted biotin. Micelles with a density of 25 mol% biotin on the surface exhibited the best internalization properties. Importantly, cellular uptake decreased drastically for micelles bearing ≥25 mol% of biotin at their surface, which was explained by the authors with the following hypotheses [118], (i) increase of the local concentration of biotin may result in non-solvated areas which alter ligand-receptor recognition, (ii) steric hindrance could also limit ligand-protein accessibility, (iii) stacking between adjacent biotin moieties might lower the availability of active targeting ligands, and/or (iv) receptor overbinding, where a single micelle is bonded to multiple receptors, reduces the overall number of interacting nanoparticles per cell.

Biotinylated polymer-based nanoparticles have shown great potential in controlled drug release, overcoming drug resistance, and optimizing the targeted release efficiency [119–124]. For instance, Wu et al. designed biotin-decorated liposomes to effectively target breast tumor cells [125]. The paclitaxel-loaded triple biotinylated liposomes exerted stronger cytotoxicity against human MCF-7 breast tumor cells *in vitro* and increased accumulation at the tumor sites *in vivo*.

(Strept)avidin is a tetrameric protein with four identical β-barrel subunits [126,127]. Each unit has a biotin-binding pocket and can bind biotin independently with an extremely high affinity (dissociation constant, K_d = ~10^{-15} M) [128,129]. The high affinity of avidin-biotin provides the possibility of determining the efficiency of biotin conjugation reaction using an avidin/4′-hydroxyazobenzene-2-carboxylic acid (HABA) competitive binding assay [116,130,131]. HABA is a dye that can bind to avidin, and HABA-avidin complexes in an aqueous solution show a characteristic absorbance at 500 nm. When biotin or biotinylated reagents are added to HABA-avidin solution, the strong binding of avidin-biotin causes the dissociation of HABA molecules. This displacement can then be quantitatively monitored by the decrease in ultraviolet (UV) absorbance at 500 nm. Despite the common application of avidin/HABA assay, Sleiman et al. reported that this assay did not apply to the luminescent PEGylated micelles with biotin decoration due to the small interference caused by the iridium-incorporated polymers [132]. Therefore, in their study, streptavidin-coated magnetic beads were employed to analyze the binding efficiency of the luminescent micelles. The streptavidin-coated magnetic beads are a suspension of magnetic particles approximately 1.5 μm in size to which streptavidin is covalently attached to the surface. This thesis describes the application of streptavidin-coated magnetic beads for the evaluation of the simultaneous release of drugs from polymeric micelles as well as their retention in the micelles in clean buffer solutions and biological media.

Aims and outline of this thesis

This thesis aimed to develop PEG-free polymeric micelles based on p(HPMAm)-b-p(HPMAm-Bz) as nanocarriers for hydrophobic anticancer drugs.

Chapter 2 describes the synthesis and characterization of a biotin-functionalized chain transfer agent and amphiphilic p(HPMAm)-b-p(HPMAm-Bz) with different molecular weights using the reversible addition–fragmentation chain-transfer (RAFT) polymerization. The copolymers self-assembled in aqueous media into biotinylated polymeric micelles. The cellular uptake and cytotoxicity of these micelles loaded with paclitaxel were evaluated using A549 human lung cancer cells overexpressing the biotin receptor as well as in HEK293 kidney cells lacking this receptor.

Chapter 3 describes the systematic study on factors impacting the size of p(HPMAm)-b-p(HPMAm-Bz) polymeric micelles, including the molecular weight of the polymers, homopolymer content, and processing methods (i.e., batch process versus continuous microfluidics). The formation of core-shell structured micelles was demonstrated by dynamic light scattering, asymmetric flow field-flow fractionation coupled with multi-angle light scattering, analytical ultracentrifugation, and Cryo-transmission electron microscopy analysis.

Chapter 4 describes a magnetic beads-enabled method for the evaluation of *in vitro* drug release from polymeric micelles in biological media. Strong interaction between biotin and streptavidin was exploited to capture paclitaxel or curcumin-loaded biotinylated micelles from PBS, PBS/Tween 80, PBS/BSA, plasma, and whole mouse blood using streptavidin-coated magnetic beads. This study aimed to determine simultaneously both the amount of drug released in the different media as well as the amount of drug still retained in the micelles.

Chapter 5 describes the effect of p(HPMA) as the shell of the polymeric micelles on circulation kinetics and possible accelerated blood clearance. The different micelles possessed the same hydrophobic core (p(HPMAm-Bz)), but different hydrophilic

shells (pHPMA and PEG). The circulation time and biodistribution of the micelles in BALB/c mice after the first and second doses, the possible impact of biotin decoration on the *in vivo* behavior of p(HPMAm)-based micelles, and the possible accelerated blood clearance were investigated.

Chapter 6 summarizes the results of this thesis and provides future perspectives for the development of biotinylated polymeric micelles from amphiphilic poly(HPMA)-based block copolymers for cancer therapy and other inflammatory diseases.

References

[1]   Cancer, (2020). https://www.who.int/news-room/fact-sheets/detail/cancer (accessed July 23, 2022).

[2]   B. Flühmann, I. Ntai, G. Borchard, S. Simoens, S. Mühlebach, Nanomedicines: the magic bullets reaching their target?, European Journal of Pharmaceutical Sciences. 128 (2019) 73–80.

[3]   Z.R. Lu, P. Qiao, Drug delivery in cancer therapy, Quo vadis?, Mol Pharm. 15 (2018) 3603–3616.

[4]   A. Tewabe, A. Abate, M. Tamrie, A. Seyfu, E.A. Siraj, Targeted drug delivery — from magic bullet to nanomedicine: Principles, challenges, and future perspectives, J Multidiscip Healthc. 14 (2021) 1711–1724.

[5]   C. Allen, Why I'm holding onto hope for nano in oncology, Mol Pharm. 13 (2016) 2603–2604.

[6]   D. Mundekkad, W.C. Cho, Nanoparticles in clinical translation for cancer therapy, Int J Mol Sci. 23 (2022) 1–29.

[7]   Y. Barenholz, Doxil® - The first FDA-approved nano-drug: Lessons learned, Journal of Controlled Release. 160 (2012) 117–134.

[8]   Y. Matsumura, H. Maeda, A new concept for macromolecular therapeutics in cancer chemotherapy: mechanism of tumoritropic accumulation of proteins and the antitumor agent smancs, Cancer Res. 46 (1986) 6387–6392.

[9]   J. Fang, H. Nakamura, H. Maeda, The EPR effect: unique features of tumor blood vessels for drug delivery, factors involved, and limitations and augmentation of the effect, Adv Drug Deliv Rev. 63 (2011) 136–151.

[10]   H. Maeda, Vascular permeability in cancer and infection as related to macromolecular drug delivery, with emphasis on the EPR effect for tumor-selective drug targeting, Proc Jpn Acad Ser B Phys Biol Sci. 88 (2012) 4–22.

[11]   H. Maeda, H. Nakamura, J. Fang, The EPR effect for macromolecular drug delivery to solid tumors: improvement of tumor uptake, lowering of systemic toxicity, and distinct tumor imaging in vivo, Adv Drug Deliv Rev. 65 (2013) 71–79.

[12]   H. Maeda, J. Wu, T. Sawa, Y. Matsumura, K. Hori, Tumor vascular permeability and the EPR effect in macromolecular therapeutics: a review, Journal of Controlled Release. 65 (2000) 271–284.

[13]   H. Maeda, The 35th anniversary of the discovery of EPR effect: a new wave of nanomedicines for tumor-targeted drug delivery—personal remarks and future prospects, J Pers Med. 11 (2021) 229.

[14]   H. Maeda, Toward a full understanding of the EPR effect in primary and metastatic tumors as well as issues related to its heterogeneity, Adv Drug Deliv Rev. 91 (2015) 3–6.

[15] T. Lammers, F. Kiessling, W.E. Hennink, G. Storm, Drug targeting to tumors: principles, pitfalls and (pre-) clinical progress, Journal of Controlled Release. 161 (2012) 175–187.

[16] W. Islam, S. Kimura, R. Islam, A. Harada, K. Ono, J. Fang, T. Niidome, T. Sawa, H. Maeda, Epr-effect enhancers strongly potentiate tumor-targeted delivery of nanomedicines to advanced cancers: Further extension to enhancement of the therapeutic effect, J Pers Med. 11 (2021) 487.

[17] P. Mi, K. Miyata, K. Kataoka, H. Cabral, Clinical Translation of Self-Assembled Cancer Nanomedicines, Adv Ther (Weinh). 4 (2021) 2000159.

[18] R. van der Meel, L.J.C. Vehmeijer, R.J. Kok, G. Storm, E.V.B. van Gaal, Ligand-targeted particulate nanomedicines undergoing clinical evaluation: Current status, Adv Drug Deliv Rev. 65 (2013) 1284–1298.

[19] S. Xu, B.Z. Olenyuk, C.T. Okamoto, S.F. Hamm-Alvarez, Targeting receptor-mediated endocytotic pathways with nanoparticles: rationale and advances, Adv Drug. 65 (2013) 121–138.

[20] N. Li, Y. Sun, Y. Fu, K. Sun, RNA drug delivery using biogenic nanovehicles for cancer therapy, Front Pharmacol. 12 (2021) 1–16.

[21] M. Liu, X. Fang, Y. Yang, C. Wang, Peptide-enabled targeted delivery systems for therapeutic applications, Front Bioeng Biotechnol. 9 (2021) 1–15.

[22] Y. Liu, L. Scrivano, J.D. Peterson, M.H.A.M. Fens, I.B. Hernández, B. Mesquita, J.S. Toraño, W.E. Hennink, C.F. van Nostrum, S. Oliveira, EGFR-targeted nanobody functionalized polymeric micelles loaded with mTHPC for selective photodynamic therapy, Mol Pharm. 17 (2020) 1276–1292.

[23] M.J. Joralemon, K.S. Murthy, E.E. Remsen, M.L. Becker, K.L. Wooley, Synthesis, characterization, and bioavailability of mannosylated shell cross-linked nanoparticles, Biomacromolecules. 5 (2004) 903–913.

[24] H. Shi, M.J. van Steenbergen, B. Lou, Y. Liu, W.E. Hennink, R.J. Kok, Folate decorated polymeric micelles for targeted delivery of the kinase inhibitor dactolisib to cancer cells, Int J Pharm. 582 (2020) 119305.

[25] W.X. Ren, J. Han, S. Uhm, Y.J. Jang, C. Kang, J.H. Kim, J.S. Kim, Recent development of biotin conjugation in biological imaging, sensing, and target delivery, Chemical Communications. 51 (2015) 10403–10418.

[26] W. Alshaer, H. Hillaireau, E. Fattal, Aptamer-guided nanomedicines for anticancer drug delivery, Adv Drug Deliv Rev. 134 (2018) 122–137.

[27] M. Hadjidemetriou, Z. Al-Ahmady, M. Mazza, R.F. Collins, K. Dawson, K. Kostarelos, In vivo biomolecule corona around blood-circulating, clinically used and antibody-targeted lipid bilayer nanoscale vesicles, ACS Nano. 9 (2015) 8142–8156.

[28] V.J. Yao, S. D'Angelo, K.S. Butler, C. Theron, T.L. Smith, S. Marchiò, J.G. Gelovani, R.L. Sidman, A.S. Dobroff, C.J. Brinker, A.R.M. Bradbury, W. Arap, R. Pasqualini, Ligand-targeted theranostic nanomedicines against cancer, Journal of Controlled Release. 240 (2016) 267–286.

[29] L. Martínez-Jothar, S. Doulkeridou, R.M. Schiffelers, J. Sastre Torano, S. Oliveira, C.F. van Nostrum, W.E. Hennink, Insights into maleimide-thiol conjugation chemistry: Conditions for efficient surface functionalization of nanoparticles for receptor targeting, Journal of Controlled Release. 282 (2018) 101–109.

[30] D.N. Heo, D.H. Yang, H.J. Moon, J.B. Lee, M.S. Bae, S.C. Lee, W.J. Lee, I.C. Sun, I.K. Kwon, Gold nanoparticles surface-functionalized with paclitaxel drug and biotin receptor as theranostic agents for cancer therapy, Biomaterials. 33 (2012) 856–866.

[31] K. Hirota, E. Czogala, W. Pedrycz, Stealth liposomes: review of the basic science, rationale, and clinical applications, existing and potential, Int J Nanomedicine. 1 (2016) 297–315.

[32] S.M. Moghimi, A.J. Andersen, S.H. Hashemi, B. Lettiero, D. Ahmadvand, A.C. Hunter, T.L. Andresen, I. Hamad, J. Szebeni, Complement activation cascade triggered by PEG-PL engineered nanomedicines and carbon nanotubes: The challenges ahead, Journal of Controlled Release. 146 (2010) 175–181.

[33] Y. Hussein, M. Youssry, Polymeric micelles of biodegradable diblock copolymers: enhanced encapsulation of hydrophobic drugs, Materials. 11 (2018) 688.

[34] N.Z. Knežević, E. Ruiz-Hernández, W.E. Hennink, M. Vallet-Regí, Magnetic mesoporous silica-based core/shell nanoparticles for biomedical applications, RSC Adv. 3 (2013) 9584–9593.

[35] H. Cabral, K. Miyata, K. Osada, K. Kataoka, Block copolymer micelles in nanomedicine applications, Chem Rev. 118 (2018) 6844–6892.

[36] A. Varela-Moreira, Y. Shi, M.H.A.M. Fens, T. Lammers, W.E. Hennink, R.M. Schiffelers, Clinical application of polymeric micelles for the treatment of cancer, Mater Chem Front. 1 (2017) 1485–1501.

[37] L. Houdaihed, J.C. Evans, C. Allen, Overcoming the road blocks: advancement of block copolymer micelles for cancer therapy in the clinic, Mol Pharm. 14 (2017) 2503–2517.

[38] D. Hwang, J.D. Ramsey, A. v. Kabanov, Polymeric micelles for the delivery of poorly soluble drugs: from nanoformulation to clinical approval, Adv Drug Deliv Rev. 156 (2020) 80–118.

[39] R. Takahashi, K. Doi, S. Fujii, K. Sakurai, Flower necklaces of controllable length formed from N-(2-hydroxypropyl) methacrylamide-based amphiphilic statistical copolymers, Langmuir. 36 (2020) 11556–11563.

[40] M. Najafi, N. Kordalivand, M.A. Moradi, J. van den Dikkenberg, R. Fokkink, H. Friedrich, N.A.J.M. Sommerdijk, M. Hembury, T. Vermonden, Native chemical ligation for cross-linking of flower-like micelles, Biomacromolecules. 19 (2018) 3766–3775.

[41] J. Bresseleers, M. Bagheri, C. Lebleu, S. Lecommandoux, O. Sandre, I.A.B. Pijpers, A.F. Mason, S. Meeuwissen, C.F. van Nostrum, W.E. Hennink, J.C.M. van Hest, Tuning size and morphology of mPEG-b-p(HPMA-Bz) copolymer self-assemblies using microfluidics, Polymers (Basel). 12 (2020) 2572.

[42] Q. Yu, M.G. Roberts, S. Pearce, A.M. Oliver, H. Zhou, C. Allen, I. Manners, M.A. Winnik, Rodlike block copolymer micelles of controlled length in water designed for biomedical applications, Macromolecules. 52 (2019) 5231–5244.

[43] N. Kang, J.C. Leroux, Triblock and star-block copolymers of N-(2-hydroxypropyl)methacrylamide or N-vinyl-2-pyrrolidone and d,l-lactide: Synthesis and self-assembling properties in water, Polymer (Guildf). 45 (2004) 8967–8980.

[44] O. Soga, C.F. Van Nostrum, A. Ramzi, T. Visser, F. Soulimani, P.M. Frederik, P.H.H. Bomans, W.E. Hennink, Physicochemical characterization of degradable thermosensitive polymeric micelles, Langmuir. 20 (2004) 9388–9395.

[45] Y. Shi, T. Lammers, G. Storm, W.E. Hennink, Physico-chemical strategies to enhance stability and drug retention of polymeric micelles for tumor-targeted drug delivery, Macromol Biosci. 17 (2017) 1600160.

[46] H. Cabral, Y. Matsumoto, K. Mizuno, Q. Chen, M. Murakami, M. Kimura, Y. Terada, M.R. Kano, K. Miyazono, M. Uesaka, N. Nishiyama, K. Kataoka, Accumulation of sub-100 nm polymeric micelles in poorly permeable tumours depends on size, Nat Nanotechnol. 6 (2011) 815–823.

[47] Q. Zhou, L. Zhang, T.H. Yang, H. Wu, Stimuli-responsive polymeric micelles for drug delivery and cancer therapy, Int J Nanomedicine. 13 (2018) 2921–2942.

[48] J. Bresseleers, M. Bagheri, G. Storm, J.M. Metselaar, W.E. Hennink, S.A. Meeuwissen, J.C.M. van Hest, Scale-Up of the manufacturing process to produce docetaxel-loaded mPEG- b -p(HPMA-Bz) block copolymer micelles for pharmaceutical applications, Org Process Res Dev. 23 (2019) 2707–2715.

[49] M. Bagheri, J. Bresseleers, A. Varela Moreira, O. Sandre, S.A. Meeuwissen, R.M. Schiffelers, J.M. Metselaar, C.F. van Nostrum, J.C.M. van Hest, W.E. Hennink, The effect of formulation and processing parameters on the size of mPEG-b-p(HPMA-Bz) polymeric micelles, Langmuir. 34 (2018) 15495–15506.

[50] M. Beck-Broichsitter, E. Rytting, T. Lebhardt, X. Wang, T. Kissel, Preparation of nanoparticles by solvent displacement for drug delivery: a shift in the "ouzo region" upon drug loading, European Journal of Pharmaceutical Sciences. 41 (2010) 244–253.

[51] E. Lepeltier, C. Bourgaux, P. Couvreur, Nanoprecipitation and the "ouzo effect": application to drug delivery devices, Adv Drug Deliv Rev. 71 (2014) 86–97.

[52] Q. Hu, C.J. Rijcken, R. Bansal, W.E. Hennink, G. Storm, J. Prakash, Complete regression of breast tumour with a single dose of docetaxel-entrapped core-cross-linked polymeric micelles, Biomaterials. 53 (2015) 370–378.

[53] R. Botet, The "ouzo effect", recent developments and application to therapeutic drug carrying, J Phys Conf Ser. 352 (2012) 012047.

[54] M.A. Tomeh, X. Zhao, Recent advances in microfluidics for the preparation of drug and gene delivery systems, Mol Pharm. 17 (2020) 4421–4434.

[55] K. Letchford, R. Liggins, H. Burt, Solubilization of hydrophobic drugs by methoxy poly(ethylene glycol)-block-polycaprolactone diblock copolymer micelles: Theoretical and experimental data and correlations, J Pharm Sci. 9 (2008) 1179–1190.

[56] F. Ullah, A. Khan, H.M. Akil, M. Siddiq, Effect of hydrophilic/hydrophobic block ratio and temperature on the surface and associative properties of oxyethylene and oxybutylene diblock copolymers in aqueous media, J Dispers Sci Technol. 36 (2015) 1777–1785.

[57] H. Yang, J. Guo, R. Tong, C. Yang, J.-K. Chen, pH-Sensitive micelles based on star copolymer Ad-(PCL-b-PDEAEMA-b-PPEGMA)4 for controlled drug delivery, Polymers (Basel). 10 (2018) 443.

[58] N. Scholz, T. Behnke, U. Resch-Genger, Determination of the critical micelle concentration of neutral and ionic surfactants with fluorometry, conductometry, and surface tension—a method comparison, J Fluoresc. 28 (2018) 465–476.

[59] C. Le Zhao, M.A. Winnik, G. Riess, M.D. Croucher, Fluorescence probe techniques used to study micelle formation in water-soluble block copolymers, Langmuir. 6 (1990) 514–516.

[60] R.M. Talom, G. Fuks, C. Mingotaud, S. Gineste, F. Gauffre, Investigation of the reversibility of the unimer-to-aggregate transition in block copolymers by surface tension-measurements, J Colloid Interface Sci. 387 (2012) 180–186.

[61] W. Huang, C. Zhang, Tuning the size of poly(lactic-co-glycolic acid) (PLGA) nanoparticles fabricated by nanoprecipitation, Biotechnol J. 13 (2018) 1700203.

[62] H. Koide, T. Asai, K. Hatanaka, T. Urakami, T. Ishii, Particle size-dependent triggering of accelerated blood clearance phenomenon, Int J Pharm. 362 (2008) 197–200.

[63] C.D. Walkey, J.B. Olsen, H. Guo, A. Emili, W.C.W. Chan, Nanoparticle size and surface chemistry determine serum protein adsorption and macrophage uptake, J Am Chem Soc. 134 (2012) 2139–2147.

[64] M. Glantz, A. Håkansson, H. Lindmark Månsson, M. Paulsson, L. Nilsson, Revealing the size, conformation, and shape of casein micelles and aggregates with asymmetrical flow field-flow fractionation and multiangle light scattering, Langmuir. 26 (2010) 12585–12591.

[65] S.E. Harding, The Svedberg lecture 2017. From nano to micro: the huge dynamic range of the analytical ultracentrifuge for characterising the sizes, shapes and interactions of molecules and assemblies in biochemistry and polymer science, European Biophysics Journal. 47 (2018) 697–707.

[66] S. Bhattacharjee, DLS and zeta potential - what they are and what they are not?, Journal of Controlled Release. 235 (2016) 337–351.

[67] M. Ghezzi, S. Pescina, C. Padula, P. Santi, E. del Favero, L. Cantù, S. Nicoli, Polymeric micelles in drug delivery: an insight of the techniques for their characterization and assessment in biorelevant conditions, Journal of Controlled Release. 332 (2021) 312–336.

2

[68] U. Sakulkhu, M. Mahmoudi, L. Maurizi, G. Coullerez, M. Hofmann-Amtenbrink, M. Vries, M. Motazacker, F. Rezaee, H. Hofmann, Significance of surface charge and shell material of superparamagnetic iron oxide nanoparticle (SPION) based core/shell nanoparticles on the composition of the protein corona, Biomater Sci. 3 (2015) 265–278.

[69] N. Schultz, G. Metreveli, M. Franzreb, F.H. Frimmel, C. Syldatk, Zeta potential measurement as a diagnostic tool in enzyme immobilisation, Colloids Surf B Biointerfaces. 66 (2008) 39–44.

[70] H. Kouchakzadeh, S.A. Shojaosadati, A. Maghsoudi, E. Vasheghani Farahani, Optimization of PEGylation conditions for BSA nanoparticles using response surface methodology, AAPS PharmSciTech. 11 (2010) 1206–1211.

[71] R.F. Pagels, J. Edelstein, C. Tang, R.K. Prud'homme, Controlling and predicting nanoparticle formation by block copolymer directed rapid precipitations, Nano Lett. 18 (2018) 1139–1144.

[72] C. Cao, J. Zhao, M. Lu, C.J. Garvey, M.H. Stenzel, Correlation between drug loading content and biological activity: the complexity demonstrated in paclitaxel-loaded glycopolymer micelle system, Biomacromolecules. 20 (2019) 1545–1554.

[73] M.H. Stenzel, The trojan horse goes wild: the effect of drug loading on the behavior of nanoparticles, Angewandte Chemie - International Edition. 60 (2021) 2202–2206.

[74] Z. He, X. Wan, A. Schulz, H. Bludau, M.A. Dobrovolskaia, S.T. Stern, S.A. Montgomery, H. Yuan, Z. Li, D. Alakhova, M. Sokolsky, D.B. Darr, C.M. Perou, R. Jordan, R. Luxenhofer, A. v. Kabanov, A high capacity polymeric micelle of paclitaxel: Implication of high dose drug therapy to safety and in vivo anti-cancer activity, Biomaterials. 101 (2016) 296–309.

[75] X. Wan, Y. Min, H. Bludau, A. Keith, S.S. Sheiko, R. Jordan, A.Z. Wang, M. Sokolsky-Papkov, A. v. Kabanov, Drug combination synergy in worm-like polymeric micelles improves treatment outcome for small cell and non-small cell lung cancer, ACS Nano. 12 (2018) 2426–2439.

[76] M.S. Haider, M.M. Lübtow, S. Endres, S. Forster, V.J. Flegler, B. Böttcher, V. Aseyev, A.C. Pöppler, R. Luxenhofer, R. Luxenhofer, Think beyond the core: impact of the hydrophilic corona on drug solubilization using polymer micelles, ACS Appl Mater Interfaces. 12 (2020) 24531–24543.

[77] M.M. Lübtow, H. Marciniak, A. Schmiedel, M. Roos, C. Lambert, R. Luxenhofer, Ultra-high to ultra-low drug-loaded micelles: probing host–guest interactions by fluorescence spectroscopy, Chemistry - A European Journal. 25 (2019) 12601–12610.

[78] C. Cao, J. Zhao, F. Chen, M. Lu, Y.Y. Khine, A. Macmillan, C.J. Garvey, M.H. Stenzel, Drug-induced morphology transition of self-assembled glycopolymers: insight into the drug-polymer interaction, Chemistry of Materials. 30 (2018) 5227–5236.

[79] K. Knop, R. Hoogenboom, D. Fischer, U.S. Schubert, Poly(ethylene glycol) in drug delivery: pros and cons as well as potential alternatives, Angewandte Chemie International Edition. 49 (2010) 6288–6308.

[80] A.A. D'souza, R. Shegokar, Polyethylene glycol (PEG): a versatile polymer for pharmaceutical applications, Expert Opin Drug Deliv. 13 (2016) 1257–1275.

[81] I. Alberg, S. Kramer, M. Schinnerer, Q. Hu, C. Seidl, C. Leps, N. Drude, D. Möckel, C. Rijcken, T. Lammers, M. Diken, M. Maskos, S. Morsbach, K. Landfester, S. Tenzer, M. Barz, R. Zentel, Polymeric Nanoparticles with Neglectable Protein Corona, Small. 16 (2020) 1907574.

[82] A. Abuchowski, T. Van Es, N.C. Palczuk, F.F. Davis, Alteration of immunological properties of bovine serum albumin by covalent attachment of polyethylene glycol, Journal of Biological Chemistry. 252 (1977) 3578–3581.

[83] E.T.M. Dams, P. Laverman, W.J.G. Oyen, G. Storm, G.L. Scherphof, J.W.M. van der Meer, F.H.M. Corstens, O.C. Boerman, Accelerated blood clearance and altered biodistribution of repeated injections of sterically stabilized liposomes, Journal of Pharmacology and Experimental Therapeutics. 292 (2000) 1071–1079.

[84] A.S. Abu Lila, H. Kiwada, T. Ishida, The accelerated blood clearance (ABC) phenomenon: clinical challenge and approaches to manage, Journal of Controlled Release. 172 (2013) 38–47.

[85] J.J.F. Verhoef, T.J. Anchordoquy, Questioning the use of PEGylation for drug delivery, Drug Deliv Transl Res. 3 (2013) 499–503.

[86] H. Koide, T. Asai, H. Kato, H. Ando, K. Shiraishi, M. Yokoyama, N. Oku, Size-dependent induction of accelerated blood clearance phenomenon by repeated injections of polymeric micelles, Int J Pharm. 432 (2012) 75–79.

[87] B. Romberg, C. Oussoren, C.J. Snel, M.G. Carstens, W.E. Hennink, G. Storm, Pharmacokinetics of poly(hydroxyethyl- L -asparagine) -coated liposomes is superior over that of PEG-coated liposomes at low lipid dose and upon repeated administration, Biochim Biophys Acta. 1768 (2007) 737–743.

[88] B. Romberg, C. Oussoren, C.J. Snel, W.E. Hennink, G. Storm, Effect of liposome characteristics and dose on the pharmacokinetics of liposomes coated with poly(amino acid)s, Pharm Res. 24 (2007) 2394–2401.

[89] T. Ishihara, T. Maeda, H. Sakamoto, N. Takasaki, M. Shigyo, T. Ishida, H. Kiwada, Y. Mizushima, T. Mizushima, Evasion of the accelerated blood clearance phenomenon by coating of nanoparticles with various hydrophilic polymers, Biomacromolecules. 11 (2010) 2700–2706.

[90] P.H. Kierstead, H. Okochi, V.J. Venditto, T.C. Chuong, S. Kivimae, J.M.J. Fréchet, F.C. Szoka, The effect of polymer backbone chemistry on the induction of the accelerated blood clearance in polymer modified liposomes, Journal of Controlled Release. 213 (2015) 1–9.

[91] B. Weber, C. Seidl, D. Schwiertz, M. Scherer, S. Bleher, R. Süss, M. Barz, Polysarcosine-based lipids: from lipopolypeptoid micelles to stealth-like lipids in Langmuir Blodgett monolayers, Polymers (Basel). 8 (2016) 427.

2

[92]   J. Yang, J. Kopeček, Design of smart HPMA copolymer-based nanomedicines, Journal of Controlled Release. 240 (2016) 9–23.

[93]   P. Chytil, L. Kostka, T. Etrych, HPMA copolymer-based nanomedicines in controlled drug delivery, J Pers Med. 11 (2021) 1–22.

[94]   J. Yang, J. Kopeček, The light at the end of the tunnel—second generation HPMA conjugates for cancer treatment, Curr Opin Colloid Interface Sci. 31 (2017) 30–42.

[95]   X. Zhang, P. Chytil, T. Etrych, W. Liu, L. Rodrigues, G. Winter, S.K. Filippov, C.M. Papadakis, Binding of HSA to macromolecular pHPMA based nanoparticles for drug delivery: an investigation using fluorescence methods, Langmuir. 34 (2018) 7998–8006.

[96]   R. Duncan, J. Kopecek, J.B. Lloyd, Development of N-(2-hydroxypropyl) methacrylamide copolymers as carriers of therapeutic agents, Polymer Science and Technology. 23 (1983) 97–113.

[97]   R. Duncan, M.J. Vicent, Do HPMA copolymer conjugates have a future as clinically useful nanomedicines? A critical overview of current status and future opportunities, Adv Drug Deliv Rev. (2010).

[98]   M. Talelli, C.J.F. Rijcken, C.F. van Nostrum, G. Storm, W.E. Hennink, Micelles based on HPMA copolymers, Adv Drug Deliv Rev. 62 (2010) 231–239.

[99]   J. Kopeček, P. Kopečková, HPMA copolymers: origins, early developments, present, and future, Adv Drug Deliv Rev. 62 (2010) 122–149.

[100]   J. Kopeček, P. Kopečková, T. Minko, Z.R. Lu, HPMA copolymer-anticancer drug conjugates: design, activity, and mechanism of action, European Journal of Pharmaceutics and Biopharmaceutics. 50 (2000) 61–81.

[101]   F. Grafe, W. Wohlrab, R.H. Neubert, M. Brandsch, Transport of biotin in human keratinocytes, Journal of Investigative Dermatology. 120 (2003) 428–433.

[102]   S.W. Polyak, Mechanisms of biotin transport, Biochemistry & Analytical Biochemistry. 4 (2015) 1–8.

[103]   P.D. Prasad, H. Wang, R. Kekuda, T. Fujita, Y.J. Fei, L.D. Devoe, F.H. Leibach, V. Ganapathy, Cloning and functional expression of a cDNA encoding a mammalian sodium- dependent vitamin transporter mediating the uptake of pantothenate, biotin, and lipoate, Journal of Biological Chemistry. 273 (1998) 7501–7508.

[104]   G. Russell-Jones, J. Mcewan, Amplification of biotin-mediated targeting, US patent 2006/0127310 A1, application no. 10/535, 269, Access Pharmaceuticals Australia PTY LTD., USA, 2006.

[105]   G. Russell-Jones, K. McTavish, J. McEwan, J. Rice, D. Nowotnik, Vitamin-mediated targeting as a potential mechanism to increase drug uptake by tumours, J Inorg Biochem. 98 (2004) 1625–1633.

[106]   S. Maiti, P. Paira, Biotin conjugated organic molecules and proteins for cancer therapy: A review, Eur J Med Chem. 145 (2018) 206–223.

[107]   D. Plaziuk, J. Zakrzewski, M. Salmain, A. Błauzì, B. Rychlik, P. Strzelczyk, A. Bujacz, G. Bujacz, Ferrocene-biotin conjugates targeting cancer cells: Synthesis, interaction with avidin, cytotoxic properties and the crystal structure of the complex of avidin with a biotin-linker-ferrocene conjugate, Organometallics. 32 (2013) 5774–5783.

[108]   L. Bildstein, C. Dubernet, P. Couvreur, Prodrug-based intracellular delivery of anticancer agents, Adv Drug Deliv Rev. 63 (2011) 3–23.

[109]   E.Y. Hanurry, T.W. Mekonnen, A.T. Andrgie, H.F. Darge, Y.S. Birhan, W.-H. Hsu, H.-Y. Chou, C.-C. Cheng, J.-Y. Lai, H.-C. Tsai, Biotin-decorated PAMAM G4.5 dendrimer nanoparticles to enhance the delivery, anti-proliferative, and apoptotic effects of chemotherapeutic drug in cancer cells, Pharmaceutics. 12 (2020) 443.

[110]   R. Narain, M. Gonzales, A.S. Hoffman, P.S. Stayton, K.M. Krishnan, Synthesis of monodisperse biotinylated p(NIPAAm)-coated iron oxide magnetic nanoparticles and their bioconjugation to streptavidin, Langmuir. 23 (2007) 6299–6304.

[111]   A. Aqil, H. Qiu, J.F. Greisch, R. Jérôme, E. De Pauw, C. Jérôme, Coating of gold nanoparticles by thermosensitive poly(N-isopropylacrylamide) end-capped by biotin, Polymer (Guildf). 49 (2008) 1145–1153.

[112]   C.Y. Hong, C.Y. Pan, Direct synthesis of biotinylated stimuli-responsive polymer and diblock copolymer by RAFT polymerization using biotinylated trithiocarbonate as RAFT agent, Macromolecules. 39 (2006) 3517–3524.

[113]   A. Doerflinger, N.N. Quang, E. Gravel, G. Pinna, M. Vandamme, F. Ducongé, E. Doris, Biotin-functionalized targeted polydiacetylene micelles, Chemical Communications. 54 (2018) 3613–3616.

[114]   W. Lv, L. Liu, Y. Luo, X. Wang, Y. Liu, Biotinylated thermoresponsive core cross-linked nanoparticles via RAFT polymerization and "click" chemistry, J Colloid Interface Sci. 356 (2011) 16–23.

[115]   H. Kakwere, S. Perrier, Orthogonal "relay" reactions for designing functionalized soft nanoparticles, J Am Chem Soc. 131 (2009) 1889–1895.

[116]   X. Jiang, S. Liu, R. Narain, Degradable thermoresponsive core cross-linked micelles: Fabrication, surface functionalization, and biorecognition, Langmuir. 25 (2009) 13344–13350.

[117]   H.S. Min, H.J. Kim, J. Ahn, M. Naito, K. Hayashi, K. Toh, B.S. Kim, Y. Matsumura, I.C. Kwon, K. Miyata, K. Kataoka, Tuned density of anti-tissue factor antibody fragment onto siRNA-loaded polyion complex micelles for optimizing targetability into pancreatic cancer cells, Biomacromolecules. 19 (2018) 2320–2329.

[118]   N. MacKiewicz, J. Nicolas, N. Handké, M. Noiray, J. Mougin, C. Daveu, H.R. Lakkireddy, D. Bazile, P. Couvreur, Precise engineering of multifunctional PEGylated polyester nanoparticles for cancer cell targeting and imaging, Chemistry of Materials. 26 (2014) 1834–1847.

2

[119]   C.Y. Quan, D.Q. Wu, C. Chang, G.B. Zhang, S.X. Cheng, X.Z. Zhang, R.X. Zhuo, Synthesis of thermo-sensitive micellar aggregates self-assembled from biotinylated PNAS-b-PNIPAAm-b-PCL triblock copolymers for tumor targeting, Journal of Physical Chemistry C. 113 (2009) 11262–11267.

[120]   C. Cheng, H. Wei, J.L. Zhu, C. Chang, H. Cheng, C. Li, S.X. Cheng, X.Z. Zhang, R.X. Zhuo, Functionalized thermoresponsive micelles self-assembled from biotin-PEG-b-P(NIPAAm-co-HMAAm)-b-PMMA for tumor cell target, Bioconjug Chem. 19 (2008) 1194–1201.

[121]   E.S. Lee, K. Na, Y.M. Bae, Super pH-sensitive multifunctional polymeric micelle, Nano Lett. 5 (2005) 325–329.

[122]   D.T. Bui, J. Nicolas, A. Maksimenko, D. Desmaële, P. Couvreur, Multifunctional squalene-based prodrug nanoparticles for targeted cancer therapy, Chemical Communications. 50 (2014) 5336–5338.

[123]   Y. Patil, T. Sadhukha, L. Ma, J. Panyam, Nanoparticle-mediated simultaneous and targeted delivery of paclitaxel and tariquidar overcomes tumor drug resistance, Journal of Controlled Release. 136 (2009) 21–29.

[124]   M. Huang, Y. Pu, Y. Peng, Q. Fu, L. Guo, Y. Wu, Y. Zheng, Biotin and glucose dual-targeting, ligand-modified liposomes promote breast tumor-specific drug delivery, Bioorg Med Chem Lett. 30 (2020) 127151.

[125]   B. Tang, Y. Peng, Q. Yue, Y. Pu, R. Li, Y. Zhao, L. Hai, L. Guo, Y. Wu, Design, preparation and evaluation of different branched biotin modified liposomes for targeting breast cancer, Eur J Med Chem. 193 (2020) 112204.

[126]   N. Michael Green, Avidin, Am J Med Sci. 243 (1962) 131.

[127]   N. Michael Green, Avidin and streptavidin, Methods Enzymol. 184 (1990) 51–67.

[128]   J. Song, Y. Li, C. Ji, J.Z.H. Zhang, Functional loop dynamics of the streptavidin-biotin complex, Sci Rep. 5 (2015) 7906.

[129]   M. Wilchek, E.A. Bayer, Introduction to avidin-biotin technology, Methods Enzymol. 184 (1990) 5–13.

[130]   Y.Z. You, D. Oupický, Synthesis of temperature-responsive heterobifunctional block copolymers of poly(ethylene glycol) and poly(N-isopropylacrylamide), Biomacromolecules. 8 (2007) 98–105.

[131]   K. Qi, Q. Ma, E.E. Remsen, C.G. Clark, K.L. Wooley, Determination of the bioavailability of biotin conjugated onto shell cross-linked (SCK) nanoparticles, J Am Chem Soc. 126 (2004) 6599–6607.

[132]   K.L. Metera, K.D. Ha-nni, G. Zhou, M.K. Nayak, H.S. Bazzi, D. Juncker, H.F. Sleiman, Luminescent iridium(III)-containing block copolymers: self-assembly into biotin-labeled micelles for biodetection assays, ACS Macro Lett. 1 (2012) 954–959.
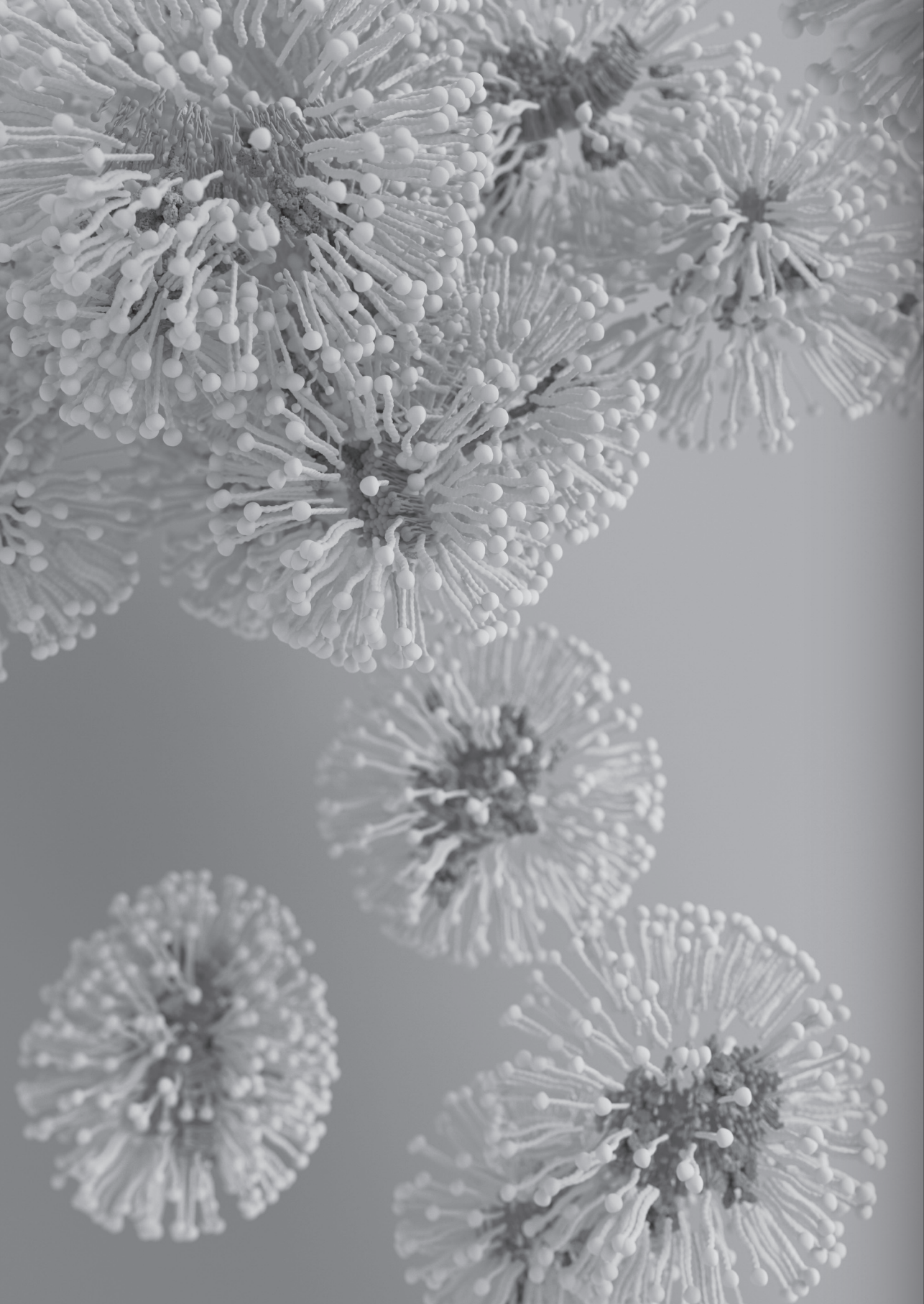
2

Biotin-decorated all-HPMA polymeric micelles for paclitaxel delivery

Yan Wang [1], Mies J. van Steenbergen [1], Nataliia Beztsinna [1], Yang Shi [2], Twan Lammers [2], Cornelus F. van Nostrum [1] and Wim E. Hennink [1]

[1] Department of Pharmaceutics, Utrecht Institute for Pharmaceutical Sciences, Utrecht University, Universiteitsweg 99, 3508 TB Utrecht, the Netherlands; y.wang3@uu.nl (Y.W.); M.J.vanSteenbergen@uu.nl (M.J.v.S.); nataliia.beztsinna@gmail.com (N.B.); C.F.vanNostrum@uu.nl (C.F.v.N.)

[2] Department of Nanomedicine and Theranostics, Institute for Experimental Molecular Imaging, RWTH Aachen University Clinic, Forckenbecktrasse 55, 52074 Aachen, Germany; yshi@ukaachen.de (Y.S.); tlammers@ukaachen.de (T.L.)

Abstract

To avoid poly(ethylene glycol)-related issues of nanomedicines such as accelerated blood clearance, fully *N*-2-hydroxypropyl methacrylamide (HPMAm)-based polymeric micelles decorated with biotin for drug delivery were designed. To this end, a biotin-functionalized chain transfer agent (CTA), 4-cyano-4-[(dodecylsulfanylthiocarbonyl)-sulfanyl]pentanoic acid (biotin-CDTPA), was synthesized for reversible addition–fragmentation chain-transfer (RAFT) polymerization. Amphiphilic poly(*N*-2-hydroxypropyl methacrylamide)-block-poly(*N*-2-benzoyloxypropyl methacrylamide) (p(HPMAm)-b-p(HPMAm-Bz)) with molecular weights ranging from 8 to 24 kDa were synthesized using CDTPA or biotin-CDTPA as CTA and 2,2'-azobis(2-methylpropionitrile) as initiator. The copolymers self-assembled in aqueous media into micelles with sizes of 40–90 nm which positively correlated to the chain length of the hydrophobic block in the polymers, whereas the critical micelle concentrations decreased with increasing hydrophobic block length. The polymer with a molecular weight of 22.1 kDa was used to prepare paclitaxel-loaded micelles which had sizes between 61 and 70 nm, and a maximum loading capacity of around 10 wt.%. A549 lung cancer cells overexpressing the biotin receptor, internalized the biotin-decorated micelles more efficiently than non-targeted micelles, while very low internalization of both types of micelles by HEK293 human embryonic kidney cells lacking the biotin receptor was observed. As a consequence, the paclitaxel-loaded micelles with biotin decoration exhibited stronger cytotoxicity in A549 cells than non-targeted micelles. Overall, a synthetic pathway to obtain actively targeted poly(ethylene glycol)-free micelles fully based on a poly(HPMAm) backbone was established. These polymeric micelles are promising systems for the delivery of hydrophobic anticancer drugs.

Introduction

During the last decades, drug delivery systems have been extensively investigated for cancer chemotherapy, and particularly, substantial attention has been devoted to polymeric micelles [1–5]. Polymeric micelles are nanosized colloidal particles with a core-shell structure, which spontaneously self-assemble from amphiphilic copolymers above a certain concentration (CMC, critical micelle concentration) in aqueous solution. The outer hydrophilic shell ensures colloidal stability of polymeric micelles and provides long circulation in the blood circulation, whereas the hydrophobic core is highly suitable for accommodating and solubilizing hydrophobic drugs [6–9]. Due to their small size (< 100 nm) and long circulation kinetics, polymeric micelles passively accumulate in cancerous or inflamed tissues by a phenomenon referred to as the enhanced permeability and retention (EPR) effect [10–12]. Besides passive targeting, micelles can be functionalized with ligands for active targeting to increase the efficacy of anti-cancer drugs while reducing their unwanted localization in healthy tissues by means of receptor-mediated endocytosis [13–15]. Various ligands, including antibody (fragments), peptides, aptamers and small molecules (such as folate) have been employed for the design of targeted nanomedicines [16–19].

Biotin, as a water-soluble vitamin, is essential for normal cellular functions, growth and development [20,21], and the sodium-dependent multivitamin transporter (SMVT) has been proved to be its main transporter [22], which is overexpressed in many cancer cells such as lung cancer cells (A549 and M109) [20,23]. In 2004 Russell-Jones et al. reported that a biotin-targeted doxorubicin- poly(*N*-2-benzoyloxypropyl methacrylamide) (pHPMAm) conjugate caused significant killing enhancement in colon carcinoma xenografts. Importantly, the same outcomes were not observed when either vitamin B$_{12}$ or folate were used as targeting agents [23,24]. Therefore, biotin has emerged as a remarkable active targeting ligand for nanocarriers [25–29]. Biotin has a valeric acid tail, through which it can be conjugated to other molecules to achieve biotinylation (Scheme 1A) [30]. Biotin can be decorated on the surface of nanocarriers either through pre-conjugation of biotin to the polymers before their assembly into nanocarriers [31–33], or by attaching biotin onto the surface of nanocarriers after formation (post-conjugation) [34,35].

Poly(ethylene glycol) (PEG) remains the 'gold standard' as hydrophilic shell-forming block in polymeric micelles, due to its high water-solubility and stealth properties that avoids adsorption of opsonins onto the surface of nanocarriers, which in turn reduces unspecific uptake of these particles by mononuclear phagocyte system (MPS) [36,37]. Several formulations based on PEGylated micelles for anti-cancer therapy are currently under evaluation in clinical trials [8,38,39]. However, in contrary

2

to the general assumption that PEGylated substances lack of immunogenicity, it has been shown that repeated injections of PEGylated nanoparticles can induce a phenomenon termed the accelerated blood clearance (ABC) effect, which is mediated by anti-PEG immunoglobulin M antibodies (IgM) [40,41]. Therefore, the search for alternative polymers that do not result in an immune response but maintain the long circulation is required. p(HPMAm) is a promising alternative for PEG, besides good hydrophilicity and biocompatibility, because of its multifunctionality, which enables modification with either hydrophobic moieties to serve as a micellar core, or conjugated with multiple drugs and bioactive ligands for targeted delivery [42–47]. Importantly, Szoka et al. reported that the ABC phenomenon was not observed upon repeated administration of p(HPMAm) modified liposomes due to the lack of formation of anti-p(HPMAm) IgM antibodies in rats, whereas a pronounced IgM response was observed for animals repeatedly treated with PEG-coated liposomes [48].

Recently the synthesis of poly(ethylene glycol)-block-poly(*N*-2-benzoyloxypropyl methacrylamide) (mPEG-b-p(HPMAm-Bz)) was reported [49]. These micelles showed high stability, drug loading and drug retention as a result of π-π stacking interactions between the aromatic groups of the drugs and the polymer chains. In the same study it was shown that paclitaxel (PTX)-loaded mPEG-b-p(HPMAm-Bz) micelles exhibited high therapeutic efficacy and complete tumor regression in mice bearing human epidermoid and breast carcinoma xenografts. Taken this in mind, we here set out to develop a biotin-decorated fully p(HPMAm)-based anti-cancer drug delivery system. To this end, p(HPMAm)-b-p(HPMAm-Bz) block copolymers with and without biotin modification were synthesized by reversible addition–fragmentation chain-transfer (RAFT) polymerization and used for the formation of biotinylated micelles. The cellular uptake and cytotoxicity of these micelles loaded with PTX were evaluated using A549 human lung cancer cells overexpressing the biotin receptor as well as in HEK293 kidney cells lacking this receptor.

Materials and Methods

Materials
D-(+)-Biotin was purchased from Santa Cruz Biotechnology, Inc. (Heidelberg, Germany). *N*-Hydroxysuccinimide (NHS), dicyclohexylcarbodiimide (DCC), *N*-Boc-1,6-hexanediamine, triethylamine (TEA), trifluoroacetic acid (TFA), 4-cyano-4-[(dodecylsulfanylthiocarbonyl)-sulfanyl]pentanoic acid (CDTPA), *N*-(3-dimethylaminopropyl)-*N'*-ethylcarbodiimide hydrochloride (EDC), sodium bicarbonate (NaHCO$_3$), sodium chloride (NaCl), anhydrous sodium sulfate (Na$_2$SO$_4$), 4-(2-hydroxyethyl)piperazine-1-ethanesulfonic acid (HEPES), pyrene,

and Dulbecco's modified Eagle's medium (DMEM) were obtained from Sigma-Aldrich (Zwijndrecht, the Netherlands) and used without further purification. Dimethylformamide (DMF, peptide synthesis grade), dichloromethane (DCM, peptide synthesis grade), tetrahydrofuran (THF, HPLC grade), dimethylacetamide (DMAc, peptide synthesis grade), 2-propanol, diethyl ether, and acetone were purchased from Biosolve Ltd (Valkenswaard, the Netherlands) and used as received, unless indicated otherwise. 2,2'-Azobis(2-methylpropionitrile) (AIBN) was obtained from Sigma-Aldrich (Zwijndrecht, the Netherlands), recrystallized from ethanol and stored at -20 °C. Phosphate buffered saline (PBS, pH 7.4, containing 11.9 mM phosphate, 137 mM sodium chloride, and 2.7 mM potassium chloride) was purchased from Fisher Scientific (Geel, Belgium). Paclitaxel (PTX) was ordered from LC Laboratories (MA, USA). *N*-2-Hydroxypropyl methacrylamide (HPMAm) was synthesized and characterized as described in a previous publication [50]. *N*-2-Benzoyloxypropyl methacrylamide (HPMAm-Bz) was synthesized and characterized as previously reported [43]. PEG standards for gel permeation chromatography (GPC) analysis were supplied by Agilent (Santa Clara, USA). Cyanine 3 (Cy3) amine was supplied by Lumiprobe GmbH (Hannover, Germany). Spectra/Por dialysis membrane (MW 6–8 kDa), DNA stain Hoechst 33430, and reduced serum medium Opti-MEM were obtained from Thermo Fisher Scientific (Landsmeer, the Netherlands), while 0.45 μm RC membrane filters were ordered from Phenomenex (Utrecht, the Netherlands). 3-(4,5-Dimethylthiazol-2-yl)-5-(3-carboxy-methoxyphenyl)-2-(4-sulfophenyl)-2H-tetrazolium (MTS) reagent was purchased from Benelux B.V. (Leiden, the Netherlands).

Synthesis of the biotin-functionalized RAFT chain transfer agent (biotin-CDTPA)

Synthesis of (+)-biotinyl-*N*-hydroxysuccinimide (NHS-biotin)
Biotin was activated according to literature procedures [51,52]. In brief, biotin (5.00 g, 20.5 mmol) and NHS (2.83 g, 24.6 mmol) were dissolved in dry DMF (150 mL) at 60 °C. DCC (5.07 g, 24.6 mmol) was added after cooling down to room temperature. The solution was stirred overnight at room temperature. Next, the formed reaction product dicyclohexylurea (DCU) was filtered off and washed with DMF. The combined filtrates were dropped into cold diethyl ether to precipitate the crude product which was then refluxed in 2-propanol, filtered, and dried under vacuum to yield NHS-biotin (4.60 g, 66%). ^{1}H NMR (600 MHz, DMSO-*d*$_6$) δ (ppm): 6.43 (s, 1H, N*H*C(=O)), 6.37 (s, 1H, N*H*C(=O)), 4.31 (ddt, 1H, *J* = 7.5, 5.1, 1.1 Hz, C*H*NHC(=O)), 4.15 (ddd, 1H, *J* = 7.7, 4.4, 1.8 Hz, C*H*NHC(=O)), 3.11 (ddd, 1H, *J* = 8.3, 6.3, 4.4 Hz, C*H*S), 2.83—2.86 (m, 1H, C*H*$_2$S), 2.78—2.83(m, 4H, (O=)C(C*H*$_2$)$_2$C(=O)), 2.65—2.70 (m, 2H, C*H*$_2$C(=O)), 2.59 (d, 1H, *J* = 12.4 Hz, C*H*$_2$S), 1.38—1.69 (m, 6H, (C*H*$_2$)$_3$CH$_2$C(=O)). ESI-MS m/z 363.0 (M + Na)$^+$, calculated for C$_{14}$H$_{19}$N$_3$O$_5$S 341.4.

Synthesis of tert-butyl(6-(5-((3aS,4S,6aR)-2-oxohexahydro-1H-thieno[3,4-d]imidazol-4-yl)pentanamido)hexyl)carbamate (*N*-boc-HDA-biotin)

N-Boc-HDA-biotin was synthesized as described in previous publications [53,54]. Briefly, NHS-biotin (3.00 g, 8.8 mmol) and *N*-Boc-1,6-hexanediamine (1.90 g, 8.8 mmol) were dissolved in anhydrous DMF (150 mL) and then TEA (1.22 mL, 12.0 mmol) was added. The reaction mixture was stirred at room temperature overnight. The product was isolated by precipitation in cold diethyl ether, dried under vacuum to yield *N*-Boc-HDA-biotin (3.50 g, 90%). ^{1}H NMR (600 MHz, DMSO-d_6) δ (ppm): 7.72 (t, 1H, J = 5.6 Hz, N$\underline{H}$), 6.75 (t, 1H, J = 5.8 Hz, N$\underline{H}$), 6.41 (s, 1H, NH-biotin), 6.35 (s, 1H, NH-biotin), 4.30 (ddt, 1H, J = 7.6, 5.2, 1.1 Hz, C$\underline{H}$NH), 4.12 (ddd, 1H, J = 7.7, 4.4, 1.9 Hz, C$\underline{H}$NH), 3.09 (ddd, 1H, J = 8.7, 6.2, 4.4 Hz, SC$\underline{H}$CH$_2$), 3.00 (q, 2H, NC$\underline{H}_2$), 2.85−2.90 (m, 2H, NC$\underline{H}_2$), 2.82 (dd, 1H, J = 12.4, 5.1 Hz, SCH$\underline{H}$), 2.57 (d, 1H, J = 12.4 Hz, SC$\underline{H}$H), 2.04 (t, 2H, J = 7.4 Hz, C$\underline{H}_2$C(=O)), 1.38−1.61 (m, 23H, 7CH$_2$, C(CH$_3$)$_3$). ESI-MS m/z 443.2 (M+H)$^+$, 465.2 (M+Na)$^+$, calculated for C$_{21}$H$_{38}$N$_4$O$_4$S 442.6.

Synthesis of *N*-(6-aminohexyl)-5-((3aS,4S,6aR)-2-oxohexahydro-1H-thieno[3,4-d]imidazole-4-yl)pentanamide trifluoroacetate (HDA-biotin)

The removal of the Boc protection group from *N*-Boc-HDA-biotin was performed following literature procedures [53,54]. In short, to a solution of *N*-Boc-HDA-biotin (3.50 g, 7.9 mmol) in DCM (43 mL), TFA (8.5 mL, 111.0 mmol) was added. The mixture was stirred at room temperature for 3 h. The solvent was evaporated under reduced pressure to yield a yellowish oil. The crude product was subsequently precipitated in an excess of cold diethyl ether. After repeatedly dissolving in methanol and evaporation under vacuum to remove residual TFA, the oil was dissolved in 10 mL water and lyophilized to yield HDA-biotin (3.50 g, 97%). ^{1}H NMR (600 MHz, DMSO-d_6) δ (ppm): 7.75 (t, J = 5.6 Hz, 1H, N$\underline{H}$), 7.40 (br, 3H, N$\underline{H}_3$), 6.43 (s, 1H, NH-biotin), 6.38 (s, 1H, NH-biotin), 4.31 (dd, 1H, J = 7.7, 5.1 Hz, C$\underline{H}$NH), 4.12 (ddd, 1H, J = 7.2, 4.4, 1.8 Hz, C$\underline{H}$NH), 3.09 (ddd, 1H, J = 8.6, 6.0, 4.4 Hz, SC$\underline{H}$CH$_2$), 3.01 (q, 2H, J = 6.6 Hz, NC$\underline{H}_2$), 2.81 (dd, 1H, J = 12.4, 5.1 Hz, SCH$\underline{H}$), 2.74−2.78 (m, 2H, NH$_2$C$\underline{H}_2$), 2.57 (d, 1H, J = 12.5 Hz, SC$\underline{H}$H), 2.04 (t, 2H, J = 7.4 Hz, C$\underline{H}_2$C(=O)), 1.22−1.61 (m, 14H, 7CH$_2$). ESI-MS m/z 343.2 (M+H)$^+$, calculated for C$_{16}$H$_{30}$N$_4$O$_2$S 342.5.

Synthesis of 4-cyano-4-[(dodecylsulfanylthiocarbonyl)-sulfanyl]pentanoic succinimide (NHS-CDTPA)

The synthesis of NHS-CDTPA was based on previously published papers [55,56]. Shortly, to a solution of 4-cyano-4-[(dodecylsulfanylthiocarbonyl)-sulfanyl]pentanoic acid (CDTPA) (5.00 g, 12.4 mmol) in 50 mL dry DCM at 0 **°C**, NHS (1.80 g, 15.6 mmol) and EDC (3.02 g, 15.9 mmol) were added. The reaction mixture was stirred at 0 **°C** for 1 h and then at room temperature for 9 h. Subsequently, the DCM solution was washed with saturated NaHCO$_3$ (aq.) and the resulting DCM phase was dried over anhydrous Na$_2$SO$_4$. After 2 h, Na$_2$SO$_4$ was filtered off and the solvent

was removed under reduced pressure and further dried under vacuum to yield NHS-CDTPA (5.30 g, 85%). ^{1}H NMR (600 MHz, chloroform-*d*) δ (ppm): 3.33 (m, 2H, CH$_2$C$\underline{H}_2$S), 2.93 (ddd, J = 9.2, 6.3, 3.9 Hz, 2H, C$\underline{H}_2$C(=O)), 2.85 (s, 4H, (O=)C(C$\underline{H}_2$)$_2$C(=O)), 2.66 (ddd, 1H, J = 14.4, 9.8, 6.5 Hz, C$\underline{H}_2$CH$_2$C(=O)), 2.53 (ddd, 1H, J = 14.4, 9.8, 6.5 Hz, C$\underline{H}_2$CH$_2$C(=O)), 1.88 (s, 3H, C(C$\underline{H}_3$)), 1.70 (tt, 2H, J = 12.8, 3.9 Hz, C$\underline{H}_2$CH$_2$S), 1.37−1.42 (m, 2H, C$\underline{H}_2$(CH$_2$)$_2$S), 1.23−1.31 (m, 16H, CH$_3$(C$\underline{H}_2$)$_8$CH$_2$), 0.88 (t, J = 7.0 Hz, 3H, C$\underline{H}_3$CH$_2$CH$_2$). ESI-MS m/z 559.2 (M+Na+2H$_2$O)$^+$, 541.2 (M+Na+H$_2$O)$^+$, calculated for C$_{23}$H$_{36}$N$_2$O$_4$S$_3$ 500.7.

Synthesis of biotin-functionalized chain transfer agent (biotin-CDTPA)

Coupling of NHS-CDTPA with HDA-biotin afforded a RAFT chain transfer agent, biotin-CDTPA. Briefly, to a solution of HDA-biotin (658 mg, 1.4 mmol) in a mixture of 18 mL anhydrous DMF and DCM (1:1, v/v), NHS-CDTPA (656 mg, 1.3 mmol) and TEA (450 µL, 3.3 mmol) were added. The reaction mixture was stirred at room temperature for 16 h. Next, DCM was evaporated under vacuum at 40 °C, and subsequently the reaction mixture was dropped into a large excess of reverse osmosis (RO) water to precipitate the crude product which was then washed with 2-propanol, filtered and dried under vacuum to yield biotin-CDTPA (~900 mg, 94%). ^{1}H NMR (600 MHz, DMSO-d_6) δ (ppm): 7.96 (t, 1H, J = 5.6 Hz, N$\underline{H}$), 7.73 (t, 1H, J = 5.6 Hz, N$\underline{H}$), 6.41 (s, 1H, NH-biotin), 6.35 (s, 1H, NH-biotin), 4.30 (dd, 1H, J = 7.8, 5.1 Hz, C$\underline{H}$NH), 4.12 (ddd, 1H, J = 7.6, 4.5, 1.8 Hz, C$\underline{H}$NH), 3.09 (ddd, 1H, J = 8.7, 6.0, 4.4 Hz, SC$\underline{H}$CH$_2$), 3.04−2.98 (m, 4H, 2NHC$\underline{H}_2$), 2.82 (dd, 1H, J = 12.4, 5.1 Hz, SCH$\underline{H}$), 2.58 (d, 1H, J = 12.4 Hz, SCH$\underline{H}$), 2.43−2.26 (m, 4H, 2C$\underline{H}_2$C(=O)), 2.04 (t, 2H, J = 7.4 Hz, CH$_2$C$\underline{H}_2$S), 1.85 (s, 3H, C(C$\underline{H}_3$)), 1.63−1.20 (m, 36H, 18CH$_2$), 0.85 (t, 3H, J = 6.9 Hz, C$\underline{H}_3$CH$_2$CH$_2$). ESI-MS m/z 728.3 (M+H)$^+$, 750.2 (M+Na)$^+$, calculated for C$_{35}$H$_{61}$N$_5$O$_3$S$_4$ 728.2.

Synthesis and characterization of p(HPMAm)-b-p(HPMAm-Bz) block copolymers with or without biotin terminus

Synthesis of poly[*N*-(2-hydroxypropyl) methacrylamide] macro chain transfer agent (p(HPMAm) macroCTA) with or without biotin terminus

The p(HPMAm) macroCTA with or without a biotin terminus was synthesized using RAFT polymerization with CDTPA or biotin-CDTPA as CTA and AIBN as initiator at 70 °C [57]. In detail, the reagents were weighed in Schlenk tubes and subsequently dissolved in dry DMAc (10 mL). The concentration of HPMAm was 300 mg/mL. To obtain p(HPMAm) of different molecular weights, molar ratios of [HPMAm]/[CDTPA]/[AIBN] of 180/5/1, 320/5/1 and 460/5/1 were applied. For the polymerization of HPMAm with a biotin terminal end, the molar ratio of [HPMAm]/[biotin-CDTPA]/[AIBN] was 460/5/1. The obtained solutions were degassed by three cycles of freeze-vacuum-thaw, backfilled with nitrogen, and the tubes were subsequently immersed in a prewarmed oil bath at 70 °C. At different time points, samples were withdrawn and analyzed by ^{1}H NMR and GPC. The reaction was carried out for 5–6

h. Next, the polymers were isolated by precipitation in diethyl ether for three times (DMAc/diethyl ether = 1/49, v/v) and dried overnight under vacuum to give the final products (entries 1–4 in Table 1).

Synthesis of block copolymers of poly[*N*-(2-hydroxypropyl) methacrylamide]-block-[*N*-(2-benzoyloxy-propyl) methacrylamide] (p(HPMAm)-b-p(HPMAm-Bz)) with or without biotin terminus

The obtained p(HPMAm) macroCTAs with or without biotin terminus were chain-extended with HPMAm-Bz under the same conditions as for the synthesis of p(HPMAm). In detail, the reagents were weighed in Schlenk tubes and subsequently dissolved in dry DMAc (7 mL). The concentration of HPMAm-Bz was 300 mg/mL. For the synthesis of copolymers with different molecular weights of the hydrophilic and hydrophobic blocks, the molar ratios of [HPMAm-Bz]/[p(HPMAm)]/[AIBN] were 250/5/1, 500/5/1 and 900/5/1, respectively. For the synthesis of biotinylated copolymer, the molar ratio of [HPMAm-Bz]/[biotinylated p(HPMAm)]/[AIBN] was 900/5/1. The solution was degassed by three cycles of freeze-vacuum-thawing, backfilled with nitrogen, and then the tube was immersed in a prewarmed oil bath at 70 °C. At different time points, samples were withdrawn and analyzed by ^{1}H NMR and GPC. The reaction was carried out for 18–20 h. The polymers were isolated by precipitation in diethyl ether for three times (DMAc/diethyl ether = 1/49, v/v) and dried overnight under vacuum to give the final products (entries 5–14 in Table 1).

Characterizations of the polymers by ^{1}H NMR spectroscopy and GPC

^{1}H NMR spectra were recorded using a Bruker 600 MHz spectrometer (Billerica, MA, USA). The polymers (5–10 mg) were dissolved in 600 μL DMSO-d_6. The DMSO-d_6 peak at 2.50 ppm was used as the reference line.

Chemical shifts of p(HPMAm) (Fig. S2B): 7.18 (b, C(=O)NHCH$_2$), 4.70 (s, CH(CH$_3$)OH), 3.68 (s, NHCH$_2$CH(CH$_3$) OH), 2.9 (b, NHCH_2CH), 0.4—2.0 (b, the rest of protons are from the methyl and backbone CH$_2$ protons). Chemical shifts of the biotinylated p(HPMAm) (Fig. S3B): in addition to protons from p(HPMAm), 7.89 (s, NH-linker), 7.74 (s, NH-linker), 6.43 (NH-biotin), 6.37 (NH-biotin), 4.30 (CHNH), 4.14 (CHNH).

The theoretical number average of molecular weight (M$_{n, theory}$) of p(HPMAm) with or without biotin terminus was calculated using the following equation (1):

$$M_{n, theory} = [monomer]/[CTA] \times conversion \times M_{monomer} + M_{CTA} \tag{1}$$

where the conversion of HPMAm was determined by comparing the integration areas of resonances from the vinyl protons of HPMAm at 5.30 ppm and the methine protons of HPMAm at 3.68 ppm (Fig. S2A & 3A), and [monomer], [CTA], M$_{monomer}$

and M$_{CTA}$ are the initial monomer and CTA concentrations, molecular weights of monomer (M$_{HPMAm}$ = 143 g/mol) and CTA (M$_{CDTPA}$ = 403 g/mol, M$_{biotin-CDTPA}$ = 727 g/mol), respectively.

The number average of molecular weight determined by ^{1}H NMR analysis (M$_{n, NMR}$) of biotinylated p(HPMAm) was calculated using the following equation (2):

$$M_{n, NMR} = degree\ of\ polymerization \times M_{monomer} + M_{CTA} \tag{2}$$

where the degree of polymerization of biotinylated p(HPMAm) was determined by comparing the integration areas of resonances from the methine protons of biotin-CDTPA at 4.14 ppm and the methine protons of biotinylated p(HPMAm) at 3.68 ppm (Fig. S3B), and M$_{monomer}$ and M$_{CTA}$ are molecular weights of monomer (M$_{HPMAm}$ = 143 g/mol) and CTA (M$_{biotin-CDTPA}$ = 727 g/mol), respectively.

Chemical shifts of p(HPMAm)-b-p(HPMAm-Bz) with or without biotin terminus (Fig. S4B & 5B): in addition to protons from p(HPMAm) with or without biotin terminus, 7.93 (s, aromatic CH), 7.34—7.65 (b, aromatic CH), 5.00 (s, NHCH$_2$CH(CH$_3$)O(O=C)), 3.15 (b, NHCH_2CH(CH$_3$)O(O=C)).

M$_{n, theory}$ of p(HPMAm)-b-p(HPMAm-Bz) with or without biotin terminus was calculated using the following equation (3):

$$M_{n, theory} = [monomer]/[macroCTA] \times conversion \times M_{monomer} + M_{n, macroCTA} \tag{3}$$

where the conversion of HPMAm-Bz was determined by comparing the integration areas of resonances from the methine protons of p(HPMAm-Bz) at 5.00 ppm and the vinyl protons of HPMAm-Bz at 5.60 ppm (Fig. S4A & 5A), and [monomer], [macroCTA], M$_{monomer}$ and M$_{n, macroCTA}$ are the initial monomer and macroCTA concentrations, molecular weights of monomer (M$_{HPMAm-Bz}$ = 247 g/mol) and macroCTA (M$_{n, p(HPMAm)}$ = 3000, 4900, and 7100 g/mol, M$_{n, biotinylated\ p(HPMAm)}$ = 6800 g/mol), respectively. M$_{n, NMR}$ of p(HPMAm)-b-p(HPMAm-Bz) with or without biotin terminus was calculated using the following equation (4):

$$M_{n, NMR} = degree\ of\ polymerization \times M_{monomer} + M_{n, macroCTA} \tag{4}$$

where the degree of polymerization of p(HPMAm)-b-(pHPMAm-Bz) with or without biotin terminus was determined by comparing the integration areas of resonances from the methine protons of p(HPMAm-Bz) at 5.00 ppm and the methine protons of p(HPMAm) with or without biotin terminus at 3.68 ppm (Fig. S4B & 5B), and M$_{monomer}$ and M$_{n, macroCTA}$ are molecular weights of monomer (M$_{HPMAm-Bz}$ = 247 g/mol)

and macroCTA ($M_{n, p(HPMAm)}$ = 3000, 4900, and 7100 g/mol, $M_{n, biotinylated\ p(HPMAm)}$ = 6800 g/mol), respectively.

GPC was carried out to determine the number average molecular weight (M_n), weight average molecular weight (M_w) and dispersity of molecular weight (PDI, equal to M_w/M_n) using two serial PLgel 5 µm MIXED-D columns and PEGs of narrow molecular weight distribution as calibration standards [58]. Samples were prepared by dissolving approximately 10 mg of the polymer in 3 mL of DMF and samples of 50 µL were injected onto the column. The eluent was DMF containing 10 mM LiCl, the elution rate was 1 mL/min, the temperature was 65 °C, and detection was done using a refractive index (RI) detector and ultraviolet (UV) detector at the wavelength of 254 and 309 nm.

Synthesis and characterizations of cyanine3 (Cy3)-labeled p(HPMAm)-b-p(HPMAm-Bz) block copolymer

The terminal carboxylic acid group of the p(HPMAm) block of p(HPMAm)-b-p(HPMAm-Bz) was first activated by NHS/EDC, yielding p(HPMAm)-b-p(HPMAm-Bz) NHS ester, followed by its reaction with the primary amine groups of Cy3 [59]. In detail, p(HPMAm)-b-p(HPMAm-Bz) (100 mg, thus 0.0046 mmol COOH end groups, entry 10 in Table 1) was dissolved in 1 mL dry DMAc and subsequently EDC (1.3 mg, 0.0069 mmol) and NHS (0.8 mg, 0.0069 mmol) dissolved in 1 mL DCM were added. The reaction mixture was stirred at room temperature for 1 h followed by addition of Cy3 amine (3.5 mg, 0.0056 mmol) dissolved in 0.5 mL dry DCM also containing TEA (8.0 µL, 0.058 mmol), and the resulting reaction mixture was stirred at room temperature overnight and subsequently transferred into a Spectra/Por dialysis membrane with a molecular weight cutoff of 6–8 kDa and sealed. Dialysis was carried out for 48 h against water/THF (1:1 v/v) which was changed every 12 h [49]. The final product (entry 15 in Table 1) was collected after lyophilization and characterized by ^{1}H NMR and GPC coupled with a UV detector (detection wavelength of 550 nm) as described above. The labeling efficiency was determined by Jasco FP8300 Spectrofluorometer (Easton, MD, USA) with a calibration curve of Cy3 amine in DMF at the concentration of 0.0625, 0.125, 0.25, 0.5 and 1 µg/mL. Fluorescence emission spectra of Cy3 from 500 to 800 nm were recorded at room temperature with an excitation wavelength at 550 nm. The excitation and emission band slits were 2.5 nm.

Preparation and characterizations of empty (Cy3-labeled) and PTX-loaded p(HPMAm)-b-p(HPMAm-Bz) micelles with or without biotin modification

Preparation of empty (Cy3-labeled) and PTX-loaded p(HPMAm)-b-p(HPMAm-Bz) micelles

Empty p(HPMAm)-b-p(HPMAm-Bz) micelles (with or without biotin modification) were prepared by solvent extraction method. In detail, 1 mL DMF solution of 18.0 mg of nonbiotinylated p(HPMAm)-b-p(HPMAm-Bz) copolymer (entry 13 in Table 1) and 2.0 mg of biotinylated p(HPMAm)-b-p(HPMAm-Bz) copolymer (entry 14 in Table 1), or 20.0 mg nonbiotinylated p(HPMAm)-b-p(HPMAm-Bz) copolymer only (entry 13 in Table 1) was pipetted into 1 mL Milli-Q water while stirring for 1 min. To remove DMF, the solution was transferred into a Spectra/Por dialysis membrane with a molecular weight cutoff of 6–8 kDa and sealed. Dialysis was carried out for 24 h against Milli-Q water which was changed at 2nd, 5th and 13th h. Next, the micellar dispersion was filtered through 0.45 µm RC membrane filter. The size of the empty p(HPMAm)-b-p(HPMAm-Bz) micelles was determined by dynamic light scattering (DLS) after 10-fold dilution in water at 25 °C using a Zetasizer Nano S at a fixed angle of 173° (Malvern Instruments Ltd., Malvern, UK). The Z-average diameter (Z_{ave}) and polydispersity index (PDI) were calculated by the Zetasizer software v.7.13. The zeta-potential of the empty p(HPMAm)-b-p(HPMAm-Bz) micelles was measured after 10-fold dilution in 10 mM HEPES buffer pH 7.4 using a Zetasizer Nano Z (Malvern Instruments Ltd., Malvern, UK). The residual DMF content of the micellar dispersion was measured by ^{1}H NMR as follows. Two hundred µL micelle dispersion was mixed with 400 µL D$_2$O, and no any peak corresponding to DMF was detected (detection limit ~50 ppm).

PTX-loaded micelles were prepared similarly as for empty micelles. In detail, 1 mL DMF in which the polymers (20 mg/mL, entries 13 and/or 14 in Table 1) and PTX (concentrations ranging from 1 to 25 mg/mL) were dissolved was rapidly pipetted into 1 mL Milli-Q water while stirring for 1 min, and DMF was subsequently removed by dialysis followed by filtration through 0.45 µm RC membrane filter to remove non-encapsulated PTX. To determine the drug content of PTX-loaded micelles, the micellar dispersions were diluted 10-fold with THF (HPLC grade) to destabilize the micelles, and the dissolved PTX was subsequently quantified by HPLC analysis (Waters Alliance System). The elution was isocratic with a mobile phase of THF/water = 55:45 (v/v) containing 0.1% formic acid. The total run time was 8 min with a flow rate of 1 mL/min. A Sunfire C18 column (5 µm, 4.6 × 150 mm) was used and the detection wavelength was 227 nm. The injection volume was 10 µL and the PTX concentration in the different samples was calculated using a calibration curve of PTX standards prepared in THF in a concentration range of 6–100 µg/mL. The

encapsulation efficiency (EE) and loading capacity (LC) were calculated by the following formulas:

$$EE = \frac{\text{amount of loaded PTX}}{\text{amount of PTX used for loading}} \times 100\% \tag{5}$$

$$LC = \frac{\text{amount of loaded PTX}}{\text{amount of loaded PTX + amount of obtained polymer}} \times 100\% \tag{6}$$

To study cellular uptake, empty Cy3-labeled p(HPMAm)-b-p(HPMAm-Bz) micelles (with or without biotin modification) were prepared similarly as for empty micelles without Cy3 label. Briefly, 1 mL DMF solution of 17.4 mg of nonbiotinylated p(HPMAm)-b-p(HPMAm-Bz) copolymer (entry 13 in Table 1), 2.0 mg of biotinylated p(HPMAm)-b-p(HPMAm-Bz) copolymer (entry 14 in Table 1) and 0.6 mg Cy3-labeled p(HPMAm)-b-p(HPMAm-Bz) (entry 15 in Table 1), or 19.4 mg nonbiotinylated p(HPMAm)-b-p(HPMAm-Bz) (entry 13 in Table 1) and 0.6 mg Cy3-labeled p(HPMAm)-b-p(HPMAm-Bz) (entry 15 in Table 1) was rapidly pipetted into 1 mL Milli-Q water while stirring for 1 min, and DMF was subsequently removed by dialysis followed by filtration through 0.45 µm RC membrane filter.

p(HPMAm)-b-p(HPMAm-Bz) polymer concentration determination
The polymer concentrations in the micellar dispersions were determined by GPC analysis (Waters Alliance System) after 10-fold dilution with DMF to destabilize the micelles. The elution was isocratic with a mobile phase of DMF containing 10 mM LiCl. Two serial PLgel 5 µm MIXED-D columns were used. Total run time was 30 min with a flow rate of 1 mL/min, the injection volume was 50 µL, the column temperature was 65 °C, and detection was done using a refractive index (RI) detector and ultraviolet (UV) detector at the wavelength of 254 and 309 nm. The polymer concentrations in the different samples were calculated using a calibration curve of samples of polymer dissolved in DMF at concentrations between 0.1–2 mg/mL. The micelle recovery yield was calculated by the following formula (7):

$$\text{Recovery yield} = \frac{\text{amount of obtained polymer}}{\text{amount of polymer used for prepearation}} \times 100\% \tag{7}$$

In vitro stability of p(HPMAm)-b-p(HPMAm-Bz) micelles
The *in vitro* colloidal stability of empty micelles, empty p(HPMAm)-b-p(HPMAm-Bz) (entry 13 in Table 1) micelles (with or without biotin decoration), prepared as described above and diluted 10-fold with PBS pH 7.4 (final polymer concentration was 0.9 and 0.6 mg/mL for biotinylated and nonbiotinylated micelles), was

investigated. The samples were incubated at 37 °C for 48 h. Small sample aliquots were analyzed by DLS.

Effect of the hydrophobic/hydrophilic block molecular weight ratio of p(HPMAm)-b-p(HPMAm-Bz) on micelle size
The effect of hydrophobic/hydrophilic block molecular weight ratio of p(HPMAm)-b-p(HPMAm-Bz) on the size of the formed micelles was investigated using the small library of copolymers synthesized as described above (entries 5–13 in Table 1). The different diblock copolymers (20 mg) were dissolved in 1 mL DMF and the obtained solutions were rapidly pipetted into 1 mL Milli-Q water while stirring for 1 min. DMF was removed by dialysis, and the obtained micellar dispersions were subsequently filtered through 0.45 µm RC membrane filter. The size of micelles was determined by DLS.

Critical micelle concentration (CMC) determination
The CMCs of the different p(HPMAm)-b-p(HPMAm-Bz) block copolymers were determined using pyrene fluorescence method as described previously [60,61]. Briefly, the p(HPMAm)-b-p(HPMAm-Bz) micelles were prepared by the solvent extraction method as described above, and the p(HPMAm)-b-p(HPMAm-Bz) polymer concentration was determined as described above. Subsequently, the micelle dispersions were diluted with distilled water to obtain concentrations that ranged from 1.0×10^{-5} to 1 mg/mL. Next, 50 µL of pyrene dissolved in acetone (0.18 mM) was added to 500 µL of the polymer dispersion. The dispersions were incubated at room temperature overnight to evaporate acetone. Fluorescence excitation spectra of pyrene from 300 to 360 nm were recorded at 37 °C while the intensity of the emitted light at 390 nm was recorded. The excitation and emission band slits were 10 and 2.5 nm, respectively. The intensity ratio of I_{338}/I_{333} was plotted against the polymer concentration to determine CMC.

Cell culture
Human adenocarcinoma alveolar based lung cancer cell line (A549) and human embryonic kidney cell line (HEK293) were obtained from the American Type Culture Collection (ATCC, Manassas, Virginia, USA). A549 cells are biotin receptor-positive whereas HEK293 cells are biotin receptor-negative [20]. A549 and HEK293 cells were cultured in DMEM supplemented with 10% of fetal bovine serum (FBS) at 37 °C in a humidified atmosphere containing 5% of CO_2. Both cell lines were grown in 75 cm^2 cell culture flasks and passaged twice a week.

In vitro cellular uptake of empty Cy3-labeled p(HPMAm)-b-p(HPMAm-Bz) micelles

A549 and HEK293 cells were seeded into 96-well plates at a density of 1×10^4 cells/well and incubated for 24 h at 37 °C in a humidified atmosphere containing 5% of CO_2. Stock solutions of empty Cy3-labeled micelles with or without biotin decoration (polymer concentration was 6 mg/mL) were prepared as described above. The cells were incubated with 100 μL of different formulations at 140 μg/mL at 37 °C in a humidified atmosphere containing 5% of CO_2 for 1, 4, 8, and 24 h. Next, Hoechst 33430 was added to the wells 30 min before imaging with a final concentration of 10 nM. The media were replaced with Opti-MEM and the plate was transferred into a Yokogawa CV7000 (Tokyo, Japan) spinning disk microscope with a 40 × 1.2 NA water objective. To investigate whether cellular internalization of the biotinylated micelles indeed occurs via biotin-receptor mediated endocytosis, A549 and HEK293 cells were pre-incubated with 2 mM free biotin for 1 h. Subsequently, the cells were incubated with the Cy3-labeled micelles with or without biotin decoration for 4 h, followed by confocal imaging according to the above procedures.

In vitro cytotoxicity of empty and PTX-loaded p(HPMAm)-b-p(HPMAm-Bz) micelles

The cell viability was evaluated after 48 h-exposure to the formulations by using the MTS assay. The tetrazolium reagent MTS can be bio-reduced by living cells into a colored formazan product that is soluble in tissue culture medium and that can be quantified by colorimetric method [58,62]. A549 and HEK293 cells were seeded into 96-well plates at a density of 5×10^3 cells/well and incubated for 24 h at 37 °C in a humidified atmosphere containing 5% of CO_2. Stock solutions of empty micelles with biotin decoration (polymer concentration was 9 mg/mL), empty micelles without biotin decoration (polymer concentration was 6 mg/mL), PTX-loaded micelles with biotin decoration (polymer concentration was 7 mg/mL) and PTX-loaded micelles without biotin decoration (polymer concentration was 6 mg/mL) were prepared as described above. PTX as Taxol formulation was prepared by dissolving 12 mg of PTX in 1 mL ethanol followed by addition of 1 mL Cremophor EL and sonication for 30 min [43]. A Taxol formulation without PTX was prepared by mixing Cremophor EL and ethanol (1:1, v/v). PTX-loaded micellar and Taxol formulations were diluted in cell culture media to yield concentrations of PTX that ranged from 1.0×10^{-5} to 100 μg/mL. The empty micelles were diluted in cell culture medium to yield polymer concentrations ranging from 1.7×10^{-4} to 1700 μg/mL, subsequently, Cremophor EL/ethanol solution was diluted in cell culture medium the same way as the Taxol formulation. The cells were incubated with 100 μL of the different formulations at 37 °C in a humidified atmosphere containing 5% of CO_2 for 48 h. Next, the media were replaced by 100 μL of fresh medium and 20 μL of MTS reagent followed by incubation for 2 h. The cell viability was determined by measuring the absorbance at 492 nm using a Biochrome EZ microplate reader (Jakarta Utara, Indonesia). IC_{50} values were calculated as drug concentration that inhibits the cell growth by 50% after 48 h of cultivation.

Statistical analysis

Statistical analysis was done by GraphPad Prism 8.3.0 software. Two-way analysis of variance (ANOVA) was used to determine the statistical significance of cell viability data. A value of $p < 0.05$ was considered significant.

Results and Discussion

Synthesis of biotin-functionalized chain transfer agent, biotin-CDTPA

A biotin-functionalized RAFT chain transfer agent, namely 4-cyano-4 [(dodecylsulfanylthiocarbonyl)-sulfanyl]pentanoic acid (biotin-CDTPA), was synthesized as shown in Scheme 1A. Amine-functionalized biotin (HDA-biotin) and NHS-activated CDTPA were synthesized as described previously [51–56], and obtained with the yield of 97 and 85%, respectively. Subsequently, biotin-CDTPA was obtained through NHS coupling of HDA-biotin with NHS-activated CDTPA with 94% yield. The ^{1}H NMR spectrum (Fig. S1) and mass spectrometric analysis (described above) demonstrate the successful synthesis of the desired CTA.
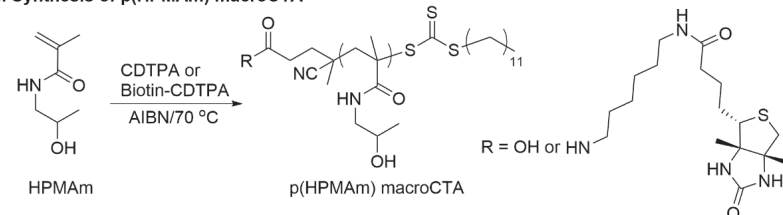
Synthesis of p(HPMAm)-b-p(HPMAm-Bz) block copolymers

The block copolymers p(HPMAm)-b-p(HPMAm-Bz) were synthesized as illustrated in Scheme 1B & C. First, HPMAm was polymerized by RAFT using either CDTPA or biotin-CDTPA as CTA and AIBN as initiator, respectively (Scheme 1B). The obtained p(HPMAm) macroCTA was subsequently extended with HPMAm-Bz (Scheme 1C). As shown in Fig. 1A, fast polymerization rates up to 8 h were observed, which slowed down after this time point likely due to loss of active thiocarbonylthio chain ends affording 'dead' polymer chains that are unable to participate in the RAFT process [63,64]. Similar pheonomenon in RAFT polymerization at high conversions was also observed in previous studies [57,65]. Fig. 1B–D show that the number average molecular weight (M_n) increased linearly with HPMAm and HPMAm-Bz conversion, which is typical for a controlled radical polymerization [66].
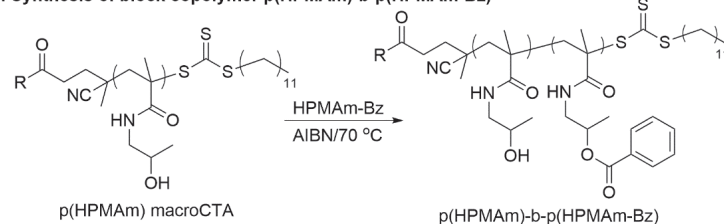
A. Synthesis of biotin-CDTPA
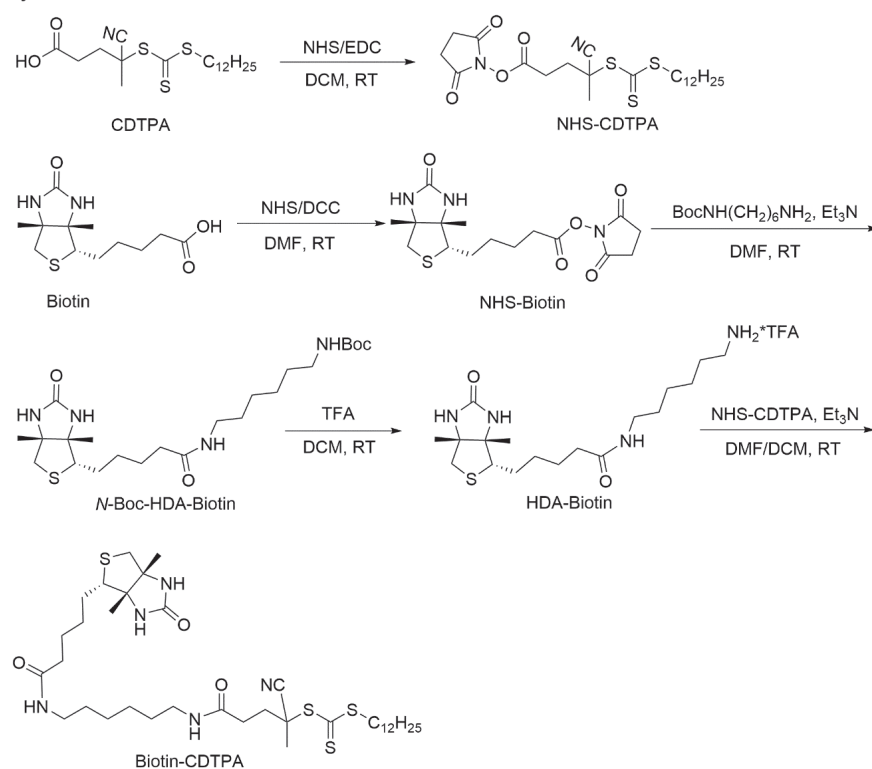
B. Synthesis of p(HPMAm) macroCTA

C. Synthesis of block copolymer p(HPMAm)-b-p(HPMAm-Bz)

Scheme 1. Synthesis of p(HPMAm)-b-p(HPMAm-Bz) block copolymer with or without a biotin terminus. (**A**) Synthesis of biotin-functionalized chain transfer agent, biotin-CDTPA. (**B**) Synthesis of macro chain trasnfer agent, p(HPMAm). (**C**) Synthesis of block copolymer p(HPMAm)-b-p(HPMAm-Bz).
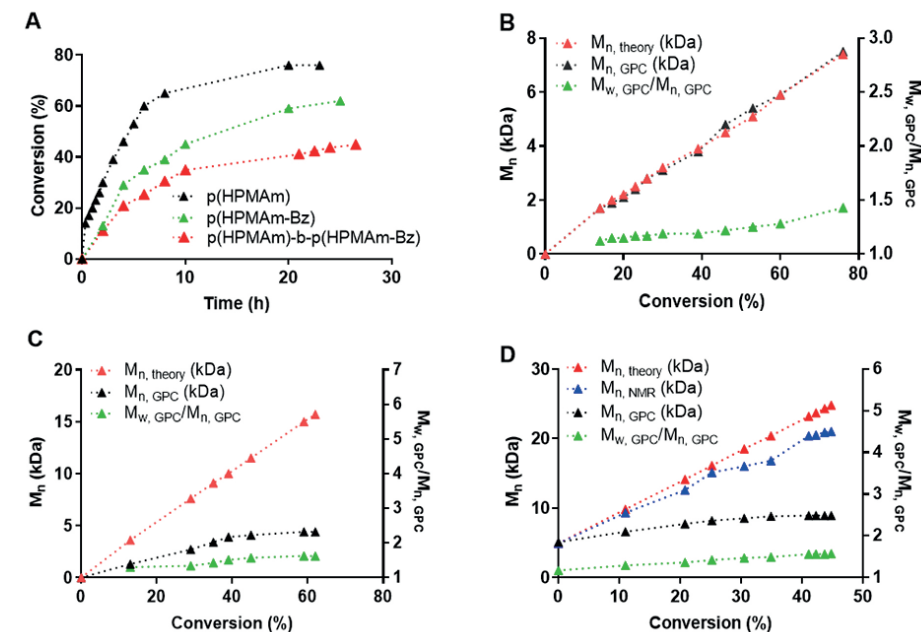

Fig. 1. Conversion as a function of reaction time for the RAFT polymerization of HPMAm and HPMAm-Bz (**A**). M_n (based on GPC and ^{1}H NMR analysis) and $M_{w, GPC}/M_{n, GPC}$ (PDI) versus conversion of HPMAm and HPMAM-Bz (**B,** p(HPMAm), molar ratio of M/CTA/I was 320/5/1; **C,** p(HPMAm-Bz), molar ratio of M/CTA/I was 500/5/1; and **D,** p(HPMAm)-b-p(HPMAm-Bz), molar ratio of M/macroCTA/I was 900/5/1).

We aimed to synthesize p(HPMAm) macroCTA with molecular weights of 3, 5 and 7 kDa, respectively, to mimic PEG (2–5 kDa) commonly used as a stealth polymer in polymeric micelles and PEGylated liposomes [67–70]. To obtain p(HPMAm) of different molecular weights, the molar ratio of HPMAm/CDTPA/AIBN ([M]/[CTA]/[I]) in the feed was varied (180/5/1, 320/5/1 and 460/5/1). For the synthesis of biotinylated p(HPMAm), the feed molar ratio of HPMAm/biotin-CDTPA/AIBN was 460/5/1. The RAFT polymerization was terminated when the conversion was around 50% to obtain p(HPMAm) with PDI of 1.19–1.33 (entries 1–4 in Table 1). The M_n's of p(HPMAm) measured by GPC were in accordance with the theoretical values calculated from the conversion of HPMAm (entries 1–4 in Table 1), by comparing the integration areas of resonances from the vinyl protons of HPMAm at 5.30 ppm and the methine protons of HPMAm at 3.68 ppm (Fig. S2A). In a typical ^{1}H NMR spectrum of the biotinylated p(HPMAm) (Fig. S3B), besides the characteristic peaks for p(HPMAm), the resonances attributed to the biotin unit could be clearly identified (chemical shifts as described above), which demonstrates that the biotin-terminated p(HPMAm) was successfully synthesized by RAFT polymerization using a biotin-functionalized trithiocarbonate chain transfer agent.

Table 1. Characteristics of the polymers synthesized by RAFT as determined by ^{1}H NMR, GPC and fluorometric analysis.

Entry	Polymers	Molar Ratio of M/CTA/I	Monomer Conversion (%)	$M_{n, theory}$ (kDa) [a]	$M_{n, NMR}$ (kDa) [b]	$M_{n, GPC}$ (kDa) [c]	PDI [c]	CMC (μg/mL) [d]
1	p(HPMAm)$_{3.0k}$	180:5:1	51	3.0	—	3.2	1.19	—
2	p(HPMAm)$_{4.9k}$	320:5:1	50	4.9	—	5.0	1.22	—
3	p(HPMAm)$_{7.1k}$	460:5:1	51	7.1	—	7.7	1.26	—
4	biotinylated p(HPMAm)$_{6.8k}$	460:5:1	46	6.8	7.0	8.1	1.33	—
5	p(HPMAm)$_{3.0k}$–b–p(HPMAm-Bz)$_{5.4k}$	250:5:1	36	7.5	8.4	6.6	1.39	33
6	p(HPMAm)$_{3.0k}$–b–p(HPMAm-Bz)$_{9.9k}$	500:5:1	39	12.6	12.9	8.7	1.43	27
7	p(HPMAm)$_{3.0k}$–b–p(HPMAm-Bz)$_{15.6k}$	900:5:1	44	22.5	18.6	10.6	1.55	21
8	p(HPMAm)$_{4.9k}$–b–p(HPMAm-Bz)$_{6.4k}$	250:5:1	42	10.1	11.3	7.4	1.36	32
9	p(HPMAm)$_{4.9k}$–b–p(HPMAm-Bz)$_{11.3k}$	500:5:1	38	14.3	16.2	9.2	1.41	22
10	p(HPMAm)$_{4.9k}$–b–p(HPMAm-Bz)$_{16.8k}$	900:5:1	40	22.8	21.7	10.0	1.41	6
11	p(HPMAm)$_{7.1k}$–b–p(HPMAm-Bz)$_{4.9k}$	250:5:1	45	12.7	12.0	9.1	1.42	43
12	p(HPMAm)$_{7.1k}$–b–p(HPMAm-Bz)$_{9.1k}$	500:5:1	39	16.7	16.2	8.5	1.49	22
13	p(HPMAm)$_{7.1k}$–b–p(HPMAm-Bz)$_{15.0k}$	900:5:1	39	24.9	22.1	11.0	1.48	6
14	biotinylated p(HPMAm)$_{6.8k}$-b-p(HPMAm-Bz)$_{16.3k}$	900:5:1	41	25.3	23.1	12.9	1.48	—
15	Cy3-labeled p(HPMAm)$_{4.9k}$-b-p(HPMAm-Bz)$_{18.7k}$ [e]	—	—	—	23.6	10.0	1.41	—

[a] $M_{n, theory}$ calculated using equations (1) and (3);
[b] $M_{n, NMR}$ calculated using equations (2) and (4);
[c] Determined by GPC analysis (DMF containing 10 mM LiCl as eluent, PEGs as standards), PDI, equal to $M_{w, GPC}/M_{n, GPC}$;
[d] Determined using pyrene fluorescence method;
[e] Obtained by labeling of p(HPMAm)$_{4.9k}$-b-p(HPMAm-Bz)$_{16.8k}$.
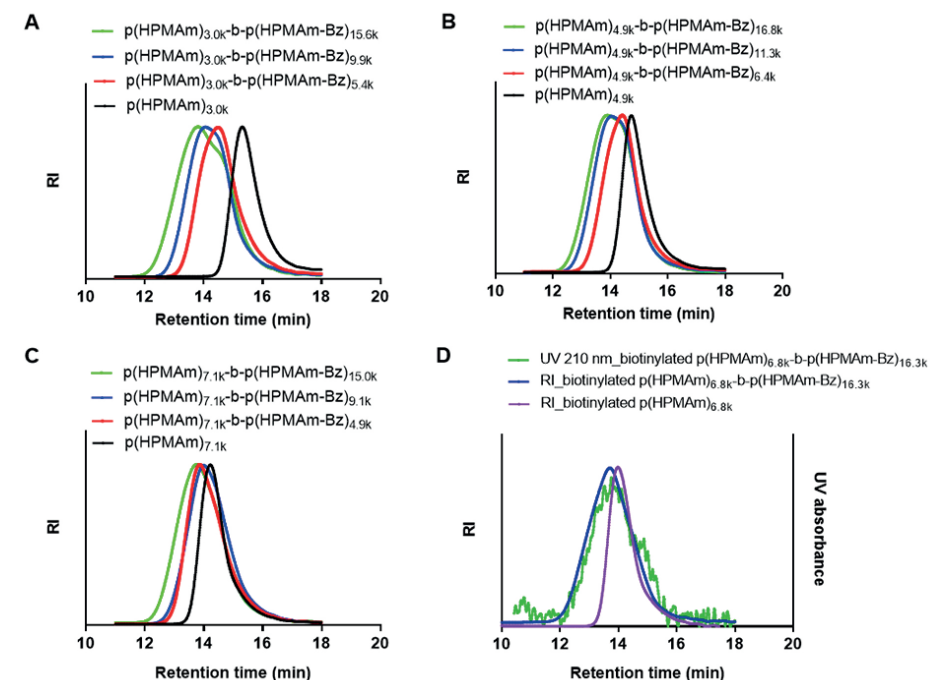
Fig. 2. GPC chromatograms of the synthesized block copolymers. (**A–C**) GPC chromatograms (RI detection) of the different p(HPMAm)-b-p(HPMAm-Bz) copolymers. (**D**) GPC chromatograms (RI and UV detection) of biotinylated p(HPMAm)-b-p(HPMAm-Bz).

To synthesize p(HPMAm)-b-p(HPMAm-Bz) diblock copolymers, the different p(HPMAm) macroCTAs were chain-extended with HPMAm-Bz under the same reaction conditions as for the synthesis of p(HPMAm). We aimed to synthesize block copolymers with a molecular weight below 45 kDa, which is the threshold of renal elimination for pHPMA [71]. To obtain p(HPMAm)-b-p(HPMAm-Bz) of different molecular weights, the molar ratios of HPMAm-Bz/p(HPMAm)/AIBN ([M]/[CTA]/[I]) in the feed were 250/5/1, 500/5/1 and 900/5/1. For the synthesis of the biotinylated block copolymer, the feed molar ratio of HPMAm-Bz/biotinylated p(HPMAm)/AIBN was 900/5/1. The RAFT polymerization was terminated when the conversion was around 40% with PDI of 1.36–1.55 (entries 5–14 in Table 1). The successful chain extension was demonstrated by GPC and ^{1}H NMR analysis. The obtained block copolymers showed a decreased GPC retention time compared to p(HPMAm), demonstrating an increased molecular weight (Fig. 2A–D). The GPC traces of the synthesized block copolymers exhibited slight tailing at low molecular weight and thus were relatively asymmetric, probably due to the presence of p(HPMAm) chains with a dead end. Such dead polymer chains formed during the macroCTA synthesis

cannot undergo chain extension, resulting in a small amount of homopolymer in the final product (Fig. S7), which is inevitable when block copolymers are synthesized via RAFT [72]. The repeating units of both HPMAm and HPMAm-Bz in the ^{1}H NMR spectra support the composition of the formed block copolymers (Fig. S4B & 5B). The theoretical M_n's of the block copolymers calculated from the HPMAm-Bz conversion were close to the molecular weight values as determined by ^{1}H NMR analysis (entries 5–14 in Table 1), by comparing the integration areas of resonances from the methine protons of p(HPMAm-Bz) at 5.00 ppm and the methine protons of p(HPMAm) at 3.68 ppm (Fig. S4B). A typical ^{1}H NMR spectrum of the biotinylated p(HPMAm)-b-p(HPMAm-Bz) shows that in addition to the characteristic resonances for p(HPMAm) and p(HPMAm-Bz) units, some small peaks ascribed to biotin were found (Fig. S5B, chemical shifts as described above) providing evidence that the block copolymer p(HPMAm)-b-p(HPMAm-Bz) indeed contains the biotin end group. Importantly, only one peak was observed in the GPC chromatogram using UV detection (wavelength 210 nm, Fig. 2D), which points to the free biotin concentration below detection.

To obtain a fluorescently labeled block copolymer suitable for cellular uptake studies, p(HPMAm)$_{4.9k}$-b-p(HPMAm-Bz)$_{16.8k}$ with a terminal NHS ester group was synthesized and subsequently reacted with Cy3 amine fluorophore (Scheme S1). The M_n of the synthesized Cy3-labeled p(HPMAm)-b-p(HPMAm-Bz) as determined by ^{1}H NMR was 23.6 kDa, which is close to the number average of molecular weight of the copolymer before Cy3 conjugation (Fig. S6A & B). The GPC chromatogram of Cy3-labeled p(HPMAm)$_{4.9k}$-b-p(HPMAm-Bz)$_{18.7k}$ (Fig. S8A) shows that the chromatograms as recorded by RI and UV detection demonstrate identical retention time, which confirms that Cy3 was conjugated to the block copolymer. Importantly, the absence of UV-Vis signal in the Cy3-labeled p(HPMAm)$_{4.9k}$-b-p(HPMAm-Bz)$_{18.7k}$ sample at 18.5 min confirms that no free Cy3 amine was present. After the coupling reaction, on average, the number of Cy3 units was 0.85 per polymer chain as demonstrated by fluorometric analysis (Fig. S8B).

Preparation of empty p(HPMAm)-b-p(HPMAm-Bz) micelles

Polymeric micelles based on the different p(HPMAm)-b-p(HPMAm-Bz) copolymers (entries 5–13 in Table 1) were prepared by rapid addition of DMF solution containing the block copolymer to the same volume of water under stirring and followed by dialysis. ^{1}H NMR analysis showed that the residual DMF concentration was < 150 ppm, which is below the 880 ppm limit according to International Community of Harmonization (ICH) guideline for residual solvents for human use [73]. The copolymers with molecular weights ranging from 8 to 24 kDa resulted in the formation of micelles with tailored sizes from 40 to 90 nm (PDI < 0.12). As shown in Fig. 3A, for block copolymers with a fixed molecular weight of the hydrophilic p(HPMAm) block (3.0, 4.9 and 7.1 kDa), the size of the micelles increased with

increasing molecular weight of hydrophobic block. This is in agreement with previous findings reported by our group, where the micelle size and aggregation number (N_{agg}) decreased with decreasing molecular weight of the hydrophobic block of the block copolymer mPEG-b-p(HPMAm-Bz) [74]. Further, the size of empty p(HPMAm)$_{7.1k}$-b-p(HPMAm-Bz)$_{15.0k}$ micelles (with or without biotin decoration) in PBS (pH 7.4) did not change upon incubation for 48 h at 37 °C (63 ± 5 and 62 ± 3 nm for biotinylated and nonbiotinylated micelles), which demonstrates good colloidal stability.
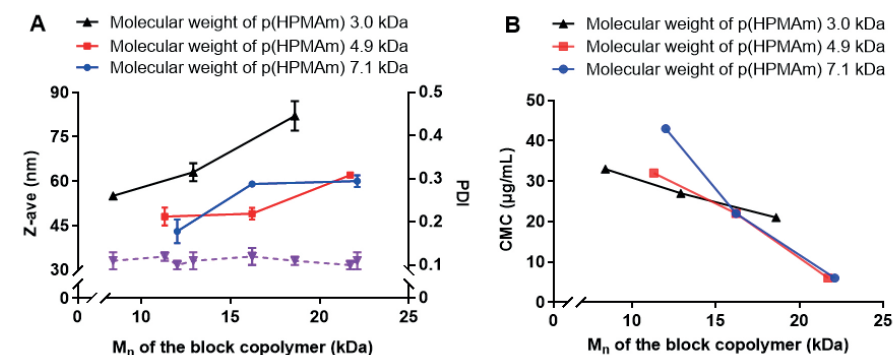

Fig. 3. (**A**) Effect of the molecular weight of the p(HPMAm)-b-p(HPMAm-Bz) block copolymers on the Z-average size (black, red, and blue line) and PDI (purple line) of the formed micelles. Data represent mean ± SD (n = 3). (**B**) Critical micelle concentration as a function of p(HPMAm)-b-p(HPMAm-Bz) polymer molecular weight.

CMC of p(HPMAm)-b-p(HPMAm-Bz)

The critical micelle concentration (CMC) of the micelles based on the library of p(HPMAm)-b-p(HPMAm-Bz) block copolymers (entries 5–13 in Table 1) was determined using pyrene as a hydrophobic fluorescence probe. In the excitation spectra of pyrene, a red shift occurs as a result of pyrene partitioning from water to the hydrophobic core of polymeric micelles [75,76]. When p(HPMAm)-b-p(HPMAm-Bz) concentrations were below the CMC, a maximum peak of pyrene was observed at 333 nm, whereas this peak shifted to 338 nm when the polymer concentrations were above CMC (Fig. S9A). The I_{338}/I_{333} fluorescence ratio can thus be used to determine the CMC of polymeric micelles (Fig. S9B). The CMCs of p(HPMAm)$_{7.1k}$-b-p(HPMAm-Bz)$_{15.0k}$, p(HPMAm)$_{7.1k}$-b-p(HPMAm-Bz)$_{9.1k}$ and p(HPMAm)$_{7.1k}$-b-p(HPMAm-Bz)$_{4.9k}$ were 6, 22 and 43 µg/mL, respectively (Table 1). It is clear that for block copolymers with a fixed molecular weight of the hydrophilic block (7.1 kDa), the CMCs of the polymers decreased with increasing hydrophobic/hydrophilic ratio and thus with increasing molecular weight of the hydrophobic block. The same trend was also observed for the block polymers with fixed hydrophilic block of p(HPMAm)$_{3.0k}$

and p(HPMAm)$_{4.9k}$ (Table 1 and Fig. 3B), which is in line with previous publications [6,74,76–79].

PTX loading capacity

PTX is an antineoplastic drug and used in the treatment of various cancers [80], which is very hydrophobic and its aqueous solubility is ≤3.5 µg/mL [81,82]. By loading this drug in p(HPMAm)$_{7.1k}$-b-p(HPMAm-Bz)$_{15.0k}$ micelles, its solubility increased to 0.5 mg/mL (Table S2). As shown in Fig. 4A, the loading capacity of p(HPMAm)$_{7.1k}$-b-p(HPMAm-Bz)$_{15.0k}$ micelles increased from 1 to 9 wt.% when increasing PTX feed from 1 to 15 wt.%. The loading capacity did not further increase at a 20 wt.% feed of PTX, which can be attributed to the effect of the preparation methods and the solvent used in this method [77]. Our results are in accordance with previous reports showing that the introduction of benzoyl group in these micelles yielded good incorporation of hydrophobic molecules due to the π–π stacking interaction between the aromatic groups of PTX and benzoyl groups of the polymer [43,49,83]. The PTX-loaded p(HPMAm)$_{7.1k}$-b-p(HPMAm-Bz)$_{15.0k}$ micelles, dependent on the PTX content, had a slightly larger size than that of empty micelles, ranging from 61 to 70 nm with a PDI < 0.12 (Fig. 4B).
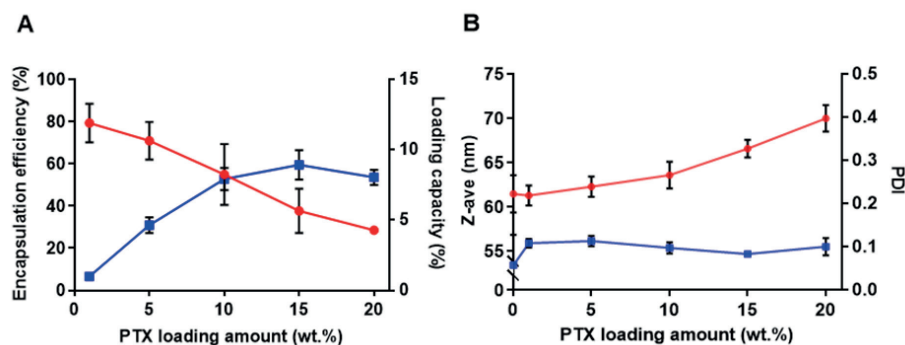

Fig. 4. (**A**) Encapsulation efficiency (red line) and loading capacity (blue line) of p(HPMAm)$_{7.1k}$-b-p(HPMAm-Bz)$_{15.0k}$ micelles at different PTX feeds. Data represent mean ± SD (n = 3). (**B**) The effect of PTX feed on the Z-average size (red line) and PDI (blue line) of p(HPMAm)$_{7.1k}$-b-p(HPMAm-Bz)$_{15.0k}$ micelles. Data represent mean ± SD (n = 3).

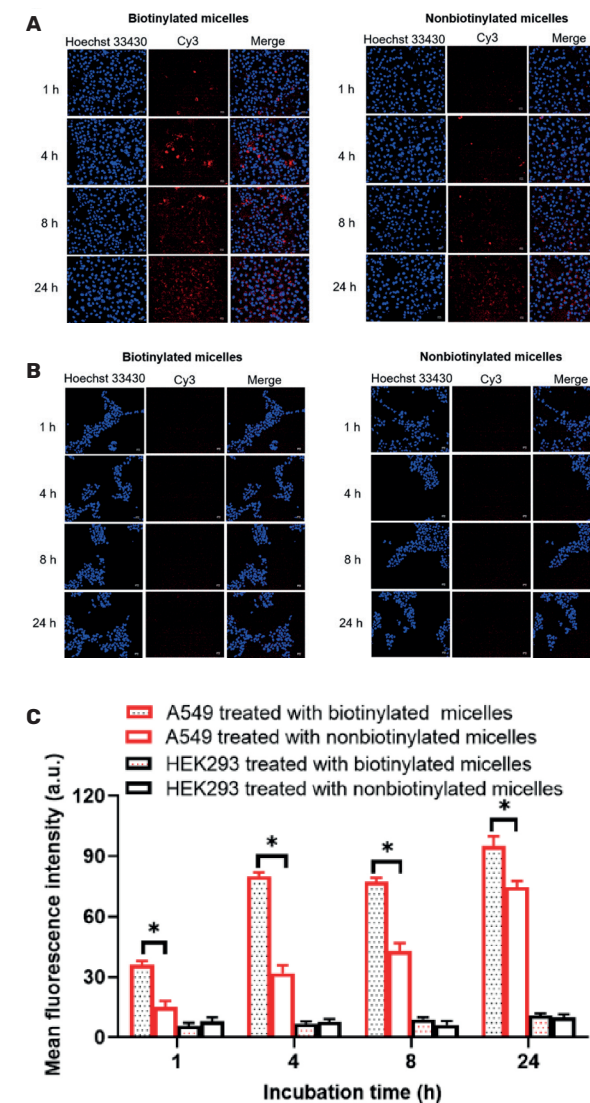## Cellular uptake of Cy3-labeled p(HPMAm)-b-p(HPMAm-Bz) micelles

Fig. 5. Internalization of the fluorescently labeled targeted and non-targeted p(HPMAm)-b-p(HPMAm-Bz) micelles. Laser confocal scanning microscopy images of A549 cells (**A**) and HEK293 cells (**B**) after incubation with Cy3-labeled p(HPMAm)-b-p(HPMAm-Bz) micelles with or without biotin decoration (140 µg/mL) for 1, 4, 8, and 24 h. Cell nuclei are stained with Hoechst 33430 in blue while the micelles are visualized in red by Cy3. (**C**) The corresponding mean fluorescence intensity calculated from the confocal images. Scale bar = 50 µm, data represent mean ± SD (n = 5 imaging fields), * p < 0.05.

Previous studies have shown that 10-20 mol% ligand (i.e., biotin and folate) density on the surface of polymeric nanoparticles was optimal for efficient cellular uptake [84,85]. We therefore fixed the biotin density at 10 mol% at the surface of the micelles. A549 (biotin receptor-positive) and HEK293 (biotin receptor-negative) cells were incubated with Cy3-labeled p(HPMAm)-b-p(HPMAm-Bz) micelles with or without biotin decoration for 1, 4, 8, and 24 h and stained with Hoechst 33430 before imaging. In non-cancerous HEK293 cells which do not express the biotin receptor, very low internalization of both biotinylated and nonbiotinylated micelles was observed (Fig. 5B & C). However, it is clear that the fluorescence intensity of biotinylated p(HPMAm)-b-p(HPMAm-Bz) micelles was significantly higher as compared to the nonbiotinylated micelles in biotin receptor–expressing A549 cells (Fig. 5A & C), confirming the enhanced internalization of biotinylated p(HPMAm)-b-p(HPMAm-Bz) micelles. Besides, the uptake of p(HPMAm)-b-p(HPMAm-Bz) micelles in these cells was time-dependent. In the presence of free biotin, biotinylated micelles showed significantly lower uptake by A549 cells whereas the uptake of nonbiotinylated micelles was not affected (Fig. S10). These observations validate that the biotinylated micelles are taken up via biotin/SMVT receptor-mediated endocytosis.

Cytotoxicity of empty and PTX-loaded p(HPMAm)-b-p(HPMAm-Bz) micelles

A549 and HEK293 cell lines were used to assess the cytocompatibility of formed micellar formulations with or without biotin modification and to determine the cytotoxicity of PTX-loaded micelles as compared to Taxol formulations. The results indicate that empty p(HPMAm)$_{7.1k}$-b-p(HPMAm-Bz)$_{15.0k}$ micelles with or without biotin modification were non-toxic at the polymer concentrations up to 1.7 mg/mL as compared to Cremophor EL/ethanol solution which showed substantial cytotoxicity above a concentration of 1.7 μg/mL (Fig. 6A & B). PTX-loaded micelles with or without biotin decoration exhibited comparable cytotoxicity for both cell lines at low PTX concentrations (up to 0.1 μg/mL) (Fig. 6C & D). This can be explained by the fact that the polymer concentration was below its CMC and thus PTX was present in its free form. At higher PTX concentrations (> 0.1 μg/mL), Taxol showed higher cytotoxicity than PTX–loaded polymeric micelles formulations due to high toxicity of Cremophor EL/ethanol mixture. Fig. 6D shows that at PTX concentration > 1 μg/mL, the cytotoxicity did not show significant difference between PTX-loaded micelles with or without biotinylation in HEK293 cells lacking the biotin receptor (p > 0.05). However, at PTX concentrations of 10 and 100 μg/mL, the biotinylated micelles were significantly more cytotoxic than PTX-loaded micelles without biotin modification in A549 cells which overexpress the biotin receptor (p < 0.05) (Fig. 6C). At PTX concentrations of 1–100 μg/mL, the polymer concentration was above CMC and therefore the significant killing enhancement of the formulation is likely caused

by the released PTX after internalization of the micelles. IC$_{50}$ values as determined using the MTS assay are summarized in Table 2, suggesting that the expression of the biotin receptor on the surface of A549 lung cancer cells induced receptor-mediated endocytosis of biotinylated micelles as compared to HEK293 cells that do not express the biotin receptor, and subsequently PTX was released from the polymeric micelles internalized by A549 cells resulting in cell killing.
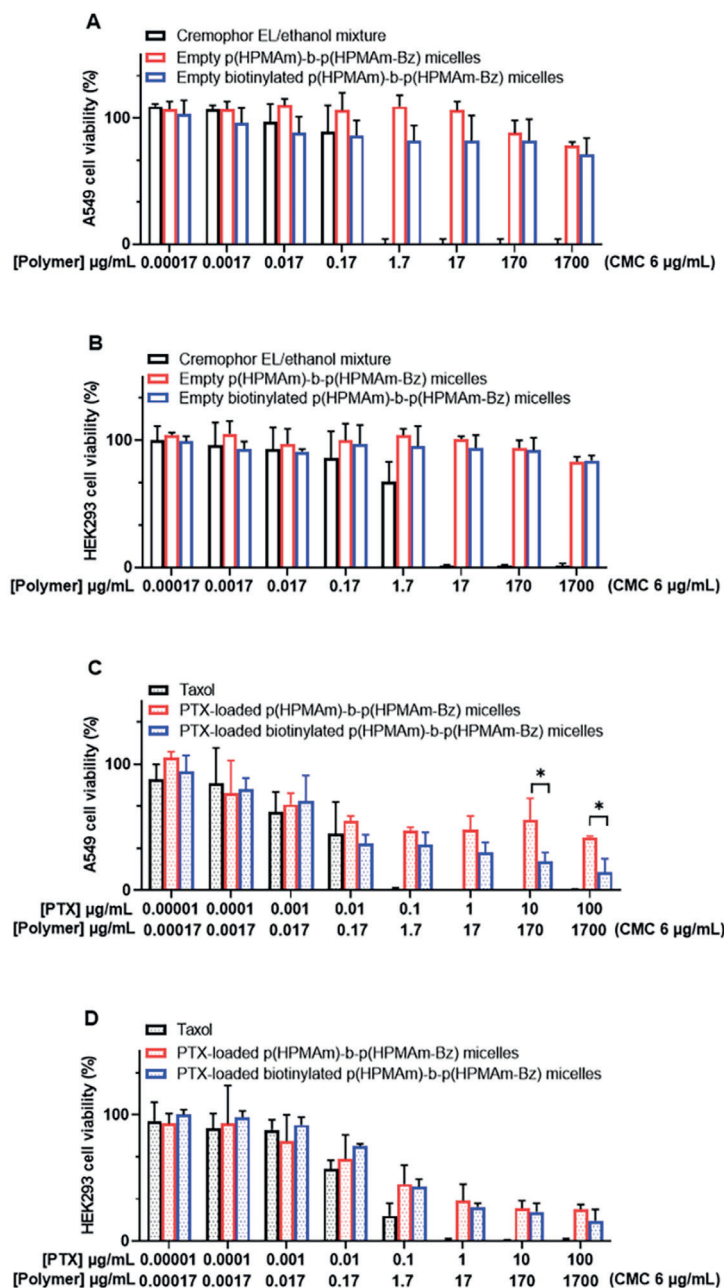
Fig. 6. Cytotoxicity of the targeted and non-targeted p(HPMAm)-b-p(HPMAm-Bz) micelles. Cell viability of A549 (**A**) and HEK293 cells (**B**) exposed to Cremophor EL/ethanol mixture and p(HPMAm)-b-p(HPMAm-Bz) micelles with or without biotin decoration. Cell viability of A549 (**C**) and HEK293 cells (**D**) exposed to Taxol and PTX-loaded p(HPMAm)-b-p(HPMAm-Bz) micelles with or without biotin decoration. Data represent mean ± SD (n = 3), * p < 0.05.

Table 2. IC$_{50}$ values in A549 and HEK293 cells after 48 h-treatment by PTX formulations.

| Cell line | IC$_{50}$ (μg/mL)[a] | | |
	Taxol	PTX-loaded micelles without biotin decoration	PTX-loaded micelles with biotin decoration
A549	0.003 ± 0.001	1.5 ± 0.3	0.021 ± 0.002
HEK293	0.013 ± 0.008	0.13 ± 0.06	0.142 ± 0.015

[a] Data represent mean ± SD (n = 3).

Conclusion

In the present study, well-controlled block copolymers p(HPMAm)-b-(pHPMAm-Bz) with and without biotin functionalization were successfully synthesized by RAFT polymerization and in aqueous solution they self-assembled into polymeric micelles with tailored size above their critical micelle concentrations. The biotin-decorated micelles were more efficiently internalized and exerted more potent cytotoxicity than non-targeted micelles in target cells, which was mediated by biotin receptor expressed on the surface of the target cells. These results provide evidence that the biotinylated polymeric micelles fully based on a poly(HPMAm) backbone are promising candidates for targeted therapy of biotin receptor-overexpressing cancers.

Acknowledgements

References

[1] C. Deng, Y. Jiang, R. Cheng, F. Meng, Z. Zhong, Biodegradable polymeric micelles for targeted and controlled anticancer drug delivery: promises, progress and prospects, Nano Today. 7 (2012) 467–480.

[2] H. Cabral, K. Kataoka, Progress of drug-loaded polymeric micelles into clinical studies, Journal of Controlled Release. 190 (2014) 465–476.

[3] A. Varela-Moreira, Y. Shi, M.H.A.M. Fens, T. Lammers, W.E. Hennink, R.M. Schiffelers, Clinical application of polymeric micelles for the treatment of cancer, Mater Chem Front. 1 (2017) 1485–1501.

[4] C. Allen, Why I'm holding onto hope for nano in oncology, Mol Pharm. 13 (2016) 2603–2604.

[5] G. Gaucher, R.H. Marchessault, J.C. Leroux, Polyester-based micelles and nanoparticles for the parenteral delivery of taxanes, Journal of Controlled Release. 143 (2010) 2–12.

[6] N. Kang, J.C. Leroux, Triblock and star-block copolymers of N-(2-hydroxypropyl)methacrylamide or N-vinyl-2-pyrrolidone and d,l-lactide: Synthesis and self-assembling properties in water, Polymer (Guildf). 45 (2004) 8967–8980.

[7] O. Soga, C.F. van Nostrum, A. Ramzi, T. Visser, F. Soulimani, P.M. Frederik, P.H.H. Bomans, W.E. Hennink, Physicochemical characterization of degradable thermosensitive polymeric micelles, Langmuir. 20 (2004) 9388–9395.

[8] H. Cabral, K. Miyata, K. Osada, K. Kataoka, Block copolymer micelles in nanomedicine applications, Chem Rev. 118 (2018) 6844–6892.

[9] Y. Shi, T. Lammers, G. Storm, W.E. Hennink, Physico-chemical strategies to enhance stability and drug retention of polymeric micelles for tumor-targeted drug delivery, Macromol Biosci. 17 (2017) 1600160.

[10] H. Maeda, H. Nakamura, J. Fang, The EPR effect for macromolecular drug delivery to solid tumors: improvement of tumor uptake, lowering of systemic toxicity, and distinct tumor imaging in vivo, Adv Drug Deliv Rev. 65 (2013) 71–79.

[11] H. Maeda, J. Wu, T. Sawa, Y. Matsumura, K. Hori, Tumor vascular permeability and the EPR effect in macromolecular therapeutics: a review, Journal of Controlled Release. 65 (2000) 271–284.

[12] V. Torchilin, Tumor delivery of macromolecular drugs based on the EPR effect, Adv Drug Deliv Rev. 63 (2011) 131–135.

[13] A. Alibakhshi, F. Abarghooi Kahaki, S. Ahangarzadeh, H. Yaghoobi, F. Yarian, R. Arezumand, J. Ranjbari, A. Mokhtarzadeh, M. de la Guardia, Targeted cancer therapy through antibody fragments-decorated nanomedicines, Journal of Controlled Release. 268 (2017) 323–334.

[14] P. Mi, H. Cabral, K. Kataoka, Ligand-Installed Nanocarriers toward Precision Therapy, Advanced Materials. 32 (2020) 1902604.

[15] V.J. Yao, S. D'Angelo, K.S. Butler, C. Theron, T.L. Smith, S. Marchiò, J.G. Gelovani, R.L. Sidman, A.S. Dobroff, C.J. Brinker, A.R.M. Bradbury, W. Arap, R. Pasqualini, Ligand-targeted theranostic nanomedicines against cancer, Journal of Controlled Release. 240 (2016) 267–286.

[16] J. Li, F. Wang, D. Sun, R. Wang, A review of the ligands and related targeting strategies for active targeting of paclitaxel to tumours, J Drug Target. 24 (2016) 590–602.

[17] Y. Lu, P.S. Low, Folate-mediated delivery of macromolecular anticancer therapeutic agents, Adv Drug Deliv Rev. 54 (2002) 675–693.

[18] R. van der Meel, L.J.C. Vehmeijer, R.J. Kok, G. Storm, E.V.B. van Gaal, Ligand-targeted particulate nanomedicines undergoing clinical evaluation: Current status, Adv Drug Deliv Rev. 65 (2013) 1284–1298.

[19] W. Alshaer, H. Hillaireau, E. Fattal, Aptamer-guided nanomedicines for anticancer drug delivery, Adv Drug Deliv Rev. 134 (2018) 122–137.

[20] W.X. Ren, J. Han, S. Uhm, Y.J. Jang, C. Kang, J.S.H. Kim, J.S.H. Kim, Recent development of biotin conjugation in biological imaging, sensing, and target delivery, Chemical Communications. 51 (2015) 10403–10418.

[21] S. Chen, X. Zhao, J. Chen, J. Chen, L. Kuznetsova, S.S. Wong, I. Ojima, Mechanism-based tumor-targeting drug delivery system. validation of efficient vitamin receptor-mediated endocytosis and drug release, Bioconjug Chem. 21 (2010) 979–987.

[22] S.W. Polyak, Mechanisms of biotin transport, Biochemistry & Analytical Biochemistry. 4 (2015) 1–8.

[23] G. Russell-Jones, K. McTavish, J. McEwan, J. Rice, D. Nowotnik, Vitamin-mediated targeting as a potential mechanism to increase drug uptake by tumours, J Inorg Biochem. 98 (2004) 1625–1633.

[24] G. Russell-Jones, J. Mcewan, Amplification of biotin-mediated targeting, US patent 2006/0127310 A1, application no. 10/535, 269, Access Pharmaceuticals Australia PTY LTD., USA, 2006.

[25] N.U. Deshpande, M. Jayakannan, Biotin-tagged polysaccharide vesicular nanocarriers for receptor-mediated anticancer drug delivery in cancer cells, Biomacromolecules. 19 (2018) 3572–3585.

[26] H. Nosrati, P. Barzegari, H. Danafar, H. Kheiri, F. Group, Biotin-functionalized copolymeric PEG-PCL micelles for in vivo tumour-targeted delivery of artemisinin, Artif Cells Nanomed Biotechnol. 47 (2019) 104–114.

[27] C.Y. Deng, Y.Y. Long, S. Liu, Z.B. Chen, C. Li, Construction of biotin-modified polymeric micelles for pancreatic cancer targeted photodynamic therapy, Yaoxue Xuebao. 50 (2015) 1038–1044.

[28] E.Y. Hanurry, T.W. Mekonnen, A.T. Andrgie, H.F. Darge, Y.S. Birhan, W.-H. Hsu, H.-Y. Chou, C.-C. Cheng, J.-Y. Lai, H.-C. Tsai, Biotin-decorated PAMAM G4.5 dendrimer nanoparticles to enhance the delivery, anti-proliferative, and apoptotic effects of chemotherapeutic drug in cancer cells, Pharmaceutics. 12 (2020) 443.

[29] Y. Jin, Z. Wu, C. Wu, Y. Zi, X. Chu, J. Liu, W. Zhang, Size-adaptable and ligand (biotin)-sheddable nanocarriers equipped with avidin scavenging technology for deep tumor penetration and reduced toxicity, Journal of Controlled Release. 320 (2020) 142–158.

[30] S. Maiti, P. Paira, Biotin conjugated organic molecules and proteins for cancer therapy: A review, Eur J Med Chem. 145 (2018) 206–223.

[31] R. Narain, M. Gonzales, A.S. Hoffman, P.S. Stayton, K.M. Krishnan, Synthesis of monodisperse biotinylated p(NIPAAm)-coated iron oxide magnetic nanoparticles and their bioconjugation to streptavidin, Langmuir. 23 (2007) 6299–6304.

[32] A. Aqil, H. Qiu, J.F. Greisch, R. Jérôme, E. de Pauw, C. Jérôme, Coating of gold nanoparticles by thermosensitive poly(N-isopropylacrylamide) end-capped by biotin, Polymer (Guildf). 49 (2008) 1145–1153.

[33] C.Y. Hong, C.Y. Pan, Direct synthesis of biotinylated stimuli-responsive polymer and diblock copolymer by RAFT polymerization using biotinylated trithiocarbonate as RAFT agent, Macromolecules. 39 (2006) 3517–3524.

[34] A. Doerflinger, N.N. Quang, E. Gravel, G. Pinna, M. Vandamme, F. Ducongé, E. Doris, Biotin-functionalized targeted polydiacetylene micelles, Chemical Communications. 54 (2018) 3613–3616.

[35] W. Lv, L. Liu, Y. Luo, X. Wang, Y. Liu, Biotinylated thermoresponsive core cross-linked nanoparticles via RAFT polymerization and "click" chemistry, J Colloid Interface Sci. 356 (2011) 16–23.

[36] K. Knop, R. Hoogenboom, D. Fischer, U.S. Schubert, Poly(ethylene glycol) in drug delivery: pros and cons as well as potential alternatives, Angewandte Chemie International Edition. 49 (2010) 6288–6308.

[37] I. Alberg, S. Kramer, M. Schinnerer, Q. Hu, C. Seidl, C. Leps, N. Drude, D. Möckel, C. Rijcken, T. Lammers, M. Diken, M. Maskos, S. Morsbach, K. Landfester, S. Tenzer, M. Barz, R. Zentel, Polymeric Nanoparticles with Neglectable Protein Corona, Small. 16 (2020) 1907574.

[38] L. Houdaihed, J.C. Evans, C. Allen, Overcoming the road blocks: advancement of block copolymer micelles for cancer therapy in the clinic, Mol Pharm. 14 (2017) 2503–2517.

[39] Z.R. Lu, P. Qiao, Drug delivery in cancer therapy, Quo vadis?, Mol Pharm. 15 (2018) 3603–3616.

[40] E.T.M. Dams, P. Laverman, W.J.G. Oyen, G. Storm, G.L. Scherphof, J.W.M. van der Meer, F.H.M. Corstens, O.C. Boerman, Accelerated blood clearance and altered biodistribution of repeated injections of sterically stabilized liposomes, Journal of Pharmacology and Experimental Therapeutics. 292 (2000) 1071–1079.

[41] A.S. Abu Lila, H. Kiwada, T. Ishida, The accelerated blood clearance (ABC) phenomenon: clinical challenge and approaches to manage, Journal of Controlled Release. 172 (2013) 38–47.

[42] M. Talelli, C.J.F. Rijcken, C.F. van Nostrum, G. Storm, W.E. Hennink, Micelles based on HPMA copolymers, Adv Drug Deliv Rev. 62 (2010) 231–239.

[43] Y. Shi, M.J. van Steenbergen, E.A. Teunissen, L. Novo, S. Gradmann, M. Baldus, C.F. van Nostrum, W.E. Hennink, Π-Π Stacking increases the stability and loading capacity of thermosensitive polymeric micelles for chemotherapeutic drugs, Biomacromolecules. 14 (2013) 1826–1837.

[44] T. Minko, P. Kopečková, V. Pozharov, J. Kopeček, HPMA copolymer bound adriamycin overcomes MDR1 gene encoded resistance in a human ovarian carcinoma cell line, Journal of Controlled Release. 54 (1998) 223–233.

[45] J. Yang, J. Kopeček, Design of smart HPMA copolymer-based nanomedicines, Journal of Controlled Release. 240 (2016) 9–23.

[46] J. Kopeček, P. Kopečková, HPMA copolymers: origins, early developments, present, and future, Adv Drug Deliv Rev. 62 (2010) 122–149.

[47] J. Yang, J. Kopeček, The light at the end of the tunnel—second generation HPMA conjugates for cancer treatment, Curr Opin Colloid Interface Sci. 31 (2017) 30–42.

[48] P.H. Kierstead, H. Okochi, V.J. Venditto, T.C. Chuong, S. Kivimae, J.M.J. Fréchet, F.C. Szoka, The effect of polymer backbone chemistry on the induction of the accelerated blood clearance in polymer modified liposomes, Journal of Controlled Release. 213 (2015) 1–9.

[49] Y. Shi, R. van der Meel, B. Theek, E. Oude Blenke, E.H.E. Pieters, M.H.A.M. Fens, J. Ehling, R.M. Schiffelers, G. Storm, C.F. van Nostrum, T. Lammers, W.E. Hennink, Complete regression of xenograft tumors upon targeted delivery of paclitaxel via Π-Π stacking stabilized polymeric micelles, ACS Nano. 9 (2015) 3740–3752.

[50] D. Oupický, Č. Koňák, K. Ulbrich, DNA complexes with block and graft copolymers of N-(2-hydroxypropyl)methacrylamide and 2-(trimethylammonio)ethyl methacrylate, J Biomater Sci Polym Ed. 10 (1999) 573–590.

[51] J. Buller, A. Laschewsky, J.F. Lutz, E. Wischerhoff, Tuning the lower critical solution temperature of thermoresponsive polymers by biospecific recognition, Polym Chem. 2 (2011) 1486–1489.

[52] D. Tong, J. Yao, H. Li, S. Han, Synthesis and characterization of thermo- and pH-sensitive block copolymers bearing a biotin group at the poly(ethylene oxide) chain end, J Appl Polym Sci. 102 (2006) 3552–3558.

[53] G. Miglietta, S. Cogoi, J. Marinello, G. Capranico, A.S. Tikhomirov, A. Shchekotikhin, L.E. Xodo, RNA G-quadruplexes in kirsten ras (KRAS) oncogene as targets for small molecules inhibiting translation, J Med Chem. 60 (2017) 9448–9461.

[54] J. Brglez, I. Ahmed, C.M. Niemeyer, Photocleavable ligands for protein decoration of DNA nanostructures, Org Biomol Chem. 13 (2015) 5102–5104.

2

[55] O.O. Oyeneye, W.Z. Xu, P.A. Charpentier, Adhesive RAFT agents for controlled polymerization of acrylamide: Effect of catechol-end R groups, RSC Adv. 5 (2015) 76919–76926.

[56] D.S.W. Benoit, S. Srinivasan, A.D. Shubin, P.S. Stayton, Synthesis of folate-functionalized RAFT polymers for targeted siRNA delivery, Biomacromolecules. 12 (2011) 2708–2714.

[57] Y. Shi, E.T.A. van den Dungen, B. Klumperman, C.F. van Nostrum, W.E. Hennink, Reversible addition-fragmentation chain transfer synthesis of a micelle-forming, structure reversible thermosensitive diblock copolymer based on the N-(2-hydroxy propyl) methacrylamide backbone, ACS Macro Lett. 2 (2013) 403–408.

[58] M. Najafi, N. Kordalivand, M.A. Moradi, J. van den Dikkenberg, R. Fokkink, H. Friedrich, N.A.J.M. Sommerdijk, M. Hembury, T. Vermonden, Native chemical ligation for cross-linking of flower-like micelles, Biomacromolecules. 19 (2018) 3766–3775.

[59] A. Swami, M.R. Reagan, P. Basto, Y. Mishima, N. Kamaly, S. Glavey, S. Zhang, M. Moschetta, D. Seevaratnam, Y. Zhang, J. Liu, M. Memarzadeh, J. Wu, S. Manier, J. Shi, N. Bertrand, Z.N. Lu, K. Nagano, R. Baron, A. Sacco, A.M. Roccaro, O.C. Farokhzad, I.M. Ghobrial, Engineered nanomedicine for myeloma and bone microenvironment targeting, Proc Natl Acad Sci U S A. 111 (2014) 10287–10292.

[60] O. Naksuriya, Y. Shi, C.F. van Nostrum, S. Anuchapreeda, W.E. Hennink, S. Okonogi, HPMA-based polymeric micelles for curcumin solubilization and inhibition of cancer cell growth, European Journal of Pharmaceutics and Biopharmaceutics. 94 (2015) 501–512.

[61] C. Cheng, H. Wei, J.L. Zhu, C. Chang, H. Cheng, C. Li, S.X. Cheng, X.Z. Zhang, R.X. Zhuo, Functionalized thermoresponsive micelles self-assembled from biotin-PEG-b-P(NIPAAm-co-HMAAm)-b-PMMA for tumor cell target, Bioconjug Chem. 19 (2008) 1194–1201.

[62] J.A. Barltrop, T.C. Owen, A.H. Cory, J.G. Cory, 5-(3-carboxymethoxyphenyl)-2-(4,5-dimethylthiazolyl)-3-(4-sulfophenyl)te trazolium, inner salt (MTS) and related analogs of 3-(4,5-dimethylthiazolyl)-2,5-diphenyltetrazolium bromide (MTT) reducing to purple water-soluble formazans as cell-viability indica, Bioorg Med Chem Lett. 1 (1991) 611–614.

[63] X. Pan, F. Zhang, B. Choi, Y. Luo, X. Guo, A. Feng, S.H. Thang, Effect of solvents on the RAFT polymerization of N-(2-hydroxypropyl) methacrylamide, Eur Polym J. 115 (2019) 166–172.

[64] B.A. Abel, C.L. McCormick, Mechanistic insights into temperature-dependent trithiocarbonate chain-end degradation during the RAFT polymerization of N-arylmethacrylamides, Macromolecules. 49 (2016) 465–474.

[65] M. Danial, S. Telwatte, D. Tyssen, A. Postma, S. Cosson, G. Tachedjian, G. Moad, A. Postma, Combination anti-HIV therapy: via tandem release of prodrugs from macromolecular carriers, Polym Chem. 7 (2016) 7477–7487.

[66] W.A. Braunecker, K. Matyjaszewski, Controlled/living radical polymerization: Features, developments, and perspectives, Prog Polym Sci. 32 (2007) 93–146.

[67] S. Eetezadi, S.N. Ekdawi, C. Allen, The challenges facing block copolymer micelles for cancer therapy: In vivo barriers and clinical translation, Adv Drug Deliv Rev. 91 (2015) 7–22.

[68] Z. Amoozgar, Y. Yeo, Recent advances in stealth coating of nanoparticle drug delivery systems, Wiley Interdiscip Rev Nanomed Nanobiotechnol. 4 (2012) 219–233.

[69] K. Hirota, E. Czogala, W. Pedrycz, Stealth liposomes: review of the basic science, rationale, and clinical applications, existing and potential, Int J Nanomedicine. 1 (2016) 297–315.

[70] S. Salmaso, P. Caliceti, Stealth properties to improve therapeutic efficacy of drug nanocarriers, J Drug Deliv. 2013 (2013) 374252.

[71] LW. Seymour, R. Duncan, J. Strohalm, J. Kopeček, Effect of molecular weight (Mw) of N-(2-hydroxypropyl)methacrylamide copolymers on body distribution and rate of excretion after subcutaneous, intraperitoneal, and intravenous administration to rats, J Biomed Mater Res. 21 (1987) 1341–1358.

[72] C. Barner-Kowollik, Handbook of RAFT polymerization, in: M.H. Stenzel (Ed.), Complex Architecture Design via the RAFT Process: Scope, Strengths and Limitations, Wiley, Sydney, 2008: pp. 315–372.

[73] International Community of Harmonization (ICH), Impurities: guideline for residual solvents Q3C (R6), International Conference on Harmonization of Technical Requirements for Registration of Pharmaceuticals for Human Use. 44 (2011) 1–29.

[74] M. Bagheri, J. Bresseleers, A. Varela Moreira, O. Sandre, S.A. Meeuwissen, R.M. Schiffelers, J.M. Metselaar, C.F. van Nostrum, J.C.M. van Hest, W.E. Hennink, The effect of formulation and processing parameters on the size of mPEG-b-p(HPMA-Bz) polymeric micelles, Langmuir. 34 (2018) 15495–15506.

[75] C. le Zhao, M.A. Winnik, G. Riess, M.D. Croucher, Fluorescence probe techniques used to study micelle formation in water-soluble block copolymers, Langmuir. 6 (1990) 514–516.

[76] C. Kim, S.C. Lee, J.H. Shin, J.S. Yoon, I.C. Kwon, S.Y. Jeong, Amphiphilic diblock copolymers based on poly(2-ethyl-2-oxazoline) and poly(1,3-trimethylene carbonate): Synthesis and micellar characteristics, Macromolecules. 33 (2000) 7448–7452.

[77] Y. Hussein, M. Youssry, Polymeric micelles of biodegradable diblock copolymers: enhanced encapsulation of hydrophobic drugs, Materials. 11 (2018) 688.

[78] K. Letchford, R. Liggins, H. Burt, Solubilization of hydrophobic drugs by methoxy poly(ethylene glycol)-block-polycaprolactone diblock copolymer micelles: Theoretical and experimental data and correlations, J Pharm Sci. 9 (2008) 1179–1190.

[79]   K. Letchford, J. Zastre, R. Liggins, H. Burt, Synthesis and micellar characterization of short block length methoxy poly(ethylene glycol)-block-poly(caprolactone) diblock copolymers, Colloids Surf B Biointerfaces. 35 (2004) 81–91.

[80]   A.M. Barbuti, Z.S. Chen, Paclitaxel through the ages of anticancer therapy: Exploring its role in chemoresistance and radiation therapy, Cancers (Basel). 7 (2015) 2360–2371.

[81]   T. Konno, J. Watanabe, K. Ishihara, Enhanced solubility of paclitaxel using water-soluble and biocompatible 2-methacryloyloxyethyl phosphorylcholine polymers, J Biomed Mater Res A. 65 (2003) 209–214.

[82]   R.T. Liggins, W.L. Hunter, H.M. Burt, Solid-state characterization of paclitaxel, J Pharm Sci. 86 (1997) 1458–1463.

[83]   M. Sheybanifard, N. Beztsinna, M. Bagheri, E.M. Buhl, J. Bresseleers, A. Varela-Moreira, Y. Shi, C.F. van Nostrum, G. van der Pluijm, G. Storm, W.E. Hennink, T. Lammers, J.M. Metselaar, Systematic evaluation of design features enables efficient selection of Π electron-stabilized polymeric micelles, Int J Pharm. 584 (2020) 119409.

[84]   N. MacKiewicz, J. Nicolas, N. Handké, M. Noiray, J. Mougin, C. Daveu, H.R. Lakkireddy, D. Bazile, P. Couvreur, Precise engineering of multifunctional PEGylated polyester nanoparticles for cancer cell targeting and imaging, Chemistry of Materials. 26 (2014) 1834–1847.

[85]   Y.C. Gong, X.Y. Xiong, X.J. Ge, Z.L. Li, Y.P. Li, Effect of the folate ligand density on the targeting property of folated-conjugated polymeric nanoparticles, Macromol Biosci. 19 (2019) 1800348.

Supplementary information
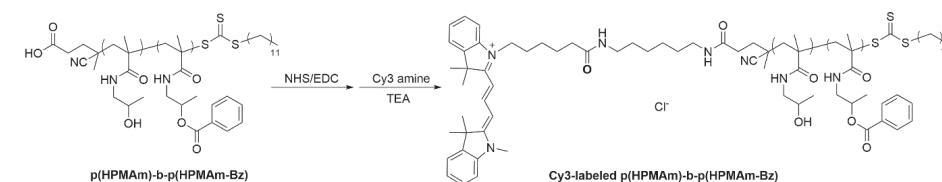
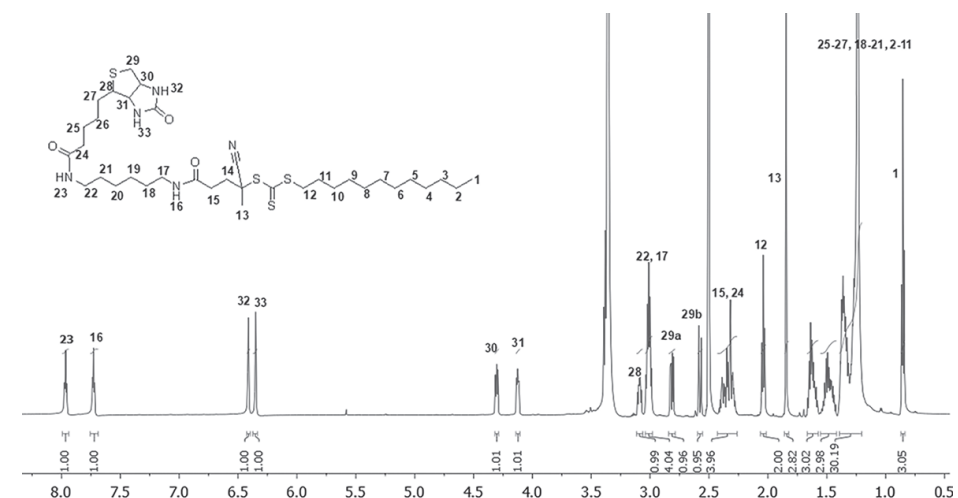**Scheme S1.** Synthesis of Cy3-labeled p(HPMAm)-b-p(HPMAm-Bz) block copolymer [1,2].

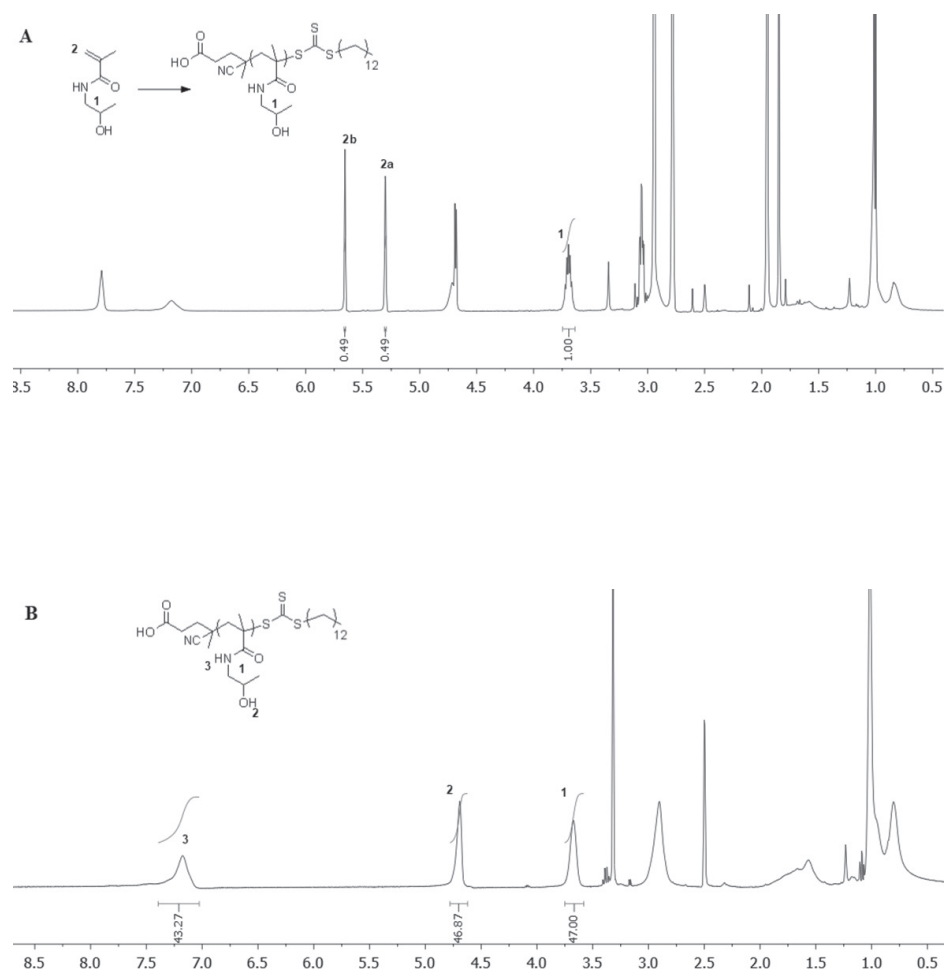**Fig. S1.** ^{1}H NMR spectrum of biotin-CDTPA.

Fig. S2. ¹H NMR spectra of the reaction mixture of HPMAm/CTA at 6 hours (**A**) and isolated p(HPMAm)₇.₁ₖ (entry 3 in Table 1) (**B**).

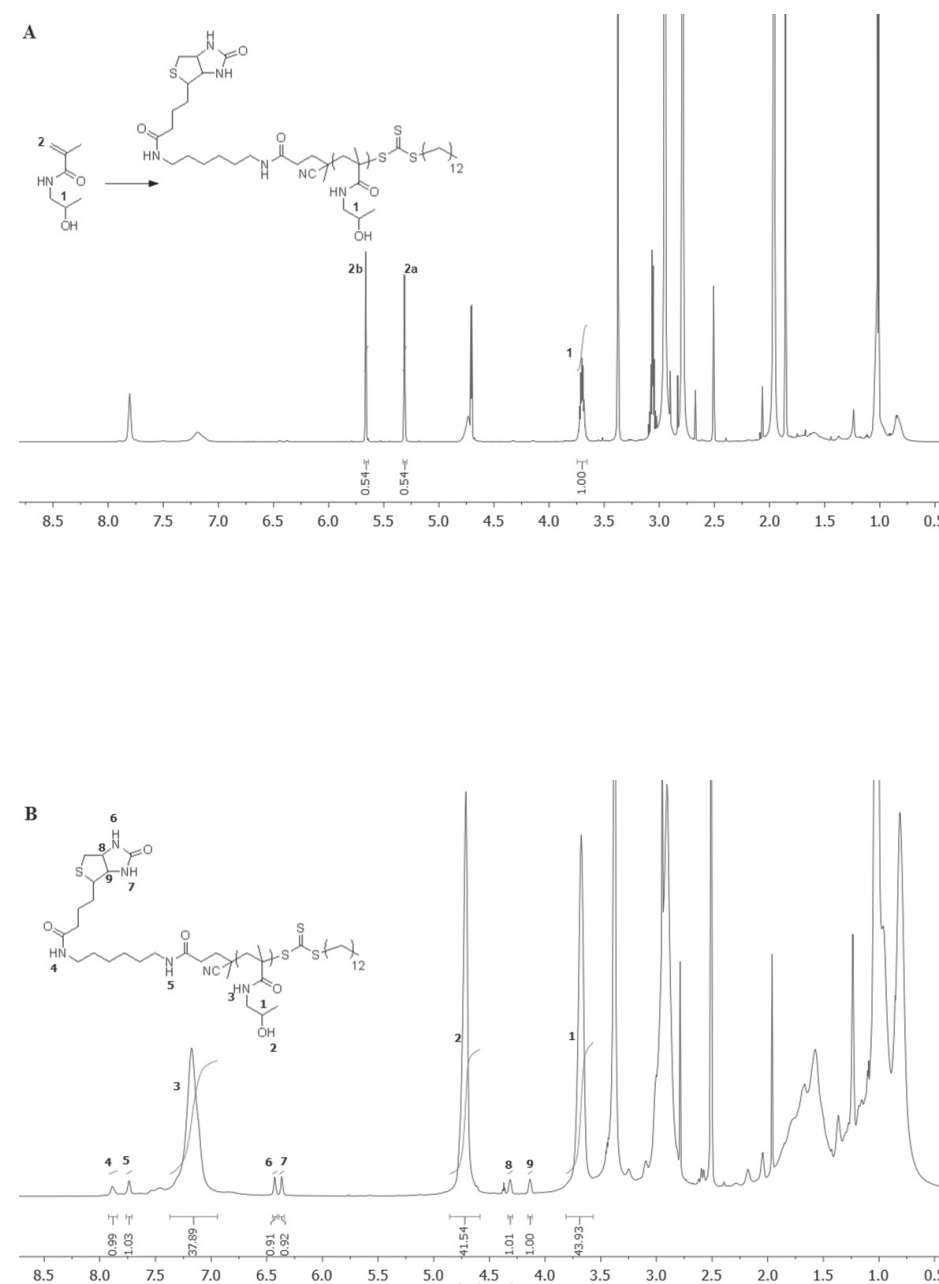**Fig. S3.** ¹H NMR spectra of the reaction mixture of HPMAm/biotin-CTA at 6 hours (**A**) and isolated biotinylated p(HPMAm)₆.₈ₖ (entry 4 in Table 1) (**B**).
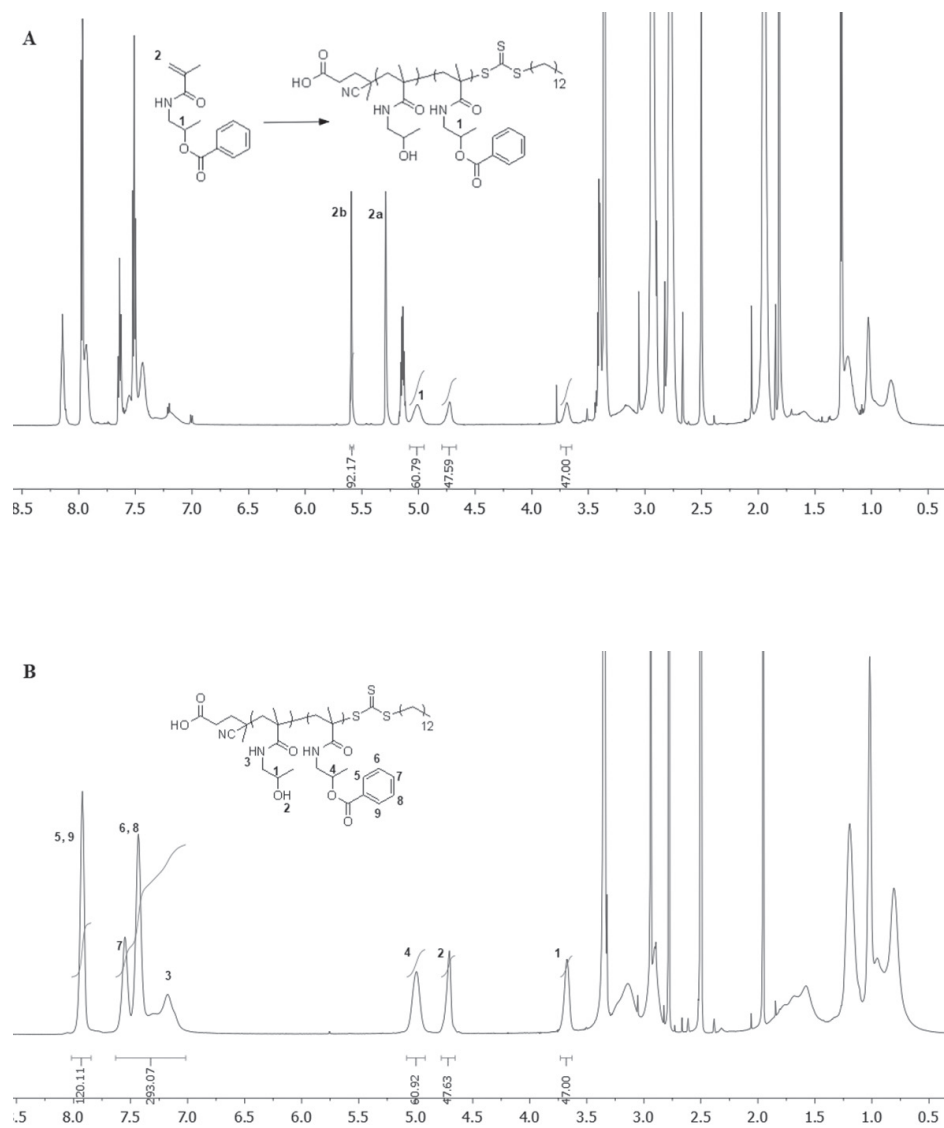
Fig. S4. ^{1}H NMR spectra of the reaction mixture of HPMAm-Bz/macroCTA at 20 hours (**A**) and isolated p(HPMAm)$_{7.1k}$-b-p(HPMAm-Bz)$_{15.0k}$ (entry 13 in Table 1) (**B**).
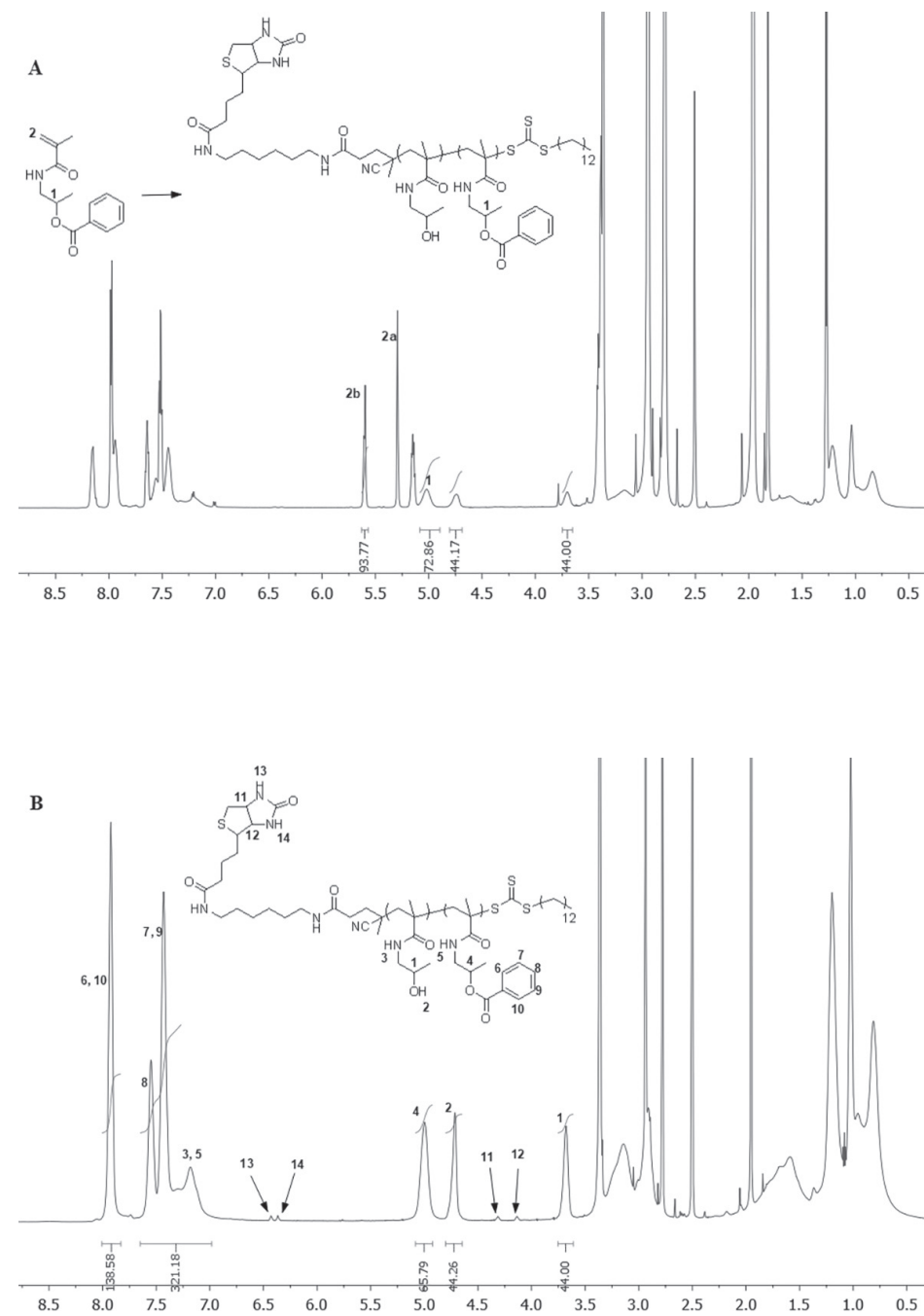

Fig. S5. ^{1}H NMR spectra of the reaction mixture of HPMAm-Bz/biotinylated macroCTA at 19 hours (**A**) and isolated biotinylated p(HPMAm)$_{6.8k}$-p(HPMAm-Bz)$_{16.3k}$ (entry 14 in Table 1) (**B**).
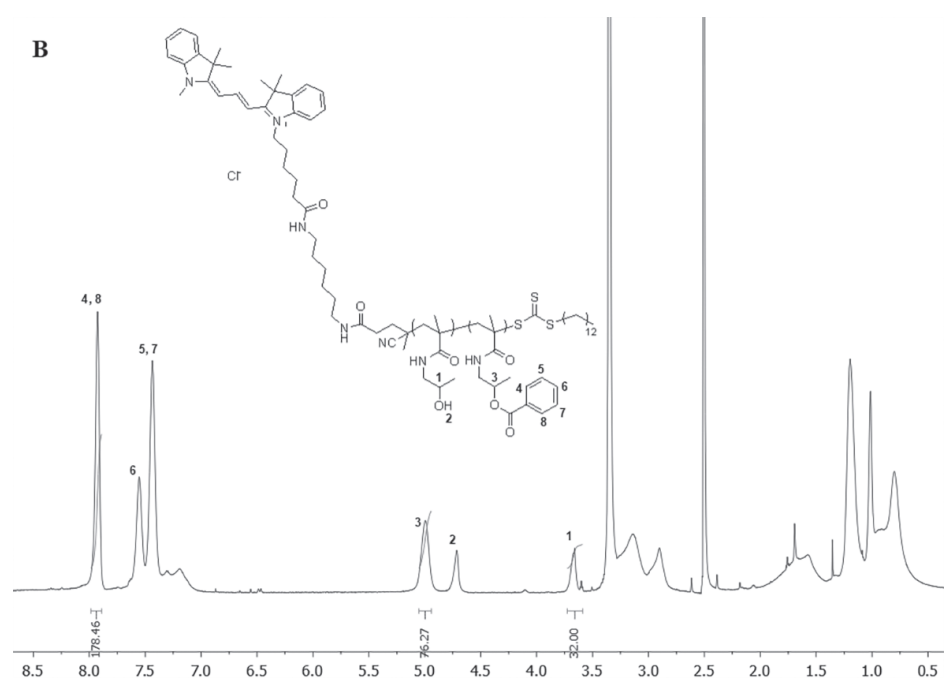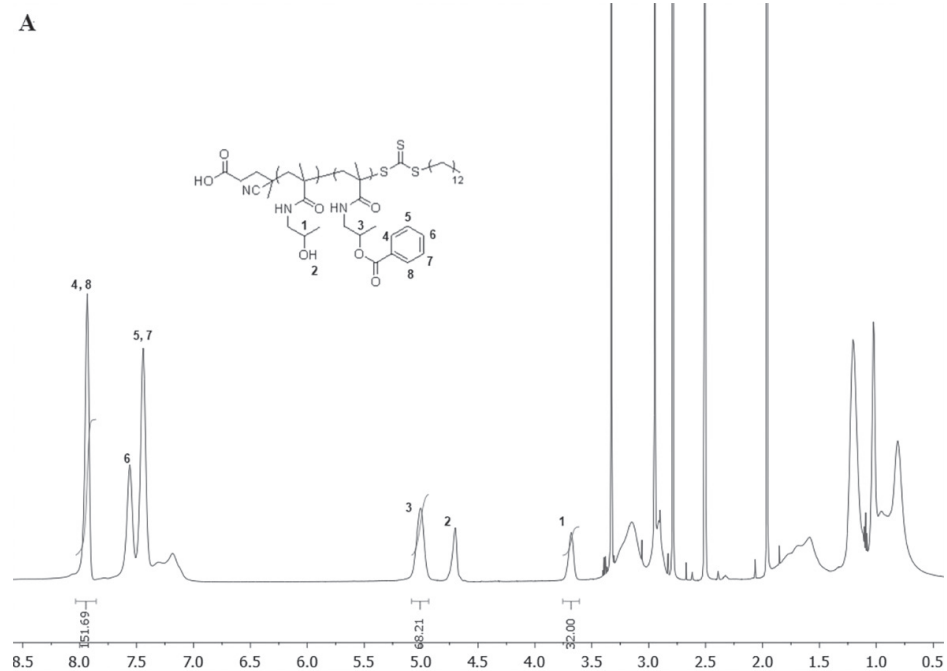
A

B

Fig. S6. ^{1}H NMR spectra of p(HPMAm)$_{4.9k}$-p(HPMAm-Bz)$_{16.8k}$ (entry 10 in Table 1) (**A**) and Cy3-labeled p(HPMAm)$_{4.9k}$-p(HPMAm-Bz)$_{18.7k}$ (entry 15 in Table 1) (**B**).

Table S1. Comparison of the molecular weight of some selected polymers using different GPC calibration standards.

Polymers	Molar Ratio of M/CTA/I	Monomer Conversion (%)	$M_{n,\,theory}$ (kDa) [a]	$M_{n,\,NMR}$ (kDa) [b]	$M_{n,\,GPC}$ (kDa)_PS	$M_{n,\,GPC}$ (kDa)_PMMA	$M_{n,\,GPC}$ (kDa)_PEG
p(HPMAm)$_{63}$	1000/5/1	31.8	9.5	−	21.7	12.4	9.7
p(HPMAm-Bz)$_{52}$	500/2.5/1	25.9	31.8	−	15.5	7.6	5.8
p(HPMAm)$_{63}$-b-p (HPMAm-Bz)$_{162}$	500/1.73/1	33.2	32.7	34.9	47.0	20.3	13.8

Notes: [a] $M_{n,\,theory}$ calculated using equations (1) and (3); [b] $M_{n,\,NMR}$ calculated using equations (2) and (4).
Abbrevivations: PS, polystyrene; PMMA, poly(methyl methacrylate); PEG, polyethylene glycol.

The results show that p(HPMAm) with a molecular weight of 9500 (and thus a DP of 63) has the same hydrodynamic volume as PEG with a molecular weight of 9700 (and thus a DP of 220), PMMA of 12400 (DP 124) and PS 21700 (DP 208). Similar discrepancies were also observed in previous publications [3–5].
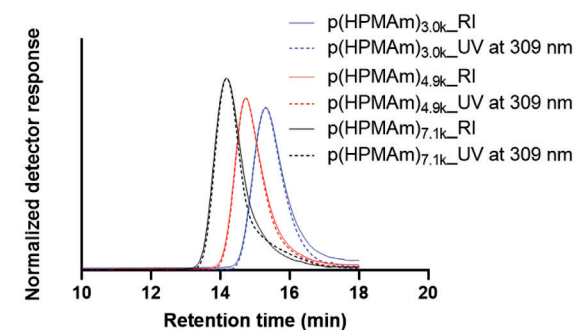

Fig. S7. GPC UV and RI traces of p(HPMAm)$_{3.0k}$, p(HPMAm)$_{4.9k}$, and p(HPMAm)$_{7.1k}$. The dead polymer chains are not visible using UV detection at 309 nm due to the absence of thiocarbonylthio moieties, but still can be seen using RI detecion. An estimation of the fraction of dead chains in p(HPMAm) was made by calculating the ratio of the normalized RI and UV signal and the area under the curve of the chromatogrammes. It was estimated that 4.8, 2.5, and 2.1% of dead polymers were present in p(HPMAm)$_{3.0k}$, p(HPMAm)$_{4.9k}$, and p(HPMAm)$_{7.1k}$, respectively.
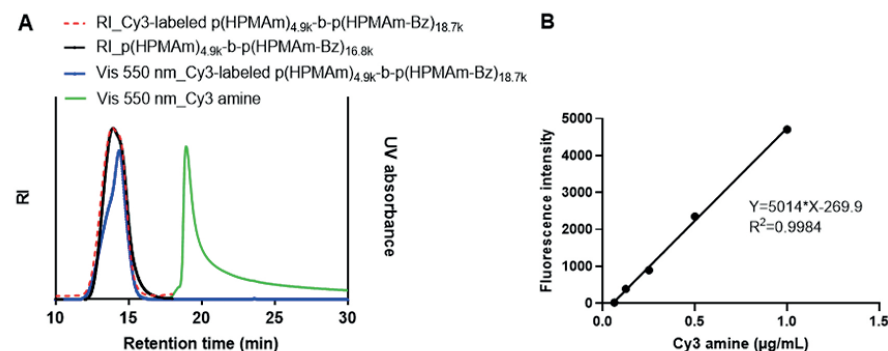
Fig. S8. (**A**) GPC chromatograms (RI and Vis detection) of the Cy3-labeled p(HPMAm)-b-p(HPMAm-Bz) copolymer before and after Cy3 conjugation. (**B**) Calibration curve of Cy3 fluorescence intensity versus Cy3 concentration in DMF. The fluorescence intensity of the Cy3-labeled p(HPMAm)-b-p(HPMAm-Bz) (15 µg/mL, in DMF) was 1432, and therefore the Cy3 amine concentration in Cy3-labeled polymer sample was 0.34 µg/mL as calculated from the calibration curve. The molecular weights of Cy3 amine and the Cy3-labeled p(HPMAm)-b-p(HPMAm-Bz) are 627 and 23600 g/mol, respectively. Thus the number of Cy3 units was 0.85 per polymer chain.
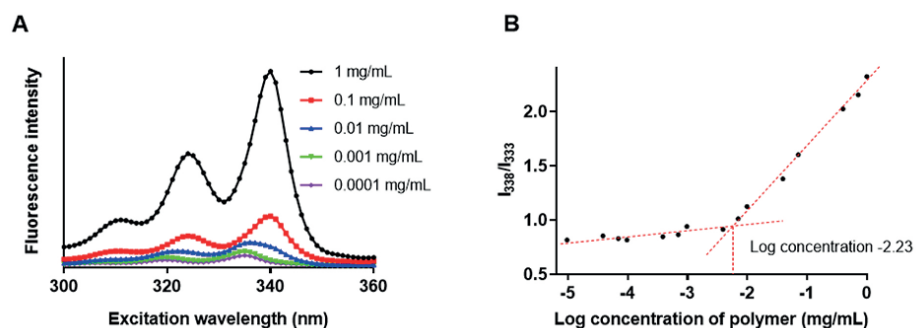

Fig. S9. (**A**) Fluorescence excitation spectra of pyrene as a function of $p(HPMAm)_{7.1k}$-b-$p(HPMAm-Bz)_{15k}$ polymer concentrations, monitored at λ_{em} = 390 nm. (**B**) I_{338}/I_{333} fluorescence ratio for pyrene as a function of the log concentration of $p(HPMAm)_{7.1k}$-b-$p(HPMAm-Bz)_{15k}$ copolymer (entry 13 in Table 1), and CMC was calculated from the intersection of two lines.
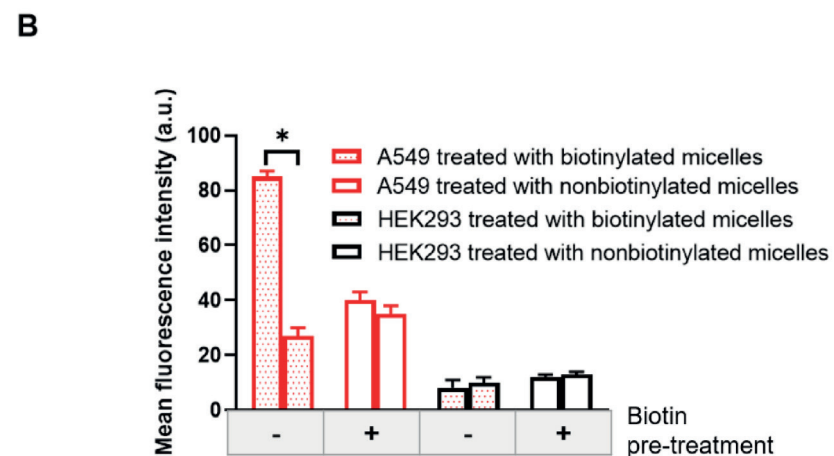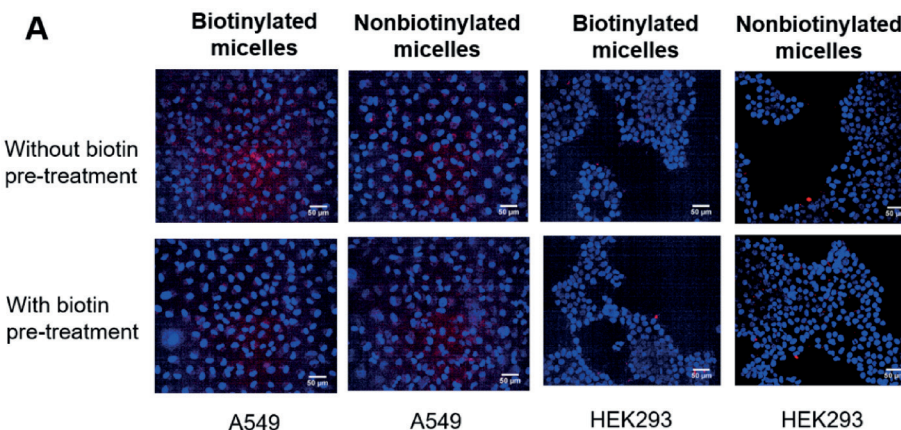
Fig. S10. Internalization of the fluorescently labeled targeted and non-targeted p(HPMAm)-b-p(HPMAm-Bz) micelles with or without biotin pre-treatment. (**A**) Laser confocal scanning microscopy images showing the cellular uptake of Cy3-labeled p(HPMAm)-b-p(HPMAm-Bz) micelles with or without biotin decoration (140 µg/mL) after 4 h-incubation by A549 cells and HEK293 cells with or without biotin pre-treatment. Cell nuclei are stained with Hoechst 33430 in blue while the micelles are visualized in red by Cy3. (**B**) The corresponding mean fluorescence intensity calculated from the confocal images. Scale bar = 50 µm, data represent mean ± SD (n = 5 imaging fields), * p < 0.05.

Table S2. PTX solubilization at different PTX loading amount as determined by HPLC analysis.

| PTX loading amount (%)	PTX concentration in micelles (mg/mL) [a]	Encapsulation efficiency (%) [a]	Loading capacity (%) [a]
1	0.06 ± 0.01	79.4 ± 9.2	1.0 ± 0.2
5	0.29 ± 0.04	71.0 ± 8.9	4.6 ± 0.6
10	0.48 ± 0.07	54.9 ± 14.5	7.9 ± 0.8
15	0.50 ± 0.10	37.7 ± 10.5	8.9 ± 1.1
20	0.46 ± 0.03	28.6 ± 2.0	8.0 ± 0.5

[a] n = 3.

References

[1]   Y. Shi, R. Van Der Meel, B. Theek, E. Oude Blenke, E.H.E. Pieters, M.H.A.M. Fens, J. Ehling, R.M. Schiffelers, G. Storm, C.F. Van Nostrum, T. Lammers, W.E. Hennink, Complete regression of xenograft tumors upon targeted delivery of paclitaxel via Π-Π stacking stabilized polymeric micelles, ACS Nano. 9 (2015) 3740–3752.

[2]   A. Swami, M.R. Reagan, P. Basto, Y. Mishima, N. Kamaly, S. Glavey, S. Zhang, M. Moschetta, D. Seevaratnam, Y. Zhang, J. Liu, M. Memarzadeh, J. Wu, S. Manier, J. Shi, N. Bertrand, Z.N. Lu, K. Nagano, R. Baron, A. Sacco, A.M. Roccaro, O.C. Farokhzad, I.M. Ghobrial, Engineered nanomedicine for myeloma and bone microenvironment targeting, Proceedings of the National Academy of Sciences of the United States of America. 111 (2014) 10287–10292.

[3]   C. Kojima, B. Turkbey, M. Ogawa, M. Bernardo, C.A.S. Regino, L.H. Bryant, P.L. Choyke, K. Kono, H. Kobayashi, Dendrimer-based MRI contrast agents: the effects of PEGylation on relaxivity and pharmacokinetics, Nanomedicine: Nanotechnology, Biology and Medicine. 7 (2011) 1001–1008.

[4]   G. Gody, T. Maschmeyer, P.B. Zetterlund, S. Perrier, Exploitation of the degenerative transfer mechanism in RAFT polymerization for synthesis of polymer of high livingness at full monomer conversion, Macromolecules. 47 (2014) 639–649.

[5]   C. Duffy, M. Phelan, P.B. Zetterlund, F. Aldabbagh, Reversible addition-fragmentation chain transfer polymerization of alkyl-2-cyanoacrylates: An assessment of livingness, Journal of Polymer Science Part A: Polymer Chemistry. 55 (2017) 1397–1408

2
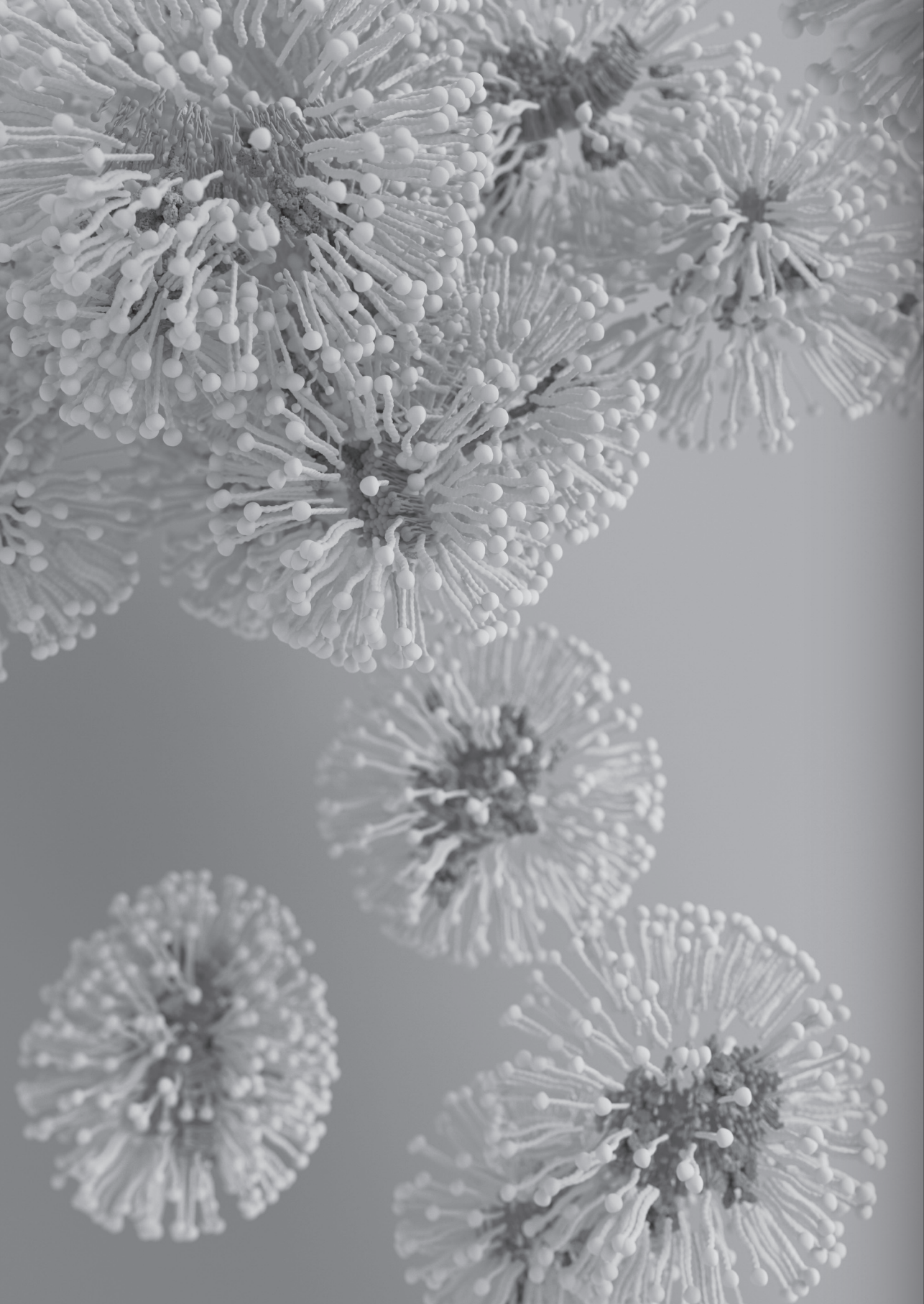
3

Tuning the size of all-HPMA polymeric micelles fabricated by solvent extraction

Yan Wang [1], Dominique M. E. Thies-Weesie [2], Esmeralda D. C. Bosman [1], Mies J. van Steenbergen [1], Joep van den Dikkenberg [1], Yang Shi [3], Twan Lammers [3], Cornelus F. van Nostrum [1] and Wim E. Hennink [1]

[1] Department of Pharmaceutics, Utrecht Institute for Pharmaceutical Sciences, Utrecht University, Universiteitsweg 99, 3508 TB Utrecht, the Netherlands
[2] Department of Physical and Colloid Chemistry, Debye Institute for Nanomaterials Science, Utrecht University, Padualaan 8, 3584 CH Utrecht, the Netherlands
[3] Department of Nanomedicine and Theranostics, Institute for Experimental Molecular Imaging, RWTH Aachen University Clinic, Forckenbecktrasse 55, 52074 Aachen, Germany

Abstract

The size of polymeric micelles crucially affects their tumor accumulation, penetration and antitumor efficacy. In the present study, micelles were formed based on amphiphilic poly(*N*-2-hydroxypropyl methacrylamide)-block-poly(*N*-2-benzoyloxypropyl methacrylamide) (p(HPMAm)-b-p(HPMAm-Bz)) via the solvent extraction method, and factors impacting micelle size were systematically studied, including the molecular weight of the polymers, homopolymer content, and processing methods (i.e., batch process versus continuous microfluidics). The formation of core-shell structured micelles was demonstrated by light scattering, sedimentation velocity and electron microscopy analysis. Micellar size and aggregation number increased with decreasing the molecular weight ratio of the hydrophilic/hydrophobic block. The presence of hydrophobic p(HPMAm-Bz) homopolymer and high copolymer concentration increased micelle size, while the presence of hydrophilic p(HPMAm) homopolymer did not affect micellar size. Regarding processing conditions, it was found that the use of tetrahydrofuran and acetone as solvents for the polymers resulted in larger micelles, likely due to their relatively high water-solvent interaction parameters as compared to other solvents tested, i.e., dimethylformamide, dimethylacetamide, and dimethyl sulfoxide. Among the latter, only dimethylformamide led to micelles with a narrow polydispersity. Addition of dimethylformamide to an aqueous solvent and faster mixing of two solvents using microfluidics favored the formation of smaller micelles. In conclusion, our results show that the size of all-HPMA polymeric micelles can be easily tailored from 40 to 120 nm by varying the formulation properties and processing parameters.

Introduction

In aqueous solution, amphiphilic block copolymers self-assemble into polymeric micelles composed of hydrophobic core – hydrophilic shell architectures which can be used for solubilization and targeted delivery of cytostatic drugs [1–5]. Their hydrophobic core is able to accommodate poorly water-soluble drugs via either physical entrapment or chemical attachment, while their hydrophilic shell ensures colloidal stability [6–8]. Upon intravenous administration, the nano-size of polymeric micelles (usually 10–100 nm) and their hydrophilic shell contribute to prolonged blood circulation by avoiding protein adsorption and uptake by the mononuclear phagocyte system (MPS) [9,10]. This prolonged circulation leads to increased accumulation of drug payloads in cancerous and inflamed tissues due to increased vascular permeability and impaired lymphatic drainage, known as the enhanced permeability and retention (EPR) effect [11,12].

The efficacy of nanoparticulate drug delivery systems is affected by many physical and chemical characteristics, including size, shape, and surface properties (i.e., surface charge and the presence of targeting ligands) [13–17]. Among these factors, the size of polymeric micelles and size distribution play a critical role regarding circulation, tumor disposition and penetration, and cellular uptake [18]. In recent years, the effect of size of nanoparticles on their efficacy of cancer treatment have been extensively studied. For example, Tang et al. prepared micelles based on polyethylene glycol (PEG) and 10-OH methacrylate ester of 7-ethyl-10-hydroxyl-camptothecin (HEMASN38). The authors showed that 100 nm PEG-b-P(HEMASN38) micelles had prolonged blood circulation and improved tumor accumulation as compared to 30 nm size micelles [19]. However, these 30 nm micelles showed better tumor penetration. Kataoka et al. reported that PEG-b-poly(glutamic acid) micelles with average size of 30, 50, 70 and 100 nm penetrated highly permeable tumors, whereas only micelles of 30 nm were able to penetrate poorly permeable pancreatic tumors and showed antitumor effects [20]. On the contrary, Liang et al. found that ultrasmall tiopronin-coated gold nanoparticles (2 and 6 nm) had longer blood circulation times than 15 nm gold nanoparticles [21]. However, ultrasmall nanodrugs may undergo rapid renal clearance, resulting in inadequate tumor accumulation [22]. Overall, the optimal size of polymeric micelles should be large enough for long circulation time and high tumor accumulation (> 5.5 nm) [23], but small enough for good tumor penetration (< 100 nm) [24].

Recently, we reported the synthesis of amphiphilic poly(*N*-2-hydroxypropyl methacrylamide)-block-poly(*N*-2-benzoyloxypropyl methacrylamide) (p(HPMAm)-b-p(HPMAm-Bz)) with a molecular weight ranging from 8 to 24 kDa via reversible addition–fragmentation chain-transfer (RAFT) polymerization [25]. Micelles based

on p(HPMAm)-b-p(HPMAm-Bz) with a molecular weight of 22.1 kDa showed good colloidal stability and drug loading. In the present study, a systematic evaluation was performed to investigate the parameters that affect the size of p(HPMAm)-b-p(HPMAm-Bz) micelles formed using batch preparation and continuous microfluidics. These include: (1) formulation variables, namely the type of solvent for the block copolymer, polymer concentration, homopolymer content, and the molecular weight ratio of the hydrophobic/hydrophilic block, as well as (2) processing variables, namely order of addition of solvent and non-solvent (water), volume ratio and mixing time of the organic phase and aqueous medium. The formed micelles were characterized using various techniques, including asymmetric flow field-flow fractionation coupled with multi-angle light scattering and dynamic light scattering, ultracentrifugation and electronic microscopy. The purpose was to find a highly reproducible method for formation of all-HPMAm based micelles with tunable size.

Materials and Methods

Materials
Dimethylformamide (DMF), tetrahydrofuran (THF), dimethylacetamide (DMAc), dimethyl sulfoxide (DMSO), and acetone were purchased from Biosolve Ltd. (Valkenswaard, the Netherlands) and used as received. Syringe filters with 0.45 µm regenerate cellulose (RC) membrane were purchased from Phenomenex (Utrecht, the Netherlands), while 0.2 µm polytetrafluoroethylene (PTFE) membrane and 0.2 µm RC membrane filters were ordered from Roth (Karlsruhe, Germany). Bovine serum albumin was purchased from Sigma-Aldrich (Zwijndrecht, the Netherlands). Poly(N-2-hydroxypropyl methacrylamide) (p(HPMAm)), poly(N-2-benzoyloxypropyl methacrylamide) (p(HPMAm-Bz)), and p(HPMAm)-b-p(HPMAm-Bz) which were synthesized and characterized as previously reported are shown in Scheme S1 & Table S1 [25].

Preparation of p(HPMAm)-b-p(HPMAm-Bz) micelles
p(HPMAm)-b-p(HPMAm-Bz) micelles were prepared by solvent extraction method. In detail, 1 mL DMF solution of 20 mg p(HPMAm)-b-p(HPMAm-Bz) copolymer was pipetted into 1 mL of Milli-Q water while stirring for 1 min. To remove DMF, the mixture was transferred into a Spectra/Por dialysis membrane with a molecular weight cutoff of 6–8 kDa which was subsequently sealed. Dialysis was carried out for 24 h against Milli-Q water which was changed at 2nd, 5th, and 13th h. Next, the micellar dispersion was filtered through 0.45 µm RC membrane filter.

Effect of solvent composition on the micellar size
THF, acetone, DMAc, DMF, and DMSO were used to investigate the effect of the type of organic solvent on the size of p(HPMAm)-b-p(HPMAm-Bz) micelles. In short, p(HPMAm)$_{7.1k}$-b-p(HPMAm-Bz)$_{15.0k}$ copolymer (20 mg) was dissolved in 1 mL of the organic solvents mentioned and the obtained solution was pipetted into 1 mL of Milli-Q water while stirring for 1 min. THF and acetone were removed by evaporation overnight at room temperature, while DMAc, DMF, and DMSO were removed by dialysis, resulting in the formation of micelles.

The effect of the composition of the aqueous solution on the size of the micelles was also investigated. Water, 0.9% NaCl solution, and phosphate-buffered saline (PBS, pH 7.4, containing 11.9 mM phosphate, 137 mM sodium chloride, and 2.7 mM potassium chloride) were used as aqueous medium. One milliliter DMF solution of 20 mg of p(HPMAm)$_{7.1k}$-b-p(HPMAm-Bz)$_{15.0k}$ copolymer was pipetted into 1 mL of Milli-Q water, 0.9% NaCl solution, or PBS while stirring for 1 min, followed by dialysis and filtration through 0.45 µm RC membrane filter.

Effect of the polymer concentration in DMF on the micellar size
The effect of polymer concentration in DMF on the size of p(HPMAm)-b-p(HPMAm-Bz) micelles was investigated. Briefly, one milliliter DMF solution of different amounts of p(HPMAm)$_{7.1k}$-b-p(HPMAm-Bz)$_{15.0k}$ copolymer (5, 10, 20, 30, and 40 mg) was pipetted into 1 mL of Milli-Q water while stirring for 1 min, followed by dialysis and filtration through 0.45 µm RC membrane filter.

Effect of organic/aqueous solvent ratio and the order of solvent addition on the micellar size
To investigate the effect of organic to aqueous solvent ratio and the order of solvent addition on the size of the formed p(HPMAm)-b-p(HPMAm-Bz) micelles, experiments were carried out where the volume ratios of the polymer solution in DMF to water were 1:1 and 0.3:1, and the addition order of two solvents (DMF to water or water to DMF) was changed. In brief, p(HPMAm)$_{7.1k}$-b-p(HPMAm-Bz)$_{15.0k}$ copolymer (20 mg) was dissolved in DMF (0.3 or 1.0 mL), and the obtained solution was either pipetted into Milli-Q water or water was added to this solution while stirring for 1 min, followed by dialysis and filtration through 0.45 µm RC membrane filter. The critical overlap concentration (C^*) of block copolymer p(HPMAm)-b-p(HPMAm-Bz) (total molecular weight 22 kDa) in DMF was calculated using the experimentally determined intrinsic viscosity [η] ($C^* = 1/[\eta]$) [26]. The flow times of DMF and solutions of this polymer (10, 21 and 28 mg/mL) were measured as the average of three readings with an accuracy of ±0.2 s. The intrinsic viscosity was calculated by extrapolating the plot of the reduced viscosity η_{sp}/c versus polymer concentration c to c = 0 using the classical Huggins equation [27].

Effect of mixing time of organic and aqueous solvent on the micellar size

The effect of mixing time of organic and aqueous solvent on the size of the formed p(HPMAm)-b-p(HPMAm-Bz) micelles was investigated using Dolomite microfluidics (Dolomite Center Ltd., Royston, UK). In detail, a solution of block copolymer in DMF (20 mg/mL, p(HPMAm)$_{7.1k}$-b-p(HPMAm-Bz)$_{15.0k}$, p(HPMAm)$_{7.1k}$-b-p(HPMAm-Bz)$_{9.1k}$, or p(HPMAm)$_{4.9k}$-b-p(HPMAm-Bz)$_{11.3k}$) was filtered with a 0.2 μm PTFE syringe filter, and Milli-Q water was filtered with a 0.2 μm RC syringe filter. Both solvents were placed in chambers which were connected to pumps. These pumps were connected to a Dolomite hydrophilic micromixer chip (Part No. 3200401) via a PTFE tubing. The polymer solution and Milli-Q water were mixed at a 1:1 volume ratio at different total flow rates (Q$_{tot}$, 100, 200, 350, 500, 1600, and 3000 μL/min) corresponding to varying mixing times (τ$_M$, 1571, 635, 306, 192, 42, and 18 ms) which were calculated based on data supplied by the manufacturer (Fig. S2). Two mL of the different micellar dispersions were collected after the mixture reached a steady-state flow. DMF was subsequently removed by dialysis against water.

Effect of the presence of free p(HPMAm) and p(HPMAm-Bz) homopolymer on the micellar size

The effect of free p(HPMAm) and p(HPMAm-Bz) homopolymer on the size of the formed p(HPMAm)-b-p(HPMAm-Bz) micelles was investigated. In short, 20 mg of p(HPMAm)$_{7.1k}$-b-p(HPMAm-Bz)$_{15.0k}$ copolymer and 0, 1, 2, 5, and 10 mg of p(HPMAm)$_{7.1k}$ or p(HPMAm-Bz)$_{14.6k}$ were dissolved in 1 mL of DMF corresponding to weight fractions of 0, 5, 9, 20, and 33 wt% of the homopolymer, respectively. These solutions were mixed with 1 mL water and subsequently, DMF was removed by dialysis. Finally, the micellar dispersions were filtered through 0.45 μm RC membrane filter.

Effect of hydrophilic/hydrophobic molecular weight of copolymers on the micellar size

The effect of the hydrophilic/hydrophobic molecular weight of the block copolymers on the size of the formed micelles was investigated. Polymers with different hydrophilic and hydrophobic lengths at a total molecular weight of 8–24 kDa (Table S1) were used to prepare micelles. Briefly, p(HPMAm)-b-p(HPMAm-Bz) copolymer (20 mg) was dissolved in 1 mL DMF and the obtained solution was pipetted into 1 mL of Milli-Q water while stirring for 1 min, followed by dialysis and filtration through 0.45 μm RC membrane filter.

Characterization of p(HPMAm)-b-p(HPMAm-Bz) micelles

^{1}H NMR spectroscopy

The residual organic solvent content of the micellar dispersion was measured by ^{1}H NMR analysis using a Bruker 600 MHz spectrometer (Bruker Corp., Massachusetts, USA) as described previously [28]. Two hundred microliter of micelle dispersion was mixed with 400 μL of D$_2$O (containing 10 mg/mL sodium acetate as an internal standard), and the amount of residual organic solvent was calculated by comparing the integral of THF (3.60 ppm), acetone (2.22 ppm), DMAc (2.08 ppm), DMF (7.92 ppm), and DMSO (2.71 ppm) to that of sodium acetate (CH$_3$ at 1.76 ppm).

Thermo gravimetric analysis (TGA)

The polymer concentration in the different micellar dispersions was determined by thermo gravimetric analysis (TGA) using a TA instrument Q50 (Waters Corp., Delaware, USA). The analysis was performed by introducing 50 μL of dialyzed micelle dispersion into a tared aluminum pan, followed by heating from 20 to 120 °C at a heating rate of 20 °C/min with an isothermal hold time of 100 min. The weight of polymer residual was recorded over time. A sample of dry polymer, analyzed for comparison, displayed no mass loss indicating the stability of p(HPMAm)-b-p(HPMAm-Bz) polymers up to at least 120 ˚C.

Dynamic light scattering (DLS)

The size and size distribution of the formed p(HPMAm)-b-p(HPMAm-Bz) micelles were determined by dynamic light scattering (DLS) at 25 °C after 10-fold dilution in water using a Zetasizer Nano S at a fixed angle of 173° (Malvern Instruments Ltd., Malvern, UK). The size of micelles was also determined after addition of 1 mL of 1.8% NaCl solution or twice concentrated PBS (pH 7.4, containing 23.8 mM phosphate, 274 mM sodium chloride, and 5.4 mM potassium chloride) to 1 mL of micellar dispersions prepared in water. The Z-average diameter (Z$_{ave}$) and polydispersity index (PDI) were calculated by the Zetasizer software v.7.13.

Asymmetric flow field-flow fractionation and multi-angle light scattering (AF4-MALS)

The radius of gyration (R$_g$), the radius of hydration (R$_h$), and the molecular weight of different micelles (M$_{w, mic}$) were determined by asymmetric flow field-flow fractionation (AF4) measurements using a Postnova AF2000 system (Postnova Analytics, Landsberg, Germany) equipped with a degasser, isocratic pumps, auto sampler, and fraction collector. A Frit-inlet channel was equipped with a ceramic frit, a 350 μm spacer, and a regenerated cellulose membrane with a molecular weight cut-off of 10 kDa and kept at a temperature of 25 ˚C. The AF4 system was coupled to a refractive index (RI) detector, a multi-angle light scattering (MALS) detector and a DLS system (Malvern Instruments Ltd., Malvern, UK). Bovine serum albumin

dissolved in 0.9% NaCl at a concentration of 5 mg/mL was used for calibration. PBS (pH 7.4, containing 11.9 mM phosphate, 137 mM sodium chloride, and 2.7 mM potassium chloride) was used as eluent. The micellar dispersions in water were diluted in PBS to a final concentration of 1.2 mg/mL. A 20 µL of sample was injected into the system and the detector flow was kept at 0.5 mL/min. The crossflow rate was initially 1.5 mL/min and then decreased exponentially in 70 min to 0.0 mL/min. After completion of the elution program, crossflow rate was maintained at 0.0 mL/min for at least 5 min to ensure complete elution of largest particles. Data acquisition and processing were executed with an AF2000 control software v.2.1.0.5, from which R_g, R_h, and $M_{w, mic}$ of micelles were calculated using a random coil fitting model [29]. The refractive index increment of the polymer (dn/dc), which is required for the determination of the molecular weight, was measured in water by injection of 20 µL of micellar dispersion (concentration accurately determined using TGA) into the AF4 channel without crossflow using a detector flow rate of 0.5 mL/min over 10 min.

Ultracentrifugation

The molecular weight of two selected micelles based on p(HPMAm)$_{3.0k}$–b–p(HPMAm-Bz)$_{15.6k}$ and p(HPMAm)$_{4.9k}$-b-p(HPMAm-Bz)$_{11.3k}$ was determined by sedimentation velocity experiments using a Proteomelab XL-I analytical ultracentrifuge (Beckman Coulter Inc., California, USA) equipped with absorbance optics. Diluted micelle dispersions were centrifuged in 3 mm pathlength double-sector Epon centerpieces with quartz centerpieces in an An-60 Ti rotor; the reference sector was filled with Milli-Q water. The micelle concentration was accurately determined using TGA and it turned out to be 0.54 mg/mL for p(HPMAm)$_{3.0k}$-b-p(HPMAm-Bz)$_{15.6k}$ and 1.21 mg/mL for p(HPMAm)$_{4.9k}$-b-p(HPMAm-Bz)$_{11.3k}$, respectively. The samples were centrifuged at 20 °C at a rotor speed of 8000 rpm (5152 g) for p(HPMAm)$_{3.0k}$-b-p(HPMAm-Bz)$_{15.6k}$ micelles and 15000 rpm (18112 g) for p(HPMAm)$_{4.9k}$-b-p(HPMAm-Bz)$_{11.3k}$, respectively. Changes in solute micelle concentrations were detected by 200-300 absorbance scans measured at 272 nm. Analysis and fitting of the data was performed using the program Sedfit v.16.1c. A continuous c(M) distribution model was fitted to the data [30]; the distribution was integrated to calculate the average molecular weight of micelles ($M_{w, mic}$). From the known molecular weight of one polymer chain, the aggregation number of polymers per micelle was calculated to obtain N_{agg}.

Partial specific volume of the micelles ($\bar{v}$), required for the determination of the molecular weight $M_{w, mic}$, was calculated from density measurements (pf series of diluted micelles (concentration ranging from 0.8 to 5.5 mg/ml at 20.00±0.01 ºC using a high-precision density meter DMA5000 (Anton Paar GmbH, Graz, Austria) according to the following equation:

$$\rho = \rho_0 + (1 - \bar{v}\,\rho_0)c$$

where ρ is density of micelle dispersion, ρ_0 is density of water, and c is concentration of micelles.

Electron microscopy (EM) analysis

The morphology of p(HPMAm)$_{7.1k}$-b-p(HPMAm-Bz)$_{15.0k}$ micelles formed under different conditions was visualized by transmission electron microscope (TEM) using a JEOL JEM-1400 TEM instrument (JEOL Ltd., Tokyo, Japan) operated with 100 kv acceleration voltages and 40 µA beam current. Samples were prepared by drying a drop of micellar dispersions in water (5 µL, 1 mg/mL) on a 400-mesh copper grid with lacey carbon support (Electron Microscopy Sciences, Pennsylvania, USA), subsequently stained with uranyl acetate solution (2%, w/v) before TEM observation. The morphology of selected micelles based on p(HPMAm)$_{3.0k}$-b-p(HPMAm-Bz)$_{15.6k}$ and p(HPMAm)$_{4.9k}$-b-p(HPMAm-Bz)$_{11.3k}$ was investigated by cryogenic TEM (Cryo-TEM) using a Philips Tecnai 20 (FEI/Philips Electrons Optics, Eindhoven, the Netherlands). Samples for Cryo-TEM were prepared by glow-discharging the 300-mesh copper grid with lacey carbon support (Electron Microscopy Sciences, Pennsylvania, USA) in a Cressington 208 carbon coater for 40 s. Then, 3 µL of micellar dispersion was pipetted onto the grid and blotted for 3-4 s in a fully automated vitrification robot (Vitrobot MARK IV, Thermo Fisher/FEI, Eindhoven, the Netherlands) at room temperature and 100% humidity. The grid was subsequently plunged into liquid ethane and stored under liquid nitrogen. Cryo-TEM images were recorded using a Gatan 626 holder (Gatan, California, USA). Brightness and contrast corrections of the acquired images were performed using the ImageJ software.

Results and Discussion

Effect of solvent and anti-solvent on the size of all-p(HPMAm) micelles

Various organic solvents were used to investigate the effect on the size of p(HPMAm)$_{7.1k}$-b-p(HPMAm-Bz)$_{15.0k}$ micelles prepared by solvent extraction. ^{1}H NMR analysis showed that the amount of THF and acetone of the micellar dispersions after solvent evaporation for 24 h was far below the recommended limit of residual solvent for humanized use according to ICH guidelines (<720 and 5000 ppm,

respectively, Table S2) [31]. However, these micellar dispersions also contained up to 2000 ppm of DMAc the solvent used for polymer synthesis that was not removed by evaporation due to its high boiling point (165 °C) (Fig. S1). Importantly, the residual concentration of the non-volatile solvent DMAc, DMF and DMSO was far below the recommended limit (<1090, 880, and 5000 ppm, respectively, Table S2) after dialysis for 24 h. Figure 1A shows that the Z_{ave} of the different micelles varied from 61 ± 1 to 113 ± 7 nm (PDI < 0.2) with the smallest and largest micelles obtained using DMAc and THF, respectively. Both DLS and TEM analyses showed that micelles obtained using DMAc, DMF, and DMSO exhibited similar sizes (60~70 nm by DLS and 30~50 nm by TEM) (Fig. 1A).
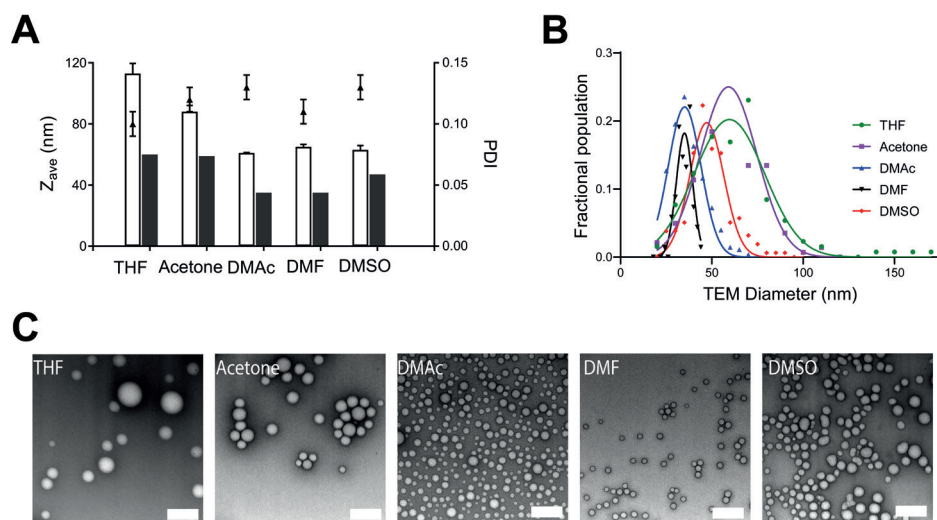
Fig. 1. Effect of organic solvent on micelle size. (**A**) Size of p(HPMAm)$_{7.1k}$-b-p(HPMAm-Bz)$_{15.0k}$ micelles prepared using different organic solvents, as determined by DLS (empty bars, n = 3 meaning three independent replicates) and TEM (filled bars, n = 1), and PDI (black dots, n = 3 meaning three independent replicates). (**B**) Size distribution of micelles as derived from TEM images. The curves of TEM diameter are the fitted Gaussian distributions. (**C**) TEM images of p(HPMAm)$_{7.1k}$-b-p(HPMAm-Bz)$_{15.0k}$ micelles prepared by using THF, acetone, DMAc, DMF, and DMSO as polymer solvent (from left to right). Scale bar represents 200 nm.

Solvent extraction, also referred to as nanoprecipitation method, was first described by Fessi et al. in 1989 and is a frequently applied method for the preparation of polymeric nanoparticles because it is a relatively fast process with low energy input [32–36]. Using this method, the formation of polymeric micelles relies on the rapid diffusion of the organic phase with dissolved polymer chains into the external aqueous phase, followed by polymer aggregation to yield colloidal particles as demonstrated by Duan et al. for the formation of pH-sensitive polysialic acid

based polymeric micelles [37]. The extent of polymer partition can be qualitatively described by comparing both solubility parameter difference ($\Delta\delta_{solvent-water}$) and solvent-water interaction parameter ($\chi_{solvent-water}$) [38–40]. Table S3 shows that DMF, DMSO, and DMAc display lower $\Delta\delta_{solvent-water}$ values (between 31.0 to 32.5 MPa$^{1/2}$) than THF and acetone (35.7 and 35.8 MPa$^{1/2}$), which points to a high solvent-water affinity of the first mentioned solvents and thus facilitates rapid polymer partition into the aqueous phase leading to rapid precipitation and the formation of smaller micelles (i.e., Z_{ave} of micelles prepared using DMF ≈ DMSO ≈ DMAc < THF and acetone). Acetone, with a lower $\chi_{solvent-water}$ value (23.4) than THF (27.1), forced more rapid polymer partition into the aqueous phase, which in turn resulted in polymeric micelles with a smaller average size as measured by DLS.

The micellar sizes measured by TEM were 25–47% smaller than those determined by DLS (Fig. 1A). This can be explained as follows. First, TEM observes nanoparticles in the dry state where the p(HPMAm) shell is invisible to the electron beam without chemical staining, whereas DLS measures the hydrodynamic diameter of nanoparticles including the solvation layers [41]. Second, TEM is a number-based measurement, whereas DLS measures intensity distributions based on Brownian motion. The detected light-scattering intensity is proportional to the six power of a particle diameter and thus larger particles are overestimated [42].

Notably, TEM images indicate that micelles formed using DMF had a narrow polydispersity (Fig. 1B & C). Therefore, DMF was selected for further micelle preparation.
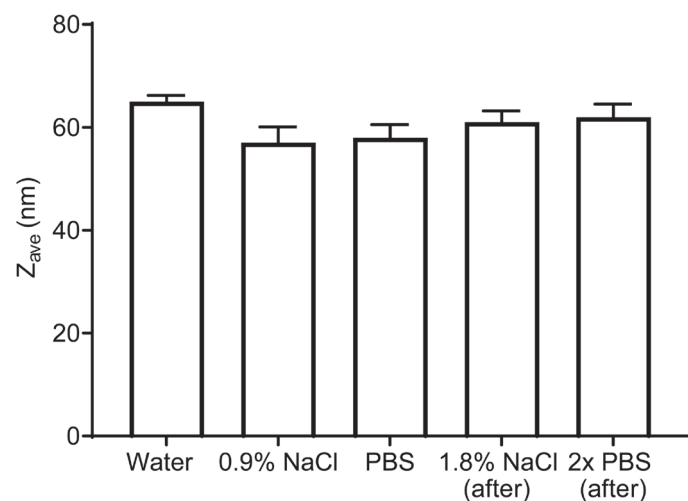
The effect of the composition of the aqueous medium on the micellar size was also investigated. As shown in Fig. 2, the micelles showed comparable sizes when they were prepared in saline solution (57 ± 3 and 58 ± 3 nm in 0.9% NaCl and PBS, respectively). Our previous paper showed that the p(HPMAm)$_{7.1k}$-b-p(HPMAm-Bz)$_{15.0k}$ micelles demonstrated good colloidal stability in PBS upon incubation for 48 h at 37 °C [25]. In the current study, the size of micelles prepared in water did not change once this dispersion was mixed with an equal volume of either 1.8% NaCl solution or twice concentrated PBS, making the resulted dispersions because of their osmotic values in principle suitable for intravenous injection, demonstrating that the micellar structures are thermodynamically stable.

Effect of the polymer concentration in DMF on the size of all-p(HPMAm) micelles

DMF solutions of p(HPMAm)$_{7.1k}$-b-p(HPMAm-Bz)$_{15.0k}$ with various concentrations were used for the preparation of micelles. As depicted in Fig. 3A, polymer concentrations from 5 to 40 mg/mL resulted in the formation of micelles in a range of 43 ± 2 to 73 ± 4 nm (PDI < 0.2). A similar phenomenon was observed for the formation of pH-sensitive micelles based on zwitterionic sulfobetaines prepared

via solvent extraction method, where the average diameter of micelles increased from 70 to 110 nm when the concentration of poly(ε-caprolactone)-b-poly-(*N*,*N*-diethylaminoethyl methacrylate)-r-poly(*N*-(3-sulfopropyl)-*N*-methacryloxethy-*N*,*N*-diethylammoniumbetaine) increased from 1 to 10 mg/mL [43]. Likely, the increase of the polymer concentration in the organic solvent slows down the diffusion of the polymer-solvent into the aqueous solution due to the increased viscosity of the organic solution, leading to larger particles [35,36,44]. Our results indicate that this explanation is also valid for the all-HPMA based polymeric micelles investigated in the present study. However, different from the positive correlation between polymer concentration in DMF with micellar size of p(HPMAm)-b-p(HPMAm-Bz), in an earlier study we reported that the size of mPEG-b-p(HPMAm-Bz) micelles decreased with increasing polymer concentration up to 30 mg/mL in THF [45]. The discrepancy with the present study can be attributed to different polymer-organic solvent interactions, which needs further investigation.
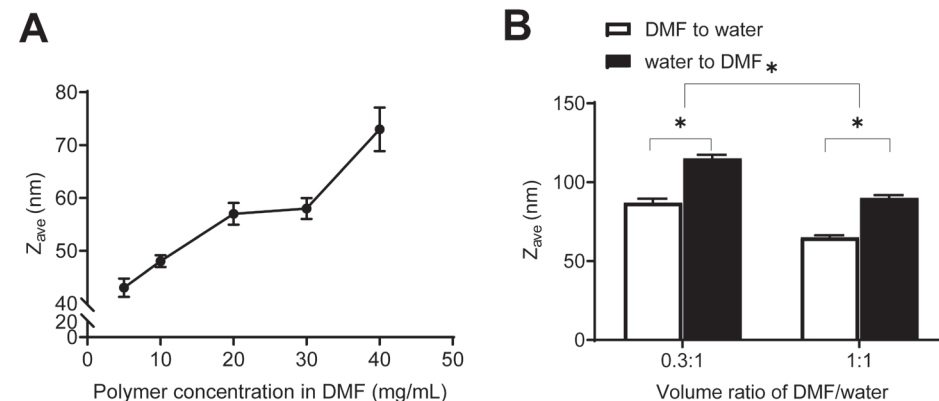
Effect of organic/aqueous solvent ratio and the order of solvent addition on the size of all-p(HPMAm) micelles

The effects of the volume ratio of organic to aqueous solvent as well as the order of solvent addition on the size of the formed micelles were investigated. When the ratio of organic solvent to water was reduced from 1:1 to 0.3:1 using less DMF (1 and 0.3 mL) to dissolve the same amount of polymer, p(HPMAm)$_{7.1k}$-b-p(HPMAm-Bz)$_{15.0k}$ micelles with average sizes of 65 ± 1 and 87 ± 3 nm were formed by adding DMF to water, respectively (Fig. 3B). When water was added to DMF at 1:1 and 0.3:1 DMF/

water volume ratios, the size of the resulting micelles was 90 ± 2 and 115 ± 2 nm, respectively. Regardless of the order of solvent addition, the reduction in the DMF/water ratio from 1:1 to 0.3:1 resulted in a significant increase in the average size of self-assembled micelles. Lower solvent-to-water ratio increased the initial weight fraction of polymer in organic solvent, i.e., polymer concentration increased from 20 to 67 mg/mL. It appears that these concentrations were below the critical overlap concentration (C* = 133 mg/mL), demonstrating that polymer chain entanglement did not occur and that this cannot explain the observation. The formation of larger particles might be therefore attributed to the increased viscosity of the organic solution with increasing initial weight fraction of the polymer, which subsequently retards diffusion of the polymer into the aqueous medium.

Effect of mixing time of organic and aqueous solvent on the size of all-p(HPMAm) micelles
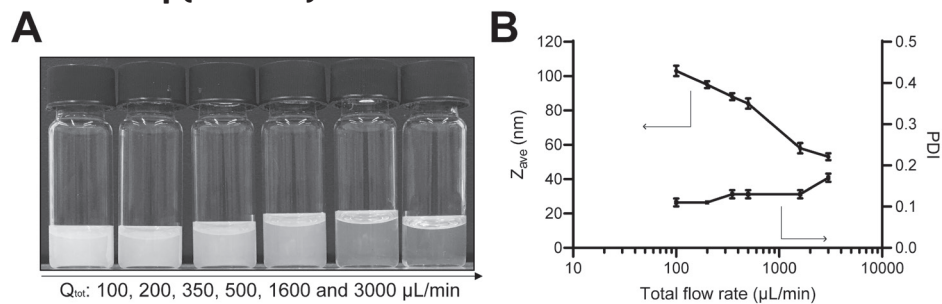
A

Q_{tot}: 100, 200, 350, 500, 1600 and 3000 µL/min

B

Fig. 4. Effect of mixing time of DMF and water on micelle size. (A) p(HPMAm)$_{7.1k}$-b-p(HPMAm-Bz)$_{15.0k}$ micelle dispersions obtained at different mixing times. (B) Size of p(HPMAm)$_{7.1k}$-b-p(HPMAm-Bz)$_{15.0k}$ micelles as a function of microfluidic flow rate (n = 3 meaning three independent replicates).

Table 1. Characteristics of p(HPMAm)-b-p(HPMAm-Bz) micelles obtained by microfluidics as determined by AF4-MALS.

Q_{tot} (µL/min)	τ_M (ms)	$M_{w, mic}$ (10^3 kDa)	N_{agg} (10^3)	R_g (nm)	R_h (nm)	R_g/R_h
100	1571	114	5.2	30	44	0.68
200	635	108	4.8	27	42	0.65
350	306	93	4.2	23	37	0.62
500	192	48	2.1	21	35	0.61
1600	42	16	0.7	15	25	0.59
3000	18	11	0.5	11	21	0.53

Q_{tot} = total flow rate, τ_M = mixing time, $M_{w, mic}$ = weight-average molecular weight of micelles determined by AF4-MALS, N_{agg} = the micelle aggregation number calculated by $M_{w, mic}/M_{n, p}$, where $M_{n, p}$ is the molar mass of a single polymer chain determined by ^{1}H NMR, R_g = radius of gyration, R_h = radius of hydration (n= 3, the standard deviation is less than 4%).

Most of polymeric micelles aimed for cancer drugs are fabricated using bulk mixing methods leading to a lack of uniformity and reproducibility, which obstacles the translation to the industrial scales. Microfluidics provides precise control over the fluid flows and mixing time [46–48]. Therefore, the effect of mixing time of the organic and aqueous solvent on the size of the formed micelles was investigated using this technology. Photographs of p(HPMAm)$_{7.1k}$-b-p(HPMAm-Bz)$_{15.0k}$ micelle dispersions shown in Fig. 4A demonstrate that micellar dispersions obtained at higher total flow rate were opalescent, while those at lower flow rate were turbid. DLS measurements (Fig. 4B) evidenced that the micellar size increased from 52 ± 2 to 103 ± 3 nm (PDI < 0.2) when the total flow rate decreased from 3000 to 100 µL/min (i.e., mixing time increased from 18 to 1571 ms). AF4-MALS analysis revealed that the aggregation number of the micelles (N_{agg}), calculated by dividing the weight-average molecular weight of micelles by the molar mass of a single polymer chain as determined by ^{1}H NMR, increased with increasing mixing time (Table 1). The ratio of radius of gyration and hydration (R_g/R_h), known as the shape factor, is 0.775 for rigid spheres with uniform density [49,50]. For particles composed of a dense core and a partly coiled less dense shell, the high concentration of the mass in the core leads to a small radius of gyration, and R_g/R_h values below the theoretical value of rigid spheres. For example, micelles with a dense spherical polystyrene core surrounded by a less dense poly(methacrylic acid) shell in a mixed solvent with dioxane and water (80:20 v/v), showed R_g/R_h values ranging from 0.37 to 0.64 [51]. It is also possible for a core-shell structure to have R_g/R_h > 0.775, as reported for core-shell spherical micelles based on cyclic poly(N-acryloylmorpholine)-grafted copolymer with R_g/R_h values ranging from 0.81 to 0.95 in water [52]. Table 1 shows

3

that the resulting R_g/R_h values of the different micelles were between 0.53 to 0.66, which are slightly lower than that of rigid spheres, suggesting the formation of spherical micelles with a dense core and a swollen hydrated shell [53,54]. Similar results were observed for p(HPMAm)$_{7.1k}$–b–p(HPMAm-Bz)$_{9.1k}$ and p(HPMAm)$_{4.9k}$–b–p(HPMAm-Bz)$_{11.3k}$ (Fig. S3 & Table S4).

The flow rate dependence indicates that the formation of core-shell structured all-p(HPMAm) micelles is explained by the nucleation-controlled process. The addition of an anti-solvent (water) entails supersaturation, which in turn results in the nucleation and diffusion-limited growth of spherical aggregates with narrow distribution [55,56]. The rate of nucleation growth depends on the magnitude of supersaturation at a given temperature [46]. High flow rate results in fast mixing, and consequently the mixing time (τ_M) is approaching the aggregation time (τ_{agg}), inducing homogeneous local high supersaturation and rapid growth of spherical particles. This eventually results in numerous smaller micelles with narrow size distribution upon displacement of the organic solvent [48,57,58]. A similar phenomenon was also reported for the formation of mPEG-b-p(HPMAm-Bz) micelles using microfluidics [59]. These results demonstrate that the tunable mixing conditions significantly impacts the particle formation and growth kinetics and thus allows for the micelle preparation with a uniform size and size distribution. Continuous flow production ensures the same mixing quality over time, which in turn reduces batch-to-batch variation. For further scalable preparation of the all-HPMA based micelles, microfluidics is preferred over batch-mode production as it offers controlled size and features.

Effect of p(HPMAm) and p(HPMAm-Bz) homopolymer presence on the size of all-p(HPMAm) micelles

It has been reported the possibility of the presence of a small amount of homopolymer in block copolymers synthesized by RAFT polymerization [60–62], therefore, the effect of the presence of free homopolymer of p(HPMAm) and p(HPMAm-Bz) on the size of the formed p(HPMAm)-b-p(HPMAm-Bz) micelles was investigated by adding ~33% of p(HPMAm) or p(HPMAm-Bz) to the block copolymer solution. Fig. 5 shows that the size of p(HPMAm)$_{7.1k}$-b-p(HPMAm-Bz)$_{15.0k}$ micelles increased proportionally with increasing amount of homopolymer p(HPMAm-Bz)$_{14.6k}$ in DMF. This increase is because the hydrophobic p(HPMAm-Bz) is solubilized into the hydrophobic core, leading to an increase in the volume and thus diameter of the micelles. Fig. S4 presents similar results for p(HPMAm)$_{7.1k}$-b-p(HPMAm-Bz)$_{9.1k}$ and p(HPMAm)$_{7.1k}$-b-p(HPMAm-Bz)$_{4.9k}$ upon addition of p(HPMAm-Bz)$_{9.2k}$ and p(HPMAm-Bz)$_{4.7k}$, respectively. In contrast, the presence of the hydrophilic p(HPMAm)$_{7.1k}$ in the feed did not cause changes in micellar sizes (Fig. 5 & Fig. S4), which is ascribed to the good aqueous solubility of p(HPMAm) resulting in its partition in the aqueous

phase. This is in agreement with the findings previously reported [45], in which the homopolymer p(HPMAm-Bz) led to an increase of mPEG-p-p(HPMAm-Bz) micelle, whereas the presence of up to 40% of free mPEG did not affect the micelle size.
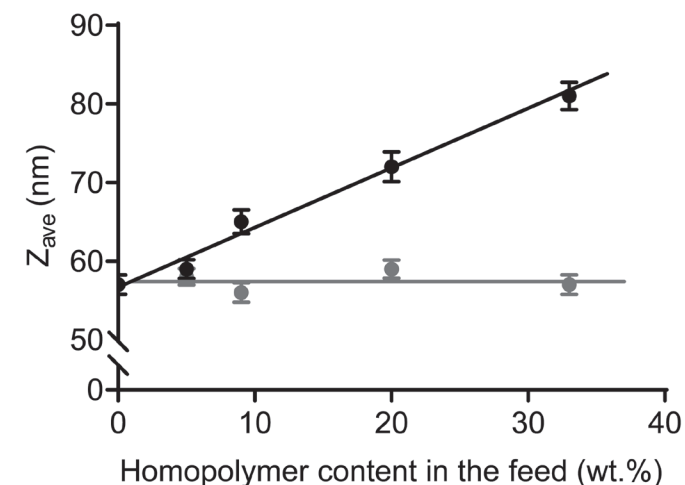
Fig. 5. Effect of the presence of free p(HPMAm)$_{7.1k}$ (gray) and p(HPMAm-Bz)$_{14.6k}$ (black) homopolymer in the feed dissolved in DMF on the size of p(HPMAm)$_{7.1k}$-b-p(HPMAm-Bz)$_{15.0k}$ micelles (n = 3 meaning three independent replicates).

Effect of hydrophilic/hydrophobic molecular weight of copolymers on the size of all-p(HPMAm) micelles

As there is no single, absolute method to characterize nanoparticles, especially in terms of morphology [63,64], to gain more insight into the impact of hydrophilic/hydrophobic molecular weight on micellar morphology, the block copolymers at fixed molecular weight of p(HPMAm) were used for the formation of micelles using batch process and further characterized by AF4-MALS, ultracentrifugation and Cryo-TEM.

Table 2. Characteristics of p(HPMAm)-b-p(HPMAm-Bz) micelles as determined by AF4-MALS.

Polymer	dn/dc (mL/g)	$M_{w,mic}$ (10^3 kDa)	N_{agg} (10^3)	R_g (nm)	R_h (nm)	R_g/R_h	σ^{-1} (nm^2)	d (nm)
p(HPMAm)$_{3.0k}$-b-p(HPMAm-Bz)$_{5.4k}$	0.169	10	1.2	10	19	0.54	3.69	1.9
p(HPMAm)$_{3.0k}$-b-p(HPMAm-Bz)$_{9.9k}$	0.193	33	2.5	17	26	0.67	3.33	1.8
p(HPMAm)$_{3.0k}$-b-p(HPMAm-Bz)$_{15.6k}$	0.216	68	3.6	30	33	0.90	3.74	1.9
p(HPMAm)$_{4.9k}$-b-p(HPMAm-Bz)$_{6.4k}$	0.151	7	0.6	8	17	0.45	6.05	2.5
p(HPMAm)$_{4.9k}$-b-p(HPMAm-Bz)$_{11.3k}$	0.179	14	0.8	12	21	0.56	6.32	2.5
p(HPMAm)$_{4.9k}$-b-p(HPMAm-Bz)$_{16.8k}$	0.201	25	1.1	16	23	0.70	5.99	2.4
p(HPMAm)$_{7.1k}$-b-p(HPMAm-Bz)$_{4.9k}$	0.163	4	0.3	7	16	0.40	9.51	3.1
p(HPMAm)$_{7.1k}$-b-p(HPMAm-Bz)$_{9.1k}$	0.180	12	0.7	11	21	0.54	7.86	2.8
p(HPMAm)$_{7.1k}$-b-p(HPMAm-Bz)$_{15.0k}$	0.194	19	0.8	12	21	0.58	6.31	2.5

dn/dc = refractive index increment of the polymer determined by AF4, $M_{w,mic}$ = weight-average molecular weight of micelles determined by AF4-MALS, N_{agg} = the micelle aggregation number calculated by $M_{w,mic}/M_{n,p}$, where $M_{n,p}$ is the molar mass of a single polymer chain determined by ^{1}H NMR, R_g = radius of gyration, R_h = radius of hydration, σ^{-1} = surface area per p(HPMAm) chain calculated by $4\pi R_h^2/N_{agg}$, d = interchain distance calculated by the root square of σ^{-1} (n=3, the standard deviation is less than 4%).

Different from DLS measurements, AF4-MALS exploits the advantages of field-flow fractionation chromatography to separate fractions of nearly monodisperse self-assemblies with the power of multi-angle laser light scattering to get insight into their morphologies [65]. Table 2 shows that for micelles with a fixed hydrophilic p(HPMAm) block length, $M_{w,mic}$ and N_{agg} increased with increasing molecular weight of the hydrophobic p(HPMAm-Bz) block. For all polymeric micelles, the R_g/R_h values varied from 0.40–0.90, which was in the same range as reported for other core-shell structured micelles [54,66–68]. The surface area available per p(HPMAm) chain (σ^{-1}), calculated by dividing the surface area of micelles by N_{agg}, was between 3 to 10 nm^2. The small surface area per p(HPMAm) chain (i.e., high grafting density) is a favorable property for drug delivery purposes as it has been reported that, for nanoparticles of equal size, an increasing PEG grafting density reduces adsorption of plasma proteins and thus prolongs blood circulation times [14,17]. The same might be expected for the all-HPMA based micelles. For block copolymers with a

fixed molecular weight of the p(HPMAm) block, despite of the increased R_h and N_{agg} with increasing p(HPMAm-Bz) block length, the space between p(HPMAm) chains remained approximately the same (1.9 ± 0.1 nm for p(HPMAm)$_{3.0k}$, 2.5 ± 0.1 nm for p(HP MAm)$_{4.9k}$, and 2.8 ± 0.3 nm for p(HPMAm)$_{7.1k}$, respectively).

Table 3. Charateristics of two selected p(HPMAm)-b-p(HPMAm-Bz) micelles as determined by ultracentrifugation.

Polymer	$\bar{v}$ (mL/g)	$M_{w,mic}$ (10^3 kDa)	N_{agg} (10^3)	f/f_0
p(HPMAm)$_{3.0k}$-b-p(HPMAm-Bz)$_{15.6k}$	0.797	71	3.8	1.19
p(HPMAm)$_{4.9k}$-b-p(HPMAm-Bz)$_{11.3k}$	0.785	12	0.7	1.17

$\bar{v}$ = partial specific volume calculated by $1/\rho$, where ρ is density of micelle dispersion determined by density meter, $M_{w,mic}$ = weight-average molecular weight of micelles determined by ultracentrifugation, N_{agg} = the micelle aggregation number calculated by $M_{w,mic}/M_{n,p}$, where $M_{n,p}$ is the molar mass of a single polymer chain obtained by ^{1}H NMR, f/f_0 = frictionl ratio (n = 3 meaning three independent replicates, the standard deviation is less than 5%).

The validity of the AF4-MALS data was confirmed by analyzing two selected samples (Table 3) by ultracentrifugation which is an established and validated technique to determine the molecular weight of synthetic polymers and colloidal particles [30,69]. First, the partial specific volume of micellar dispersion was determined from the linear regression of a density-concentration profile of the micelles [70,71]. The concentration profiles were analyzed with Sedfit to obtain weight-average molecular weight of the micelles. The derived $M_{w,mic}$ and the deduced N_{agg} of p(HPMAm)$_{4.9k}$-b-p(HPMAm-Bz)$_{11.3k}$ micelles from ultracentrifugation were 12 × 10^3 kDa and 0.7 × 10^3, respectively, which is in good agreement with those determined by AF4-MALS technique ($M_{w,mic}$ = 14 × 10^3 kDa and N_{agg} = 0.8 × 10^3). The consistency of two techniques was also demonstrated by p(HPMAm)$_{3.0k}$-b-p(HPMAm-Bz)$_{15.6k}$ (Table 2 & 3). The determined value of frictional ratio f/f_0, providing valuable information regarding the shape of particles, is nearly one for spherical particles [30,72]. The f/f_0 value of both micelles was slightly above one (1.1–1.2), pointing to spherical structures, as evidenced by AF4-MALS that the R_g/R_h value was 0.56–0.90.
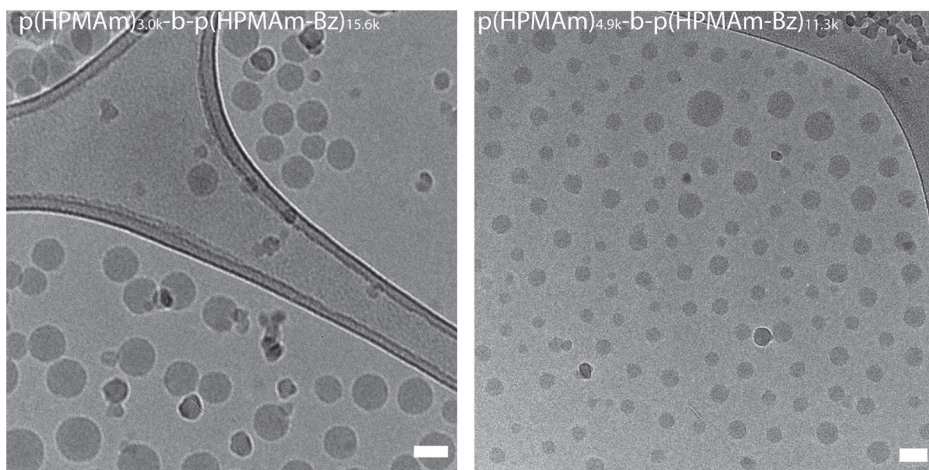
Fig. 6. Cryo-TEM images of micelles prepared from p(HPMAm)$_{3.0k}$-b-p(HPMAm-Bz)$_{15.6k}$ (left) and p(HPMAm)$_{4.9k}$-b-p(HPMAm-Bz)$_{11.3k}$ (right). Scale bar represents 50 nm.

To corroborate AF4-MALS and ultracentrifugation analyses regarding the morphology of samples, the selected micelle dispersions were further analyzed using Cryo-TEM. In line with AF4-MALS and ultracentrifugation data, both of p(HPMAm)$_{3.0k}$-b-p(HPMAm-Bz)$_{15.6k}$ and p(HPMAm)$_{4.9k}$-b-p(HPMAm-Bz)$_{11.3k}$ micelles showed spherical structures (Fig. 6). The average size as measured by Cryo-TEM was smaller than those of DLS (Table S6), which is indicative of partially coiled less dense shell making it invisible to the electron beam under Cryo-TEM.

The EPR effect as investigated and described by prof. Maeda in many papers is a hallmark in nanomedicine research as well as for the development of preclinical/clinical nanomedicine formulations. The size of nanomedicine is a crucial physicochemical factor for EPR-based drug delivery and targeting systems, and it has been reported that nanoparticles ranging from 10 to 150 nm are able to reach tumor sites through passive targeting after intravenous administration provided that these particles show sufficiently long circulating kinetics. Once accumulated in the tumor, size is also an important factor affecting tumor penetration of nanomedicines, and as general rule: the smaller the better. In the present study, several critical parameters that influence the size of all-HPMAm based micelles were investigated and discussed. In a nutshell, smaller micelles can be obtained by either proper selection of the organic solvent for the amphiphilic p(HPMAm)-b-p(HPMAm-Bz) block copolymer with faster mixing with water via microfluidics, or by using well-defined block copolymers with higher hydrophilic/hydrophobic ratios. A robust method was established to produce micelles in the size range of 40 to 120 nm, which can be exploited for EPR-driven tumor targeting.

Conclusion

This systematic study demonstrates that the self-assembly of p(HPMAm)-b-p(HPMAm-Bz) block copolymers into micelles can be tailored in size by solvent extraction method. The size control relies on the polymer hydrophobicity and hydrophilicity as well as processing method. It is important to take these parameters into consideration in practical applications of micelles.

Acknowledgements

3

References

[1]   H. Cabral, K. Miyata, K. Osada, K. Kataoka, Block copolymer micelles in nanomedicine applications, Chem Rev. 118 (2018) 6844–6892.

[2]   S. Eetezadi, S.N. Ekdawi, C. Allen, The challenges facing block copolymer micelles for cancer therapy: In vivo barriers and clinical translation, Adv Drug Deliv Rev. 91 (2015) 7–22.

[3]   L. Houdaihed, J.C. Evans, C. Allen, Overcoming the road blocks: advancement of block copolymer micelles for cancer therapy in the clinic, Mol Pharm. 14 (2017) 2503–2517.

[4]   J. Kopeček, J. Yang, Polymer nanomedicines, Advanced Drug Delivery Reviews. 156 (2020) 40–64.

[5]   R. Van Der Meel, E. Sulheim, Y. Shi, F. Kiessling, W.J.M. Mulder, Smart cancer nanomedicine, Nature Nanotechnology. 14 (2019) 1007–1017.

[6]   Y. Hussein, M. Youssry, Polymeric micelles of biodegradable diblock copolymers: enhanced encapsulation of hydrophobic drugs, Materials. 11 (2018) 688.

[7]   A. Varela-Moreira, Y. Shi, M.H.A.M. Fens, T. Lammers, W.E. Hennink, R.M. Schiffelers, Clinical application of polymeric micelles for the treatment of cancer, Mater Chem Front. 1 (2017) 1485–1501.

[8]   M. Talelli, C.J.F. Rijcken, C.F. van Nostrum, G. Storm, W.E. Hennink, Micelles based on HPMA copolymers, Adv Drug Deliv Rev. 62 (2010) 231–239.

[9]   C. Deng, Y. Jiang, R. Cheng, F. Meng, Z. Zhong, Biodegradable polymeric micelles for targeted and controlled anticancer drug delivery: promises, progress and prospects, Nano Today. 7 (2012) 467–480.

[10]   K. Knop, R. Hoogenboom, D. Fischer, U.S. Schubert, Poly(ethylene glycol) in drug delivery: pros and cons as well as potential alternatives, Angewandte Chemie International Edition. 49 (2010) 6288–6308.

[11]   J. Fang, W. Islam, H. Maeda, Exploiting the dynamics of the EPR effect and strategies to improve the therapeutic effects of nanomedicines by using EPR effect enhancers, Advanced Drug Delivery Reviews. 157 (2020) 142–160.

[12]   H. Maeda, J. Wu, T. Sawa, Y. Matsumura, K. Hori, Tumor vascular permeability and the EPR effect in macromolecular therapeutics: a review, Journal of Controlled Release. 65 (2000) 271–284.

[13]   H.S. Min, H.J. Kim, J. Ahn, M. Naito, K. Hayashi, K. Toh, B.S. Kim, Y. Matsumura, I.C. Kwon, K. Miyata, K. Kataoka, Tuned density of anti-tissue factor antibody fragment onto siRNA-loaded polyion complex micelles for optimizing targetability into pancreatic cancer cells, Biomacromolecules. 19 (2018) 2320–2329.

[14]   H. Zhou, Z. Fan, P.Y. Li, J. Deng, D.C. Arhontoulis, C.Y. Li, W.B. Bowne, H. Cheng, Dense and dynamic polyethylene glycol shells cloak nanoparticles from uptake by liver endothelial cells for long blood circulation, ACS Nano. 12 (2018) 10130–10141.

[15]   W. Huang, C. Zhang, Tuning the size of poly(lactic-co-glycolic acid) (PLGA) nanoparticles fabricated by nanoprecipitation, Biotechnol J. 13 (2018) 1700203.

[16]   M. Najafi, N. Kordalivand, M.A. Moradi, J. van den Dikkenberg, R. Fokkink, H. Friedrich, N.A.J.M. Sommerdijk, M. Hembury, T. Vermonden, Native chemical ligation for cross-linking of flower-like micelles, Biomacromolecules. 19 (2018) 3766–3775.

[17]   C.D. Walkey, J.B. Olsen, H. Guo, A. Emili, W.C.W. Chan, Nanoparticle size and surface chemistry determine serum protein adsorption and macrophage uptake, J Am Chem Soc. 134 (2012) 2139–2147.

[18]   D. Hwang, J.D. Ramsey, A. v. Kabanov, Polymeric micelles for the delivery of poorly soluble drugs: from nanoformulation to clinical approval, Adv Drug Deliv Rev. 156 (2020) 80–118.

[19]   J. Wang, W. Mao, L.L. Lock, J. Tang, M. Sui, W. Sun, H. Cui, D. Xu, Y. Shen, The role of micelle size in tumor accumulation, penetration, and treatment, ACS Nano. 9 (2015) 7195–7206.

[20]   H. Cabral, Y. Matsumoto, K. Mizuno, Q. Chen, M. Murakami, M. Kimura, Y. Terada, M.R. Kano, K. Miyazono, M. Uesaka, N. Nishiyama, K. Kataoka, Accumulation of sub-100 nm polymeric micelles in poorly permeable tumours depends on size, Nat Nanotechnol. 6 (2011) 815–823.

[21]   K. Huang, H. Ma, J. Liu, S. Huo, A. Kumar, T. Wei, X. Zhang, S. Jin, Y. Gan, P.C. Wang, S. He, X. Zhang, X.J. Liang, Size-dependent localization and penetration of ultrasmall gold nanoparticles in cancer cells, multicellular spheroids, and tumors in vivo, ACS Nano. 6 (2012) 4483–4493.

[22]   Y. Wang, Z. Wang, C. Xu, H. Tian, X. Chen, A disassembling strategy overcomes the EPR effect and renal clearance dilemma of the multifunctional theranostic nanoparticles for cancer therapy, Biomaterials. 197 (2019) 284–293.

[23]   H. Soo Choi, W. Liu, P. Misra, E. Tanaka, J.P. Zimmer, B. Itty Ipe, M.G. Bawendi, J. V. Frangioni, Renal clearance of quantum dots, Nature Biotechnology. 25 (2007) 1165–1170.

[24]   H. Maeda, The 35th anniversary of the discovery of EPR effect: a new wave of nanomedicines for tumor-targeted drug delivery—personal remarks and future prospects, J Pers Med. 11 (2021) 229.

[25]   Y. Wang, M.J. van Steenbergen, N. Beztsinna, Y. Shi, T. Lammers, C.F. van Nostrum, W.E. Hennink, Biotin-decorated all-HPMA polymeric micelles for paclitaxel delivery, Journal of Controlled Release. 328 (2020) 970–984.

[26]   S.G. Weissberg, R. Simba, S. Rothman, Viscosity of dilute to moderately concentrated polymer solutions, Polymer. 47 (1951) 298–314.

[27]   M.L. Huggins, The viscosity of dilute solutions of long-chain molecules. IV. dependence on concentration, Journal of the American Chemical Society. 64 (1942) 2716–2718.

3

[28] Y. Shi, R. Van Der Meel, B. Theek, E. Oude Blenke, E.H.E. Pieters, M.H.A.M. Fens, J. Ehling, R.M. Schiffelers, G. Storm, C.F. Van Nostrum, T. Lammers, W.E. Hennink, Complete regression of xenograft tumors upon targeted delivery of paclitaxel via Π-Π stacking stabilized polymeric micelles, ACS Nano. 9 (2015) 3740–3752.

[29] M. Andersson, B. Wittgren, K.G. Wahlund, Accuracy in multiangle light scattering measurements for molar mass and radius estimations, Anal Chem. 75 (2003) 4279–4291.

[30] P. Schuck, Size-distribution analysis of macromolecules by sedimentation velocity ultracentrifugation and Lamm equation modeling, Biophysical Journal. 78 (2000) 1606–1619.

[31] International Community of Harmonization (ICH), Impurities: guideline for residual solvents Q3C (R6), International Conference on Harmonization of Technical Requirements for Registration of Pharmaceuticals for Human Use. 44 (2011) 1–29.

[32] H. Fessi, F. Puisieux, J.P. Devissaguet, N. Ammoury, S. Benita, Nanocapsule formation by interfacial polymer deposition following solvent displacement, International Journal of Pharmaceutics. 55 (1989) 1–4.

[33] T. Jung, A. Breitenbach, T. Kissel, Sulfobutylated poly(vinyl alcohol)-graft-poly(lactide-co-glycolide)s facilitate the preparation of small negatively charged biodegradable nanospheres, Journal of Controlled Release. 67 (2000) 157–169.

[34] M. Beck-Broichsitter, J. Nicolas, P. Couvreur, Solvent selection causes remarkable shifts of the "ouzo region" for poly(lactide-co-glycolide) nanoparticles prepared by nanoprecipitation, Nanoscale. 7 (2015) 9215–9221.

[35] S. Galindo-Rodriguez, E. Allémann, H. Fessi, E. Doelker, Physicochemical parameters associated with nanoparticle formation in the salting-out, emulsification-diffusion, and nanoprecipitation methods, Pharmaceutical Research. 21 (2004) 1428–1439.

[36] C.E. Mora-Huertas, H. Fessi, A. Elaissari, Influence of process and formulation parameters on the formation of submicron particles by solvent displacement and emulsification-diffusion methods: critical comparison, Advances in Colloid and Interface Science. 163 (2011) 90–122.

[37] W. Zhang, D. Dong, P. Li, D. Wang, H. Mu, H. Niu, J. Duan, Novel pH-sensitive polysialic acid based polymeric micelles for triggered intracellular release of hydrophobic drug, Carbohydrate Polymers. 139 (2016) 75–81.

[38] U. Bilati, E. Allémann, E. Doelker, Development of a nanoprecipitation method intended for the entrapment of hydrophilic drugs into nanoparticles, European Journal of Pharmaceutical Sciences. 24 (2005) 67–75.

[39] A. Martin, P. Bustamante, A.H.C. Chun, Physical pharmacy, 4th ed., Waverly International, 1993.

[40] C.M. Hansen, Hansen solubility parameters: a user's handbook, 2nd ed., CRC Press, 2007.

[41] H. He, Y. Ren, Z. Wang, Z. Xie, A pH-responsive poly(ether amine) micelle with hollow structure for controllable drug release, RSC Advances. 6 (2016) 91940–91948.

[42] H. Hinterwirth, S.K. Wiedmer, M. Moilanen, A. Lehner, G. Allmaier, T. Waitz, W. Lindner, M. Lämmerhofer, Comparative method evaluation for size and size-distribution analysis of gold nanoparticles, Journal of Separation Science. 36 (2013) 2952–2961.

[43] X. Xie, Y. Ma, L. Huang, M. Cai, Y. Chen, X. Luo, Effect factors of micelle preparation for a pH-sensitive copolymer containing zwitterionic sulfobetaines, Colloids and Surfaces A: Physicochemical and Engineering Aspects. 468 (2015) 31–39.

[44] M. Beck-Broichsitter, E. Rytting, T. Lebhardt, X. Wang, T. Kissel, Preparation of nanoparticles by solvent displacement for drug delivery: a shift in the "ouzo region" upon drug loading, European Journal of Pharmaceutical Sciences. 41 (2010) 244–253.

[45] M. Bagheri, J. Bresseleers, A. Varela Moreira, O. Sandre, S.A. Meeuwissen, R.M. Schiffelers, J.M. Metselaar, C.F. van Nostrum, J.C.M. van Hest, W.E. Hennink, The effect of formulation and processing parameters on the size of mPEG-b-p(HPMA-Bz) polymeric micelles, Langmuir. 34 (2018) 15495–15506.

[46] M.A. Tomeh, X. Zhao, Recent advances in microfluidics for the preparation of drug and gene delivery systems, Mol Pharm. 17 (2020) 4421–4434.

[47] S. Rezvantalab, M. Keshavarz Moraveji, Microfluidic assisted synthesis of PLGA drug delivery systems, RSC Advances. 9 (2019) 2055–2072.

[48] R. Karnik, F. Gu, P. Basto, C. Cannizzaro, L. Dean, W. Kyei-Manu, R. Langer, O.C. Farokhzad, Microfluidic platform for controlled synthesis of polymeric nanoparticles, Nano Letters. 8 (2008) 2906–2912.

[49] D. Kunz, A. Thurn, W. Burchard, Dynamic light scattering from spherical particles, Colloid & Polymer Science. 261 (1983) 635–644.

[50] S. Ohno, K. Ishihara, S.I. Yusa, Formation of polyion complex (PIC) micelles and vesicles with anionic pH-responsive unimer micelles and cationic diblock copolymers in water, Langmuir. 32 (2016) 3945–3953.

[51] A. Qin, M. Tian, C. Ramireddy, S.E. Webber, P. Munk, Polystyrene-poly(methacrylic acid) block copolymer micelles, Macromolecules. 27 (1994) 120–126.

[52] R.J. Williams, A. Pitto-Barry, N. Kirby, A.P. Dove, R.K. O'Reilly, Cyclic graft copolymer unimolecular micelles: effects of cyclization on particle morphology and thermoresponsive behavior, Macromolecules. 49 (2016) 2802–2813.

[53] C. Ma, P. Pan, G. Shan, Y. Bao, M. Fujita, M. Maeda, Core-shell structure, biodegradation, and drug release behavior of poly(lactic acid)/poly(ethylene glycol) block copolymer micelles tuned by macromolecular stereostructure, Langmuir. 31 (2015) 1527–1536.

[54]   V.T.A. Nguyen, M.-C. De Pauw-Gillet, O. Sandre, M. Gauthier, Biocompatible polyion complex micelles synthesized from arborescent polymers, Langmuir. 32 (2016) 13482–13492.

[55]   S.M. D'Addio, R.K. Prud'homme, Controlling drug nanoparticle formation by rapid precipitation, Advanced Drug Delivery Reviews. 63 (2011) 417–426.

[56]   D. Horn, J. Rieger, Organic nanoparticles in aqueous phase, Angew. Chem. 40 (2001) 4330–4361.

[57]   B.K. Johnson, R.K. Prud'homme, Mechanism for rapid self-assembly of block copolymer nanoparticles, Physical Review Letters. 91 (2003) 118302.

[58]   E. Lepeltier, C. Bourgaux, P. Couvreur, Nanoprecipitation and the "ouzo effect": application to drug delivery devices, Adv Drug Deliv Rev. 71 (2014) 86–97.

[59]   J. Bresseleers, M. Bagheri, C. Lebleu, S. Lecommandoux, O. Sandre, I.A.B. Pijpers, A.F. Mason, S. Meeuwissen, C.F. van Nostrum, W.E. Hennink, J.C.M. van Hest, Tuning size and morphology of mPEG-b-p(HPMA-Bz) copolymer self-assemblies using microfluidics, Polymers (Basel). 12 (2020) 2572.

[60]   P. Yang, P. Pageni, M.P. Kabir, T. Zhu, C. Tang, Metallocene-containing homopolymers and heterobimetallic block copolymers via photoinduced RAFT polymerization, ACS Macro Letters. 5 (2016) 1293–1300.

[61]   J. Arredondo, P. Champagne, M.F. Cunningham, RAFT-mediated polymerisation of dialkylaminoethyl methacrylates in tert -butanol, Polymer Chemistry. 10 (2019) 1938–1946.

[62]   M. Danial, S. Telwatte, D. Tyssen, A. Postma, S. Cosson, G. Tachedjian, G. Moad, A. Postma, Combination anti-HIV therapy: via tandem release of prodrugs from macromolecular carriers, Polym Chem. 7 (2016) 7477–7487.

[63]   S. Mourdikoudis, R.M. Pallares, N.T.K. Thanh, Characterization techniques for nanoparticles: comparison and complementarity upon studying nanoparticle properties, Nanoscale. 10 (2018) 12871–12934.

[64]   M.M. Modena, B. Rühle, T.P. Burg, S. Wuttke, Nanoparticle characterization: what to measure?, Advanced Materials. 31 (2019) 1–26.

[65]   Y. Hu, R.M. Crist, J.D. Clogston, The utility of asymmetric flow field-flow fractionation for preclinical characterization of nanomedicines, Analytical and Bioanalytical Chemistry. 412 (2020) 425–438.

[66]   C.J.F. Rijcken, T.F.J. Veldhuis, A. Ramzi, J.D. Meeldijk, C. van Nostrum, W.E. Hennink, Novel fast degradable thermosensitive polymeric micelles based on PEG-block-poly(N-(2-hydroxyethyl)methacrylamide-oligolactates), Biomacromolecules. 6 (2005) 2343–2351.

[67]   S. Dai, P. Ravi, C.Y. Leong, K.C. Tam, L.H. Gan, Synthesis and aggregation behavior of amphiphilic block copolymers in aqueous solution: di- and triblock copolymers of poly(ethylene oxide) and poly(ethyl acrylate), Langmuir. 20 (2004) 1597–1604.

[68]   L.T.T. Trinh, H.M.L. Lambermont-Thijs, U.S. Schubert, R. Hoogenboom, A. Kjøniksen, Thermoresponsive poly(2-oxazoline) block copolymers exhibiting two cloud points: complex multistep assembly behavior, Macromolecules. 45 (2012) 4337–4345.

[69]   J.L. Cole, J.W. Lary, T. P. Moody, T.M. Laue, Analytical ultracentrifugation: sedimentation velocity and sedimentation equilibrium, Methods in Cell Biology. 84 (2008) 143–179.

[70]   M. Raşa, U.S. Schubert, Progress in the characterization of synthetic (supramolecular) polymers by analytical ultracentrifugation, Soft Matter. 2 (2006) 561–572.

[71]   T.M. Laue, W.F. Stafford, Modern applications of analytical ultracentrifugation, Annual Review of Biophysics and Biomolecular Structure. 28 (1999) 75–100.

[72]   Z. Bedö, E. Berecz, I. Lakatos, Mass, size and shape of micelles formed in aqueous solutions of ethoxylated nonyl-phenols, Colloid & Polymer Science. 265 (1987) 715–722.
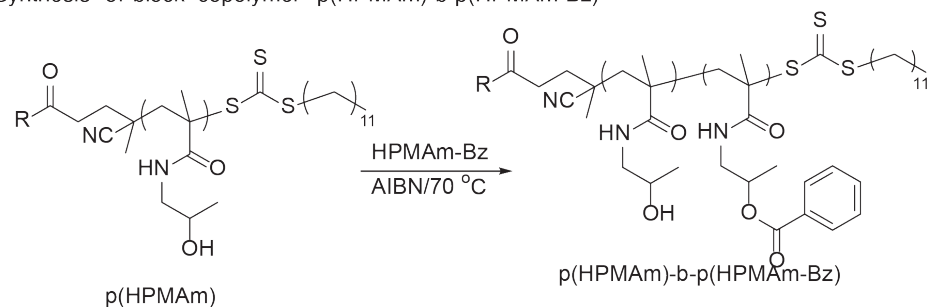
3

Supporting information

Synthesis of p(HPMAm)
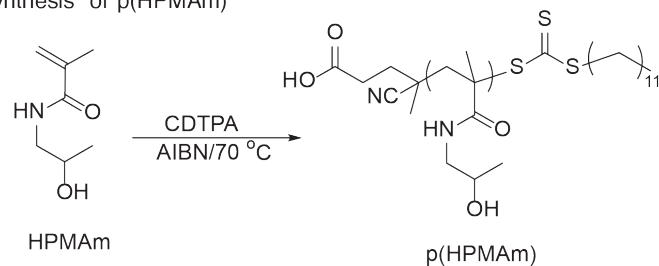
Synthesis of p(HPMAm-Bz)
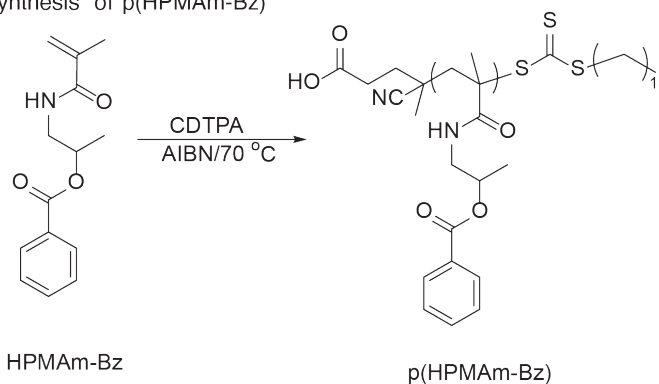
Synthesis of block copolymer p(HPMAm)-b-p(HPMAm-Bz)

Scheme S1. Synthesis of p(HPMAm) and p(HPMAm-Bz), and block copolymer p(HPMAm)-b-p(HPMAm-Bz) by reversible addition–fragmentation chain-transfer (RAFT) polymerization. [1] CDTPA: 4-cyano-4-[(dodecylsulfanylthiocarbonyl)-sulfanyl]pentanoic acid. AIBN: 2,2'-azobis(2-methylpropionitrile).

Table S1. Characterization of p(HPMAm) and p(HPMAm-Bz), and block copolymer p(HPMAm)-b-p(HPMAm-Bz) [1]. For convenience for the reader, those characteristics of the synthesized polymers are shown again.

Entry	Polymers	[M]/[CTA]/[I]	Monomer Conversion (%)	$M_{n, theory}$ (kDa)	$M_{n, NMR}$ (kDa)	$M_{n, GPC}$ (kDa)	PDI
1	p(HPMAm)$_{7.1k}$	460:5:1	51	7.1	–	7.7	1.26
2	p(HPMAm-Bz)$_{4.7k}$	250:5:1	35	4.7	–	4.0	1.25
3	p(HPMAm-Bz)$_{9.2k}$	500:5:1	36	9.2	–	7.8	1.28
4	p(HPMAm-Bz)$_{14.6k}$	900:5:1	32	14.6	–	10.1	1.29
5	p(HPMAm)$_{3.0k}$-b-p(HPMAm-Bz)$_{5.4k}$	250:5:1	36v	7.5	8.4	6.6	1.39
6	p(HPMAm)$_{3.0k}$-b-p(HPMAm-Bz)$_{9.9k}$	500:5:1	39	12.6	12.9	8.7	1.43
7	p(HPMAm)$_{3.0k}$-b-p(HPMAm-Bz)$_{15.6k}$	900:5:1	44	22.5	18.6	10.6	1.55
8	p(HPMAm)$_{4.9k}$-b-p(HPMAm-Bz)$_{6.4k}$	250:5:1	42	10.1	11.3	7.4	1.36
9	p(HPMAm)$_{4.9k}$-b-p(HPMAm-Bz)$_{11.3k}$	500:5:1	38	14.3	16.2	9.2	1.41
10	p(HPMAm)$_{4.9k}$-b-p(HPMAm-Bz)$_{16.8k}$	900:5:1	40	22.8	21.7	10.0	1.41
11	p(HPMAm)$_{7.1k}$-b-p(HPMAm-Bz)$_{4.9k}$	250:5:1	45	12.7	12.0	9.1	1.42
12	p(HPMAm)$_{7.1k}$-b-p(HPMAm-Bz)$_{9.1k}$	500:5:1	39	16.7	16.2	8.5	1.49
13	p(HPMAm)$_{7.1k}$-b-p(HPMAm-Bz)$_{15.0k}$	900:5:1	39	24.9	22.1	11.0	1.48

[M]/[CTA]/[I] = the molar ratio of HPMAm/CDTPA/AIBN, HPMAm-Bz/CDTPA/AIBN, or HPMAm-Bz/p(HPMAm)/AIBN, $M_{n, theory}$ = theoretical number average of molecular weight, $M_{n, NMR}$ = number average of molecular weight determined by ^{1}H NMR analysis, $M_{n, GPC}$ is determined by GPC analysis (DMF containing 10 mM LiCl as eluent, PEGs as standards), PDI = $M_{w, GPC}/M_{n, GPC}$

3

Table S2. Solvent residual in micellar dispersion obtained using different organic solvents as determined by ^{1}H NMR.

Organic solvent	Solvent removal method	Solvent residual determined by ^{1}H NMR (ppm)	Solvent residual limit for human use (ppm) [2]
THF	Evaporation	250 (containing 2000 ppm of DMAc)*	720
Acetone	Evaporation	200 (containing 2000 ppm of DMAc)*	5000
DMAc	Dialysis	150	1090
DMF	Dialysis	150	880
DMSO	Dialysis	160	5000

*The residual of DMAc is because the solvent used for polymer synthesis that was not removed by evaporation due to its high boiling point (165 °C).

Sample: p(HPMAm)$_{7.1k}$-b-p(HPMAm-Bz)$_{15.0k}$
Initial weight: 6.4340 mg
Method: Isothermal at 120 °C for 100 min

TGA
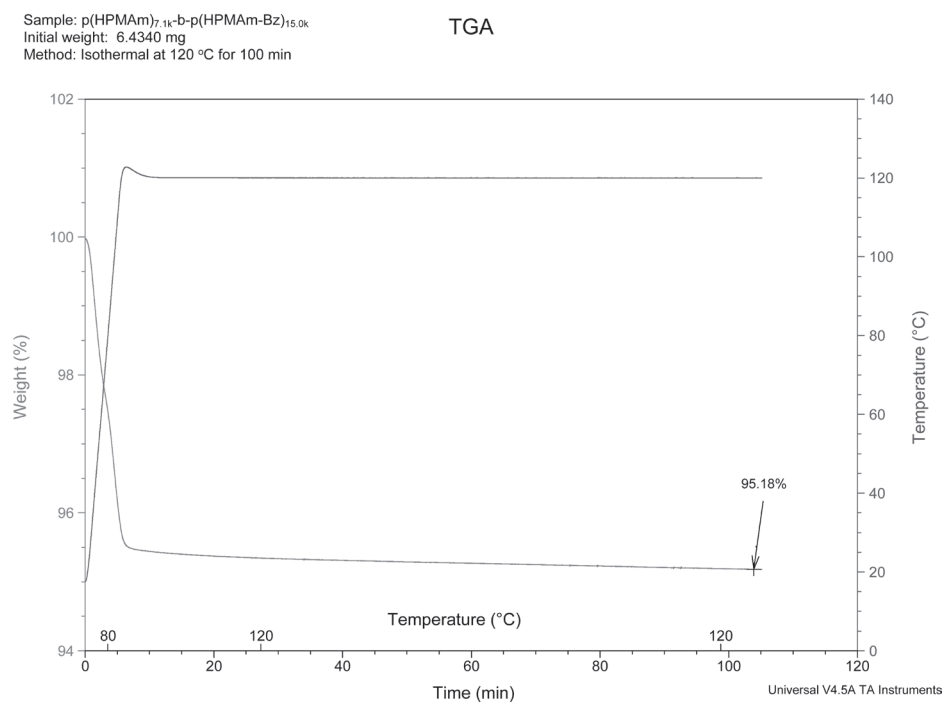
Fig. S1. Thermogravimetric analysis of block copolymer p(HPMAm)$_{7.1k}$-b-p(HPMAm-Bz)$_{15.0k}$ shows the presence of ~5% DMAc.

The extent of polymer partition can be qualitatively described by comparing both solubility parameter difference ($\Delta\delta_{solvent-water}$) and solvent–water interaction parameter ($\chi_{solvent-water}$) using the following equations [3–5]:

$$\Delta\delta_{solvent-water} = \left[\left(\delta_{d,s} - \delta_{d,w}\right)^2 + \left(\delta_{p,s} - \delta_{p,w}\right)^2 + \left(\delta_{h,s} - \delta_{h,w}\right)^2\right]^{1/2}$$

where δ_d is the dispersion force component, δ_p is the polar component, and δ_h is the hydrogen bonding component of the total solubility parameter. Subscripts s and w are corresponded to these partial solubility parameters of the organic solvent and water, respectively.

$$\chi_{solvent-water} = V_s/RT \left(\delta_{solvent} - \delta_{water}\right)^2$$

where V_s is the molar volume of the organic solvent, R is the gas constant (8.314 J·mol^{-1}·K^{-1}), T is absolute temperature (298.15 K), and $\delta_{solvent}$ and δ_{water} are the total solubility parameters of organic solvent and water, respectively.

Table S3. Physicochemical characteristics of the solvents used in the solvent extraction method

Solvent	V_s (mL/mol)	$\Delta_{solvent}$ (MPa$^{1/2}$)	δ_d (MPa$^{1/2}$)	δ_p (MPa$^{1/2}$)	δ_h (MPa$^{1/2}$)	$\Delta\delta_{solvent-water}$ (MPa$^{1/2}$)	$\chi_{solvent-water}$
THF	81.7	19.4	16.8	5.7	8.0	35.8	27.1
Acetone	74.0	20.1	15.5	10.4	7.0	35.7	23.4
DMF	77.0	24.8	17.4	13.7	11.3	31.1	16.9
DMSO	71.3	26.6	18.4	16.4	10.2	32.2	13.4
DMAc	92.5	22.7	16.8	11.5	10.2	32.4	23.9
Water	18.0	48.0	15.5	16.0	42.3	—	—

3
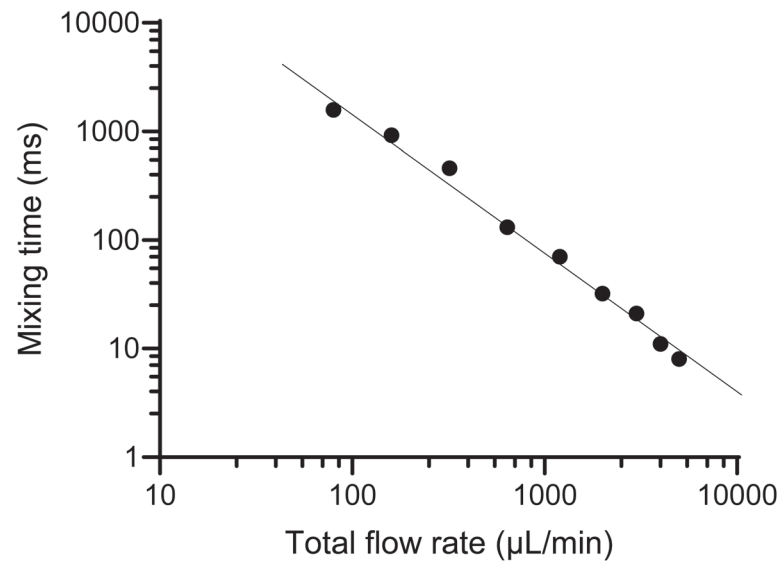
Fig. S2. Mixing time τ_M (ms) of alkaline solution and phenolphthalein pH marker plotted against total flow rate Q_{tot} (µL/min) at 1:1 ratio and extrapolated to the following equation: $\log(\tau_M) = -1.3068 \times \log(Q_{tot}) + 5.8098$. Data were obtained from the datasheet of the manufacturer's website [6].

A

Q_{tot}: 100, 200, 350, 500, 1600 and 3000 µL/min

B

Q_{tot}: 100, 200, 350, 500, 1600 and 3000 µL/min
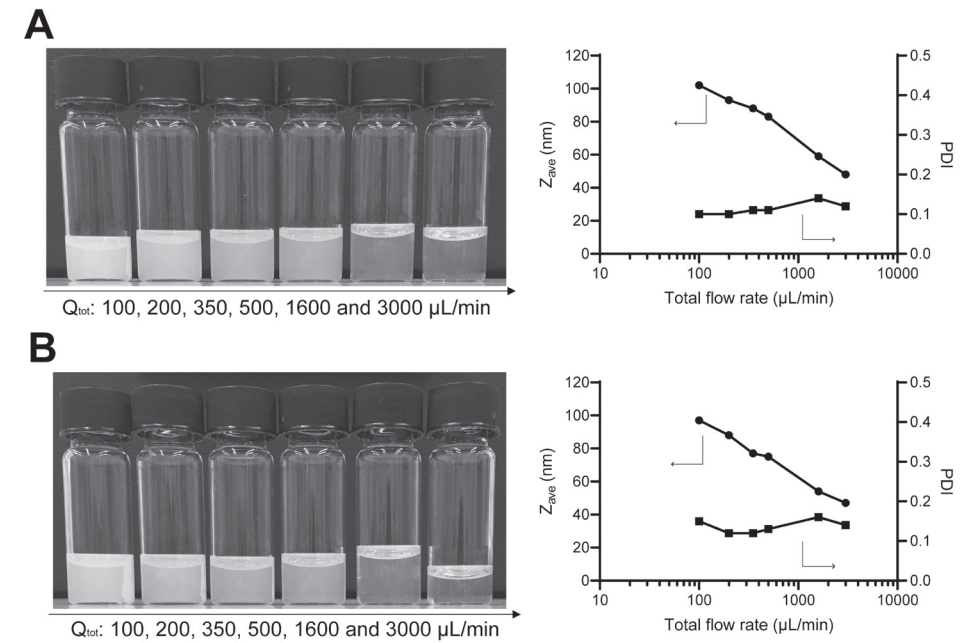
Fig. S3. The effect of mixing time on the size of $p(HPMAm)_{7.1k}$-b-$p(HPMAm-Bz)_{9.1k}$ (**A**) and $p(HPMAm)_{4.9k}$-b-$p(HPMAm-Bz)_{11.3k}$ micelles (**B**).

3

Table S4. Characteristics of p(HPMAm)$_{7.1k}$–b–p(HPMAm-Bz)$_{9.1k}$ and p(HPMAm)$_{4.9k}$–b–p(HPMAm-Bz)$_{11.3k}$ micelles obtained by microfluidics as determined by AF4-MALS.

Polymer	Q_{tot} (µL/min)	τ_M (ms)	$M_{w,mic}$ (10³ kDa)	N_{agg} (10³)	R_g (nm)	R_h (nm)	R_g/R_h
p(HPMAm)$_{7.1k}$–b–p(HPMAm-Bz)$_{9.1k}$	100	1571	75	4.6	33	48	0.69
	200	635	51	3.1	28	44	0.66
	350	306	39	2.3	23	37	0.65
	500	192	33	2.0	22	35	0.63
	1600	42	11	0.6	12	25	0.50
	3000	18	9	0.5	10	21	0.50
p(HPMAm)$_{4.9k}$–b–p(HPMAm-Bz)$_{11.3k}$	100	1571	75	4.6	35	41	0.85
	200	635	45	2.7	21	35	0.61
	350	306	40	2.4	20	32	0.60
	500	192	25	1.5	18	30	0.60
	1600	42	11	0.7	12	22	0.60
	3000	18	8	0.5	11	18	0.60

Q_{tot} = total flow rate, τ_M = mixing time, $M_{w,mic}$ = weight-average molecular weight of micelles determined by AF4-MALS, N_{agg} = the micelle aggregation number calculated by $M_{w,mic}/M_{n,p}$, where $M_{n,p}$ is the molar mass of a single polymer chain determined by ^{1}H NMR, R_g = radius of gyration, R_h = radius of hydration.
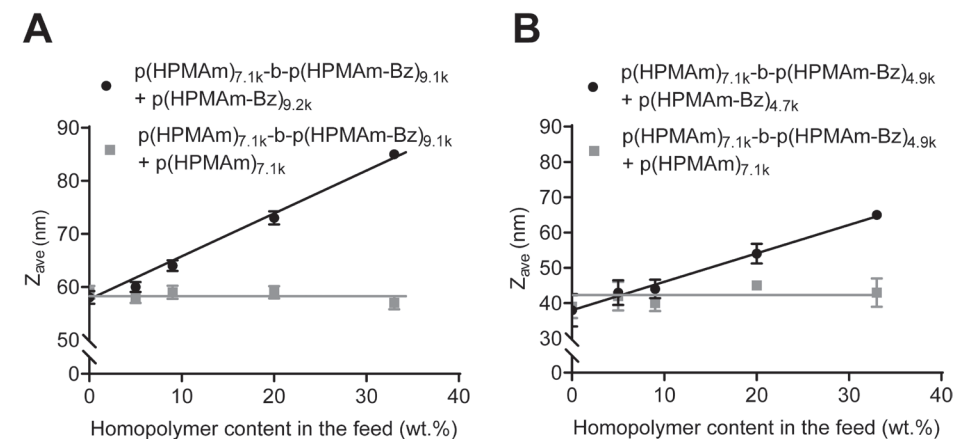
Fig. S4. Effect of the presence of free p(HPMAm)$_{7.1k}$ (gray), p(HPMAm-Bz)$_{9.2k}$ and p(HPMAm-Bz)$_{4.7k}$ homopolymer (black) in the feed on the size of p(HPMAm)$_{7.1k}$–b–p(HPMAm-Bz)$_{9.1k}$ (**A**) and p(HPMAm)$_{7.1k}$–b–p(HPMAm-Bz)$_{4.9k}$ micelles (**B**). (n = 3).

Table S5. Calculation of dn/dc of p(HPMAm-Bz).

Polymer	dn/dc of copolymer (mL/g)	dn/dc of p (HPMAm-Bz)* (mL/g)
p(HPMAm)$_{3.0k}$–b–p(HPMAm-Bz)$_{5.4k}$	0.169	0.221
p(HPMAm)$_{3.0k}$–b–p(HPMAm-Bz)$_{9.9k}$	0.193	0.228
p(HPMAm)$_{3.0k}$–b–p(HPMAm-Bz)$_{15.6k}$	0.216	0.243
p(HPMAm)$_{4.9k}$–b–p(HPMAm-Bz)$_{6.4k}$	0.151	0.209
p(HPMAm)$_{4.9k}$–b–p(HPMAm-Bz)$_{11.3k}$	0.179	0.224
p(HPMAm)$_{4.9k}$–b–p(HPMAm-Bz)$_{16.8k}$	0.201	0.237
p(HPMAm)$_{7.1k}$–b–p(HPMAm-Bz)$_{4.9k}$	0.163	0.290
p(HPMAm)$_{7.1k}$–b–p(HPMAm-Bz)$_{9.1k}$	0.180	0.261
p(HPMAm)$_{7.1k}$–b–p(HPMAm-Bz)$_{15.0k}$	0.194	0.250

*As it is not possible to determine dn/dc of p(HPMAm-Bz) due to the insolubility in aqueous medium, an estimation of the dn/dc value was made by taking into account the molecular weight ratio of two blocks, and dn/dc of homopolymer p(HPMAm) and copolymer as determined by AF4 in table 2. The dn/dc value of p(HPMAm) is 0.0751 mL/g [7]. The average calculated dn/dc value of p(HPMAm-Bz) is 0.24 mL/g, which is within experimental error with that of p(HPMAm-Bz) (0.23 mL/g) calculated from polymer mPEG-b-p(HPMAm-Bz) (n=3, the standard deviation is less than 5%) [8].

3

Table S6. The average diameter of two selected micelles as measured by DLS in comparison with Cryo-TEM.

Micelles	Diameter_DLS (nm)	Diameter_Cryo-TEM (nm)
p(HPMAm)$_{3.0k}$-b-p(HPMAm-Bz)$_{15.6k}$	75	55
p(HPMAm)$_{4.9k}$-b-p(HPMAm-Bz)$_{11.3k}$	56	32

References

[1] Y. Wang, M.J. van Steenbergen, N. Beztsinna, Y. Shi, T. Lammers, C.F. van Nostrum, W.E. Hennink, Biotin-decorated all-HPMA polymeric micelles for paclitaxel delivery, Journal of Controlled Release. 328 (2020) 970–984.

[2] International Community of Harmonization (ICH), Impurities: guideline for residual solvents Q3C (R6), International Conference on Harmonization of Technical Requirements for Registration of Pharmaceuticals for Human Use. 44 (2011) 1–29.

[3] U. Bilati, E. Allémann, E. Doelker, Development of a nanoprecipitation method intended for the entrapment of hydrophilic drugs into nanoparticles, European Journal of Pharmaceutical Sciences. 24 (2005) 67–75.

[4] A. Martin, P. Bustamante, A.H.C. Chun, Physical pharmacy, 4th ed., Waverly International, 1993.

[5] C.M. Hansen, Hansen solubility parameters: a user's handbook, 2nd ed., CRC Press, 2007.

[6] Micromixer chips, (n.d.). https://www.dolomite-microfluidics.com/product-category/microfluidic-components/microfluidic-chips/ (accessed March 24, 2021).

[7] B.S. Tucker, S.G. Getchell, M.R. Hill, B.S. Sumerlin, Facile synthesis of drug-conjugated PHPMA core-crosslinked star polymers, Polymer Chemistry. 6 (2015) 4258–4263.

[8] M. Bagheri, J. Bresseleers, A. Varela Moreira, O. Sandre, S.A. Meeuwissen, R.M. Schiffelers, J.M. Metselaar, C.F. van Nostrum, J.C.M. van Hest, W.E. Hennink, The effect of formulation and processing parameters on the size of mPEG-b-p(HPMA-Bz) polymeric micelles, Langmuir. 34 (2018) 15495–15506.

3

4

Magnetic beads for the evaluation of drug release from biotinylated polymeric micelles in biological media

Yan Wang [1], Marcel H. Fens [1], Nicky C.H. van Kronenburg [2], Yang Shi [3], Twan Lammers [3], Michal Heger [1,4], Cornelus F. van Nostrum [1] and Wim E. Hennink [1]

[1] Department of Pharmaceutics, Utrecht Institute for Pharmaceutical Sciences, Utrecht University, Universiteitsweg 99, 3508 TB Utrecht, the Netherlands

[2] Department of Translational Neuroscience, University Medical Center Utrecht Brain Center, Universiteitsweg 100, 3584 CG Utrecht, the Netherlands

[3] Department of Nanomedicine and Theranostics, Institute for Experimental Molecular Imaging, RWTH Aachen University Clinic, Forckenbecktrasse 55, 52074 Aachen, Germany

[4] Department of Pharmaceutics, Jiaxing Key Laboratory for Photonanomedicine and Experimental Therapeutics, College of Medicine, Jiaxing University, Jiaxing 314001, Zhejiang, P. R. China

Abstract

To improve the reliability of *in vitro* release studies of drug delivery systems, we developed a novel *in vitro* method for the evaluation of drug release from polymeric micelles in complex biological media. Polymeric micelles based on poly(*N*-2-hydroxypropyl methacrylamide)-block-poly(*N*-2-benzoyloxypropyl methacrylamide) (p(HPMAm)-b-p(HPMAm-Bz)) of which 10% of the chains was functionalized with biotin at the p(HPMAm) terminus were prepared using a solvent extraction method. The size of the micelles when loaded with a hydrophobic agent, namely paclitaxel (a clinically used cytostatic drug) or curcumin (a compound with multiple pharmacological activities), was around 65 nm. The biotin decoration allowed the binding of the micelles to streptavidin-coated magnetic beads which occurred within 10 min and reached a binding efficiency of 90 ± 6%. Drug release in different media was studied after the magnetic separation of micelles bound to the streptavidin-coated beads, by determination of the released drug in the media as well as the retained drug in the micellar fraction bound to the beads. The *in vitro* release of paclitaxel and curcumin at 37 °C in PBS, PBS containing 2% v/v Tween 80, PBS containing 4.5% w/v bovine serum albumin, mouse plasma, and whole mouse blood was highly medium-dependent. In all media studied, paclitaxel showed superior micellar retention compared to curcumin. Importantly, the presence of serum proteins accelerated the release of both paclitaxel and curcumin. The results presented in this study show great potential for predicting drug release from nanomedicines in biological media which in turn is crucial for their further pharmaceutical development.

Introduction

Polymeric micelles are widely investigated for their potential to incorporate a wide range of poorly water-soluble drugs to improve safety and therapeutic efficacy [1–4], and several formulations have been approved for clinical use in cancer therapy, e.g., the Cremophor-free based formulation of paclitaxel, in particular, Genexol-PM and Apealea [5]. Polymeric micelles are appreciated to *i)* protect the encapsulated drug against degradation and metabolic conversion upon administration, *ii)* prolong blood circulation and tumor accumulation, *iii)* release the drug in a sustained and controlled manner at specific systemic sites, and ultimately, *iv)* increase the therapeutic index of hydrophobic drugs. *In vitro* stability and drug release studies (also called dissolution kinetics) are key parameters in the (pre-)clinical evaluation of nanomedicines.

Present drug release assays for nanocarriers are commonly performed using separation or dialysis methods [6–8]. In the separation method, nanoparticles are dispersed in release media and incubated under constant agitation at physiological temperature. The media with the released drug are subsequently separated from the nanoparticles using centrifugation, size-exclusion chromatography (SEC), or field-flow fractionation (FFF). However, the complete separation of the nano-sized particles from the release media is challenging, particularly in complex media such as blood, leading to inaccurate determination of the released drugs. In the dialysis method, nanoparticles are transferred into a dialysis bag containing a certain release medium. The nanoparticles are retained in the dialysis bag, whereas the released drug diffuses through the dialysis membrane to the external phase containing the same release medium that is frequently sampled for quantitative analysis of the drug concentration. The dialysis membrane itself functions as a diffusion barrier, however, precipitation of released drugs in the bag and adsorption to the bag may occur. Consequently, the amount of drug determined in the bulk solution does not properly reflect the release profile of the investigated nanoformulation [9,10].

Besides the type of release assay, the selection of appropriate release media is also an important consideration. Phosphate buffered saline (PBS) is the most used medium for drug release studies. However, to maintain sink conditions, defined as the volume of the selected medium which can dissolve at least three to ten times the amount of drugs present in the dosage form [11], an exceedingly large volume of buffer or addition of surfactants is required to solubilize the released hydrophobic drugs. The former makes drug quantification difficult due to the low concentration [12], and the latter might destabilize polymeric micelles resulting in misleading release profiles [13,14]. Moreover, the mentioned *in vitro* assays fail to predict *in vivo* retention due to the complexity of the physiological media such as plasma and

blood. For instance, the presence of plasma proteins and cells or the formation of the protein corona might act as a sink or barrier for the released drug [15–20].

In the present study, a novel *in vitro* assay based on biotin-streptavidin interaction was developed and validated. Biotinylated polymeric micelles loaded with paclitaxel and curcumin were employed for evaluation of their release properties in different media. Micelles based on poly(*N*-2-hydroxypropyl methacrylamide)-block-poly(*N*-2-benzoyloxypropyl methacrylamide) (p(HPMAm)-b-p(HPMAm-Bz)) were selected because of their good stability and drug loading capacity [21,22]. Biotin, also known as vitamin B7, binds to biotin receptors, which are (over)expressed by certain cells, such as lung cancer cells [23], and when decorated on the micelle surface, it can thus potentially be used as a targeting ligand. Moreover, biotin binds to the protein streptavidin with high affinity [23]. Therefore, in the present study, this strong interaction was exploited to capture drug-loaded biotinylated micelles from media (from PBS to whole mouse blood) using streptavidin-coated magnetic beads. This method allows determining simultaneously both the amount of drug released in the different media as well as the amount of drug still retained in the micelles. Overall, this study aimed to validate the novel *in vitro* release method based on biotinylated polymeric micelles loaded with paclitaxel and curcumin using streptavidin-coated magnetic beads to get insights into the drug retention capability of micelles in biological fluids.

Materials and Methods

Materials

Streptavidin-coated magnetic beads (cat# BM551) dispersed in phosphate-buffered saline (pH = 7.5) containing 0.1% bovine serum albumin with EDTA and sodium azide were purchased from Bangs labs (Fishers, IN, USA). The characteristics are given by the supplier as follows, mean diameter = 1.5 μm, binding capacity = 2 μg biotin per 1 mg beads, and particle concentration = 5 mg/mL. Paclitaxel (PTX, cat# P9600) was supplied by LC labs (Woburn, MA, USA). Curcumin (cat# C7727), bovine serum albumin (BSA, cat# A7030, fatty acid-free), and HEPES (4-(2-hydroxyethyl)-1-piperazineethanesulfonic acid, cat# H7006) were purchased from Sigma-Aldrich (Zwijndrecht, the Netherlands), and dimethylformamide (DMF, cat# 041933) and acetonitrile (ACN, cat# 012013) were from Biosolve (Valkenswaard, the Netherlands). RC membrane syringe filters (0.45 μm, cat# AF0-2123-51) were supplied by Phenomenex (Utrecht, the Netherlands). Magnetic rack (DynaMag-2 Magnet, cat# 12321D), Spectra/Por dialysis membrane (MW 6–8 kDa, cat# 11495839), and phosphate-buffered saline (PBS, pH = 7.4, containing 11.9 mM phosphate, 137 mM sodium chloride, and 2.7 mM potassium chloride, cat# BP2438-20) were purchased from Thermo Fisher Scientific (Landsmeer, the Netherlands).

Polysorbate 80 (Tween 80, cat# T164-500) was ordered from Fisher Scientific (Loughborough, Leicestershire, UK). Block copolymers p(HPMAm)-b-p(HPMAm-Bz) with or without biotin conjugated to the p(HPMAm) terminus, as well as Cy3-labeled block copolymers, were synthesized and characterized as previously reported (characteristics given in Table S1) [21]. Mouse blood from C57BL/6J mice was collected into EDTA-containing (0.184 M) tubes and plasma was prepared by centrifugation at 1000 g for 15 min at 4 °C.

Preparation and characterization of biotinylated polymeric micelles

Empty biotinylated p(HPMAm)-b-p(HPMAm-Bz) micelles co-labeled with Cy3 were prepared by a solvent extraction method [21]. In detail, 20 mg of polymers, comprising nonbiotinylated polymer (entry 1 in Table S1), biotinylated polymer (0, 2.5, 5, 10, 15, and 20 %, respectively; entry 2 in Table S1) and Cy3-labeled polymer (2.5 %; entry 3 in Table S1) were dissolved in 1 mL of DMF. Subsequently, the polymer solution was transferred into 1 mL of Milli-Q water while stirring for 1 min. DMF was subsequently removed by dialysis in a Spectra/Por dialysis membrane with a molecular weight cutoff of 6–8 kDa followed by filtration through a 0.45 μm RC membrane syringe filter.

Drug-loaded biotinylated p(HPMAm)-b-p(HPMAm-Bz) micelles were prepared using the same method as for the empty micelles. In brief, 18 mg of nonbiotinylated polymer (entry 1 in Table S1), 2 mg of biotinylated polymer (entry 2 in Table S1), and drug (0.6 or 2 mg of PTX, or 2 mg of curcumin) were dissolved in 1 mL DMF. Micelles were formed and dialyzed as described above for empty micelles.

The size of the obtained biotinylated polymeric micelles was determined by dynamic light scattering (DLS) after 10-fold dilution in water at 25 °C using a Zetasizer Nano S 173 (Malvern Instruments, Malvern, Worcestershire, UK). The Z-average diameter (Z_{ave}) and polydispersity index (PDI) were calculated by the Zetasizer software v.7.13. The zeta-potential of the biotinylated micelles was measured after 10-fold dilution in 10 mM HEPES buffer, pH = 7.4, using a Zetasizer Nano Z (Malvern Instruments).

To determine the amount of the loaded drug, the micellar aqueous dispersions were diluted 10-fold with ACN to destabilize the micelles, and the dissolved PTX or curcumin was subsequently quantified by HPLC (Waters Alliance System). HPLC methods for the detection and quantification of these two compounds can be found in section 1 of the Supporting Information (SI). The encapsulation efficiency (EE) and loading capacity (LC) were calculated by the following formulas:

$$\text{EE}(\%) \ = \ \frac{\text{weight of loaded drug}}{\text{weight of drug used for loading}} \times 100\%$$

$$\text{LC}(\%) \ = \ \frac{\text{weight of loaded drug}}{\text{weight of loaded drug} + \text{weight of loaded polymer}} \times 100\%.$$

The concentration of the micelles was measured by thermogravimetric analysis (TGA) using a TA instrument Q50 (Waters, Milford, MA, USA). In detail, 50 μL of homogenized micelle dispersion was transferred into a tared aluminum pan, followed by heating from 20 to 120 °C at 20 °C/min with an isothermal hold time of 100 min. The maximum temperature was far below the degradation temperature of PTX (220 °C) and curcumin (180 °C) [24,25]. A sample of dry polymer, analyzed for comparison, displayed no mass loss, indicating the stability of p(HPMAm)-b-p(HPMAm-Bz) up to 120 °C.

Binding kinetics and binding efficiency of biotinylated polymeric micelles to streptavidin-coated magnetic beads

To determine the binding kinetics of biotinylated micelles on streptavidin-coated magnetic beads, nine aliquots of 13 μL of biotinylated micelles labeled with Cy3 (prepared as described above weight fraction of biotinylated polymer was 10%), corresponding to nine different time points, were mixed with 55 μL prewashed beads suspension dispersed in 117 μL of PBS resulting in a molar ratio of streptavidin/biotin (S/B) of 1.3:1. Nonbiotinylated micelles were used to study possible nonspecific binding to the beads. Subsequently, the mixtures were incubated under constant agitation for 0.5 (set as 100% fluorescence signal), 5, 10, 20, 30, 60, 120, 240, and 960 min at 4 °C. The incubation temperature was chosen to avoid any preliminary drug release from the micelles. Next, the samples were placed in a magnetic rack for 1 min resulting in forced sedimentation of the beads. The supernatants were collected and diluted with DMF (1:1, v/v) for fluorescence measurement with excitation and emission wavelengths of 555 and 570 nm, respectively (model FP-8300, JASCO, Hachioji-shi, Tokyo, Japan). To the bead fractions, 130 μL of DMF was added to destabilize the captured biotinylated micelles, and an equal volume of PBS was added prior to fluorescence measurement. The Cy3 fluorescence signals in the supernatant and the bead fraction were taken as the amount of the unbound and bound micelles, respectively. A calibration curve was obtained by diluting Cy3-labeled biotinylated micelles in DMF/PBS (1:1, v/v) at concentrations between 10 to 400 μg/mL.

To determine the binding efficiency of biotinylated micelles to streptavidin-coated magnetic beads, nine aliquots of 13 μL of Cy3-labeled micelles with different weight fractions of the biotinylated block copolymers (0, 2.5, 5, 10, 15, and 20%, respectively), corresponding to nine different amount of beads in the tubes, were mixed with 0 (set as 100% fluorescence signal), 5, 15, 25, 35, 45, 55, 65, and 75 μL prewashed beads suspension in 117 μL of PBS, corresponding to molar ratios of streptavidin/biotin ranging from 0 to 7, respectively, followed by incubation under constant agitation for 10 min at 4 °C. Subsequently, the different samples were placed in a magnetic rack for 1 min, and the amount of free and captured biotinylated micelles was determined by fluorescence measurement of the supernatant and beads fraction.

In vitro drug release from biotinylated polymeric micelles associated with streptavidin-coated magnetic beads

The release study was conducted using drug-loaded biotinylated micelles in five different media, namely PBS, PBS containing 2% v/v Tween 80, PBS containing 4.5% w/v fatty acid-free BSA, mouse plasma, and whole mouse blood. Tween 80 is a surfactant that can solubilize the released compound and therefore act as a sink for hydrophobic compounds in aqueous environments. PTX solubility in PBS containing 2% v/v Tween 80 was reported to be 70 μg/mL (>210× the solubility in PBS) [26], whereas curcumin solubility in PBS/2% v/v Tween 80 was measured to be 28 μg/mL (>2500× solubility in PBS) [27]. In the release assay, the selected volume of PBS/2% Tween 80 (240 μL for 10% drug feed) was sufficient to solubilize the entire dose of PTX (4.8 ± 0.1 μg) and curcumin (4.9 ± 0.1 μg) present in the micellar formulation. Albumin is a transporter/solubilizer for a great variety of both endogenous ligands such as fatty acids and drugs including paclitaxel and curcumin [28–30], and therefore fatty acid-free BSA was used to solubilize the released drug and thus maintain sink conditions. Since one albumin contains two PTX/curcumin-binding sites [29,31], the molar ratio of albumin/drug used in this assay was more than sufficient to solubilize the dose of drug initially present in the micelles (Table S2).

The release of the drugs was studied as follows: 9 aliquots of 13 μL of drug-loaded micelles containing 10% biotinylated polymers (3 or 10% PTX feed, or 10% curcumin feed), corresponding to nine different time points, were mixed with 55 μL prewashed beads which were dispersed in 117 μL of PBS (Fig. 2). After constant agitation for 10 min at 4 °C, the tubes were placed in a magnetic rack for 1 min causing the beads to move to one side of the Eppendorf tubes. The supernatants, possibly containing non-bound micelles and non-encapsulated drugs, were discarded. Predetermined volumes of release medium PBS, PBS/Tween 80, PBS/BSA, mouse plasma, and whole mouse blood (240 μL for 10% drug feed, 130 μL for 3% drug feed) were added to the beads and the samples were subsequently incubated at 37 °C under constant agitation. After 0.5 (set as 100% drug content), 15, 30, 60, 120, 240, 360, 1440, and

2880 min, sample tubes were placed in a magnet rack for 1 min. The supernatants containing the released drug were collected and diluted with ACN (1:1, v/v). In the case of serum protein-containing media (PBS/BSA, mouse plasma, and mouse blood), the precipitated albumin and/or other plasma proteins were centrifuged at 12000 g for 10 min prior to HPLC analysis. The method was validated by spiking PBS/BSA, mouse plasma, and whole mouse blood with known amounts of drugs, followed by precipitation of proteins and determination of the amounts of drugs in the supernatants. Full recovery of the added drug was achieved in all media (Table S3). Next, 130 µL of ACN was added to the bead fractions containing the bound micelles plus their retained drug content, to destabilize the micelles. Finally, the drug concentrations were quantified by HPLC analysis. The amounts of drugs in the release media and the bead fractions were taken as the percentage of drug release and drug retention, respectively. The HPLC methods for the detection and quantification of paclitaxel and curcumin can be found in the SI. Each experiment was repeated three times and data are given as the average values based on these three independent measurements.

Results and Discussion

Characterization of empty and drug-loaded biotinylated polymeric micelles

Empty biotinylated micelles were prepared by solvent extraction using DMF as a solvent for p(HPMAm)-b-p(HPMAm-Bz) with or without biotin at the p(HPMAm) terminus and water as non-solvent. Table 1 shows that the hydrodynamic diameter of the obtained micelles containing different percentages of the biotinylated polymer ranged between 62 and 77 nm with a low polydispersity (PDI ≤ 0.14), demonstrating a small size distribution. The micelles had a negative zeta potential at pH = 7.4, which is attributed to the carboxylic acid group at the terminal end of the polymer chains that is deprotonated at the measurement conditions (pH = 7.4, Fig. S2). The zeta potential of the micelles became less negative from -16.2 ± 0.5 to -9.0 ± 0.7 mV with an increasing weight fraction of biotinylated block copolymer from 0 to 20%, which most likely can be ascribed to the loss of carboxyl groups upon biotinylation.

Table 1. Physicochemical characteristics of empty micelles [a]

Weight fraction of biotinylated block copolymer (%)	Z_{ave} (nm)	PDI	Zeta potential (mV)
0	70 ± 3	0.13 ± 0.02	-16.2 ± 0.5
2.5	63 ± 5	0.14 ± 0.01	-14.2 ± 0.3
5	62 ± 6	0.14 ± 0.01	-14.0 ± 0.1
10	65 ± 2	0.13 ± 0.01	-13.9 ± 0.2
15	77 ± 4	0.10 ± 0.01	-12.9 ± 0.4
20	75 ± 6	0.13 ± 0.01	-9.0 ± 0.7

[a] Data are presented as mean ± SD of three independently prepared batches.

Table 2 shows that 10% biotinylated micelles loaded with different feeds of either PTX or curcumin exhibited similar sizes and polydispersity (~65 nm with PDI ≤ 0.14). The micelles showed good encapsulation efficiency (79 ± 4%) and loading capacity (2.6 ± 0.1%) at 3% feed of PTX, whereas the encapsulation efficiency was 51 ± 1% at 10% PTX feed, resulting in a loading capacity of 6.1 ± 0.1%. On the other hand, curcumin was more efficiently loaded in the core of the biotinylated micelles at 10% feed with a high encapsulation efficiency (82 ± 6%) and a loading capacity of 9.0 ± 0.1%. These results are in line with previous studies, in which PTX and curcumin were loaded with high encapsulation efficiency into structurally related micelles based on poly(ethylene glycol)-b-p(HPMAm-Bz) polymers [6,19,32,33].

Table 2. Physicochemical characteristics of drug-loaded biotinylated micelles [a]

Drug and feed	Z_{ave} (nm)	PDI	EE (%)	LC (%)
PTX, 3%	65 ± 1	0.10 ± 0.01	79 ± 4	2.6 ± 0.1
PTX, 10%	65 ± 5	0.14 ± 0.01	51 ± 1	6.1 ± 0.1
Curcumin, 10%	62 ± 1	0.09 ± 0.01	82 ± 6	9.0 ± 0.1

[a] Data are presented as mean ± SD of three independently prepared batches.

Binding properties of biotinylated polymeric micelles

The binding kinetics and binding efficiency of Cy3-labeled biotinylated polymeric micelles with streptavidin-coated magnetic beads were investigated. Our previous study revealed the binding ability of the micelles containing 10% biotinylated polymers by cells that overexpress biotin receptors [21], demonstrating that the biotin groups are exposed at the p(HPMAm) shell of the micelles. Therefore, as expected and shown in Fig. 1A, biotinylated micelles also bound to the streptavidin-coated beads and reached equilibrium within 10 min. This resulted in binding of 90 ± 6% micelles at a molar ratio of streptavidin/biotin (S/B) 1.3:1. Importantly, nonbiotinylated micelles did not show any affinity for the beads upon incubation up to 960 min under the same conditions (Fig. S3), nor with increasing amount of streptavidin beads (Fig. S4), confirming that observed binding of the biotinylated micelles indeed occurred through biotin-streptavidin interactions.
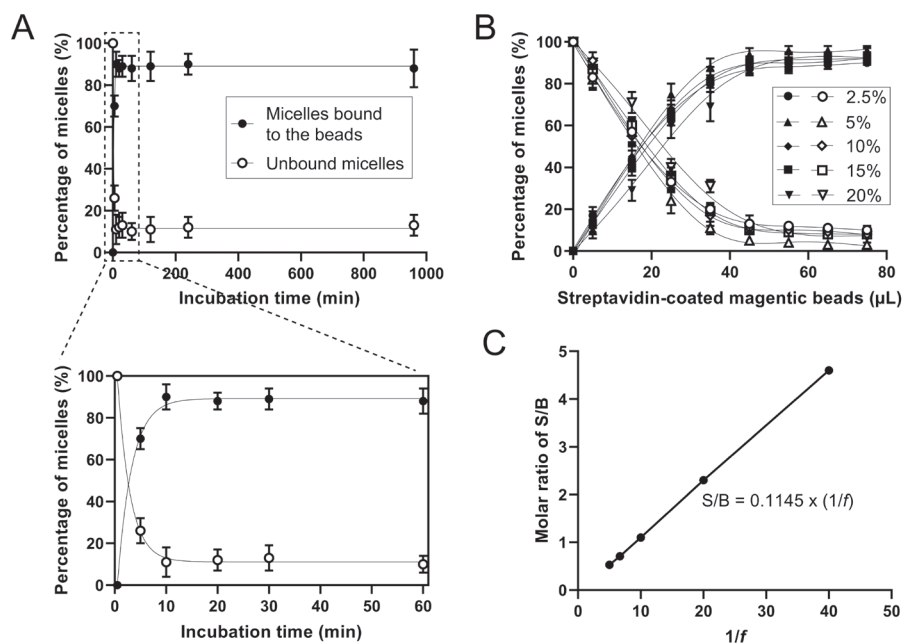

Previous publications have demonstrated that <25% biotin coverage of the surface of polymeric micelles exhibited good surface accessibility and efficient cellular uptake through binding to the biotin receptor [34–37]. Therefore, the weight fraction of biotinylated polymer in the Cy3-labeled micelles was tuned from 2.5 to 20%. Fig. 1B shows that the amounts of bound micelles increased with increasing amounts of beads added to a fixed concentration of micelles. Surprisingly, this was independent of the degree of biotinylation. As shown in Fig. 1C, S/B was linearly related to $1/f$, in which f is the fraction of biotinylated polymers in micelles. As pointed out in section 2 in the Supporting Information, this corresponds to a model in which the surface coverage of the beads by the micelles is indeed independent of the percentage of biotin on the micelles. According to this model, the molar ratio of streptavidin to biotin (S/B) was 0.11. Sleiman *et al.* reported the application of streptavidin-coated magnetic beads in the quantification of biotin accessibility on the surface of PEGylated luminescent iridium micelles [38]. In their study, a biotinylated PEG-based triblock copolymer was synthesized, and each polymer has on average one biotin unit at the terminal end and thus these micelles were composed of 100% biotinylated polymers. In that case, 24 µg of biotinylated triblock polymer (M_n 20400) was bound to 1 mL beads (1 mg/mL, containing 0.125 µM streptavidin). Therefore, 1.18 nmol biotinylated polymer (or biotin) was bound to 0.125 nmol streptavidin. The experimental S/B ratio was 0.125/1.18 = 0.11, which is in excellent agreement with our value. In our study, the number of streptavidin units that are covered by each micelle is equal to 0.11 × N_{agg} = ~90, assuming an aggregation number (N_{agg}) of 800 [22]. The surface of a projected circle with a diameter of 70 nm is 3848 nm^2 which covers those 90 streptavidin molecules, which in turn equals ~42 nm^2 per streptavidin molecule assuming that the surface of the beads is fully covered with streptavidin. This corresponds to a diameter of 7.3 nm for one streptavidin molecule, which is close to the previously reported size of streptavidin (4.2×4.2×5.6 nm) [39].

Fig. 1. Binding of biotinylated micelles to streptavidin-coated magnetic beads. (**A**) Binding kinetics of micelles (with 10% biotinylated polymers) at 4 °C in PBS at S/B = 1.3:1 mol/mol. Data are presented as mean ± SD of three independent replicates. (**B**) Binding efficiency of micelles upon incubation with increasing volume of streptavidin-coated magnetic beads (added from a stock solution 5 mg/mL) for 10 min at 4 °C in 117 mL PBS. The concentration of micelles was constant, whereas the weight fractions of biotinylated block copolymer were varied. Closed symbols represent the percentage of biotinylated micelles bound to the beads, and open symbols represent the percentage of unbound micelles. (**C**) The molar ratio of streptavidin/biotin (S/B) as a function of $1/f$, where f is the fraction of biotinylated polymers in micelles.
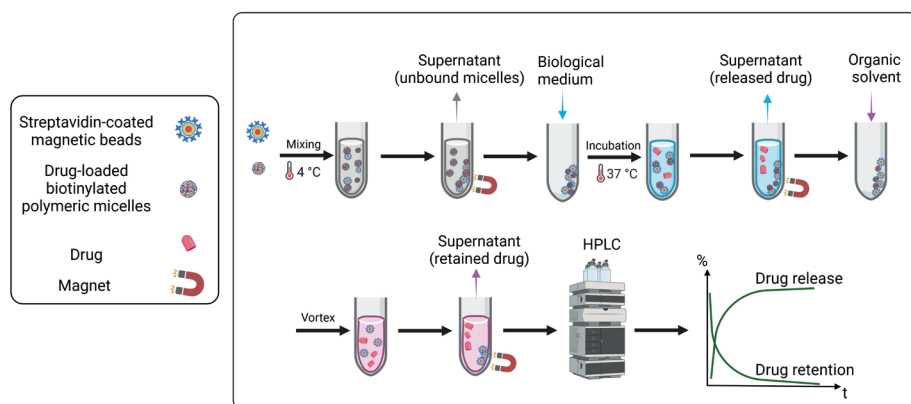
Fig. 2. Schematic illustration of the developed method to study *in vitro* drug release of drugs from polymeric micelles in complex biological media, using biotinylated micelles and streptavidin-coated magnetic beads. The figure was created using BioRender (https://biorender.com/).

Drug release from biotinylated polymeric micelles

To confirm that polymeric micelles do not dissociate in the release media nor fuse with components of the media, PBS, PBS containing 2% v/v Tween 80, and 4.5% w/v fatty acid-free BSA were incubated with drug-loaded biotinylated micelles at 37 °C for 48 h. The size of micelles was not changed as measured by DLS and Tween micelles (± 20 nm) and BSA (± 6 nm) were detected as separate peaks (Fig. S5). As shown in Fig. 2, the drug-loaded micelles were pre-captured by the beads after incubation at 4 °C for 10 min in PBS and subsequent collection by a magnetic rack. PBS was then discarded to remove non-encapsulated drug molecules or loosely bound drug-loaded micelles. The PTX and curcumin in the micelles captured by the beads was 90 ± 3% and 89 ± 3% of the initially loaded drug, respectively (Fig. S6), which is consistent with the binding efficiency of micelles to the beads (Fig. 1A). For the release studies, the captured beads containing drug-loaded micelles were resuspended in the release medium and incubated at 37 °C under constant agitation for 48 h.

Release of PTX from biotinylated polymeric micelles

Upon incubation in PBS, the amount of PTX retained in the micelles first dropped during the first 6 h to 82 and 65%, for micelles with 3 or 10% PTX feed, respectively, followed by a slight decrease reaching 72 and 56% after 48-h incubation, respectively (Fig. 3A). After the first 2 h, the release medium contained 15-20% of the loaded PTX, and thereafter no further increase was observed for the

micelles with both 3 and 10% PTX feed. This resulted in a mass balance, which is the sum of released and retained drug, of 70-90% which can likely be ascribed to PTX degradation in the release medium. Representative HPLC chromatograms of free and encapsulated PTX in micelles incubated in PBS/BSA are shown in Fig. S7. Indeed, we found a major degradation peak in the HPLC chromatogram (retention time 6.5 min, UV 227 nm) of released PTX, whereas PTX that was retained in the polymeric micelles was degraded to a lesser extent at the same time interval. This demonstrates that the drug loaded in the hydrophobic core is less degraded than that in the solution, which has been reported previously for other combinations of drugs and polymeric micelles [40–42]. Different from the ~20% PTX release in PBS observed in the current study, it was reported that only 8% of PTX release was observed for mPEG-b-p(HPMAm-Bz) micelles after 48 h incubation in PBS using a centrifugation method [33], supporting that this centrifugation method gives an underestimation of drug release. The novel drug release model can benefit from a dual-parameter metric, i.e., drug release and drug retention. Although the released PTX undergoes degradation in PBS, an accurate release profile can be provided by measuring the drug retention. Moreover, our release method provides additional parameter, i.e., the rate of drug degradation in release medium, which could be useful information in nanoformulation design and application.

As shown in Fig. 3B, 80% of the loaded PTX was released in the medium during the first 4 h incubation in PBS buffer containing 2% v/v Tween 80 as a solubilizer. Thereafter the micelles only showed a slow release of about 2% during the next 44 hours. Analysis of the micelles showed that the remaining ~20% of loaded drugs was detected in the micelles, indeed meaning that the mass balance was around 100%. Compared to our novel release approach, the conventional dialysis method showed similar fast PTX release from π- π stacking polymeric micelles during the first 2 h incubation in PBS/Tween 80 or PBS/Triton X-100, which was followed by a gradual release during the following 7 days [6,43]. As the released PTX does not undergo degradation in PBS/Tween, drug release profile can be accurately obtained from the dual parameter of drug release and retention. Fig. 3B also shows that the observed fast release was independent of the initial drug loading. Similar observations have been previously reported for other PTX formulations upon incubation in PBS/Tween 80 [6,44].

A release of 20–25% of the loaded PTX was seen during the first 4-6 h of incubation of the micelles in PBS containing 4.5% w/v BSA and thereafter further release was hardly observed (Fig. 3C). The same figure also shows that around 65% of PTX loading was retained in the micelles after 4-6 h of incubation. Our novel release method showed a similar PTX release profile from π- π stacking polymeric micelles in PBS/BSA as for the conventional dialysis method [6]. Again, the release profile was not dependent on the initial drug loading (3 and 10%). Further, to prove that

4

drug release is release medium volume-independent, a release study was performed with a fixed volume and concentration of micelles (10% PTX loading) using a 2-fold volume of PBS/BSA. As shown in Fig. 3D, the PTX release and retention profiles were within the experimental error like those in a 2-fold smaller volume of PBS/BSA (Fig. 3C), demonstrating that sink conditions were valid at both conditions.
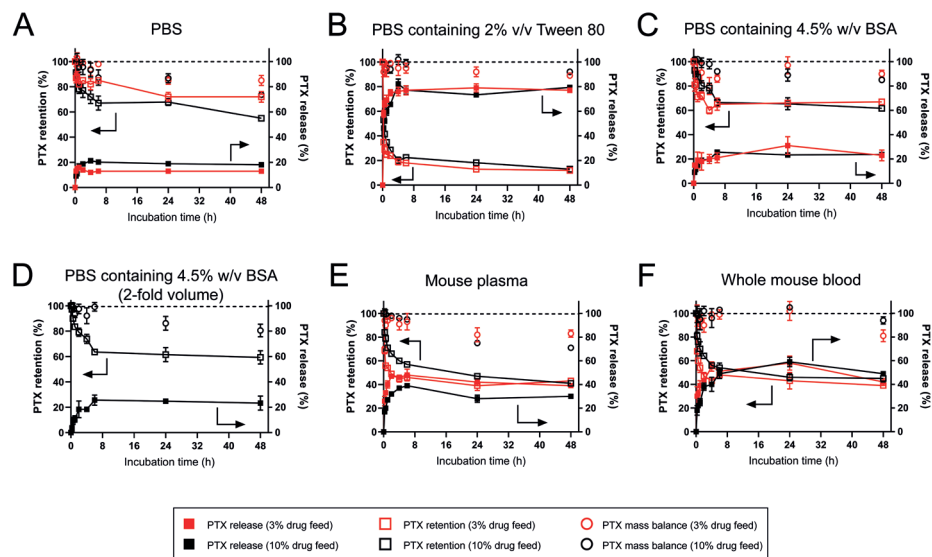

Fig. 3. PTX release and retention profiles. Released and retained PTX were measured (as schematically shown in Fig. 2) by capturing drug-loaded biotinylated micelles with streptavidin-coated magnetic beads from various media upon incubation at 37 °C under constant agitation (in 240 µL medium for 10% PTX feed, 130 µL for 3% PTX feed): (**A**) PBS, (**B**) PBS containing 2% v/v Tween 80, (**C**) PBS containing 4.5% w/w BSA, (**D**) PBS containing 4.5% w/w BSA (2-fold higher volume), (**E**) mouse plasma, and (**F**) whole mouse blood. Filled squares represent released PTX, open squares represent retained PTX, and circles represent the total amount of the measured PTX (= released + retained PTX). Red symbols represent micelles with 3% PTX feed; black symbols represent micelles with 10% PTX feed. The left arrow points to PTX retention; the right arrow points to PTX release. Data are presented as mean ± SD of three independent replicates.

When micelles with 3 and 10% PTX loading were incubated in mouse plasma at 37 °C, the PTX retention decreased to about 50% during the first 6 h, and thereafter gradually decreased to 40% at 48 h. Accordingly, up to 50% of the loaded drug was observed in the release medium during the first 6 h (Fig. 3E). However, during the next 6 to 48 h of incubation, total PTX measured in the medium did not further increase but decreased to 30-45%. Eventually, the total mass balance was around

80% at 48 h for both micelles with 3 and 10% PTX loading, which is likely due to the above-mentioned degradation of PTX.

Fig. 3C and E show that PTX was released faster in mouse plasma than in PBS/BSA. Also, the amount of PTX released is higher in plasma than that in BSA. It has previously been reported that the photosensitizer meta-tetra(hydroxyphenyl) chlorin (mTHPC) was released from benzyl-poly(ε-caprolactone)-b-poly(ethylene glycol) micelles in a medium-dependent manner using asymmetric flow field flow fractionation (AF4) [45]. It was found that the release of mTHPC in human plasma occurred faster and to a higher extent than that in human serum albumin (HSA), likely due to the high affinity of the photosensitizer for specific plasma proteins, i.e., lipoproteins. Kumar *et al.* reported that, PTX, besides to HSA, also binds to alpha 1-acid glycoprotein and lipoprotein [46]. Therefore, the presence of these proteins in mouse plasma may accelerate PTX release as compared to PBS/BSA as a release medium.

Upon incubation in whole mouse blood, independent of the initial loading, around 50% of the loaded PTX was released from the micelles during the first 6 h, and 40-45% of PTX was retained in the micelles after 48 h incubation, resulting in a mass balance of >90% (Fig. 3F). Hence, very similar PTX retention profiles were observed in whole mouse blood and plasma (Fig. 3E & F). However, the amount of PTX measured in whole blood medium was 1.5-fold higher than that in plasma at 24 h-incubation. This discrepancy of PTX released in plasma and whole blood requires further investigation.

Release of curcumin from biotinylated polymeric micelles
Incubation of curcumin-loaded micelles with 10% loading in PBS at 37 °C showed that 50% of the initial amount was still retained in the micelles after 6 h (Fig. 4A). The faster release of curcumin compared to PTX is likely due to less compatibility of curcumin with the hydrophobic core of the micelles. Thereafter the retained curcumin slowly dropped to ~30% during the next 42 hours. However, no released curcumin was detected in PBS, resulting in a mass balance of only 30% at 48 h. Given the near insolubility of curcumin in an aqueous solution and poor stability at pH > 6.5 [47–49], it is plausible that the released curcumin was precipitated and/or degraded. Indeed, we did observe curcumin degradation products (UV 254 nm) in the chromatogram with retention times of 1.50-2.20 min after 48-h incubation (Fig. S8), probably including bicyclopentadione as demonstrated by Naksuriya *et al.* [48].

When PBS was supplemented with 2% v/v Tween 80, loaded curcumin was quantitatively released in the first hour of incubation, and the mass balance was ~100% (Fig. 4B). Obviously, the Tween micelles solubilized the released curcumin and also protected it against degradation which is in line with our previous findings [48].
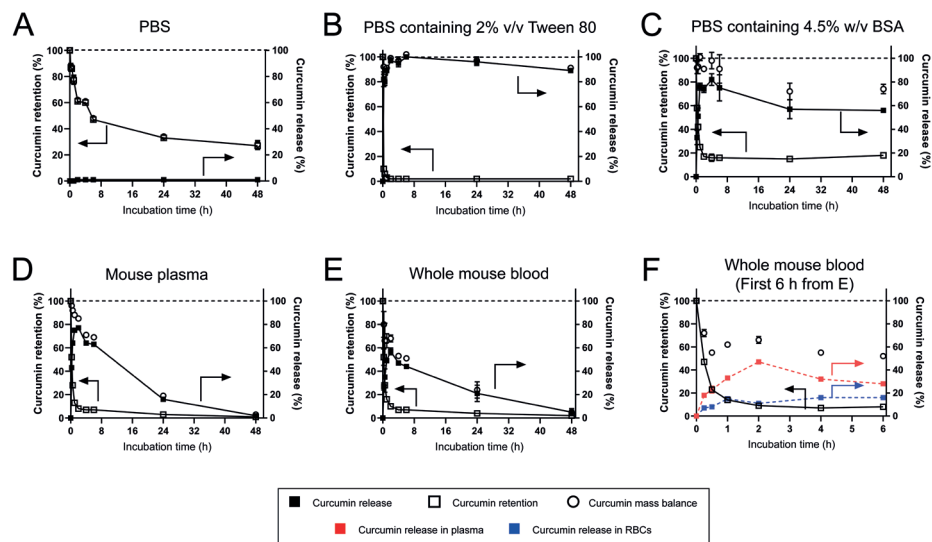
Fig. 4. Curcumin release profiles. Curcumin retention and release were measured in various media by capturing drug-loaded biotinylated micelles with streptavidin-coated magnetic beads upon incubation at 37 °C under constant agitation: (**A**) PBS, (**B**) PBS containing 2% v/v Tween 80, (**C**) PBS containing 4.5% w/w BSA, (**D**) mouse plasma, (**E**) whole mouse blood, and (**F**) first 6 h in whole mouse blood. Filled black squares represent curcumin release, open black squares represent curcumin retention, and black circles represent the total amount of the measured curcumin. The left arrow points to curcumin retention; the right arrow points to curcumin release. Data are presented as mean ± SD of three independent replicates.

Fig. 4C shows that when curcumin-loaded micelles were incubated in PBS containing 4.5% w/v BSA, 80% of the loaded curcumin was rapidly released in the first 1-2 h and 20% of loading was retained in the micelles. This graph also shows that micelles did not release the remaining 20% curcumin whereas the released amount gradually dropped from 80% to 60% after 48 h, leading to a mass balance of ~80%. The gradual drop is likely caused by the degradation of the albumin-bound curcumin. Although one albumin molecule can bind two curcumin molecules and protect curcumin against decomposition [19,50], obviously, the protection of curcumin degradation by albumin is inferior to that of Tween micelles (Fig. 4B & C). Fig. 4D shows that incubation of curcumin-loaded micelles at 37 °C in plasma also showed a rapid release in the first 1-2 h of up to 80% of the loading, and the released curcumin was fully degraded within 48 h. Curcumin degradation peaks with retention times of 1.50-2.20 min at UV 254 nm were observed in the HPLC chromatogram. Around 5% of loaded curcumin was retained in the micelles between 2-6 h of incubation with plasma and at 48 h no curcumin was detected in the micelles. Finally, during

the incubation of curcumin-loaded micelles in whole blood, the same retention profile for curcumin was observed as for plasma (Fig. 4E). It is remarked that the degradation rate of curcumin was faster in whole mouse blood than that in plasma (Fig. 4D & E). By spinning down the blood cells, ~20% of curcumin was observed to be associated with RBCs in the first 6 h-incubation (Fig. 4F), yet the AUC of degradation peaks in RBCs fraction also increased within 6 h. This can be possibly explained by the redistribution of curcumin from the plasma fraction to the RBCs. These results support the instability of curcumin in the presence of albumin and particularly erythrocytes, which is in line with previous reports that curcumin is distributed into, and metabolized by RBCs in a species-dependent manner [51–53]. Our release method provides a useful tool to study the association of released curcumin with erythrocytes, which will provide useful insights for the investigation of the pharmacokinetics and the tissue distribution of curcumin.

These results show that the curcumin release in PBS/Tween > plasma ≈ whole blood > PBS/BSA > PBS within 8 h incubation. The released curcumin was stabilized by albumin to some extent, and a delayed curcumin degradation in PBS/BSA and plasma was seen within 6 h incubation as compared to curcumin released in PBS (Fig. 4A & C), which is in good agreement with a previous publication that the released curcumin from mPEG-b-p(HPMAm-Bz) micelles was subsequently solubilized by albumin as determined by AF4 analysis [19]. Similarly, Wang *et al.* also reported that curcumin degradation was significantly reduced in cell culture medium containing 10% fetal calf serum and in human blood than in 0.1 M phosphate buffer during 8 h incubation [54]. Kee *et al.* revealed that albumin and fibrinogen are responsible for binding curcumin in human plasma, and more importantly, these proteins suppress the hydrolysis of curcumin and thus retard degradation [55].

Conclusion

A new *in vitro* method for studying the release kinetics of water-insoluble drugs from polymeric micelles in complex biological media is described. The proposed "fishing" approach of biotinylated nanoparticles by streptavidin-coated magnetic beads enables the determination of time-dependent drug retention and release (and thus total mass balance) in biological media. Moreover, our results illustrate how inappropriate *in vitro* release media, like PBS and PBS supplemented with solubilization agents such as surfactant or BSA, can lead to underestimated or overestimated drug release kinetics and profiles, and result in a misleading conclusion of drug retention. In this work, we demonstrate that this assay allows studying the release of PTX and curcumin from polymeric micelles in mouse plasma and whole mouse blood *in vitro*. Since biotinylated polymers and lipids can be easily

synthesized and are also commercially available, this novel method can be extended to other biotinylated nanoformulations in a broad range of biological media, e.g., homogenate suspensions of tumor tissues, and loaded with a wide variety of drugs, both of hydrophobic and hydrophilic nature. In conclusion, the further development and application of the magnetic beads-enabled method potentially improves the reliability of the *in vitro* release assay, thereby facilitating high throughput testing of various nanomedicines and reducing the number of animal experiments needed.

References

[1]   D. Hwang, J.D. Ramsey, A. v. Kabanov, Polymeric micelles for the delivery of poorly soluble drugs: from nanoformulation to clinical approval, Adv Drug Deliv Rev. 156 (2020) 80–118.

[2]   A. Varela-Moreira, Y. Shi, M.H.A.M. Fens, T. Lammers, W.E. Hennink, R.M. Schiffelers, Clinical application of polymeric micelles for the treatment of cancer, Mater Chem Front. 1 (2017) 1485–1501.

[3]   H. Cabral, K. Miyata, K. Osada, K. Kataoka, Block copolymer micelles in nanomedicine applications, Chem Rev. 118 (2018) 6844–6892.

[4]   L. Houdaihed, J.C. Evans, C. Allen, Overcoming the road blocks: advancement of block copolymer micelles for cancer therapy in the clinic, Mol Pharm. 14 (2017) 2503–2517.

[5]   P. Mi, K. Miyata, K. Kataoka, H. Cabral, Clinical Translation of Self-Assembled Cancer Nanomedicines, Adv Ther (Weinh). 4 (2021) 2000159.

[6]   M. Sheybanifard, N. Beztsinna, M. Bagheri, E.M. Buhl, J. Bresseleers, A. Varela-Moreira, Y. Shi, C.F. van Nostrum, G. van der Pluijm, G. Storm, W.E. Hennink, T. Lammers, J.M. Metselaar, Systematic evaluation of design features enables efficient selection of Π electron-stabilized polymeric micelles, Int J Pharm. 584 (2020) 119409.

[7]   A. Ranjan, P.K. Jha, Experiments and modeling of controlled release behavior of commercial and model polymer-drug formulations using dialysis membrane method, Drug Delivery and Translational Research. 10 (2020) 515–528.

[8]   M. Ghezzi, S. Pescina, C. Padula, P. Santi, E. del Favero, L. Cantù, S. Nicoli, Polymeric micelles in drug delivery: an insight of the techniques for their characterization and assessment in biorelevant conditions, Journal of Controlled Release. 332 (2021) 312–336.

[9]   M. Yu, W. Yuan, D. Li, A. Schwendeman, S.P. Schwendeman, Predicting drug release kinetics from nanocarriers inside dialysis bags, Journal of Controlled Release. 315 (2019) 23–30.

[10]   S.A. Abouelmagd, B. Sun, A.C. Chang, Y.J. Ku, Y. Yeo, Release kinetics study of poorly water-soluble drugs from nanoparticles: are we doing it right?, Molecular Pharmaceutics. 12 (2015) 997–1003.

[11]   Council of Europe, Chapter 2.9.3 Dissolution test for solid dosage forms, in: European Pharmacopoeia, 8th ed., EDQM, Strasbourg Cedex, France, 2014.

[12]   D.J. Phillips, S.R. Pygall, V.B. Cooper, J.C. Mann, Overcoming sink limitations in dissolution testing: a review of traditional methods and the potential utility of biphasic systems, Journal of Pharmacy and Pharmacology. 64 (2012) 1549–1559.

[13]   S.C. Wang, T.C. Wei, W. Bin Chen, H.K. Tsao, Effects of surfactant micelles on viscosity and conductivity of poly(ethylene glycol) solutions, Journal of Chemical Physics. 120 (2004) 4980–4988.

[14]   S. Myhre, M. Amann, L. Willner, K.D. Knudsen, R. Lund, How detergents dissolve polymeric micelles: kinetic pathways of hybrid micelle formation in SDS and block copolymer mixtures, Langmuir. 36 (2020) 12887–12899.

[15]   S. D'Souza, A review of in vitro drug release test methods for nano-sized dosage forms, Advances in Pharmaceutics. 2014 (2014) 1–12.

[16]   J. Weng, H.H.Y. Tong, S.F. Chow, In vitro release study of the polymeric drug nanoparticles: development and validation of a novel method, Pharmaceutics. 12 (2020) 732.

[17]   Y. Zhao, F. Fay, S. Hak, J. Manuel Perez-Aguilar, B.L. Sanchez-Gaytan, B. Goode, R. Duivenvoorden, C. de Lange Davies, A. Bjørkøy, H. Weinstein, Z.A. Fayad, C. Pérez-Medina, W.J.M. Mulder, Augmenting drug–carrier compatibility improves tumour nanotherapy efficacy, Nature Communications. 7 (2016) 11221.

[18]   V. Gray, S. Cady, D. Curran, J. Demuth, O. Eradiri, M. Hussain, J. Krämer, J. Shabushnig, E. Stippler, D.G. Hunt, In vitro release test methods for drug formulations for parenteral applications, Dissolution Technologies. 25 (2018) 8–13.

[19]   M. Bagheri, M.H. Fens, T.G. Kleijn, R.B. Capomaccio, D. Mehn, P.M. Krawczyk, E.M. Scutigliani, A. Gurinov, M. Baldus, N.C.H. van Kronenburg, R.J. Kok, M. Heger, C.F. van Nostrum, W.E. Hennink, In vitro and in vivo studies on HPMA-based polymeric micelles loaded with curcumin., Mol Pharm. 18 (2021) 1247–1263.

[20]   Z.S. Al-Ahmady, M. Hadjidemetriou, J. Gubbins, K. Kostarelos, Formation of protein corona in vivo affects drug release from temperature-sensitive liposomes, Journal of Controlled Release. 276 (2018) 157–167.

[21]   Y. Wang, M.J. van Steenbergen, N. Beztsinna, Y. Shi, T. Lammers, C.F. van Nostrum, W.E. Hennink, Biotin-decorated all-HPMA polymeric micelles for paclitaxel delivery, Journal of Controlled Release. 328 (2020) 970–984.

[22]   Y. Wang, D.M.E. Thies-Weesie, E.D.C. Bosman, M.J. van Steenbergen, J. van den Dikkenberg, Y. Shi, T. Lammers, C.F. van Nostrum, W.E. Hennink, Tuning the size of all-HPMA polymeric micelles fabricated by solvent extraction, Journal of Controlled Release. 343 (2022) 338–346.

[23]   W.X. Ren, J. Han, S. Uhm, Y.J. Jang, C. Kang, J.S.H. Kim, J.S.H. Kim, Recent development of biotin conjugation in biological imaging, sensing, and target delivery, Chemical Communications. 51 (2015) 10403–10418.

[24]   S. Kenth, J.P. Sylvestre, K. Fuhrmann, M. Meunier, J.C. Leroux, Fabrication of paclitaxel nanocrystals by femtosecond laser ablation and fragmentation, Journal of Pharmaceutical Sciences. 100 (2011) 1022–1030.

[25]   T. Esatbeyoglu, K. Ulbrich, C. Rehberg, S. Rohn, G. Rimbach, Thermal stability, antioxidant, and anti-inflammatory activity of curcumin and its degradation product 4-vinyl guaiacol, Food and Function. 6 (2015) 887–893.

[26]   T. Yang, F. De Cui, M.K. Choi, J.W. Cho, S.J. Chung, C.K. Shim, D.D. Kim, Enhanced solubility and stability of PEGylated liposomal paclitaxel: In vitro and in vivo evaluation, International Journal of Pharmaceutics. 338 (2007) 317–326.

[27]   A. Umerska, C. Gaucher, F. Oyarzun-Ampuero, I. Fries-Raeth, F. Colin, M.G. Villamizar-Sarmiento, P. Maincent, A. Sapin-Minet, Polymeric nanoparticles for increasing oral bioavailability of curcumin, Antioxidants. 7 (2018) 1–18.

[28]   M.T. Larsen, M. Kuhlmann, M.L. Hvam, K.A. Howard, Albumin-based drug delivery: harnessing nature to cure disease, Molecular and Cellular Therapies. 4 (2016) 1–12.

[29]   K. Paál, J. Müller, L. Hegedûs, High affinity binding of paclitaxel to human serum albumin, European Journal of Biochemistry. 268 (2001) 2187–2191.

[30]   T. Kar, P. Basak, S. Sen, R.K. Ghosh, M. Bhattacharyya, Analysis of curcumin interaction with human serum albumin using spectroscopic studies with molecular simulation, Frontiers in Biology. 12 (2017) 199–209.

[31]   A. Barik, B. Mishra, A. Kunwar, K. Indira Priyadarsini, Interaction of curcumin with human serum albumin: Thermodynamic properties, fluorescence energy transfer and denaturation effects, Chemical Physics Letters. 436 (2007) 239–243.

[32]   Y. Shi, M.J. Van Steenbergen, E.A. Teunissen, L. Novo, S. Gradmann, M. Baldus, C.F. Van Nostrum, W.E. Hennink, Π-Π Stacking increases the stability and loading capacity of thermosensitive polymeric micelles for chemotherapeutic drugs, Biomacromolecules. 14 (2013) 1826–1837.

[33]   Y. Shi, R. Van Der Meel, B. Theek, E. Oude Blenke, E.H.E. Pieters, M.H.A.M. Fens, J. Ehling, R.M. Schiffelers, G. Storm, C.F. Van Nostrum, T. Lammers, W.E. Hennink, Complete regression of xenograft tumors upon targeted delivery of paclitaxel via Π-Π stacking stabilized polymeric micelles, ACS Nano. 9 (2015) 3740–3752.

[34]   J. Jin, D. Wu, P. Sun, L. Liu, H. Zhao, Amphiphilic triblock copolymer bioconjugates with biotin groups at the junction points: synthesis, self-assembly, and bioactivity, Macromolecules. 44 (2011) 2016–2024.

[35]   X. Wang, L. Liu, Y. Luo, H. Zhao, Bioconjugation of biotin to the interfaces of polymeric micelles via in situ click chemistry, Langmuir. 25 (2009) 744–750.

[36]   K. Qi, Q. Ma, E.E. Remsen, C.G. Clark, K.L. Wooley, Determination of the bioavailability of biotin conjugated onto shell cross-linked (SCK) nanoparticles, J Am Chem Soc. 126 (2004) 6599–6607.

[37]   A. Doerflinger, N.N. Quang, E. Gravel, G. Pinna, M. Vandamme, F. Ducongé, E. Doris, Biotin-functionalized targeted polydiacetylene micelles, Chemical Communications. 54 (2018) 3613–3616.

[38]   K.L. Metera, K.D. Ha-nni, G. Zhou, M.K. Nayak, H.S. Bazzi, D. Juncker, H.F. Sleiman, Luminescent iridium(III)-containing block copolymers: self-assembly into biotin-labeled micelles for biodetection assays, ACS Macro Lett. 1 (2012) 954–959.

4

[39]   E.H. Williams, A. V. Davydov, A. Motayed, S.G. Sundaresan, P. Bocchini, L.J. Richter, G. Stan, K. Steffens, R. Zangmeister, J.A. Schreifels, M. V. Rao, Immobilization of streptavidin on 4H-SiC for biosensor development, Applied Surface Science. 258 (2012) 6056–6063.

[40]   M. Elsabahy, M.É. Perron, N. Bertrand, G.E. Yu, J.C. Leroux, Solubilization of docetaxel in poly(ethylene oxide)-block-poly(butylene/styrene oxide) micelles, Biomacromolecules. 8 (2007) 2250–2257.

[41]   A. Kara, N. Ozturk, G. Esendagli, U.U. Ozkose, S. Gulyuz, O. Yilmaz, D. Telci, A. Bozkir, I. Vural, Development of novel self-assembled polymeric micelles from partially hydrolysed poly(2-ethyl-2-oxazoline)-co-PEI-b-PCL block copolymer as non-viral vectors for plasmid DNA in vitro transfection, Artificial Cells, Nanomedicine and Biotechnology. 46 (2018) S264–S273.

[42]   M.S. Alai, W.J. Lin, S.S. Pingale, Application of polymeric nanoparticles and micelles in insulin oral delivery, Journal of Food and Drug Analysis. 23 (2015) 351–358.

[43]   A. Varela-moreira, H. Van Leur, D. Krijgsman, V. Ecker, M. Braun, M. Buchner, M.H.A.M. Fens, W.E. Hennink, M. Schiffelers, Utilizing in vitro drug release assays to predict in vivo drug retention in micelles, International Journal of Pharmaceutics. 618 (2022) 121638.

[44]   Y. Wei, Z. Xue, Y. Ye, Y. Huang, L. Zhao, Paclitaxel targeting to lungs by way of liposomes prepared by the effervescent dispersion technique, Archives of Pharmacal Research. 37 (2014) 728–737.

[45]   Y. Liu, M.H.A.M. Fens, R.B. Capomaccio, D. Mehn, L. Scrivano, R.J. Kok, S. Oliveira, W.E. Hennink, C.F. van Nostrum, Correlation between in vitro stability and pharmacokinetics of poly(ε-caprolactone)-based micelles loaded with a photosensitizer, Journal of Controlled Release. 328 (2020) 942–951.

[46]   G.N. Kumar, U.K. Walle, K.N. Bhalla, T. Walle, Binding of taxol to human plasma, albumin and alpha 1-acid glycoprotein, Research Communications in Chemical Pathology and Pharmacology. 80 (1993) 337–344.

[47]   M. Kharat, Z. Du, G. Zhang, D.J. McClements, Physical and chemical stability of curcumin in aqueous solutions and emulsions: impact of pH, temperature, and molecular environment, Journal of Agricultural and Food Chemistry. 65 (2017) 1525–1532.

[48]   O. Naksuriya, M.J. Vansteenbergen, J.S. Torano, S. Okonogi, W.E. Hennink, A kinetic degradation study of curcumin in its free form and loaded in polymeric micelles, AAPS Journal. 18 (2016) 777–787.

[49]   M. Heger, R.F. van Golen, M. Broekgaarden, M.C. Michel, The molecular basis for the pharmacokinetics and pharmacodynamics of curcumin and its metabolites in relation to cancers, Pharmacological Reviews. 66 (2014) 222–307.

[50]   A. Basu, G. Suresh Kumar, Elucidating the energetics of the interaction of non-toxic dietary pigment curcumin with human serum albumin: a calorimetric study, Journal of Chemical Thermodynamics. 70 (2014) 176–181.

[51]   G.T. Bolger, A. Licollari, A. Tan, R. Greil, B. Vcelar, M. Majeed, L. Helson, Distribution and metabolism of lipocurc™ (liposomal curcumin) in dog and human blood cells: species selectivity and pharmacokinetic relevance, Anticancer Research. 37 (2017) 3483–3492.

[52]   A. Storka, B. Vcelar, L. Helson, M. Wolzt, PP119—effect of liposomal curcumin on red blood cells in vitro, Clinical Therapeutics. 35 (2013) 52.

[53]   M.M. Yallapu, M.C. Ebeling, N. Chauhan, M. Jaggi, S.C. Chauhan, Interaction of curcumin nanoformulations with human plasma proteins and erythrocytes., International Journal of Nanomedicine. 6 (2011) 2779–2790.

[54]   Y.J. Wang, M.H. Pan, A.L. Cheng, L.I. Lin, Y.S. Ho, C.Y. Hsieh, J.K. Lin, Stability of curcumin in buffer solutions and characterization of its degradation products, Journal of Pharmaceutical and Biomedical Analysis. 15 (1997) 1867–1876.

[55]   M.H.M. Leung, T.W. Kee, Effective stabilization of curcumin by association to plasma proteins: human serum albumin and fibrinogen, Langmuir. 25 (2009) 5773–5777.

4

Supporting information

Section 1. HPLC methods for detection and quantification of paclitaxel and curcumin.

PTX was determined with HPLC using an isocratic method with a mobile phase of ACN/water = 55:45 (v/v) with 0.1% formic acid. The run time was 7 min with a flow rate of 1.5 mL/min. A Sunfire C18 column (5 µm, 4.6 × 150 mm) was used, and the detection wavelength was 227 nm. To calculate PTX encapsulation efficiency and loading capacity of the biotinylated micelles, the injection volume was 30 µL and the PTX concentration in micelle samples was calculated using a calibration curve of PTX standards in ACN in a concentration range of 3–100 µg/mL. To quantify the released and retained PTX in biotinylated micelles, for the samples of supernatant fraction containing released PTX, 60 µL was injected and PTX calibration was done in ACN/PBS (1:1, v/v) in a concentration range of 0.3–25 µg/mL. For the samples of beads fraction containing non-released PTX, 30 µL was injected and PTX calibration was done in ACN in a concentration range of 1-50 µg/mL.

The curcumin concentration in the different samples was determined using HPLC. In detail, the elution was isocratic with a mobile phase of ACN/water = 55:45 (v/v) with 0.25% acetic acid. The total run time was 10 min with a flow rate of 1.3 mL/min. A Sunfire C18 column was used, and the detection wavelengths were 425 and 254 nm. To calculate the curcumin encapsulation efficiency and loading capacity of the biotinylated micelles, the injection volume was 20 µL and calibration was done using standards in ACN in a concentration range of 3–100 µg/mL. To quantify the released and retained curcumin in biotinylated micelles, for the samples of supernatant fraction containing released curcumin, 40 µL was injected and curcumin calibration was done in ACN/PBS (1:1, v/v) in a concentration range of 0.01-25 µg/mL. For the samples of beads fraction containing non-released curcumin, 20 µL was injected and curcumin calibration was done in ACN in a concentration range of 0.3-25 µg/mL.

Table S1. Characteristics of block copolymer p(HPMAm)-b-p(HPMAm-Bz). Data were reproduced from previous publication [1].

Entry	Polymers	$M_{n,\ theory}$ (kDa)	$M_{n,\ NMR}$ (kDa)	$M_{n,\ GPC}$ (kDa)	PDI
1	p(HPMAm)$_{7.1k}$-b-p(HPMAm-Bz)$_{15.0k}$	24.9	22.1	11.0	1.48
2	biotinylated p(HPMAm)$_{6.8k}$-b-p(HPMAm-Bz)$_{16.3k}$	25.3	23.1	12.9	1.48
3	Cy3-labeled p(HPMAm)$_{4.9k}$-b-p(HPMAm-Bz)$_{18.7k}$	22.8	23.6	10.0	1.41

$M_{n,\ theory}$ = theoretical number average of molecular weight, $M_{n,\ NMR}$ = number average of molecular weight determined by ^{1}H NMR analysis, $M_{n,\ GPC}$ is determined by GPC analysis (DMF containing 10 mM LiCl as eluent, PEGs as standards), PDI = $M_{w,\ GPC}/M_{n,\ GPC}$.

The molecular weight discrepancy between NMR and GPC data can be explained as follows. Polyethylene glycols (PEG) of different molecular weight were used as calibration standards for the determination of the relative molecular weight of p(HPMAm)-b-p(HPMAm-Bz) using GPC analysis. GPC separation is not based on molecular weight but rather on the hydrodynamic volume of polymers. Since PEG is a very flexible polymer, it has for a given molecular weight (in fact we should talk about the degree polymerization, DP) a smaller hydrodynamic volume than a less flexible polymer with the same DP, such as p(HPMAm)-b-p(HPMAm-Bz). This leads to an underestimation of the molecular weight of linear polymers using PEG calibration [2]. Similar discrepancies were also observed in previous publications [3,4].

Table S2. The molar ratio of albumin to the potentially released drug from 13 µL biotinylated micelles upon incubation in PBS containing 4.5% w/v BSA.

Drug feed	Volume of PBS/BSA (µL)	Albumin/drug (mol/mol)
PTX, 3%	130	31
PTX, 10%	240	27
PTX, 10%	480	55
Curcumin, 10%	240	8

Table S3. Determination of drug recovery yield in protein-containing media spiked with drugs at different concentrations [a].

Concentration of drug added (µg/mL)	Medium	Recovery yield of PTX (%)	Recovery yield of curcumin (%)
40	PBS/BSA	95%	96%
	Mouse plasma	96%	96%
	Mouse blood	98%	99%
20	PBS/BSA	98%	97%
	Mouse plasma	99%	97%
	Mouse blood	100%	100%
2	PBS/BSA	96%	98%
	Mouse plasma	97%	98%
	Mouse blood	100%	100%

[a] A known amount of drugs was spiked with PBS/BSA, mouse plasma, and mouse blood, respectively, followed by precipitation of proteins and determination of the drug amount in the supernatant.

Section 2. Calculation of the number of streptavidin molecules covered by the micelles.
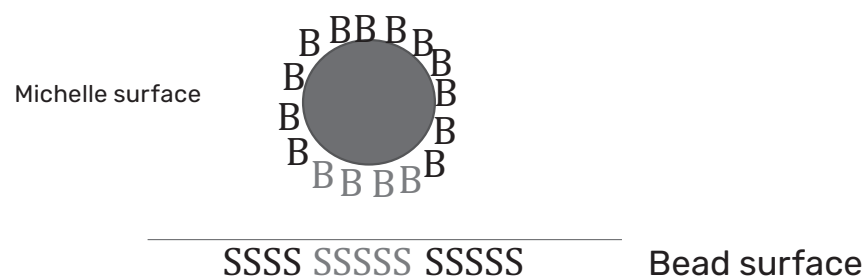
Fig. S1. Schematic illustration of streptavidin coverage on micelle surface.

As illustrated in **Fig. S1**, an unknown number of streptavidin units (S) is covered by a micelle, referred to as x.

For the 100% biotinylated micelles, the number of biotin units (B) per micelle is equal to the aggregation number (N_{agg}). Therefore, S/B at 100% biotinylation (referred to as y) is equal to $y = x / N_{agg}$.

For the <100% biotinylated micelles, the fraction of biotinylated polymers in the micelles is equal to f (e.g., $f = 0.2$ in case of 20% biotinylation):

(1) The number of S units covered by one micelle of the same diameter (i.e., 70 nm) is always the same and remains equal to $y \times N_{agg}$.

(2) However, the number of B units per micelle is reduced to $f \times N_{agg}$.

(1) and (2) together means that the molar ratio of streptavidin/biotin (S/B) $= \frac{y \times N_{agg}}{f \times N_{agg}} = y / f,$, therefore, the measured S/B as a function of 1/f should give a straight line with a slope y.

The measured S/B is plotted against 1/f in **Fig. 1C**, and a linear relation S/B = 0.1145 × (1/f) was established. Therefore, the number of covered streptavidin units $x = y \times N_{agg} = 0.1145 \times N_{agg}$.

Table S4. The molar ratio of streptavidin/biotin (S/B) determined at the maximal binding efficiency (see Fig. 1B) of biotinylated micelles upon adding streptavidin-coated magnetic beads.

f	S/B [a]	1/f
0.025	4.60	40
0.05	2.30	20
0.1	1.10	10
0.15	0.71	6.7
0.2	0.53	5

[a] The amount of streptavidin on the surface of the beads was calculated based on the information supplied by the manufacturer Bangs labs, i.e., 1 mg (200 µL) of BioMag streptavidin particles bind 2 µg of biotin.
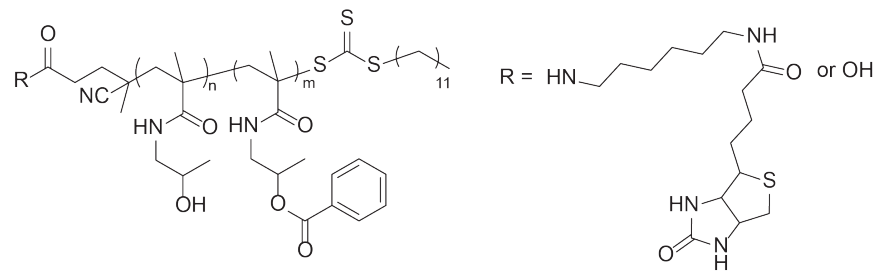
Fig. S2. Structure of p(HPMAm)-b-p(HPMAm-Bz) block copolymer with or without biotin terminus [1].
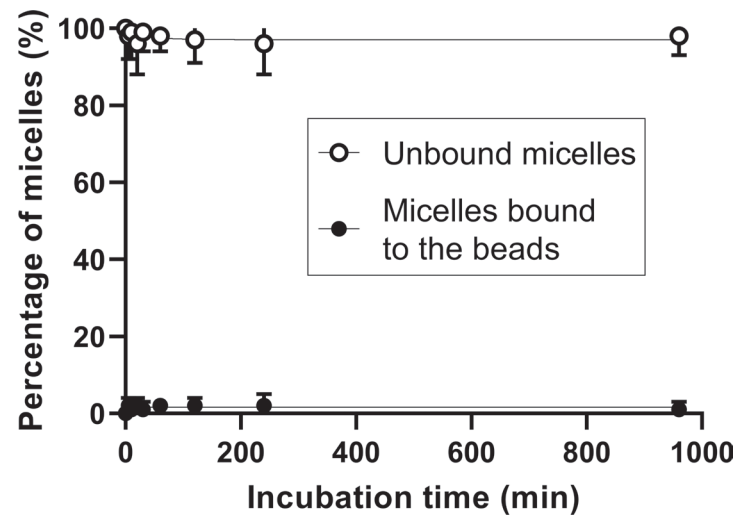

Fig. S3. Binding kinetics of nonbiotinylated micelles to streptavidin-coated magnetic beads. Data are presented as mean ± SD of three independent replicates.
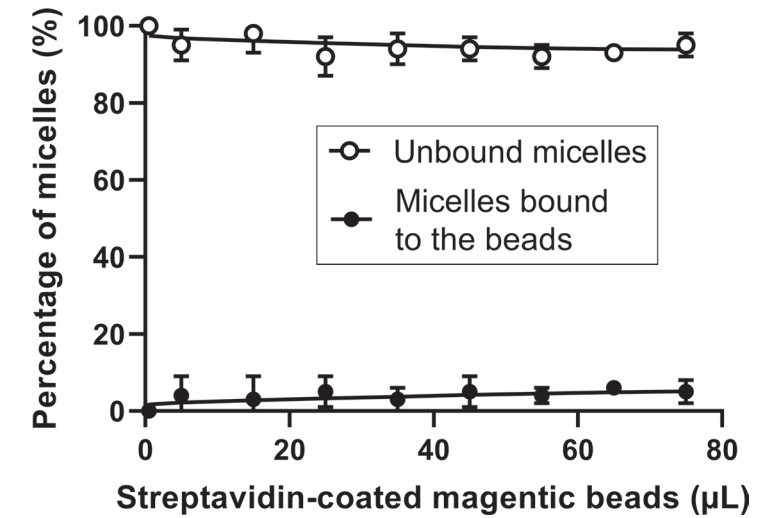
Fig. S4. Binding efficiency of nonbiotinylated micelles after 10 min upon adding increasing amounts of streptavidin-coated magnetic beads (5 mg/mL). Data are presented as mean ± SD of two independent replicates.

Fig. S5. Dynamic light scattering analysis of drug-loaded biotinylated micelles incubated with PBS, PBS containing 2% v/v Tween 80, and PBS containing 4.5% w/v BSA for 48 h at 37 °C, respectively. Green lines represent the size distribution by intensity before incubation, and red lines represent the size distribution by intensity after incubation.
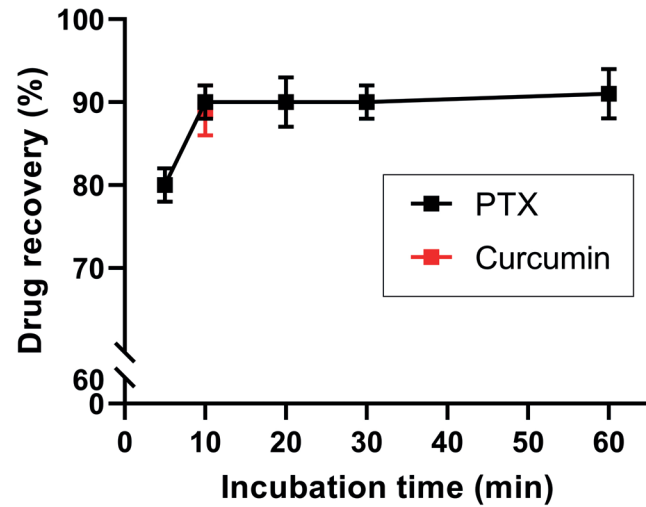
Fig. S6. Drug recovery from biotinylated micelles associated with streptavidin-coated magnetic beads upon incubation at 4 °C in PBS for 60 min. Data are presented as mean ± SD of three independent replicates.
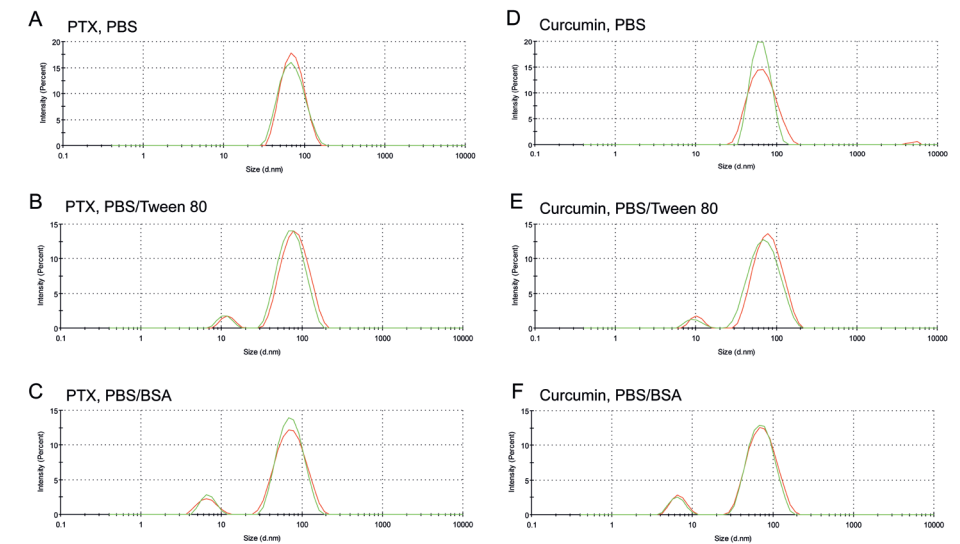
A

B
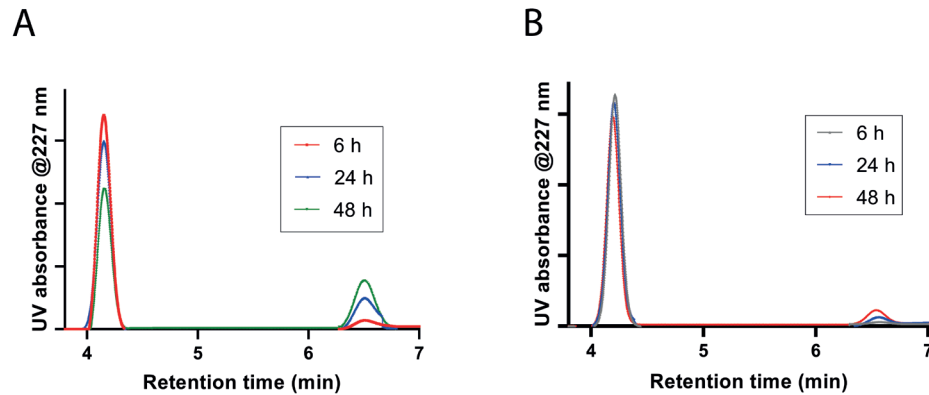
Fig. S7. Representative HPLC chromatograms of PTX and its degradation product. Free PTX (**A**) and encapsulated PTX in biotinylated micelles (**B**) were incubated in PBS containing 4.5% w/w BSA at 37 °C over 48 h. The peak at 4.5 min is corresponding to PTX, and the peak at 6.5 min is the major degradation product of PTX.
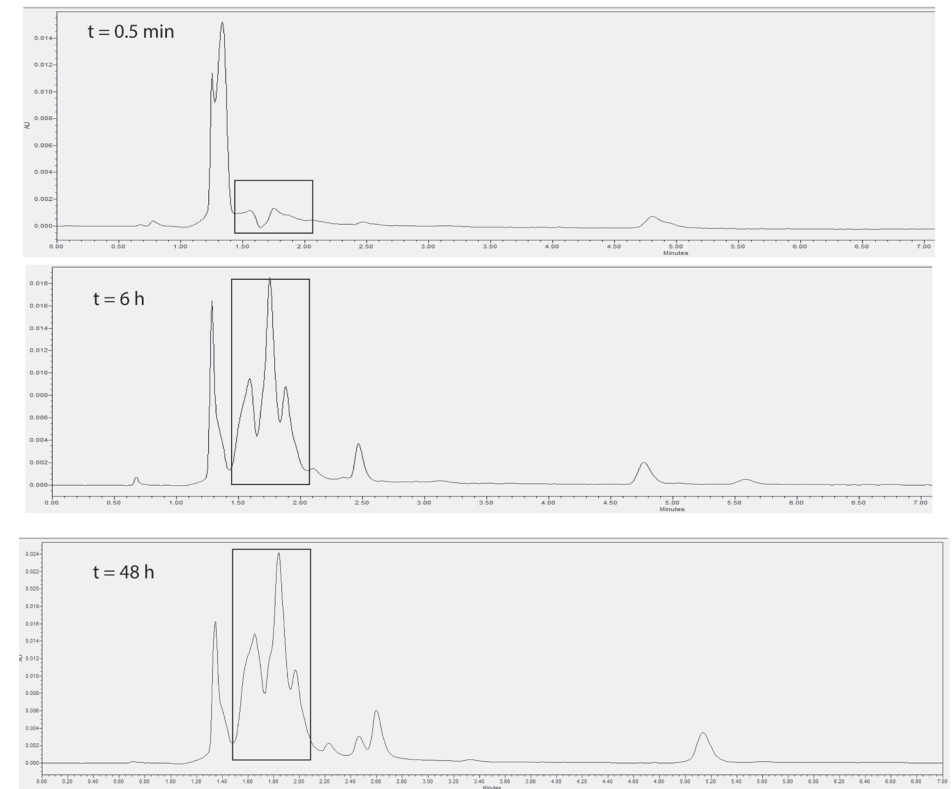
Fig. S8. Representative HPLC chromatogram (UV 254 nm) of curcumin and its degradation products released from biotinylated micelles upon incubation in PBS buffer at 37 °C over 48 h. The peak with a retention time of around 5 min corresponds to curcumin, and the peaks between 1.50–2.20 min are degradation products of curcumin.

References

[1]   Y. Wang, M.J. van Steenbergen, N. Beztsinna, Y. Shi, T. Lammers, C.F. van Nostrum, W.E. Hennink, Biotin-decorated all-HPMA polymeric micelles for paclitaxel delivery, Journal of Controlled Release. 328 (2020) 970–984.

[2]   C. Kojima, B. Turkbey, M. Ogawa, M. Bernardo, C.A.S. Regino, L.H. Bryant, P.L. Choyke, K. Kono, H. Kobayashi, Dendrimer-based MRI contrast agents: the effects of PEGylation on relaxivity and pharmacokinetics, Nanomedicine. 7 (2011) 1001–1008.

[3]   G. Gody, T. Maschmeyer, P.B. Zetterlund, S. Perrier, Exploitation of the degenerative transfer mechanism in RAFT polymerization for synthesis of polymer of high livingness at full monomer conversion, Macromolecules. 47 (2014) 639–649.

[4]   C. Duffy, M. Phelan, P.B. Zetterlund, F. Aldabbagh, Reversible addition-fragmentation chain transfer polymerization of alkyl-2-cyanoacrylates: An assessment of livingness, J Polym Sci A Polym Chem. 55 (2017) 1397–1408.

4

5

The effect of pHPMA as PEG alternative in polymeric micelles on circulation kinetics and possible accelerated blood clearance

Yan Wang [1], Marcel H. Fens [1], Aida Varela-Moreira [1], Mahsa Bagheri [1], Nicky C.H. van Kronenburg [2], Mariona Estapé Senti [3], Robbert J. Kok [1], Yang Shi [4], Twan Lammers [4], Cornelus F. van Nostrum [1], Wim E. Hennink [1]

[1] Department of Pharmaceutics, Utrecht Institute for Pharmaceutical Sciences, Utrecht University, Universiteitsweg 99, 3508 TB Utrecht, the Netherlands
[2] Department of Translational Neuroscience, University Medical Center Utrecht Brain Center, Universiteitsweg 100, 3584 CG Utrecht, the Netherlands
[3] Department of Translational Immunology, University Medical Center Utrecht Brain Center, Universiteitsweg 100, 3584 CG Utrecht, the Netherlands
[4] Department of Nanomedicine and Theranostics, Institute for Experimental Molecular Imaging, RWTH Aachen University Clinic, Forckenbecktrasse 55, 52074 Aachen, Germany

Abstract

It is well known that the decoration of nanocarriers with polyethylene glycol (PEG) results in reduced and delayed opsonization and reduced non-specific cellular uptake, and consequently leads to prolonged circulation times. However, accelerated blood clearance (ABC) is observed after repeated intravenous injections of PEGylated nanoparticles, which is caused by the formation of anti-PEG antibodies. Consequently, there is a need for alternative hydrophilic polymers, of which poly(N-2-hydroxypropyl methacrylamide) (pHPMA) is a promising candidate due to its biocompatibility and multifunctionality that allows the conjugation of drug and targeting molecules as well as imaging agents. In the present study, the circulation kinetics after first and second injections of (pHPMA)-based micelles and whether decoration of the surface with biotin as a targeting ligand induces immunogenicity and altered circulation profiles were investigated and compared with PEGylated micelles. Block copolymers of pHPMA or PEG with a poly(N-2-benzoyloxypropyl methacrylamide) (p(HPMAm-Bz)) hydrophobic block, having a similar molecular weight of 23 kDa, self-assembled into micelles in water with an average hydrodynamic diameter of 55 nm. The circulation behavior of the different micelles was evaluated upon first and second (intervals of seven days) intravenous injections in immunocompetent mice. Biotintin decoration on the surface of p(HPMAm)-b-p(HPMAm-Bz) micelles did not alter the blood circulation and biodistribution upon first and second injection. After the first injection, pHPMA micelles showed biphasic elimination kinetics that is similar to PEGylated liposomes at low lipid dose, whereas the PEGylated micelles followed first-order elimination kinetics. Single-dose injected pHPMA micelles with or without biotin decoration showed a shorter circulation half-life (12.5±2.8 and 16.3±2.6 h, respectively) compared to PEGylated micelles (24.5±2.6 h). 13±1% of single-dose injected pHPMA accumulated in the liver at 48 h, which was similar to PEGylated micelles (15±3%). After the second injection, 10-30% dose of pHPMA and PEGylated micelles showed very rapid clearance at 1 min upon injection due to a yet unknown phenomenon. The remaining dose was eliminated with a half-life of 9.8±1.6, 11.1±0.7, and 14.7±3.2 h for pHPMA micelles with or without biotin decoration, and PEGylated micelles, respectively, which is slightly faster than the elimination of the first injected dose. Anti-pHPMA and anti-PEG IgG and IgM antibodies were not detected using enzyme-linked immunosorbent assay (ELISA). Although the formation of anti-PEG antibodies was expected based on studies with PEGylated liposomes, their absence can be ascribed to the smaller sizes of the studied micelles and the high PEG intensity.
It is therefore recommended that in a future study the circulation kinetics of the pHPMA micelles is compared with that of PEGylated liposomes after the first and second injection.

Introduction

Polyethylene glycol (PEG) is the most used polymer for the design of long circulation nanoparticles [1,2]. PEGylated surfaces are considered bioinert by avoiding protein adsorption [3]. In recent years it has been demonstrated that certain plasma proteins do adsorb onto PEGylated nanoparticles, referred to as the biomolecular corona [4]. The occurrence and composition of this protein corona depend on the molecular weight of PEG as well as on the PEG density on the surface [5,6]. The phenomenon of accelerated blood clearance (ABC) has gained a lot of attention due to its apparent detrimental effects on the long circulation properties of nanoparticle therapeutics [7].

The ABC effect was first reported by Dams et al. [8]. They showed that upon intravenous injection of PEGylated liposomes in rats or rhesus monkeys, the second dose of PEGylated liposomes was cleared very rapidly from the blood circulation when the interval between the first and second injected dose was 5–21 days. This effect was subsequently observed in a broad range of animal species, e.g., mice, rabbits, and Beagle dogs, and reflects a major change in the pharmacokinetics of consecutive injections of PEGylated nanoparticles [9–12]. It was observed that the first injection of PEGylated nanoparticles triggers the production of anti-PEG IgM antibodies [13,14]. Upon repeated administration of PEGylated nanocarriers, these antibodies recognize and specifically bind to the particles leading to opsonization by C3 fragments and ultimately rapid clearance from the circulation [15]. The fast clearance of the second dose of PEGylated nanoparticles is accompanied by an increased accumulation in liver and spleen indicating a role for hepatosplenic macrophages [16,17]. Furthermore, the ABC phenomenon has potential implications for PEGylated therapeutic agents in clinical use. In a Phase I study, patients were treated with the doxorubicin liposome formulation, Doxil®, and about half of them showed symptoms of complement-activation-related hypersensitivity reactions after initial treatment of Doxil®, indicating the ability of Doxil® to induce the formation of anti-PEG antibodies [18]. Anti-PEG antibodies can induce the adsorption of complement fragments onto the surface of PEGylated lipid-based nanoparticles which induce cellular uptake by macrophages and their subsequent intracellular lysis [19,20]. For many clinical applications, repeated administration is often required to achieve adequate treatment and prevent disease sequelae or progression It is therefore of great importance to study how to modify or prevent the induction of the ABC effect upon the repeated use of PEGylated nanoparticles [21].

The occurrence and extent of the ABC effect are influenced by the type, size, surface charge, PEG density, terminal PEG end group, administration regimen, and payload of the nanoparticles [9,10,22–25]. For instance, Koide and coworkers reported that a preceding injection of PEGylated polymeric micelles or liposomes

with a size of 50-795 nm in BALB/c mice induced accelerated clearance from the bloodstream and significant accumulation in the liver after the second injection [26,27]. Conversely, the polymeric micelles with a size of 10-32 nm did not induce the ABC effect, suggesting that triggering and susceptibility for ABC are micelle size-dependent. In addition to the factors mentioned above, the type of polymer coating has also been shown to influence the induction of the ABC effect. A number of polymer coatings, such as poly(amino acid) (PAA), poly(hydroxyethyl L-asparagine) (PHEA), poly(vinylpyrrolidone) (PVP), poly(N-2-hydroxypropyl methacrylamide) (pHPMA), poly(N,N-dimethylacrylamide) (PDMA), poly(N-acryloyl morpholine) (PAcM), and polysarcosine (pSar), have all demonstrated the ability to prolong circulation times of liposomes and other nanoparticles upon repeated administration [28–33]. Particularly, pHPMA has favorable characteristics as hydrophilic material such as its versatility, possibilities for conjugation, and low protein binding [34–37]. In our previous publications, it was shown that polymeric micelles based on mPEG-b-p(HPMAm-Bz) diblock copolymers are promising nano delivery systems for curcumin or paclitaxel to treat cancer [38–40]. To avoid the use of PEG, we developed micelles based on all-pHPMA block copolymer [41]. However, it is not known whether antibodies are formed against pHPMA shell of these micelles upon intravenous injection. Therefore, in the present study, micelles based on p(HPMAm)-b-p(HPMAm-Bz) as well as the structurally related mPEG-b-p(HPMAm-Bz) were investigated for their *in vivo* behavior upon intravenous injection.

Our previous study showed that biotin-decorated p(HPMAm) micelles loaded with paclitaxel showed high *in vitro* cellular uptake and cytotoxicity in lung cancer cells [41]. Surface modification of a nanoparticle with a tumor-targeting ligand might cause immunogenicity, leading to rapid blood clearance [42]. Therefore, the effect of biotin decoration on circulation kinetics of p(HPMAm) micelles was also investigated after the first and second administration.

In the current study, different micelles possessed the same hydrophobic core poly(N-2-benzoyloxypropyl methacrylamide) (p(HPMAm-Bz)), but different hydrophilic shells (pHPMA, biotinylated pHPMA, or PEG). The circulation time and biodistribution of the micelles in BALB/c mice after the first and second doses were investigated. Finally, the possible formation of anti-p(HPMAm)- and anti-PEG antibodies was investigated.

Materials and Methods

Materials
p(HPMAm)-b-p(HPMAm-Bz) with or without biotin terminus, mPEG-b-p(HPMAm-Bz), and Cy7-labeled polymers were synthesized and characterized as previously reported [41,43]. Dimethylformamide (DMF), tetrahydrofuran (THF), and dimethyl sulfoxide (DMSO) were purchased from Biosolve Ltd. (Valkenswaard, the Netherlands). Phosphate buffered saline (PBS, pH 7.4, containing 11.9 mM phosphate, 137 mM sodium chloride, and 2.7 mM potassium chloride) and polysorbate 20 (Tween 20) were purchased from Fisher Scientific (Geel, Belgium). Spectra/Por dialysis membrane (MW 6-8 kDa) and protein A/L pre-coated microplates were obtained from Thermo Fisher Scientific (Landsmeer, the Netherlands). Syringe filters with 0.45 µm regenerate cellulose (RC) membrane were purchased from Phenomenex (Utrecht, the Netherlands). Vivaspin™ 20 centrifugal concentrators (MW 3 kDa) were ordered from Sartorius AG (Goettingen, Germany). Ethylenediaminetetraacetic acid (EDTA) containing tubes were obtained from Sarstedt (Numbrecht, Germany). Sodium chloride (NaCl), D_2O, 4-(2-hydroxyethyl)piperazine-1-ethanesulfonic acid (HEPES), bovine serum albumin (BSA), hydrochloride (HCl), 3-[(3-cholamidopropyl) dimethylammonio]-1-propanesulfonate (CHAPS), and mPEG (average molecular weight of 5 kDa) were purchased from Sigma-Aldrich (Zwijndrecht, the Netherlands). Radio-immunoprecipitation assay (RIPA) lysis buffer (0.5 M Tris-HCl, pH 7.4, 1.5 M NaCl, 2.5% deoxycholic acid, 10% NP-40, 10 mM EDTA) was purchased from Merck KGaA (Darmstadt, Germany). Human plasma was obtained from University Medical Center Utrecht mini donor service (donors ID: 201746 and 201927). PEGylated granulocyte colony-stimulating factor (PEG-G-CSF) (PEGfilgrastim/Neulasta) was purchased from Amgen (California, CA, USA). Horseradish peroxidase (HRP)-conjugated anti-mouse immunoglobulin G (IgG) and biotinylated anti-mouse immunoglobulin M (IgM) were purchased from Southern Biotech (Birmingham, AL, USA). Streptavidin-horseradish peroxidase (SA-HRP) was ordered from Roche (Basel, Switzerland) and 3,3',5,5'-tetramethylbenzidine (TMB) from Invitrogen (California, MA, USA).

Preparation and characterization of polymeric micelles with or without Cy7 label
p(HPMAm), biotinylated p(HPMAm), and PEGylated micelles with or without Cy7 label were prepared by solvent extraction as previously described [43,44]. In brief, for the preparation of p(HPMAm) micelles without biotin decoration, 400 mg of p(HPMAm)-b-p(HPMAm-Bz) (entry 1 in Table S1) containing 3 wt% Cy7-labeled polymer (entry 3 in Table S1), was dissolved in 20 mL of DMF. Subsequently, the polymer solution was mixed with 8 mL PBS while stirring for 1 min. DMF was removed by dialysis against PBS for 2 days in a Spectra/Por dialysis membrane with a molecular weight cut-off of

6–8 kDa. For the preparation of biotinylated p(HPMAm) micelles, a mixture of 90% of p(HPMAm)-b-p(HPMAm-Bz) (entry 1 in Table S1) and 10% of biotinylated p(HPMAm)-b-p(HPMAm-Bz) (entry 2 in Table S1) was dissolved in DMF followed by mixing with PBS and dialysis as described above. For the preparation of PEGylated micelles, 400 mg of mPEG-b-p(HPMAm-Bz) polymer (entry 4 in Table S1) containing 3% Cy7-labeled polymer (entry 5 in Table S1), was dissolved in 8 mL of THF. Subsequently, the polymer solution was mixed with 8 mL of PBS while stirring for 1 min. THF was removed by evaporation overnight and subsequent dialysis against PBS for 24 h. After dialysis, the micellar dispersions were concentrated to around 30 mg/mL using a Sartorius Vivaspin™ 20 centrifugal concentrator with a molecular weight cut-off of 3 kDa. The micellar dispersions were filtered through a 0.45 μm RC membrane sterile syringe filter before injection in the mice.

The concentration of the micelles in PBS was determined by thermogravimetric analysis (TGA) using a TA instrument Q50 (Waters Corp., Delaware, USA). In brief, 50 μL of homogenized micelle dispersion was transferred into a tared aluminum pan to allow gradual heating from 20 to 120 °C at 20 °C/min with an isothermal hold time of 100 min. Fifty μL of PBS was used for the blank subtraction. Samples of dry polymer displayed no mass loss indicating thermal stability of p(HPMAm)-b-p(HPMAm-Bz) and mPEG-b-p(HPMAm-Bz) polymers up to at least 120 °C.

The residual organic solvent content of the micellar dispersion was measured by ^{1}H NMR analysis using a Bruker 600 MHz spectrometer (Bruker Corp., Massachusetts, USA). In short, 200 μL of micelle dispersion was mixed with 400 μL of D_2O, and no peaks corresponding to DMF and THF were detected (detection limit ≤ 50 ppm).

The size of micelles was determined by dynamic light scattering (DLS) after 10-fold dilution in PBS at 25 °C using a Zetasizer Nano S 173 (Malvern Instruments Ltd., Malvern, UK). The Z-average diameter (Z_{ave}) and polydispersity index (PDI) were calculated by the Zetasizer software v.7.13. The zeta-potential of the micelles was measured after 10-fold dilution in 10 mM HEPES buffer pH 7.4 using a Zetasizer Nano Z (Malvern Instruments Ltd., Malvern, UK).

The weight-average molecular weight, the aggregation number (N_{agg}), the radius of gyration (R_g), and the radius of hydration (R_h) of the micelles were determined after asymmetric flow field-flow fractionation (AF4) using a Postnova AF2000 system (Postnova Analytics, Landsberg, Germany) equipped with a degasser, isocratic pumps, autosampler, and fraction collector. A Frit-inlet channel was equipped with a ceramic frit, a 350 μm spacer, and a regenerated cellulose membrane with a molecular weight cut-off of 10 kDa and kept at 25 °C. The AF4 system was coupled to a refractive index (RI) detector, a multi-angle light scattering (MALS) detector, and a DLS system (Malvern Instrument Ltd., Malvern, UK). BSA dissolved in 0.9%

NaCl at 5 mg/mL was used for calibration and PBS was used as eluent. The micellar dispersions were diluted in PBS to a concentration of 1.2 mg/mL. A 20 μL of the sample was injected into the system and the detector flow was kept at 0.5 mL/min. The crossflow rate was initially 1.5 mL/min and then decreased exponentially in 70 min to 0.0 mL/min. After completion of the elution program, no crossflow was applied for at least 5 min to ensure complete elution of the largest particles. Data acquisition and processing were executed with an AF2000 control software v.2.1.0.5, from which R_g, R_h, and $M_{w,mic}$ of micelles were calculated using a random coil fitting model [45].

Animals

The animal study was performed according to national regulations and approved by the animal experimental committee of Utrecht University. Female (8–10 weeks old, 60 in total) immunocompetent BALB/c mice were used (Envigo, Horst, the Netherlands). The mice were housed in groups of four with free access to rodent chow and water at a 12 h light/dark cycle. Before the experiments, mice were randomized, and the different micelle formulations were blinded for the investigator who performed the injections.
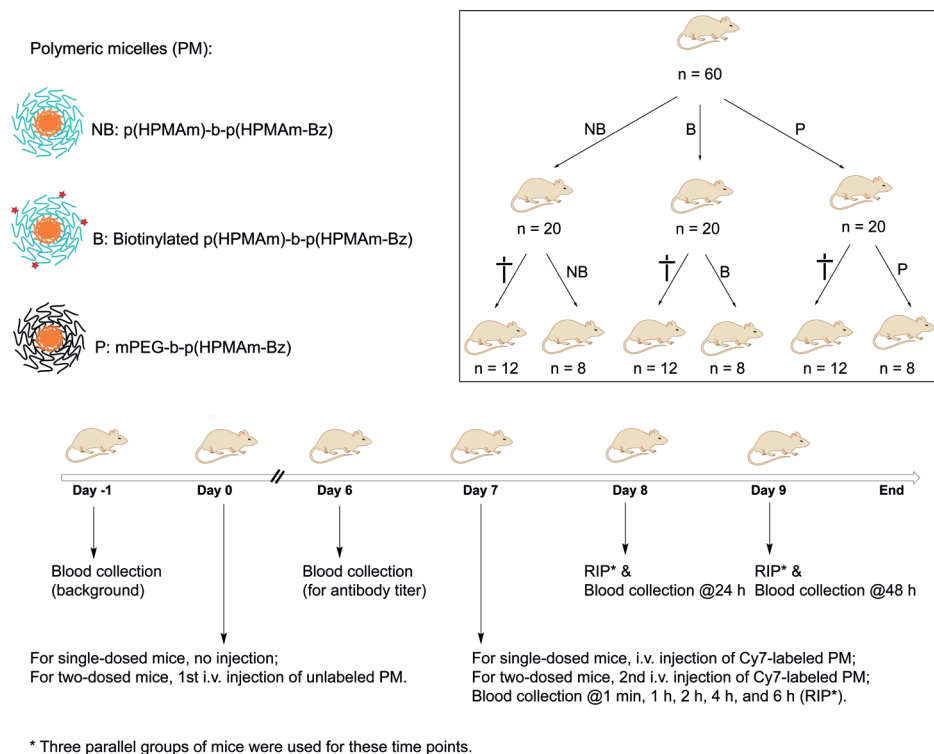
Polymeric micelles (PM):

NB: p(HPMAm)-b-p(HPMAm-Bz)

B: Biotinylated p(HPMAm)-b-p(HPMAm-Bz)

P: mPEG-b-p(HPMAm-Bz)

n = 60

NB   B   P

n = 20   n = 20   n = 20

† / NB   † / B   † / P

n = 12   n = 8   n = 12   n = 8   n = 12   n = 8

Day -1   Day 0   Day 6   Day 7   Day 8   Day 9   End

Blood collection (background)

Blood collection (for antibody titer)

RIP* & Blood collection @24 h

RIP* & Blood collection @48 h

For single-dosed mice, no injection;
For two-dosed mice, 1st i.v. injection of unlabeled PM.

For single-dosed mice, i.v. injection of Cy7-labeled PM;
For two-dosed mice, 2nd i.v. injection of Cy7-labeled PM;
Blood collection @1 min, 1 h, 2 h, 4 h, and 6 h (RIP*).

* Three parallel groups of mice were used for these time points.

Fig. 1. Schematic representation of the animal study design. For single injections, Cy7-labeled p(HPMAm), biotinylated p(HPMAm), and PEGylated micelles were injected. The second dose of micelles (Cy7-labeled dose) was given 7 days after the first injection of p(HPMAm), biotinylated p(HPMAm), and PEGylated micelles (unlabeled dose).

Circulation kinetics and biodistribution of polymeric micelles in mice

For the single-dose pharmacokinetics (PK) and biodistribution study, mice (n = 12 per group) were intravenously injected with Cy7-labeled micelles (either HPMA decorated, biotin-HPMA decorated, or PEG decorated micelles). All formulations were administered at a dose of 150 mg polymer per kg of mouse body weight via the tail vein in 100-200 µL in PBS (Fig. 1). After administration, blood was collected into EDTA tubes at predetermined time points: 1 min (set as 100% injected dose), 1, 2, 4 h via submandibular puncture (50-80 µL), and after 6, 24, and 48 h via cardiac puncture after mice were sacrificed by cervical dislocation. It is noted that three parallel groups of mice were used for these time points because the total volume of blood drawn was aimed at not exceeding 10% of the body weight of mice, and thus only two submandibular punctures per mouse were performed. Plasma samples

were prepared by centrifugation at 1500 g for 10 min at 4 °C and stored at -20 °C prior to analysis. Major organs (brain, lungs, kidneys, liver, spleen, and heart) from the mice were excised and imaged for whole organ fluorescence using a Pearl impulse imager (LI-COR, Nebraska, USA) at λ_{ex} = 785 nm and λ_{em} = 820 nm. Finally, the organs were snap-frozen in liquid nitrogen and stored at -80 °C until further analysis.

For the second dose PK and biodistribution, mice (n = 8 per group) were intravenously injected with unlabeled PEGylated micelles and HPMA-based micelles with or without biotin decoration. All formulations were administrated at a dose of 150 mg polymer per kg of mouse body weight via the tail vein in 100-200 µL in PBS. Seven days later, mice were again intravenously injected with Cy7-labeled HPMA-based micelles with or without biotin decoration and Cy7-labeled PEGylated micelles at the same dose. Blood samples were collected as mentioned above unless indicated. To investigate the formation of anti-polymer antibodies, pre-dose (before any injection) and post-dose blood samples of 50-80 µL (six days after the initial dose) were collected via submandibular puncture. Plasma samples were prepared by centrifugation at 1500 g for 10 min at 4 °C and stored at -20 °C prior to analysis. After 24 h, organs were dissected, imaged, snap-frozen in liquid nitrogen, and stored at -80 °C until further analysis.

The concentration of the Cy7-labeled micelles in plasma samples was measured using FP-8300 spectrofluorometer (JASCO Benelux B.V., Utrecht, the Netherlands). Plasma samples were diluted 10 times in DMSO and vortexed for 2 min, followed by centrifugation at 15000 g for 10 min. The fluorescence intensity of supernatants was measured in an ultra-micro quartz cuvette at an excitation wavelength of 750 nm and an emission wavelength of 773 nm. A calibration curve was made by spiking Cy7-labeled micelles in human plasma which was also subsequently diluted 10 times in DMSO resulting in a polymer concentration of 2-500 µg/mL. The protein precipitation was removed by centrifugation at 12000 g for 15 min at RT. The concentration of Cy7-labeled micelles in plasma was calculated by extrapolating from the linear fit function and corrected for recovery yield as well as the dilution factor.

To measure the accumulation of Cy7-labeled polymer in different organs, frozen organs were cut and weighed (~100 mg was used per sample) before transferring them into tubes with ceramic beads, and subsequently, 100 µL of cold RIPA lysis buffer was added. The mixture was homogenized at a speed of 6000/s for 60 s using a Precellys 24 tissue grinder (Bertin Instruments, Montigny-le-Bretonneux, France). DMSO (1:9 v/v) was subsequently added to the homogenate and vortexed for 2 min, followed by centrifugation at 15000 g for 10 min. The concentration of Cy7-labeled polymers in different tissues was determined as described above by

5

measuring the fluorescence intensity of the supernatants. A calibration curve was made by first dissolving Cy7-labeled polymer in DMSO and subsequently spiking this into tissue homogenates obtained from untreated mice resulting in a Cy7-labeled polymer concentration of 0.04-12 µg/mL.

Detection of anti-polymer antibodies in mouse plasma using ELISA

To investigate the specificity of antibodies against PEG and p(HPMAm), an enzyme-linked immunosorbent assay (ELISA) was performed. Anti-PEG antibodies were determined as previously reported [19,46]. In detail, PEGfilgrastim was dissolved in PBS (1 µg/mL) and added to 96-well plates (Greiner, 655101). The wells were air-dried overnight at room temperature (RT). Next, the plates were blocked for 2 h at RT with a solution of 2% (w/v) BSA in PBS. Diluted plasma samples, i.e., both background (pre-dose) levels (before any injection) and post-dose levels (seven days after the initial injection), collected from mice treated with PEG-b-p(HPMAm-Bz) micelles, were added to the plate. To check the specificity of the binding, 1% (w/v) mPEG (average molecular weight of 5 kDa) in PBS/BSA was added to paralleled wells containing post-dose plasma samples, and thus free mPEG would compete with the pre-coated PEGfilgrastim for binding anti-PEG antibodies. The plate was incubated at 37 °C for 1.5 h and then washed five times with a solution of 0.05% (w/v) CHAPS in PBS. 100 µL of detection antibodies of either HRP-conjugated anti-mouse IgG (diluted 1:2000 in 2% BSA/PBS) or biotinylated anti-mouse IgM (diluted 1:8000 in 2% BSA/PBA) was added to wells and incubated for 1 h under constant agitation at RT. Following five washes with 0.05% CHAPS in PBS, 100 µL of SA-HRP (diluted 1:1000 in 2% BSA/PBS) was added in case of IgM detection, whereas only PBS was added in case of IgG detection, and then incubated for 30 min at RT. Subsequently, 100 µL of TMB was added to wells and incubated for 5.5 min at RT. The reaction was stopped with 100 µL of 1 M HCl and the optical density (OD) was monitored on an iMark ELISA reader (Bio-Rad Laboratories Inc., CA, USA) at 450 nm.

Due to the absence of commercially available antibodies against p(HPMAm), anti-p(HPMAm) antibodies were determined using protein A pre-coated microplates (Pierce™ cat# 15155) allowing the Fc portion of IgG to bind and protein L pre-coated (Pierce™ cat# 15190) to allow kappa light chain of both IgG and IgM to bind [47,48], and subsequently, the specific binding was established using Cy7-labeled p(HPMAm)-b-p(HPMAm-Bz) micelles. In detail, the wells were rinsed three times with a solution of 0.05% Tween 20 in PBS. Diluted plasma samples, collected from mice injected with p(HPMAm)-b-p(HPMAm-Bz) micelles with or without biotin decoration, were introduced into the wells of a 96-well plate and subsequently incubated at RT for 1 h under constant agitation and then washed three times with PBS containing 0.05% Tween 20. 100 µL of Cy7-labeled p(HPMAm)-b-p(HPMAm-

Bz) micelles (Cy7-labeled polymer 15 µg/mL) was added to the wells followed by incubation at 37 °C for 1 h. Subsequently, the wells were washed three times with PBS containing 0.05% Tween 20 and the fluorescence intensity in the wells was measured at a wavelength of 800 nm using an Odyssey scanner (LI-COR, Nebraska, USA).

Results and Discussion

Micelle formation and characterization

Polymeric micelles were prepared by solvent extraction using THF as solvent for mPEG-b-p(HPMAm-Bz) polymers and DMF as a solvent for p(HPMAm)-b-p(HPMAm-Bz) with or without biotin conjugated to the terminus p(HPMAm); PBS was used as the non-solvent. Table 1 shows that the micelles obtained had similar sizes and size ranges, as well as surface charges, i.e., PEGylated and p(HPMAm) micelles, had mean sizes of 55 nm with a polydispersity index (PDI) below 0.14, and their zeta potential at pH 7.4 was slightly negative (-1.6, -7.7, and -6.3 mV for PEGylated, pHPMA, and biotinylated pHPMA micelles, respectively). The shape factor R_g/R_h, as characterized by AF4-MALS, was below 0.775 (0.48, 0.65, and 0.53 for PEGylated, pHPMA, and biotinylated pHPMA micelles, respectively), indicating the formation of core-shell structures [49,50]. The p(HPMAm) and PEG micelles dispersed in PBS showed a smaller aggregation number (N_{agg} = 400) as compared to what has been reported for similar micelles that had been reported with water as non-solvent (N_{agg} = 900) [43,44]. This lower N_{agg} value might be ascribed to the effect of the ionic strength on the formation of the micelles. Our previous study showed that slightly smaller micelles were formed in ionic solutions as compared to water [44]. For a bigger batch of micelles (400 mg polymers containing Cy7-labeled polymers instead of 50 mg copolymers without Cy7 label), both PEGylated and p(HPMAm) micelles showed a slightly larger size of 73 nm (PDI ≤ 0.14), a nearly neutral zeta potential (-1.0, -9.3, and -8.8 mV for PEGylated, pHPMA, and biotinylated pHPMA micelles, respectively), and an R_g/R_h value of below 0.775 (i.e., 0.65, 0.61, and 0.52 for PEGylated, pHPMA, and biotinylated pHPMA micelles, respectively). The higher N_{agg} (= 1000) of the Cy7-labeled batch as compared to the unlabeled batch (N_{agg} = 400) can probably be ascribed to the different scales at which the micelles were prepared. At a small scale, i.e., 20 mg polymer was fed in 1 mL organic solvent, Cy7-labeled and unlabeled polymers resulted in micelles of the same size (55 nm). However, once scaled up to 400 mg polymers in a volume of 20 mL organic solvent, micelles of 73 nm were formed likely due to the longer mixing time of organic solvent and anti-solvent resulting in a slow rate of nucleation growth and thus bigger micelles size and aggregation number [44,51]. The use of microfluidics mixing could circumvent scale-up issues which are recommended for future studies.

Table 1. Characteristics of p(HPMAm)-b-p(HPMAm-Bz) micelles with or without biotin decoration and mPEG-b-p(HPMAm-Bz) micelles as determined by TGA, DLS, and AF4-MALS.

Polymeric micelles	Concentration (mg/mL)	Z_{ave} (nm)	ζ (–mV)	R_g (nm)	R_h (nm)	R_g/R_h	$M_{w, mic}$ (10^6 Da)	N_{agg}
mPEG-b-p(HPMAm-Bz), 50 mg batch	29.7	55	-1.6	12	25	0.48	9.8	417
p(HPMAm)-b-p(HPMAm-Bz), 50 mg batch	29.8	55	-7.7	17	27	0.65	9.3	421
Biotinylated p(HPMAm)-b-p(HPMAm-Bz), 50 mg batch	28.6	55	-6.3	14	26	0.53	8.8	398
Cy7-labeled mPEG-b-p(HPMAm-Bz), 400 mg batch	29.1	73	-1.0	23	36	0.65	24.2	1029
Cy7-labeled p(HPMAm)-b-p(HPMAm-Bz), 400 mg batch	29.9	72	-9.3	22	35	0.61	22.4	1013
Cy7-labeled biotinylated p(HPMAm)-b-p(HPMAm-Bz), 400 mg batch	29.0	73	-8.8	22	35	0.52	23.5	1063

Conc. = polymer concentration in micellar dispersion determined by TGA, Z_{ave} = Z-average diameter determined by DLS, ζ = zeta potential determined by zetasizer in 10 mM HEPES buffer (pH 7.4), R_g = radius of gyration determined by AF4-MALS, R_h = radius of hydration determined by AF4-MALS, $M_{w, mic}$ = weight-average molecular weight of micelles determined by AF4-MALS, N_{agg} = the micelle aggregation number calculated by $M_{w, mic}/M_{n, p}$, where $M_{n, p}$ is the number-averaged molecular weight of a single polymer chain determined by ^{1}H NMR.

Circulation kinetics of PEGylated and p(HPMAm) micelles

The circulation kinetics and biodistribution of p(HPMAm) micelles with or without biotin decoration and PEGylated micelles were studied in immunocompetent BALB/c mice at a polymer dose of 150 mg per kg of body weight upon the first intravenous injection. Additionally, all three micelle formulations were injected two consecutive times into mice to establish whether accelerated clearance from the blood occurred. Previously, it was reported that the ABC effect is the most pronounced at the time interval of 6–8 days between the first and second administration in immunocompetent mice [52,53]. Hence in our study, the chosen injection interval between two doses was 7 days. Fig. 2 shows that the first injected dose of p(HPMAm)-b-p(HPMAm-Bz) micelles was eliminated faster from the circulation

than the corresponding PEGylated micelles of the same size, i.e., 8 and 30% of the injected dose of p(HPMAm) and PEGylated micelles were detected in plasma after 48 h, respectively. It appears that the biotin decoration had no significant impact on the circulation kinetics. It is further noted that the p(HPMAm) micelles showed biphasic elimination kinetics which is similar to PEGylated liposomes at low lipid dose [28], whereas the PEGylated micelles followed first-order elimination kinetics. The initial elimination phase half-life ($t_{1/2}$-α) of the p(HPMAm) micelles with or without biotin decoration was estimated to be around 0.6 h or <0.5 h, and terminal elimination phase half-lives ($t_{1/2}$-β) of a non-compartment analysis were 16.3±2.6 and 12.5±2.8 h, respectively, which were lower than the half-life ($t_{1/2}$ = 24.5±2.6 h) of PEGylated micelles (Table 2). The AUC values of p(HPMAm) micelles in plasma were 2.5–3.0 times lower compared to mPEG-b-p(HPMAm-Bz) micelles. The total distribution volumes of p(HPMAm)-b-p(HPMAm-Bz) micelles with or without biotin decoration were above 70 mL/kg, whereas the distribution volume of mPEG-b-p(HPMAm-Bz) micelles was 49±1 mL/kg that is slightly below a standard mouse blood volume of 58.5 mL/kg [54], indicating that a fraction of the injected dose of the p(HPMAm) micelles left the vascular space more extensively than the PEGylated micelles after 48 hours. Although the clearance of the first injection dose of p(HPMAm)-b-p(HPMAm-Bz) micelles with or without biotin decoration was slightly faster than mPEG-b-p(HPMAm-Bz) micelles, the good circulation half-lives of p(HPMAm) micelles are adequate for further pharmaceutical development as drug delivery systems.

Table 2. Pharmacokinetic parameters of the first and second injected dose of p(HPMAm)-b-p(HPMAm-Bz) micelles (with or without biotin decoration) and mPEG-b-p(HPMAm-Bz) micelles in plasma.

Polymeric micelles	Injection	Half-life (h)		$AUC_{0-\infty}$ ($\mu g \cdot h/mL$)	V (mL/kg)	CL (mL/h/kg)
		α Phase	β Phase			
p(HPMAm)-b-p(HPMAm-Bz)	1	<0.5	16.3±2.6	44600±5700	79±10	3.4±0.5
	2	<0.5	9.8±1.6	28600±3800	76±16	5.3±0.8
Biotinylated p(HPMAm)-b-p(HPMAm-Bz)	1	0.6	12.5±2.8	38400±2600	71±18	3.9±0.3
	2	<0.5	11.1±0.7	24800±3500	98±19	6.1±0.9
mPEG-b-p(HPMAm-Bz)	1	24.5±2.6	–	108200±12800	49±1	1.4±0.2
	2	14.7±3.2	–	54500±16200	63±28	2.9±0.9

α Phase, initial phase half-lives of p(HPMAm) micelles were estimated from plasma disappearance rates during the first hour after injection, whereas initial phase half-lives of PEGylated micelles were calculated from the non-compartment analysis. β Phase, half-lives of p(HPMAm) micelles were calculated from the non-compartment analysis. $AUC_{0-\infty}$, extrapolated area under the curve from time zero to infinity. V, volumes of distribution. CL, clearances. Volumes of distribution and clearances were calculated assuming that an average mouse has a standard blood volume of 58.5 mL/kg [54].

For the second injected dose of both the p(HPMAm)-b-p(HPMAm-Bz) micelles (with or without biotin decoration) and the mPEG-b-p(HPMAm-Bz) micelles, we set micellar concentration in plasma at 1 min as 100% injection dose, and similar circulation kinetics in plasma as for the first injected dose were observed (Fig. 2). However, it should be noted that the second injection of all three types of micelles showed 10-30% less of micellar concentration at 1 min post-administration as compared to the first injection. Therefore, although the second dose of PEGylated and p(HPMAm) micelles showed similar circulation kinetics as for the first dose, the AUC values of the second dose were 35-50% smaller than those of the first dose, suggesting that the circulation kinetics of second injection dose was actually different from the first dose for the different micelles. As the second injection of two-dose groups occurred on the same day as the single-dosed injections, using the same batch of Cy7-labeled micelles, it is not very likely that the instability of micelles and/or fluoroprobe quenching caused this very rapid clearance (<1 min) of the micelles. Importantly, the biodistribution analysis showed similarly low polymer accumulation in the kidneys (Fig. 4 & 5), suggesting that the PEGylated and p(HPMAm) micelles did not dissociate. Further investigation is required to understand the fast removal of the 10-30% of the second dose of the PEGylated and p(HPMAm) micelles at 1 min upon injection. Moreover, it should be noted that in the present study the circulation of p(HPMAm)-b-p(HPMAm-Bz) micelles was compared with mPEG-b-p(HPMAm-Bz) micelles of similar molecular weight of block copolymers. However, PEG has an expanded conformation, whereas pHPMA is a random coil as shown in a rat study of the blood circulation time of nanospheres surface-modified with semitelechelic pHPMA of different molecular weights [55]. One of the factors that determine the circulation time of decorated nanospheres is the hydrodynamic thickness of the coating layer. It has been shown using polystyrene microspheres coated with poloxamers that the thickness of the PEG coating layer is greater than a layer of pHPMA at the same molecular weight [56]. In future investigation, PEG and pHPMA of different molecular weights should be used for the preparation of micelles and evaluation of their ABC-related properties.
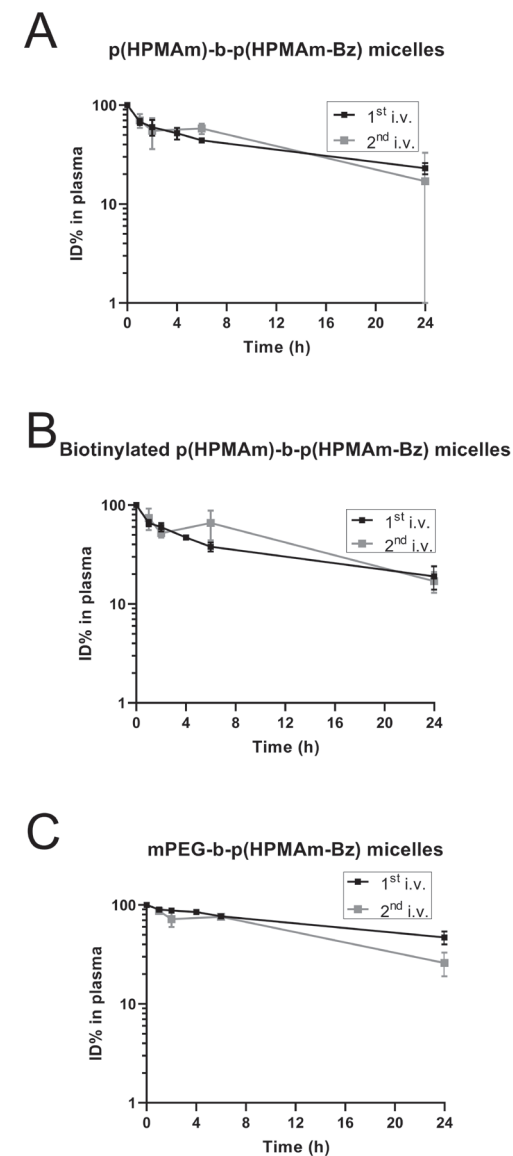

Fig. 2. Circulation kinetics of the first and second injected dose of p(HPMAm)-b-p(HPMAm-Bz) micelles with or without biotin decoration and mPEG-b-p(HPMAm-Bz) micelles in plasma of immunocompetent BALB/c mice. Micellar concentrations in plasma at 1 min were set at 100% injected dose. It should be noted that the second injection of the three different types of micelles showed 10-30% less micellar concentration at 1 min post-administration as compared to the first injection. For single injections, Cy7-labeled p(HPMAm), biotinylated p(HPMAm), and PEG micelles were injected. For repeated injections, an equivalent second dose of micelles (labeled dose) was given 7 days after the first injection of p(HPMAm), biotinylated p(HPMAm), and PEG micelles (non-labeled dose). Data are shown as mean ± SD of n = 3-4 mice per time point (n = 12 for first injection dose per group, n = 8 for second injection dose per group).

Determination of anti-PEG and anti-p(HPMAm) antibodies

The specific anti-polymer IgG and IgM antibody levels were measured in plasma using ELISA. In case of anti-PEG antibodies detection, wells containing post-dose plasma samples and free mPEG (1% w/v in PBS/BSA, average molecular weight of 5 kDa) showed a low response signal, pointing out the specificity towards PEG or the absence of anti-PEG antibodies in the plasma samples. As compared to pre-dose, anti-PEG IgM production was only observed in one out of eight mice. This mouse, however, did not show accelerated clearance from the circulation after the second injection of the PEGylated micelles. Fig. 3B shows the absence of specific anti-(pHPMAm) IgG and IgM antibodies. The absence of anti-polymer antibodies does not explain the very rapid clearance of p(HPMAm) and PEGylated micelles (10-30% of the injected dose) at 1 min upon injection. It is noted that although the study set up aimed that mPEG-b-p(HPMAm-Bz) micelles produced anti-PEG antibodies upon repeated administration, as observed for PEGylated liposomes, this was not observed. This might be ascribed to the small sizes and/or low aggregation number of micelles. It has been reported that micelles of small sizes and a low number of particles suppressed the induction of the ABC effect [13,27]. Another reason can be the high PEG density of the micelles. It has been reported that a high PEG density reduces protein adsorption onto the surface of nanoparticles leading to the suppression of the ABC effect [23,57]. On the other hand, since the ABC effect was usually reported to occur after 1 h upon repeated injection of PEGylated nanoparticles, the very rapid clearance of p(HPMAm) and PEGylated micelles within 1 min upon 2nd dose is likely caused due to some unknown effects. It is likely that the current assay was not sensitive enough to detect the antibodies against polymers. Because this assay was not validated due to the lack of positive control, namely a pool of sera from BALB/c mice immunized by pHPMA micelles. However, it should be noted that in serval studies it was shown that pHPMA does not induce an immune response *in vitro* and *in vivo* [58–60], so the sera might not contain anti-HPMA IgG and IgM antibodies.
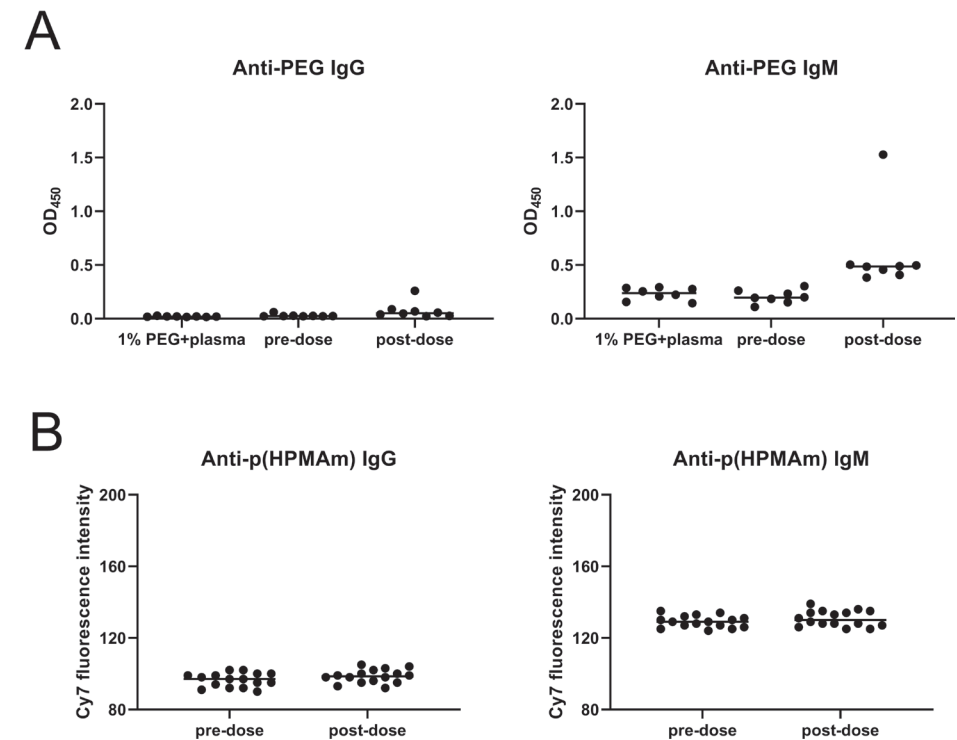
Fig. 3. Anti-polymer IgG and IgM detection using ELISA in mice pre-dose and post-dose plasma. Pre-dose occurred one day before any injections. Post-dose occurred seven days after i.v. administration of the first dose of the micelles. (**A**) Anti-PEG antibodies were determined using a sandwich ELISA as described above. Free mPEG (1% w/v in PBS/BSA, average molecular weight of 5 kDa) was added to establish the specificity of the formed anti-PEG antibodies. Data are shown as mean ± SD of n = 8. (**B**) Anti-p(HPMAm) antibodies were determined using protein A and L pre-coated microplates as described above. Data are shown as mean ± SD of n = 16.

Biodistribution of the micelles after i.v. administration

The biodistribution profiles of p(HPMAm)-b-p(HPMAm-Bz) micelles with or without biotin decoration and mPEG-b-p(HPMAm-Bz) micelles after i.v. administration were evaluated by measuring the fluorescence intensity in different organs. Fig. 4A & B show that the biotin decoration did not affect the distribution of the p(HPMAm) micelles in the different organs. After a single dose, 13±1% and 15±3% of the p(HPMAm) and PEGylated micelles accumulated in the liver at 48 h (Fig. 5A & C), respectively. Particularly, as shown in Fig. 4, 15±3% of the injected dose of p(HPMAm) micelles per g tissue accumulated in the liver at 48 h, respectively, which was similar to PEGylated micelles (17±3% per g tissue). Their accumulation

data (ID% per g tissue) were in good agreement with the imaging data of Cy7-labeled PEGylated micelles (Fig S1 in Supporting Information). Fig. 4 also shows that the accumulation of the studied micelles in the liver increased in time, which suggests hepatosis clearance by the reticuloendothelial system (RES) [61]. It is remarked that p(HPMAm) micelles with or without biotin decoration accumulated in the spleen to a less extent than PEGylated micelles (Fig. 5), suggesting that the removal of p(HPMAm) micelles occurs with less involvement of the splenic macrophages. As shown in Fig. 4, 6±1% and 5±2% of the injected dose per g tissue of p(HPMAm) micelles showed comparable accumulation in kidneys as compared to PEGylated micelles (6±1% and 5±1% per g tissue, respectively), which can be ascribed to the dissociation of micelles to unimers that have a molecular weight of around 23 kDa which is below renal clearance [62]. It is noted that 5±1% and 5±2% per g tissue of p(HPMAm) and PEGylated micelles accumulated in lungs at 48 h post single dose, respectively (Fig. 4), which can be explained by the disposition in hyper vascularized tissue due to prolonged blood circulation of the micelles and/or uptake by lung macrophages. The accumulation of the studied micelles in the heart and brain was negligible (Fig. 4 & 5). The p(HPMAm) micelles were cleared faster from the circulation than PEGylared micelles, however, the accumulation of these micelles in major organs was not significantly elevated (Fig. 5). Moreover, about 50-80% of p(HPMAm) micelles with or without biotin decoration were found back from major organs and blood at 6 h upon first and second injection, whereas close to 90-95% of PEGylated micelles were found back (Fig. 5). These results suggest that a large amount of the injected dose of p(HPMAm) micelles might accumulate in other organs which requires further investigation.

Biodistribution of p(HPMAm) micelles with or without biotin decoration and PEGylated micelles after the second dose did not show significant differences from the results found after the single-dose administrations (Fig. 4A-C).
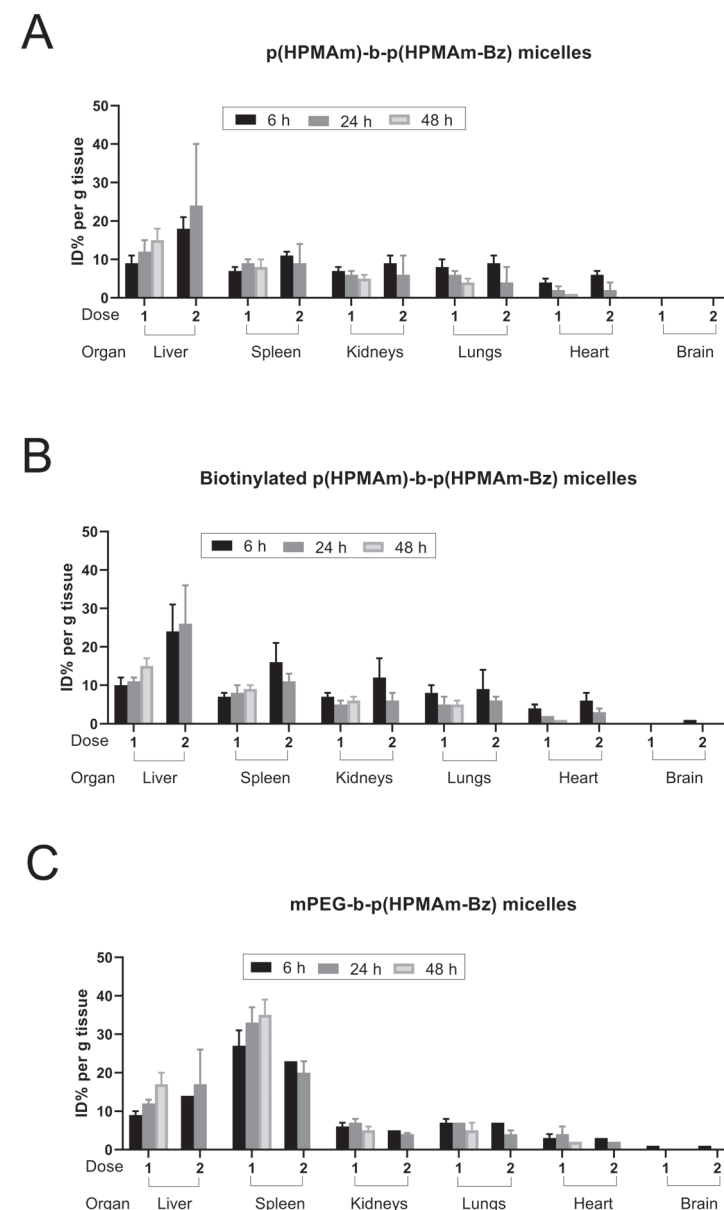

Fig. 4. Biodistribution (ID% per g tissue) of the first and second dose of p(HPMAm)-b-p(HPMAm-Bz) micelles with (**A**) or without biotin decoration (**B**) and mPEG-b-p(HPMAm-Bz) micelles (**C**) in the major organs (liver, spleen, kidneys, lungs, heart, and brain) of immunocompetent BALB/c mice. Paralleled groups of mice receiving a single dose were sacrificed at 6, 24, and 48 h post-administration, respectively, whereas paralleled groups of mice receiving a second dose were sacrificed at 6, and 24 h post-administration, respectively. Data are shown as mean ± SD of n = 3–4 mice per time point (n = 12 for first injection dose per group, n = 8 for second injection dose per group).
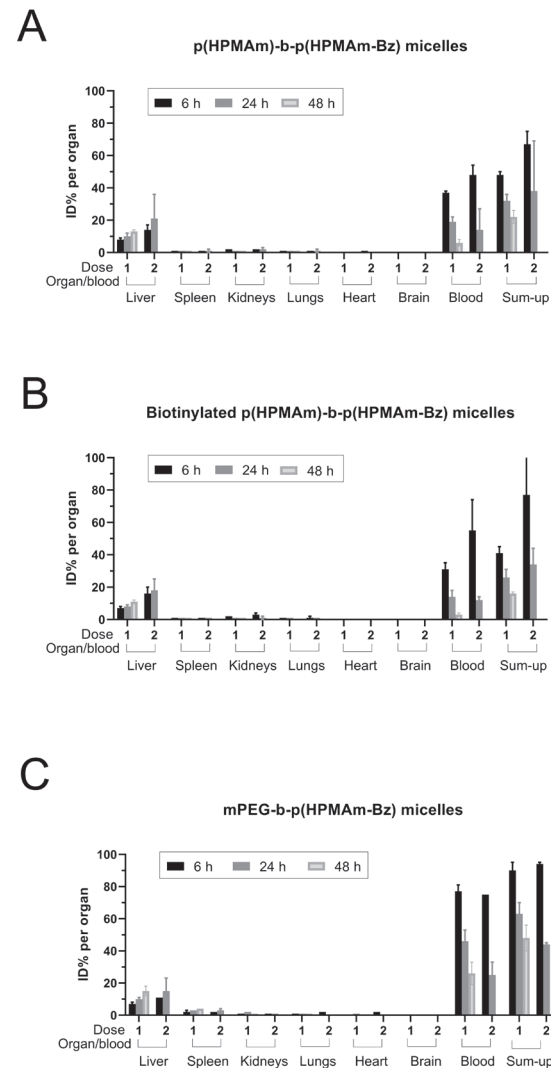
A

B

C

Fig. 5. Biodistribution (ID% per organ) of the first and second dose of p(HPMAm)-b-p(HPMAm-Bz) micelles with (**A**) or without biotin decoration (**B**) and mPEG-b-p(HPMAm-Bz) micelles (**C**) in the major organs (liver, spleen, kidneys, lungs, heart, and brain) and blood of immunocompetent BALB/c mice. Micellar concentrations in plasma at 1 min were set at 100% injected dose. Micellar concentrations in blood were converted from plasma concentrations considering a standard blood volume of 58.5 mL/kg and plasma recovery (Supporting Information). It should be noted that the second injection of the three types of micelles showed 10-30% less micellar concentration at 1 min post-administration as compared to the first injection. Paralleled groups of mice receiving a single dose were sacrificed at 6, 24, and 48 h post-administration, respectively, whereas paralleled groups of mice receiving a second dose were sacrificed at 6, and 24 h post-administration, respectively. Data are shown as mean ± SD of n = 3–4 mice per time point (n = 12 for first injection dose per group, n = 8 for second injection dose per group).

Conclusion

In this study, we investigated the *in vivo* circulation kinetics and biodistribution of micelles decorated with p(HPMAm) (with or without biotin decoration) as compared to PEG as the hydrophilic micellar shell to facilitate prolonged circulation in blood upon intravenous injection in mice. We found that the biotinylated p(HPMAm) micelles showed similar circulation kinetics compared to p(HPMAm) micelles without biotin decoration, thus the biotin targeting ligand did not cause immunogenicity. After the first administration, p(HPMAm) micelles showed slightly faster clearance than PEGylated micelles. The second administration 7 days after the first dose p(HPMAm) and PEGylared micelles showed rapid clearance of 10-30% of the injected dose at 1 min due to a yet unknown phenomenon with the absence of anti-polymer antibodies. These results suggest that additional investigations are required to have a better understanding of blood circulation and biodistribution of p(HPMAm) micelles.

5

References

[1]   K. Knop, R. Hoogenboom, D. Fischer, U.S. Schubert, Poly(ethylene glycol) in drug delivery: pros and cons as well as potential alternatives, Angewandte Chemie International Edition. 49 (2010) 6288–6308.

[2]   A.A. D'souza, R. Shegokar, Polyethylene glycol (PEG): a versatile polymer for pharmaceutical applications, Expert Opin Drug Deliv. 13 (2016) 1257–1275.

[3]   A. Abuchowski, T. Van Es, N.C. Palczuk, F.F. Davis, Alteration of immunological properties of bovine serum albumin by covalent attachment of polyethylene glycol, Journal of Biological Chemistry. 252 (1977) 3578–3581.

[4]   V. Francia, R.M. Schiffelers, P.R. Cullis, D. Witzigmann, The biomolecular corona of lipid nanoparticles for gene therapy, Bioconjug Chem. 31 (2020) 2046–2059.

[5]   I. Alberg, S. Kramer, M. Schinnerer, Q. Hu, C. Seidl, C. Leps, N. Drude, D. Möckel, C. Rijcken, T. Lammers, M. Diken, M. Maskos, S. Morsbach, K. Landfester, S. Tenzer, M. Barz, R. Zentel, Polymeric Nanoparticles with Neglectable Protein Corona, Small. 16 (2020) 1907574.

[6]   L. Digiacomo, D. Pozzi, S. Palchetti, A. Zingoni, G. Caracciolo, Impact of the protein corona on nanomaterial immune response and targeting ability, Wiley Interdiscip Rev Nanomed Nanobiotechnol. 12 (2020) 1–15.

[7]   J.J.F. Verhoef, T.J. Anchordoquy, Questioning the use of PEGylation for drug delivery, Drug Deliv Transl Res. 3 (2013) 499–503.

[8]   E.T.M. Dams, P. Laverman, W.J.G. Oyen, G. Storm, G.L. Scherphof, J.W.M. van der Meer, F.H.M. Corstens, O.C. Boerman, Accelerated blood clearance and altered biodistribution of repeated injections of sterically stabilized liposomes, Journal of Pharmacology and Experimental Therapeutics. 292 (2000) 1071–1079.

[9]   Y.W. Xin, T. Ishida, M. Ichihara, H. Kiwada, X.Y. Wang, T. Ishida, M. Ichihara, H.K. T, Influence of the physicochemical properties of liposomes on the accelerated blood clearance phenomenon in rats, Journal of Controlled Release. 104 (2005) 91–102.

[10]   T. Ishida, K. Masuda, T. Ichikawa, M. Ichihara, K. Irimura, H. Kiwada, Accelerated clearance of a second injection of PEGylated liposomes in mice, 255 (2003) 167–174.

[11]   T. Suzuki, M. Ichihara, K. Hyodo, E. Yamamoto, T. Ishida, H. Kiwada, H. Ishihara, H. Kikuchi, Accelerated blood clearance of PEGylated liposomes containing doxorubicin upon repeated administration to dogs, Int J Pharm. 436 (2012) 636–643.

[12]   B. Coins, W.T. Phillips, R. Klipper, Repeat injection studies of technetium-99M-labeled PEG-liposomes in the same animal, J Liposome Res. 8 (1998) 265–281.

[13]   K. Shiraishi, K. Kawano, Y. Maitani, T. Aoshi, K.J. Ishii, Y. Sanada, S. Mochizuki, K. Sakurai, M. Yokoyama, Exploring the relationship between anti-PEG IgM behaviors and PEGylated nanoparticles and its significance for accelerated blood clearance, Journal of Controlled Release. 234 (2016) 59–67.

[14]   X.Y. Wang, T. Ishida, H. Kiwada, Anti-PEG IgM elicited by injection of liposomes is involved in the enhanced blood clearance of a subsequent dose of PEGylated liposomes, Journal of Controlled Release. 119 (2007) 236–244.

[15]   T. Ishida, M. Ichihara, X.Y. Wang, K. Yamamoto, J. Kimura, E. Majima, H. Kiwada, Injection of PEGylated liposomes in rats elicits PEG-specific IgM, which is responsible for rapid elimination of a second dose of PEGylated liposomes, Journal of Controlled Release. 112 (2006) 15–25.

[16]   T. Ishida, M. Ichihara, X.Y. Wang, H. Kiwada, Spleen plays an important role in the induction of accelerated blood clearance of PEGylated liposomes, Journal of Controlled Release. 115 (2006) 243–250.

[17]   T. Ishida, R. Maeda, M. Ichihara, K. Irimura, H. Kiwada, Accelerated clearance of PEGylated liposomes in rats after repeated injections, Journal of Controlled Release. 88 (2003) 35–42.

[18]   J. Szebeni, S. Savay, L. Liebes, N.M. Rafique, C.R. Alving, F.M. Muggia, Complement activation following first exposure to pegylated liposomal doxorubicin (Doxil ®): possible role in hypersensitivity reactions, Annals of Oncology. 14 (2003) 1430–1437.

[19]   M. Estapé Senti, C.A. de Jongh, K. Dijkxhoorn, J.J.F. Verhoef, J. Szebeni, G. Storm, C.E. Hack, R.M. Schiffelers, M.H. Fens, P. Boross, Anti-PEG antibodies compromise the integrity of PEGylated lipid-based nanoparticles via complement, Journal of Controlled Release. 341 (2022) 475–486.

[20]   E. Chen, B.M. Chen, Y.C. Su, Y.C. Chang, T.L. Cheng, Y. Barenholz, S.R. Roffler, Premature drug release from polyethylene glycol (PEG)-coated liposomal doxorubicin via formation of the membrane attack complex, ACS Nano. 14 (2020) 7808–7822.

[21]   A.S. Abu Lila, H. Kiwada, T. Ishida, The accelerated blood clearance (ABC) phenomenon: clinical challenge and approaches to manage, Journal of Controlled Release. 172 (2013) 38–47.

[22]   H. Ma, K. Shiraishi, T. Minowa, K. Kawano, M. Yokoyama, Y. Hattori, Y. Maitani, Accelerated blood clearance was not induced for a gadolinium-containing PEG-poly (L-lysine) -based polymeric micelle in mice, Pharm Res. 27 (2010) 296–302.

[23]   T. Ishida, M. Harada, X. Yu, M. Ichihara, Y.W. Xin, M. Ichihara, K. Irimura, H. Kiwada, Accelerated blood clearance of PEGylated liposomes following preceding liposome injection : effects of lipid dose and PEG surface-density and chain length of the first-dose liposomes, Journal of Controlled Release. 105 (2005) 305–317.

[24]   L.M. Kaminskas, V.M. Mcleod, C.J. Christopher, B.J. Boyd, Differences in colloidal structure of PEGylated nanomaterials dictate the likelihood of accelerated blood clearance, J Pharm Sci. 100 (2011) 5069–5077.

[25]   M.R. Sherman, L.D. Williams, M.A. Sobczyk, S.J. Michaels, M.G.P. Saifer, Role of the methoxy group in immune responses to mpeg-protein conjugates, Bioconjug Chem. 23 (2012) 485–499.

[26]   H. Koide, T. Asai, K. Hatanaka, T. Urakami, T. Ishii, Particle size-dependent triggering of accelerated blood clearance phenomenon, Int J Pharm. 362 (2008) 197–200.

[27]   H. Koide, T. Asai, H. Kato, H. Ando, K. Shiraishi, M. Yokoyama, N. Oku, Size-dependent induction of accelerated blood clearance phenomenon by repeated injections of polymeric micelles, Int J Pharm. 432 (2012) 75–79.

[28]   B. Romberg, C. Oussoren, C.J. Snel, M.G. Carstens, W.E. Hennink, G. Storm, Pharmacokinetics of poly(hydroxyethyl- L -asparagine) -coated liposomes is superior over that of PEG-coated liposomes at low lipid dose and upon repeated administration, Biochim Biophys Acta. 1768 (2007) 737–743.

[29]   B. Romberg, C. Oussoren, C.J. Snel, W.E. Hennink, G. Storm, Effect of liposome characteristics and dose on the pharmacokinetics of liposomes coated with poly(amino acid)s, Pharm Res. 24 (2007) 2394–2401.

[30]   T. Ishihara, T. Maeda, H. Sakamoto, N. Takasaki, M. Shigyo, T. Ishida, H. Kiwada, Y. Mizushima, T. Mizushima, Evasion of the accelerated blood clearance phenomenon by coating of nanoparticles with various hydrophilic polymers, Biomacromolecules. 11 (2010) 2700–2706.

[31]   P.H. Kierstead, H. Okochi, V.J. Venditto, T.C. Chuong, S. Kivimae, J.M.J. Fréchet, F.C. Szoka, The effect of polymer backbone chemistry on the induction of the accelerated blood clearance in polymer modified liposomes, Journal of Controlled Release. 213 (2015) 1–9.

[32]   D. Hwang, J.D. Ramsey, A. v. Kabanov, Polymeric micelles for the delivery of poorly soluble drugs: from nanoformulation to clinical approval, Adv Drug Deliv Rev. 156 (2020) 80–118.

[33]   B. Weber, C. Seidl, D. Schwiertz, M. Scherer, S. Bleher, R. Süss, M. Barz, Polysarcosine-based lipids: from lipopolypeptoid micelles to stealth-like lipids in Langmuir Blodgett monolayers, Polymers (Basel). 8 (2016) 427.

[34]   J. Yang, J. Kopeček, Design of smart HPMA copolymer-based nanomedicines, Journal of Controlled Release. 240 (2016) 9–23.

[35]   P. Chytil, L. Kostka, T. Etrych, HPMA copolymer-based nanomedicines in controlled drug delivery, J Pers Med. 11 (2021) 1–22.

[36]   J. Yang, J. Kopeček, The light at the end of the tunnel—second generation HPMA conjugates for cancer treatment, Curr Opin Colloid Interface Sci. 31 (2017) 30–42.

[37]   X. Zhang, P. Chytil, T. Etrych, W. Liu, L. Rodrigues, G. Winter, S.K. Filippov, C.M. Papadakis, Binding of HSA to macromolecular pHPMA based nanoparticles for drug delivery: an investigation using fluorescence methods, Langmuir. 34 (2018) 7998–8006.

[38]   O. Naksuriya, Y. Shi, C.F. Van Nostrum, S. Anuchapreeda, W.E. Hennink, S. Okonogi, HPMA-based polymeric micelles for curcumin solubilization and inhibition of cancer cell growth, European Journal of Pharmaceutics and Biopharmaceutics. 94 (2015) 501–512.

[39]   Y. Shi, R. Van Der Meel, B. Theek, E. Oude Blenke, E.H.E. Pieters, M.H.A.M. Fens, J. Ehling, R.M. Schiffelers, G. Storm, C.F. Van Nostrum, T. Lammers, W.E. Hennink, Complete regression of xenograft tumors upon targeted delivery of paclitaxel via Π-Π stacking stabilized polymeric micelles, ACS Nano. 9 (2015) 3740–3752.

[40]   M. Bagheri, M.H. Fens, T.G. Kleijn, R.B. Capomaccio, D. Mehn, P.M. Krawczyk, E.M. Scutigliani, A. Gurinov, M. Baldus, N.C.H. van Kronenburg, R.J. Kok, M. Heger, C.F. van Nostrum, W.E. Hennink, In vitro and in vivo studies on HPMA-based polymeric micelles loaded with curcumin., Mol Pharm. 18 (2021) 1247–1263.

[41]   Y. Wang, M.J. van Steenbergen, N. Beztsinna, Y. Shi, T. Lammers, C.F. van Nostrum, W.E. Hennink, Biotin-decorated all-HPMA polymeric micelles for paclitaxel delivery, Journal of Controlled Release. 328 (2020) 970–984.

[42]   W.C. Chen, A.X. Zhang, S.D. Li, Limitations and niches of the active targeting approach for nanoparticle drug delivery, Eur J Nanomed. 4 (2012) 89–93.

[43]   M. Bagheri, J. Bresseleers, A. Varela Moreira, O. Sandre, S.A. Meeuwissen, R.M. Schiffelers, J.M. Metselaar, C.F. van Nostrum, J.C.M. van Hest, W.E. Hennink, The effect of formulation and processing parameters on the size of mPEG-b-p(HPMA-Bz) polymeric micelles, Langmuir. 34 (2018) 15495–15506.

[44]   Y. Wang, D.M.E. Thies-Weesie, E.D.C. Bosman, M.J. van Steenbergen, J. van den Dikkenberg, Y. Shi, T. Lammers, C.F. van Nostrum, W.E. Hennink, Tuning the size of all-HPMA polymeric micelles fabricated by solvent extraction, Journal of Controlled Release. 343 (2022) 338–346.

[45]   M. Andersson, B. Wittgren, K.G. Wahlund, Accuracy in multiangle light scattering measurements for molar mass and radius estimations, Anal Chem. 75 (2003) 4279–4291.

[46]   R. Kloos, I.M. Sluis, E. Mastrobattista, W.E. Hennink, R. Pieters, J. Verhoef, Acute lymphoblastic leukaemia patients treated with PEGasparaginase develop antibodies to PEG and the succinate linker, Br J Haematol. 189 (2020) 442–451.

[47]   Pierce ® protein A , protein G and protein A / G coated 96-well plates, (2022). https://www.thermofisher.com/document-connect/document-connect. html?url=https%3A%2F%2Fassets.thermofisher.com%2FTFS-Assets%2FL SG%2Fmanuals%2FMAN0011310_Pierce_ProteinA_G_AG_Coat_96Well_ UG.pdf (accessed March 27, 2022).

[48]   Pierce ™ protein L coated plates, (2022). https://www.thermofisher. com/document-connect/document-connect.html?url=https://assets. thermofisher.com/TFS-Assets%2FLSG%2Fmanuals%2FMAN0011366_ Pierce_ProteinL_Coat_Plate_UG.pdf (accessed March 27, 2022).

5

[49]   C. Ma, P. Pan, G. Shan, Y. Bao, M. Fujita, M. Maeda, Core-shell structure, biodegradation, and drug release behavior of poly(lactic acid)/poly(ethylene glycol) block copolymer micelles tuned by macromolecular stereostructure, Langmuir. 31 (2015) 1527–1536.

[50]   V.T.A. Nguyen, M.-C. De Pauw-Gillet, O. Sandre, M. Gauthier, Biocompatible polyion complex micelles synthesized from arborescent polymers, Langmuir. 32 (2016) 13482–13492.

[51]   E. Lepeltier, C. Bourgaux, P. Couvreur, Nanoprecipitation and the "ouzo effect": application to drug delivery devices, Adv Drug Deliv Rev. 71 (2014) 86–97.

[52]   T. Ishihara, M. Takeda, H. Sakamoto, A. Kimoto, C. Kobayashi, N. Takasaki, K. Yuki, K.I. Tanaka, M. Takenaga, R. Igarashi, T. Maeda, N. Yamakawa, Y. Okamoto, M. Otsuka, T. Ishida, H. Kiwada, Y. Mizushima, T. Mizushima, Accelerated blood clearance phenomenon upon repeated injection of peg-modified pla-nanoparticles, Pharm Res. 26 (2009) 2270–2279.

[53]   S.C. Semple, T.O. Harasym, K.A. Clow, S.M. Ansell, S.K. Klimuk, M.J. Hope, Immunogenicity and rapid blood clearance of liposomes containing polyethylene glycol-lipid conjugates and nucleic acid, Journal of Pharmacology and Experimental Therapeutics. 312 (2005) 1020–1026.

[54]   Approaches for sampling blood in the mouse, covering non-surgical, surgical and terminal techniques, (2021). https://nc3rs.org.uk/3rs-resources/blood-sampling/blood-sampling-mouse (accessed March 28, 2022).

[55]   S.S. Kamei, Prolonged blood circulation in rats of nanospheres surface-modified with semitelechelic poly[N-(2-hydroxypropyl)methacrylamide], Pharm Res. 12 (1995) 663–668.

[56]   L. Ilhm, L.O. Jacobsen, R.H. Miiller, E. Mak, S.S. Davis, Surface characteristics and the interaction of colloidal particles with mouse peritoneal macrophages, Biomaterials. 8 (1987) 113-117.

[57]   H. Zhou, Z. Fan, P.Y. Li, J. Deng, D.C. Arhontoulis, C.Y. Li, W.B. Bowne, H. Cheng, Dense and dynamic polyethylene glycol shells cloak nanoparticles from uptake by liver endothelial cells for long blood circulation, ACS Nano. 12 (2018) 10130–10141.

[58]   M. Kverka, J.M. Hartley, T.W. Chu, J. Yang, R. Heidchen, J. Kopeček, Immunogenicity of coiled-coil based drug-free macromolecular therapeutics, Biomaterials. 35 (2014) 5886–5896.

[59]   B. Říhová, M. Kovář, Immunogenicity and immunomodulatory properties of HPMA-based polymers, Adv Drug Deliv Rev. 62 (2010) 184–191.

[60]   B. Ri~ovx, K. Ulbricr, J. Kope~ek, P. Manual, Immunogenicity of N-(2-hydroxypropyl)-methacrylamide copolymers potential hapten or drug carriers, Folia Microbiol. 28 (1983) 217-227.

[61]   P. Laverman, A.H. Brouwers, E.T.M. Dams, W.J.G. Oyen, G. Storm, N. Van Rooijen, F.H.M. Corstens, O.C. Boerman, Preclinical and clinical evidence for disappearance of long-circulating characteristics of polyethylene glycol liposomes at low lipid dose, Journal of Pharmacology and Experimental Therapeutics. 293 (2000) 996–1001.

[62]   LW. Seymour, R. Duncan, J. Strohalm, J. Kopeček, Effect of molecular weight (Mw) of N-(2-hydroxypropyl)methacrylamide copolymers on body distribution and rate of excretion after subcutaneous, intraperitoneal, and intravenous administration to rats, J Biomed Mater Res. 21 (1987) 1341–1358.

5

Supporting information

Table S1. Characteristics of block copolymer p(HPMAm)-b-p(HPMAm-Bz) with or without biotin functionality and mPEG-b-p(HPMAm-Bz). Data were reproduced from previous publications [1–3].

Entry	Polymers	$M_{n, theory}$ (kDa)	$M_{n, NMR}$ (kDa)	$M_{n, GPC}$ (kDa)	PDI
1	p(HPMAm)$_{7.1k}$-b-p(HPMAm-Bz)$_{15.0k}$	24.9	22.1	11.0	1.48
2	biotinylated p(HPMAm)$_{6.8k}$-b-p(HPMAm-Bz)$_{16.3k}$	25.3	23.1	12.9	1.48
3	Cy7-labeled p(HPMAm)$_{7.1k}$-b-p(HPMAm-Bz)$_{14.1k}$	–	21.2	10.0	1.41
4	mPEG$_{5.0k}$-b-p(HPMAm-Bz)$_{18.5k}$	–	23.5	18.9	1.12
5	Cy7-labeled mPEG$_{5.0k}$-b-p(HPMAm-Bz)$_{17.5k}$	–	22.5	17.5	1.11

$M_{n, theory}$ = theoretical number average of molecular weight, $M_{n, NMR}$ = number average of molecular weight determined by ^{1}H NMR analysis, $M_{n, GPC}$ is determined by GPC analysis (DMF containing 10 mM LiCl as eluent, PEGs as standards), PDI = $M_{w, GPC}/M_{n, GPC}$.

Determination of recovery yield of Cy7-labeled micelles in mouse blood

Cy7-labeled pHPMA or PEGylated micelles at different concentrations (0.3, 3, and 30 mg/mL) were spiked into whole blood from BALB/c mice, followed by gentle mix and centrifugation at 1000 g for 15 min at 4 °C. The concentration of Cy7-labeled micelles in plasma was determined as described above. The red blood cell fractions were mixed with DMSO leading to lysis of the red blood cells, followed by vortexing and centrifugation at 15000 g for 15 min. The fluorescence intensity of the supernatant was measured and the concentration of Cy7-labeled micelles was determined as described above. Around ~7% of Cy7-labeled pHPMA micelles were in the red blood cell fractions which were either cellular bound or internalized micelles, whereas a negligible amount of Cy7-labeled PEGylared micelles was observed in red blood cells.
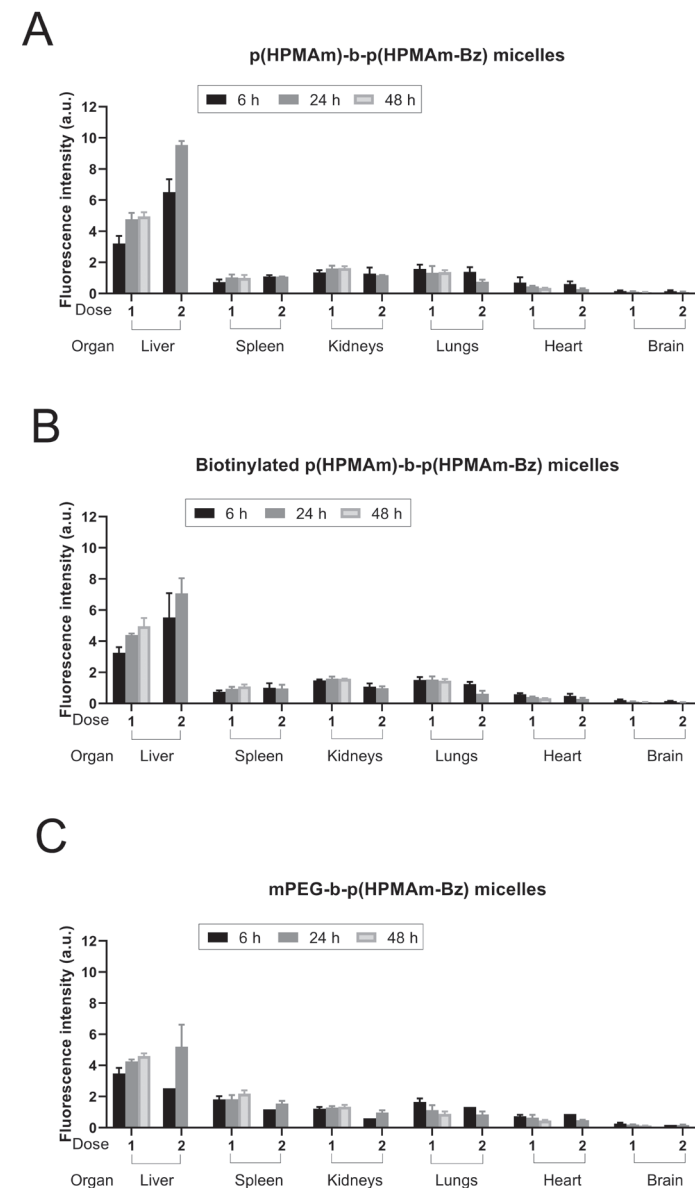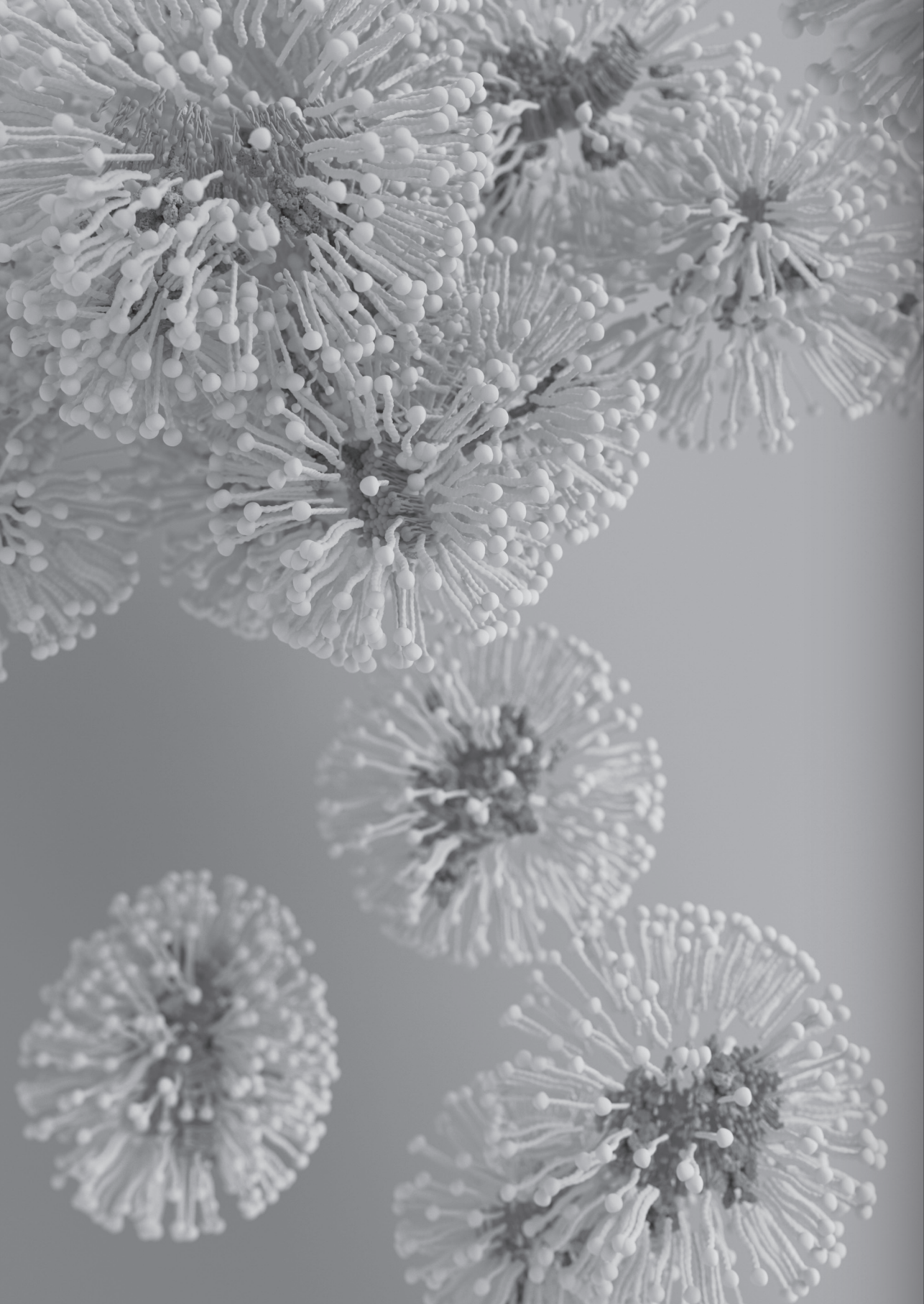

Fig. S1. *Ex vivo* fluorescence reflectance imaging (FRI) analysis of the accumulation of the Cy7-labeled p(HPMAm)-b-p(HPMAm-Bz) micelles with (**A**) or without biotin decoration (**B**) and mPEG-b-p(HPMAm-Bz) micelles (**C**) in the major organs (liver, spleen, kidneys, lungs, heart, and brain) of immunocompetent BALB/c mice. Images were obtained at λ_{ex} = 785 nm and λ_{em} = 820 nm and analyzed using Image Studio Lite Ver 5.2. Paralleled groups of mice receiving a single dose were sacrificed at 6, 24, and 48 h post-administration, respectively, whereas paralleled groups of mice receiving a second dose were sacrificed at 6, and 24 h post-administration, respectively. Data are shown as mean ± SD of n = 3–4 mice per time point (n = 12 for first injection dose per group, n = 8 for second injection dose per group).

References

[1]   Y. Wang, M.J. van Steenbergen, N. Beztsinna, Y. Shi, T. Lammers, C.F. van Nostrum, W.E. Hennink, Biotin-decorated all-HPMA polymeric micelles for paclitaxel delivery, Journal of Controlled Release. 328 (2020) 970–984.

[2]   M. Bagheri, J. Bresseleers, A. Varela Moreira, O. Sandre, S.A. Meeuwissen, R.M. Schiffelers, J.M. Metselaar, C.F. van Nostrum, J.C.M. van Hest, W.E. Hennink, The effect of formulation and processing parameters on the size of mPEG-b-p(HPMA-Bz) polymeric micelles, Langmuir. 34 (2018) 15495–15506.

[3]   A. Varela-moreira, H. Van Leur, D. Krijgsman, V. Ecker, M. Braun, M. Buchner, M.H.A.M. Fens, W.E. Hennink, M. Schiffelers, Utilizing in vitro drug release assays to predict in vivo drug retention in micelles, Int J Pharm. 618 (2022) 121638.

5

6

Summary and perspectives

Summary

Polymeric micelles have attracted growing attention for drug delivery purposes during the last three decades. They are composed of hydrophobic core – hydrophilic shell architectures which can be utilized for the solubilization of hydrophobic drugs [1–4]. The small size (<100 nm) endows polymeric micelles with good colloidal stability and prolonged circulation for passive accumulation in inflamed pathological tissues exploiting the enhanced permeability and retention (EPR) effect [5,6]. After reaching a tumor via the EPR effect, actively targeted micelles can be recognized by specific receptors overexpressed on the surface of cancer cells, which can subsequently be followed by cellular internalization and intracellular drug release [7]. Cellular internalization is particularly important for the intracellular delivery of nucleic acid-based drugs (single interfering RNA, plasmid DNA, messenger RNA, or oligonucleotides) that do not spontaneously permeate the cell membrane by Fickian diffusion [8]. An additional benefit of active targeting cell binding/internalization is that nanomedicines are retained in the tumor sites for a longer period and thus do not re-enter the systemic circulation whereas also their lymphatic drainage is retarded [9]. For nearly two decades, the small molecule biotin was covalently linked to nanomedicines for active targeting of nanomedicines because this ligand can be recognized by receptors overexpressed on cancer cells [10–12]. Poly(ethylene glycol) (PEG) has been widely used for coating of drug-loaded nanoparticles to increase their colloidal stability, prolong their circulation after intravenous administration, and finally accumulate in tumors and other inflamed tissues exploiting the EPR effect [13]. However, the pharmacokinetics after administration of the second dose of PEGylated nanoformulations can be changed due to the production of anti-PEG IgM by splenic marginal zone B cells resulting in their faster clearance [14–18]. The unwanted pharmacokinetic issue after the second dose is referred to as the accelerated blood clearance (ABC) effect, leading to drastically reduced therapeutic efficacy of PEGylated therapeutics as well as possibly resulting in acute anaphylaxis and hypersensitivity reaction [19,20]. This effect was initially revealed in numerous animal species and humans for PEGylated liposomes but was later on also reported in other PEGylated nanocarriers, such as PEG poly(lactide) (PLA) nanoparticles, PEGylated proteins pegfilgrastim (trade names Neulasta or G-Lasta), EGasparaginase, PEGylated lipid nanoparticles (LNPs), PEGylated polymeric micelles, and PEGylated exosomes [15,19,21–24]. To address this clinical concern, several strategies have been designed to overcome this limitation of PEGylation by tailoring the PEG conformation on the surface of nanoparticles and by exploring other synthetic hydrophilic uncharged polymers [25–27]. Poly(N-(2-hydroxypropyl) methacrylamide) (pHPMA) is a promising PEG alternative as the shell-forming polymer of polymeric micelles due to its high hydrophilicity, its proven biocompatibility in many applications as a component of drug delivery systems, and possibilities for functionalization [28–32]. This thesis describes the development of PEG-free and fully p(HPMA)-based polymeric micelles potentially suitable for cancer treatment. To render these micelles with targeting potential for cancer cells, biotin was decorated on their surface.

Chapter 1 provides a brief introduction of nanomedicines with a particular focus on biotinylated polymeric micelles for cancer treatment. The formulation technologies and characterization methodologies of polymeric micelles are shortly described and discussed. The quest for avoiding the ABC effect and searching for PEG-free alternative hydrophilic polymers is highlighted. Biotin as called vitamin B7 is highly water-soluble and can be conjugated to polymer-based drug delivery systems for active targeting. In this chapter, avidin-biotin technology is also shortly discussed.

Poly(N-2-benzoyloxypropyl methacrylamide) (p(HPMAm-Bz)) is a hydrophobic polymer that has been investigated as the hydrophobic core of PEGylated micelles which showed good stability and high drug loading capacity exploiting π-π stacking interactions between aromatic groups of the polymer chains as well as of the loaded drugs [33,34]. Taking this in mind, p(HPMAm)-b-p(HPMAm-Bz)-based polymeric micelles were developed and described in **Chapter 2**. Cyano-4-[(dodecylsulfanylthiocarbonyl)-sulfanyl]pentanoic acid (CDTPA) was used as a chain transfer agent (CTA) and 2,2′−azobis(2-methylpropionitrile) was used as initiator for reversible addition–fragmentation chain-transfer (RAFT) polymerization yielding a small library of p(HPMAm)-b-p(HPMAm-Bz) block copolymers with varying molecular weights (8 to 24 kDa). As anticipated, for block copolymers with a fixed molecular weight of the hydrophilic p(HPMAm) block, the critical micellar concentrations (CMC) of the polymers decreased with increasing molecular weight of the hydrophobic block. These polymers resulted in the formation of polymeric micelles in water via a solvent extraction method with tailored sizes from 40 to 90 nm. In this chapter, was coupled to the chain transfer agent CDTPA that was used subsequently for the synthesis of a biotinylated amphiphilic block copolymer p(HPMAm)-b-p(HPMAm-Bz). Paclitaxel-loaded polymeric micelles with 10% of the biotinylated polymer were formed through a solvent extraction method. The biotin-decorated micelles were more efficiently internalized by A549 lung cancer cells overexpressing the biotin receptor (SMVT, sodium multivitamin transporter) than non-targeted micelles, whereas very low internalization of both types of micelles by HEK293 human embryonic kidney cells lacking the biotin receptor was observed. Consequently, the paclitaxel-loaded micelles with biotin decoration exhibited stronger cytotoxicity in A549 cells than non-targeted micelles.

Chapter 3 demonstrates that for micelles with a fixed hydrophilic p(HPMAm) block molecular weight of 3, 5, and 7 kDa, respectively, the size, molecular weight ($M_{w,mic}$), and aggregation number (N_{agg}) of the obtained micelles increased with an increased molecular weight of the hydrophobic p(HPMAm-Bz) block, as determined by

asymmetric flow field-flow fractionation and multi-angle light scattering (AF4-MALS) coupled with dynamic light scattering (DLS). The micelles indeed possess a core-shell structure as determined by AF4-MALS-DLS, analytical ultracentrifugation, and Cryo-transmission electron microscopy (TEM). The effect of the processing conditions such as batch process versus continuous microfluidics, type of solvent, and solvent mixing parameters on micellar size was also investigated. The use of tetrahydrofuran and acetone as solvents for the polymers resulted in larger micelles, likely due to their relatively high water-solvent interaction parameters as compared to other solvents tested, i.e., dimethylformamide, dimethylacetamide, and dimethyl sulfoxide. Among the latter, only dimethylformamide led to micelles with a low polydispersity and thus narrow size distribution. The addition of dimethylformamide in which the p(HPMAm)-b-p(HPMAm-Bz) block copolymer was dissolved to the non-solvent water and a faster mixing of two solvents using microfluidics favored the formation of smaller micelles. The tunable mixing conditions significantly impact the particle formation and growth kinetics and thus allows for the preparation of micelles with small size and narrow size distribution.

Besides the application of biotin as a targeting ligand, its strong interaction with avidin was exploited in **Chapter 4** to study the *in vitro* drug release characteristics of polymeric micelles in defined buffer solutions as well as in biological fluids like plasma and blood using streptavidin-coated magnetic beads. Paclitaxel and curcumin release in different media was studied after the magnetic separation of micelles bound to the streptavidin-coated beads, by simultaneous determination of both the amount of drug released in the different media as well as the amount of drug still retained in the micelles. The *in vitro* release of paclitaxel and curcumin at 37 °C in PBS, PBS containing 2% v/v Tween 80, PBS containing 4.5% w/v bovine serum albumin (BSA), mouse plasma, and whole mouse blood was highly medium-dependent. In the different media studied, paclitaxel showed superior micellar retention compared to curcumin. Moreover, the presence of serum proteins accelerated the release of both paclitaxel and curcumin.

In **Chapter 5**, the circulation kinetics of p(HPMAm)-b-p(HPMAm-Bz) micelles with or without biotin decoration after a single and second injection were investigated in immunocompetent BALB/c mice and compared with the kinetics of PEG-b-p(HPMAm-Bz) micelles. After the first injection, pHPMA micelles showed biphasic elimination kinetics that is similar to PEGylated liposomes at low lipid dose, whereas the PEGylated micelles followed the first order of elimination kinetics. Single-dose injected p(HPMAm) micelles with or without biotin decoration were cleared faster than PEGylated micelles (16.3±2.6, 12.5±2.8, and 24.5±2.6 h, respectively). The studied micelles mainly accumulated in the liver. Moreover, the biotin decoration on the surface of the micelles did not impact the circulation, thus biotin decoration on the surface of p(HPMAm) micelles did not cause immunogenicity. The formation

of anti-pHPMA and anti-PEG antibodies was not detected after the first dose. The second dose was administrated seven days after the first injection because it was reported that the most pronounced accelerated blood clearance (ABC) effect occurred in immunocompetent mice using this dosing schedule [15,35]. After the second injection, PEGylated and pHPMA micelles showed very rapid clearance of 10-30% of the injected dose at 1 min compared to their first dose due to a yet unknown phenomenon. And the remaining dose was eliminated slightly faster than the first injected dose.

Perspectives

Driven by the idea of PEG-free nanoparticles, a micellar drug delivery system based on amphiphilic block copolymer p(HPMAm)-b-p(HPMAm-Bz) was prepared and investigated in this thesis. The small molecule biotin was decorated on the surface of p(HPMAm)-b-p(HPMAm-Bz) micelles as targeting ligand for improved cellular recognition and internalization by tumor cells as well as a platform to evaluate *in vitro* drug release in biological media such as whole blood. A few critical characteristics of p(HPMAm)-b-p(HPMAm-Bz) micelles were studied, i.e., size, stability, drug loading, drug retention, and blood circulation after a first and second administration.

The size of nanomedicines is a crucial physicochemical factor for EPR-based drug delivery and targeting systems. Lots of preclinical studies with nanoparticles have been published, which showed that nanocarriers can target drugs to tumors and other sites of inflammation via the EPR effect [5,36–39]. Smaller micelles with narrow size distribution are favored in terms of tumor accumulation and penetration [40]. **Chapter 3** describes the preparation of polymeric micelles based on p(HPMAm)-b-p(HPMAm-Bz) with tunable sizes using the solvent extraction method. The solvent-nonsolvent mixing results in local supersaturation and nucleation of the polymer leading to the spontaneous formation of micellar particles. The solvent extraction method is also suitable to encapsulate various therapeutic agents including poorly water-soluble drugs. The main advantage of this method is that it allows controlling the size of micelles by tuning the processing parameters such as total flow rate using microfluidics and solvent/nonsolvent ratio. This chapter demonstrates that micelles with a relatively small size of 40 to 90 nm can be prepared by a proper selection of the organic solvent for the amphiphilic p(HPMAm)-b-p(HPMAm-Bz) block copolymer in combination with a fast and controlled mixing rate with water as nonsolvent via a continuous process such as microfluidics. This robust method and continuous processing technology can be further developed for the reproducible production of large and sterile batches of p(HPMAm)-b-p(HPMAm-Bz) micelles for further preclinical and clinical studies. However, since an organic solvent is used

to produce the micelles, its removal and simultaneously controlling the stability of the micelles are major challenges. The residual organic solvent can lead to the the growth and subsequent unwanted aggregation of polymeric micelles due to Ostwald ripening, as well as can cause toxicity for animals and patients [41]. The organic solvent can be removed by e.g., dialysis, tangential flow filtration, and freeze-drying [42,43]. Also, the use of supercritical solvents e.g., trifluoromethane and carbon dioxide, allows for faster processing and easy solvent removal by rapidly withdrawing the pressure [44]. Implementing quality management systems based on the 'quality-by-design' concept introduced by the FDA in 2000 is a powerful tool to control pharmaceutical scale-up manufacturing processes [45].

Previous publications show that surface modification of nanoparticles with a tumor-targeting ligand does hardly or not affect the circulation properties and biodistribution profile, but does improve cellular uptake by target cells after extravasation, leading to enhanced therapeutic efficacy, particularly for drugs that need to be delivered intracellularly [46]. In line with previous publications, **Chapter 2** reports that compared to the non-targeted micelles, the biotinylated micelles triggered internalized and exerted higher cytotoxicity than non-targeted micelles using an *in vitro* cell assay. **Chapter 5** shows that the biotin decoration on the surface of the micelles did not have an effect on the circulation kinetics and biodistribution of the micelles upon single administration in mice as compared to non-biotinylated micelles. More importantly, after a second injection, the circulation kinetics of both micelles was not changed, indicating the absence of immunogenicity of pHPMA shell as well as the biotin ligand. This property makes drug-loaded biotinylated p(HPMAm)-b-p(HPMAm-Bz) micelles promising candidates for targeted therapies.

Stability and drug retention in circulation are key factors for the clinical success of polymeric micelles. Premature drug release in the bloodstream reduces the amount of drug that potentially can be delivered in the tumor as well as results in systemic drug exposure. To avoid premature drug release shortly after administration, drug-loaded micelles should have good thermodynamic as well as kinetic stability. **Chapter 2** describes the effect of block copolymers with different hydrophilic/hydrophobic molecular weights on the critical micellar concentrations (CMC). Our study showed that increasing the hydrophobic chain length of the block copolymer is a powerful approach to decreasing the CMC and thus improving the stability of the polymeric micelles. Other strategies such as core-cross linking and chemically coupling the drugs to the micelles via a degradable linker are also useful to circumvent micelle disassembly and uncontrolled drug release [47].

The stability and drug release of the micelles should be investigated in biological media such as plasma and blood for a better understanding of *in vivo* release

kinetics and to avoid the excessive use of animal models [48]. The biotinylated p(HPMAm)-b-p(HPMAm-Bz) micelles provide a tool for evaluation of *in vitro* drug release in biorelevant conditions as stated in **Chapter 4**. The avidin-biotin technology was implemented in this work, allowing the simultaneous determination of drug release and retention in different media including plasma and whole blood. As biotin can be easily introduced onto nanoparticles through published and relatively easy conjugation chemistries, this novel method can be extended to other nanoformulations loaded with a variety of drugs to study their stability in a great variety of biological media, e.g., blood and homogenate suspensions of tumor tissues. This approach can provide reliable *in vitro* drug release profiles for drugs that are of importance before further (pre)clinical and even clinical studies are planned.

Chapter 5 provides the comparison between pHPMA and PEGylated micelles in terms of circulation kinetics, biodistribution, and potential accelerated blood clearance after a first and second intravenous administration in mice. Although this study set up aimed that the second dose of PEGylated micelles, as observed for PEGylated liposomes, was rapidly cleared, this was not observed. The absence of an ABC effect in the selected animal might be ascribed to their small size of 70 nm as compared to other PEGylated polymeric micelles and liposomes that undergo the ABC effect [49,50]. Moreover, the higher PEG density on the surface of the micelles compared to that of liposomes also likely diminished the ABC effect [51]. It is therefore recommended that in a future study the circulation kinetics of the pHPMA micelles is compared with that of PEGylated liposomes and/or pHPMA micelles with larger sizes after the first and second injection. Furthermore, the rapid clearance of 10-30% of the second injected dose of pHPMA with or without biotin decoration, and PEGylated micelles occurred at 1 min due to a yet unknown phenomenon, which requires additional investigation.

Although the biotinylated p(HPMAm)-b-p(HPMAm-Bz) micelles as studied in this thesis are designed for the targeted delivery of anti-cancer agents, it is also possible to deliver other hydrophobic drugs in the treatment of inflammatory diseases and infectious diseases [52]. Furthermore, the biotinylated micellar systems and avidin-biotin technology can be also explored for imaging, biosensing, diagnosis, and tissue engineering in a variety of fields such as cell biology, pharmacology, and proteomics [53].

Despite the progress that has been achieved and described in this thesis regarding their physical chemical and pharmaceutical properties, many challenges and crucial issues remain for their further preclinical and ultimately clinical translation and development. For instance, nanoparticles encounter a variety of biological components once they are introduced to the bloodstream. Their surface is rapidly

6

coated with a layer of proteins, forming the so-called biomolecular corona which changes the surface properties, determines the overall biological behavior of the nanoparticle, and eventually affects the therapeutic efficacy [54–56]. Therefore, it is crucial to determine the composition of the biomolecular corona and understand the biological and therapeutic alterations of nanoparticles in the development of targeted nanomedicines. Separation of the biomolecular corona from unbound proteins is a major challenge because this soft protein corona (loosely bound proteins) is more fragile to preserve than the hard protein corona [57]. In this thesis, AF4 conjugated with MALS and DLS was used for the measurement of micelle size and shape as shown in **Chapter 3**. However, the separation and fractionation function of AF4 can be further exploited to separate micelle-protein complexes ranging from 1 nm to 1 μm under mild conditions, resulting in the preservation of the integrity of the soft protein corona [58]. Alberg et al. reported negligible protein adsorption on both core-cross-linked HPMA-based and PEGylated micelles and thus prolonging the circulation kinetics of the micelles. Therefore, identification of the proteins that form the corona as well as their effect on the pharmacological action of these micelles is a challenging research item.

Overall, this thesis sheds light on the synthesis, characterization, *in vitro* stability and release, and *in vivo* applications of biotin-decorated p(HPMAm)-b-p(HPMAm-Bz) micelles for targeted drug delivery. The biotinylated micelles can not only act as solubilizers and actively targeted drug carriers but also as a platform to quantify drug release and retention. The obtained results show that the biotinylated polymeric micelles fully based on a poly(HPMAm) backbone are promising candidates for targeted therapy and encourage further pharmaceutical development.

References

[1]   D. Hwang, J.D. Ramsey, A. V. Kabanov, Polymeric micelles for the delivery of poorly soluble drugs: from nanoformulation to clinical approval, Adv Drug Deliv Rev. 156 (2020) 80–118.

[2]   H. Cabral, K. Kataoka, Progress of drug-loaded polymeric micelles into clinical studies, Journal of Controlled Release. 190 (2014) 465–476.

[3]   S. Eetezadi, S.N. Ekdawi, C. Allen, The challenges facing block copolymer micelles for cancer therapy: In vivo barriers and clinical translation, Advanced Drug Delivery Reviews. 91 (2015) 7–22.

[4]   A. Varela-Moreira, Y. Shi, M.H.A.M. Fens, T. Lammers, W.E. Hennink, R.M. Schiffelers, Clinical application of polymeric micelles for the treatment of cancer, Mater Chem Front. 1 (2017) 1485–1501.

[5]   J. Fang, H. Nakamura, H. Maeda, The EPR effect: unique features of tumor blood vessels for drug delivery, factors involved, and limitations and augmentation of the effect, Adv Drug Deliv Rev. 63 (2011) 136–151.

[6]   H. Maeda, The 35th anniversary of the discovery of EPR effect: a new wave of nanomedicines for tumor-targeted drug delivery—personal remarks and future prospects, J Pers Med. 11 (2021) 229.

[7]   T. Lammers, F. Kiessling, W.E. Hennink, G. Storm, Drug targeting to tumors: principles, pitfalls and (pre-) clinical progress, Journal of Controlled Release. 161 (2012) 175–187.

[8]   U. Lächelt, E. Wagner, Nucleic acid therapeutics using polyplexes: a journey of 50 years (and beyond), Chemical Reviews. 115 (2015) 11043–11078.

[9]   A.G. Arranja, V. Pathak, T. Lammers, Y. Shi, Tumor-targeted nanomedicines for cancer theranostics, Pharmacological Research. 115 (2017) 87–95.

[10]   C. Wang, S. Ai, B. Wu, S.-W. Huang, Z. Liu, Biotinylated and fluorophore-incorporated polymeric mixed micelles for tumor cell-specific turn-on fluorescence imaging of Al 3+, J Mater Chem B. 8 (2020) 3557–3565.

[11]   G. Russell-Jones, K. McTavish, J. McEwan, J. Rice, D. Nowotnik, Vitamin-mediated targeting as a potential mechanism to increase drug uptake by tumours, J Inorg Biochem. 98 (2004) 1625–1633.

[12]   G. Russell-Jones, K. McTavish, J. McEwan, Preliminary studies on the selective accumulation of vitamin-targeted polymers within tumors, J Drug Target. 19 (2011) 133–139.

[13]   A.A. D'souza, R. Shegokar, Polyethylene glycol (PEG): a versatile polymer for pharmaceutical applications, Expert Opin Drug Deliv. 13 (2016) 1257–1275.

[14]   E.T.M. Dams, P. Laverman, W.J.G. Oyen, G. Storm, G.L. Scherphof, J.W.M. van der Meer, F.H.M. Corstens, O.C. Boerman, Accelerated blood clearance and altered biodistribution of repeated injections of sterically stabilized liposomes, Journal of Pharmacology and Experimental Therapeutics. 292 (2000) 1071–1079.

6

[15]   T. Ishihara, M. Takeda, H. Sakamoto, A. Kimoto, C. Kobayashi, N. Takasaki, K. Yuki, K.I. Tanaka, M. Takenaga, R. Igarashi, T. Maeda, N. Yamakawa, Y. Okamoto, M. Otsuka, T. Ishida, H. Kiwada, Y. Mizushima, T. Mizushima, Accelerated blood clearance phenomenon upon repeated injection of peg-modified pla-nanoparticles, Pharm Res. 26 (2009) 2270–2279.

[16]   A.S. Abu Lila, H. Kiwada, T. Ishida, The accelerated blood clearance (ABC) phenomenon: Clinical challenge and approaches to manage, Journal of Controlled Release. 172 (2013) 38–47.

[17]   M. Kawanishi, Y. Hashimoto, T. Shimizu, Comprehensive analysis of PEGylated liposome-associated proteins relating to the accelerated blood clearance phenomenon by combination with shotgun analysis and conventional methods, (2014) 547–555.

[18]   K. Shiraishi, K. Kawano, Y. Maitani, T. Aoshi, K.J. Ishii, Y. Sanada, S. Mochizuki, K. Sakurai, M. Yokoyama, Exploring the relationship between anti-PEG IgM behaviors and PEGylated nanoparticles and its significance for accelerated blood clearance, Journal of Controlled Release. 234 (2016) 59–67.

[19]   M. Estapé Senti, C.A. de Jongh, K. Dijkxhoorn, J.J.F. Verhoef, J. Szebeni, G. Storm, C.E. Hack, R.M. Schiffelers, M.H. Fens, P. Boross, Anti-PEG antibodies compromise the integrity of PEGylated lipid-based nanoparticles via complement, Journal of Controlled Release. 341 (2022) 475–486.

[20]   N. Longo, C.O. Harding, B.K. Burton, D.K. Grange, J. Vockley, M. Wasserstein, G.M. Rice, A. Dorenbaum, J.K. Neuenburg, D.G. Musson, Z. Gu, S. Sile, Single-dose, subcutaneous recombinant phenylalanine ammonia lyase conjugated with polyethylene glycol in adult patients with phenylketonuria: An open-label, multicentre, phase 1 dose-escalation trial, The Lancet. 384 (2014) 37–44.

[21]   N.E. Elsadek, A.S.A. Lila, S.E. Emam, T. Shimizu, H. Takata, H. Ando, Y. Ishima, T. Ishida, Pegfilgrastim (PEG-G-CSF) induces anti-PEG IgM in a dose dependent manner and causes the accelerated blood clearance (ABC) phenomenon upon repeated administration in mice, European Journal of Pharmaceutics and Biopharmaceutics. 152 (2020) 56–62.

[22]   R. Kloos, I.M. Sluis, E. Mastrobattista, W.E. Hennink, R. Pieters, J. Verhoef, Acute lymphoblastic leukaemia patients treated with PEGasparaginase develop antibodies to PEG and the succinate linker, Br J Haematol. 189 (2020) 442–451.

[23]   S.E. Emam, N.E. Elsadek, A.S. Abu, H. Takata, Y. Kawaguchi, T. Shimizu, H. Ando, Y. Ishima, T. Ishida, Anti-PEG IgM production and accelerated blood clearance phenomenon after the administration of PEGylated exosomes in mice, Journal of Controlled Release. 334 (2021) 327–334.

[24]   H. Koide, T. Asai, H. Kato, H. Ando, K. Shiraishi, M. Yokoyama, N. Oku, Size-dependent induction of accelerated blood clearance phenomenon by repeated injections of polymeric micelles, Int J Pharm. 432 (2012) 75–79.

[25]   J. McCallen, J. Prybylski, Q. Yang, S.K. Lai, Cross-reactivity of select PEG-binding antibodies to other polymers containing a C-C-O backbone, ACS Biomater Sci Eng. 3 (2017) 1605–1615.

[26]   H. Ma, K. Shiraishi, T. Minowa, K. Kawano, M. Yokoyama, Y. Hattori, Y. Maitani, Accelerated blood clearance was not induced for a gadolinium-containing PEG-poly (L-lysine) -based polymeric micelle in mice, Pharm Res. 27 (2010) 296–302.

[27]   Y. Fang, J. Xue, S. Gao, A. Lu, D. Yang, H. Jiang, Y. He, K. Shi, Cleavable PEGylation: a strategy for overcoming the "PEG dilemma" in efficient drug delivery, Drug Deliv. 24 (2017) 22–32.

[28]   J. Yang, J. Kopeček, Design of smart HPMA copolymer-based nanomedicines, Journal of Controlled Release. 240 (2016) 9–23.

[29]   P. Chytil, L. Kostka, T. Etrych, HPMA copolymer-based nanomedicines in controlled drug delivery, J Pers Med. 11 (2021) 1–22.

[30]   T. Lammers, K. Ulbrich, HPMA copolymers: 30years of advances, Advanced Drug Delivery Reviews. 62 (2010) 119–121.

[31]   M. Talelli, C.J.F. Rijcken, C.F. van Nostrum, G. Storm, W.E. Hennink, Micelles based on HPMA copolymers, Adv Drug Deliv Rev. 62 (2010) 231–239.

[32]   J. Kopeček, P. Kopečková, HPMA copolymers: origins, early developments, present, and future, Adv Drug Deliv Rev. 62 (2010) 122–149.

[33]   Y. Shi, R. Van Der Meel, B. Theek, E. Oude Blenke, E.H.E. Pieters, M.H.A.M. Fens, J. Ehling, R.M. Schiffelers, G. Storm, C.F. Van Nostrum, T. Lammers, W.E. Hennink, Complete regression of xenograft tumors upon targeted delivery of paclitaxel via Π-Π stacking stabilized polymeric micelles, ACS Nano. 9 (2015) 3740–3752.

[34]   M. Bagheri, M.H. Fens, T.G. Kleijn, R.B. Capomaccio, D. Mehn, P.M. Krawczyk, E.M. Scutigliani, A. Gurinov, M. Baldus, N.C.H. van Kronenburg, R.J. Kok, M. Heger, C.F. van Nostrum, W.E. Hennink, In vitro and in vivo studies on HPMA-based polymeric micelles loaded with curcumin., Mol Pharm. 18 (2021) 1247–1263.

[35]   S.C. Semple, T.O. Harasym, K.A. Clow, S.M. Ansell, S.K. Klimuk, M.J. Hope, Immunogenicity and rapid blood clearance of liposomes containing polyethylene glycol-lipid conjugates and nucleic acid, Journal of Pharmacology and Experimental Therapeutics. 312 (2005) 1020–1026.

[36]   H. Maeda, J. Wu, T. Sawa, Y. Matsumura, K. Hori, Tumor vascular permeability and the EPR effect in macromolecular therapeutics: a review, Journal of Controlled Release. 65 (2000) 271–284.

[37]   H. Maeda, The enhanced permeability and retention (EPR) effect in tumor vasculature: The key role of tumor-selective macromolecular drug targeting, Advances in Enzyme Regulation. 41 (2001) 189–207.

[38]   H. Maeda, Toward a full understanding of the EPR effect in primary and metastatic tumors as well as issues related to its heterogeneity, Adv Drug Deliv Rev. 91 (2015) 3–6.

6

[39]   H. Maeda, H. Nakamura, J. Fang, The EPR effect for macromolecular drug delivery to solid tumors: improvement of tumor uptake, lowering of systemic toxicity, and distinct tumor imaging in vivo, Adv Drug Deliv Rev. 65 (2013) 71–79.

[40]   H. Cabral, Y. Matsumoto, K. Mizuno, Q. Chen, M. Murakami, M. Kimura, Y. Terada, M.R. Kano, K. Miyazono, M. Uesaka, N. Nishiyama, K. Kataoka, Accumulation of sub-100 nm polymeric micelles in poorly permeable tumours depends on size, Nat Nanotechnol. 6 (2011) 815–823.

[41]   E. Lepeltier, C. Bourgaux, P. Couvreur, Nanoprecipitation and the "ouzo effect": application to drug delivery devices, Adv Drug Deliv Rev. 71 (2014) 86–97.

[42]   S. Đorđević, M.M. Gonzalez, I. Conejos-Sánchez, B. Carreira, S. Pozzi, R.C. Acúrcio, R. Satchi-Fainaro, H.F. Florindo, M.J. Vicent, Current hurdles to the translation of nanomedicines from bench to the clinic, Drug Delivery and Translational Research. 12 (2022) 500–525.

[43]   R. Kumar, S. v. Dalvi, P.F. Siril, Nanoparticle-based drugs and formulations: current status and emerging applications, ACS Appl Nano Mater. 3 (2020) 4944–4961.

[44]   P. Chakravarty, A. Famili, K. Nagapudi, M.A. Al-Sayah, Using supercritical fluid technology as a green alternative during the preparation of drug delivery systems, Pharmaceutics. 11 (2019) 1–34.

[45]   E. Sjögren, B. Abrahamsson, P. Augustijns, D. Becker, M.B. Bolger, M. Brewster, J. Brouwers, T. Flanagan, M. Harwood, C. Heinen, R. Holm, H.-P. Juretschke, M. Kubbinga, A. Lindahl, V. Lukacova, U. Münster, S. Neuhoff, M.A. Nguyen, A. Van Peer, C. Reppas, A.R. Hodjegan, C. Tannergren, W. Weitschies, C. Wilson, P. Zane, H. Lennernäs, P. Langguth, In vivo methods for drug absorption-comparative physiologies, model selection, correlations with in vitro methods (IVIVC), and applications for formulation/API/excipient characterization including food effects, European Journal of Pharmaceutical Sciences. 57 (2014) 99–151.

[46]   W.C. Chen, A.X. Zhang, S.D. Li, Limitations and niches of the active targeting approach for nanoparticle drug delivery, Eur J Nanomed. 4 (2012) 89–93.

[47]   Q. Hu, C.J. Rijcken, R. Bansal, W.E. Hennink, G. Storm, J. Prakash, Complete regression of breast tumour with a single dose of docetaxel-entrapped core-cross-linked polymeric micelles, Biomaterials. 53 (2015) 370–378.

[48]   M. Ghezzi, S. Pescina, C. Padula, P. Santi, E. del Favero, L. Cantù, S. Nicoli, Polymeric micelles in drug delivery: an insight of the techniques for their characterization and assessment in biorelevant conditions, Journal of Controlled Release. 332 (2021) 312–336.

[49]   T. Ishida, K. Masuda, T. Ichikawa, M. Ichihara, K. Irimura, H. Kiwada, Accelerated clearance of a second injection of PEGylated liposomes in mice, 255 (2003) 167–174.

[50]   H. Koide, T. Asai, K. Hatanaka, T. Urakami, T. Ishii, Particle size-dependent triggering of accelerated blood clearance phenomenon, Int J Pharm. 362 (2008) 197–200.

[51]   T. Ishida, M. Harada, X. Yu, M. Ichihara, Y.W. Xin, M. Ichihara, K. Irimura, H. Kiwada, Accelerated blood clearance of PEGylated liposomes following preceding liposome injection : effects of lipid dose and PEG surface-density and chain length of the first-dose liposomes, Journal of Controlled Release. 105 (2005) 305–317.

[52]   A. Jain, K. Cheng, The principles and applications of avidin-based nanoparticles in drug delivery and diagnosis, Journal of Controlled Release. 245 (2017) 27–40.

[53]   W.X. Ren, J. Han, S. Uhm, Y.J. Jang, C. Kang, J.S.H. Kim, J.S.H. Kim, Recent development of biotin conjugation in biological imaging, sensing, and target delivery, Chemical Communications. 51 (2015) 10403–10418.

[54]   X. Li, E. He, K. Jiang, W.J.G.M. Peijnenburg, H. Qiu, The crucial role of a protein corona in determining the aggregation kinetics and colloidal stability of polystyrene nanoplastics, Water Research. 190 (2021) 116742.

[55]   V. Francia, R.M. Schiffelers, P.R. Cullis, D. Witzigmann, The biomolecular corona of lipid nanoparticles for gene therapy, Bioconjug Chem. 31 (2020) 2046–2059.

[56]   Z.S. Al-Ahmady, M. Hadjidemetriou, J. Gubbins, K. Kostarelos, Formation of protein corona in vivo affects drug release from temperature-sensitive liposomes, Journal of Controlled Release. 276 (2018) 157–167.

[57]   M. Hadjidemetriou, K. Kostarelos, Nanomedicine: evolution of the nanoparticle corona, Nature Nanotechnology. 12 (2017) 288–290.

[58]   C. Weber, J. Simon, V. Mailänder, S. Morsbach, K. Landfester, Preservation of the soft protein corona in distinct flow allows identification of weakly bound proteins, Acta Biomaterialia. 76 (2018) 217–224.

6

Appendices

Nederlandse samenvatting

Polymere micellen hebben gedurende de laatste drie decennia steeds meer aandacht getrokken voor het toedienen van geneesmiddelen. Ze zijn samengesteld uit een hydrofobe kern en een hydrofiele schaal en kunnen worden gebruikt voor het oplossen van hydrofobe geneesmiddelen. De kleine afmeting (<100 nm), goede colloïdale stabiliteit en lange circulatie maken polymere micellen geschikt voor passieve accumulatie in ontstoken pathologische weefsels, waarbij gebruik wordt gemaakt van het 'enhanced permeation and retention' (EPR) effect. Na het bereiken van een tumor via het EPR-effect, kunnen micellen die voorzien van targeting liganden worden herkend door specifieke receptoren die tot overexpressie worden gebracht op het oppervlak van kankercellen, wat vervolgens kan worden gevolgd door cellulaire internalisatie en intracellulaire geneesmiddelafgifte. Cellulaire internalisatie is met name belangrijk voor de intracellulaire afgifte van op nucleïnezuur gebaseerde geneesmiddelen (siRNA, plasmide-DNA, mRNA of oligonucleotiden) die niet spontaan het celmembraan kunnen passeren door Fickiaanse diffusie. Een bijkomend voordeel van actieve targeting celbinding/internalisatie is dat nanomedicijnen voor een langere periode in de tumor worden vastgehouden en dus niet opnieuw in de systemische circulatie komen, terwijl ook hun lymfatische drainage wordt vertraagd. In recente studies werd het kleine molecuul biotine covalent gekoppeld aan nanomedicijnen voor actieve targeting omdat dit ligand kan worden herkend door biotinereceptoren die aanwezig zijn op kankercellen. Poly(ethyleenglycol) (PEG) wordt vaak gebruikt voor het coaten van met farmaca beladen nanodeeltjes om hun colloïdale stabiliteit te vergroten en ook om na intraveneuze toediening hun circulatie te verlengen waardoor deze deeltjes zich uiteindelijk ophopen in tumoren en andere ontstoken weefsels via het genoemde EPR-effect. De farmacokinetiek na toediening van de tweede dosis gePEGyleerde nanoformuleringen kan echter nadelig worden beïnvloed door de productie van anti-PEG IgM door B-cellen van de milt, wat resulteert in hun snellere klaring. Poly(N-(2-hydroxypropyl) methacrylamide) (pHPMA) is een veelbelovend PEG-alternatief voor het schilvormende polymeer van polymere micellen vanwege de hoge hydrofiliciteit, de in veel farmaceutische toepassingen bewezen biocompatibiliteit en mogelijkheden voor functionalisering. Dit proefschrift beschrijft de ontwikkeling van PEG-vrije en volledig p(HPMA)-gebaseerde polymere micellen die mogelijk geschikt zijn voor de behandeling van kanker. Deze micellen werden uitgerust met biotine op hun oppervlak om deze specifiek te maken voor kankercellen.

Hoofdstuk 1 geeft een korte introductie van nanomedicijnen met een bijzondere focus op gebiotinyleerde polymere micellen voor de behandeling van kanker. De formuleringstechnologieën en karakteriseringsmethodologieën van polymere micellen worden kort beschreven en besproken. Onderzoek naar het vermijden van het versnelde bloedklaringseffect (ABC) en naar PEG-vrije alternatieve hydrofiele polymeren wordt benadrukt. Biotine, ook vitamine B7 genoemd, is zeer goed oplosbaar in water en kan worden geconjugeerd aan polymeer gebaseerde medicijnafgiftesystemen voor actieve targeting. In dit hoofdstuk wordt ook kort de avidine-biotine-technologie besproken.

Poly(N-2-benzoyloxypropylmethacrylamide) (p(HPMAm-Bz)) is een hydrofoob polymeer dat is onderzocht als de hydrofobe kern van gePEGyleerde micellen die een goede stabiliteit en een hoge geneesmiddelbeladinscapaciteit vertoonden door gebruik te maken van π-π-'stacking' interacties tussen aromatische groepen van de polymeerketens en die van de beladen geneesmiddelen. Met dit in gedachten werden op p(HPMAm)-b-p(HPMAm-Bz) gebaseerde polymere micellen ontwikkeld en beschreven in **Hoofdstuk 2**. Cyano-4-[(dodecylsulfa-nylthiocarbonyl)-sulfanyl] pentaanzuur (CDTPA) werd gebruikt als ketenoverdrachtsagens (CTA) en 2,2'-azobis (2-methylpropionitril) werd gebruikt als initiator voor reversibele additie-fragmentatieketen-transfer (RAFT) polymerisatie die een kleine bibliotheek van p(HPMAm)-b-p(HPMAm-Bz) blokcopolymeren met variërende molecuulgewichten (8 tot 24 kDa) opleverde. Zoals verwacht nam voor blokcopolymeren met een vast molecuulgewicht van het hydrofiele p(HPMAm)-blok de kritische micellaire concentratie (CMC) van de polymeren af met toenemend molecuulgewicht van het hydrofobe blok. Deze polymeren resulteerden in water in de vorming van polymere micellen via een oplosmiddelextractiemethode met stuurbare afmetingen van 40 tot 90 nm. In dit hoofdstuk werd biotine gekoppeld aan het ketenoverdrachtsagens CDTPA dat vervolgens werd gebruikt voor de synthese van een gebiotinyleerd amfifiel blokcopolymeer p(HPMAm)-b-p(HPMAm-Bz). Met paclitaxel beladen polymere micellen met 10% van het gebiotinyleerde polymeer werden gevormd door middel van een oplosmiddelextractiemethode. De met biotine uitgeruste micellen werden efficiënter geïnternaliseerd door A549-longkankercellen die de biotinereceptor (SMVT, de natriummultivitaminetransporter) tot overexpressie brengen dan niet-getargete micellen, terwijl een zeer lage internalisatie van beide soorten micellen door HEK293 menselijke embryonale niercellen die de biotinereceptor niet tot expressie brengen, werd waargenomen. Bijgevolg vertoonden de met paclitaxel beladen micellen met biotinedecoratie een sterkere cytotoxiciteit voor A549-cellen dan voor niet-getargete micellen.

Hoofdstuk 3 laat zien dat voor micellen met een hydrofiel p(HPMAm) molecuulgewicht van respectievelijk 3, 5 en 7 kDa, de grootte, het molecuulgewicht ($M_{w,mic}$) en het aggregatiegetal (N_{agg}) van de verkregen micellen toenamen met een toenemend molecuulgewicht van het hydrofobe p(HPMAm-Bz)-blok, zoals bepaald door asymmetrische stroomveldfractionering en lichtverstrooiing met meerdere hoeken (AF4-MALS) gekoppeld aan dynamische lichtverstrooiing (DLS). De micellen hebben inderdaad een kern-schilstructuur zoals bepaald met AF4-MALS-DLS,

analytische ultracentrifugatie en cryotransmissie-elektronenmicroscopie (TEM). Het effect van de proces-omstandigheden zoals batchproces versus continue microfluïdica, type oplosmiddel en oplosmiddelmengparameters op micellaire grootte werd ook onderzocht. Het gebruik van tetrahydrofuran en aceton als oplosmiddelen voor de polymeren resulteerde in grotere micellen, waarschijnlijk vanwege hun relatief hoge water-oplosmiddel-interactieparameters in vergelijking met andere geteste oplosmiddelen, in het bijzonder dimethylformamide, dimethylacetamide en dimethylsulfoxide. Van de laatst genoemde oplosmiddelen leidde alleen dimethylformamide tot micellen met een lage polydispersiteit en dus een nauwe grootteverdeling. De toevoeging van dimethylformamide waarin het p(HPMAm)-b-p(HPMAm-Bz) blokcopolymeer was opgelost aan het niet-oplosmiddel water en een snellere menging van de twee oplosmiddelen met behulp van microfluïdische middelen bevorderden de vorming van kleinere micellen. De stuurbare mengomstandigheden hebben een aanzienlijke invloed op de deeltjesvorming en groeikinetiek en maken zo de bereiding van micellen met een kleine grootte en een smalle grootteverdeling mogelijk.

In **Hoofdstuk 4** wordt gebruik gemaakt van de sterke interactie van biotine met avidine om de *in vitro* geneesmiddelafgifte van polymere micellen in gedefinieerde bufferoplossingen en ook in biologische vloeistoffen zoals plasma en bloed te bestuderen met behulp van met streptavidine gecoate magnetische deeltjes. De afgifte van paclitaxel en curcumine in verschillende media werd bestudeerd na de magnetische scheiding van micellen die waren gebonden aan de met streptavidine gecoate deeltjes, door gelijktijdige bepaling van zowel de hoeveelheid geneesmiddel die in de verschillende media was afgegeven als de hoeveelheid geneesmiddel die nog in de micellen aanwezig was. De *in vitro* afgifte van paclitaxel en curcumine bij 37 °C in PBS, PBS met 2% v/v Tween 80, PBS met 4,5% w/v runderserumalbumine (BSA), muizenplasma en bloed van muizen was zeer medium afhankelijk. In de verschillende onderzochte media vertoonde paclitaxel een superieure micellaire retentie in vergelijking met curcumine. Bovendien versnelde de aanwezigheid van serumeiwitten de afgifte van zowel paclitaxel als curcumine.

In **Hoofdstuk 5** werd de circulatiekinetiek van p(HPMAm)-b-p(HPMAm-Bz) micellen met of zonder biotinedecoratie na een enkele en tweede injectie onderzocht in immunocompetente BALB/c muizen, en vergeleken met de kinetiek van PEG-b-p(HPMAm-Bz) micellen. Na de eerste injectie vertoonden pHPMA- micellen een bifasische eliminatiekinetiek die vergelijkbaar is met gePEGyleerde liposomen bij een lage lipidedosis, terwijl de gePEGyleerde micellen eerste orde eliminatiekinetiek vertoonden. Een enkele dosis geïnjecteerde p(HPMAm)-micellen met of zonder biotinedecoratie werden sneller geklaard dan gePEGyleerde micellen (halfwaardetijd respectievelijk 16,3 ± 2,6, 12,5 ± 2,8 en 24,5 ± 2,6 uur). De bestudeerde micellen hoopten zich voornamelijk op in de lever. Bovendien had de biotinedecoratie

op het oppervlak van de micellen geen invloed op de circulatiekinetiek, waaruit geconludeerd kan worden dat de aanwezigheid van biotine op het oppervlak van p(HPMAm)-micellen geen immunogeniciteit veroorzaakte. De vorming van anti-pHPMA- en anti-PEG-antilichamen werd niet gedetecteerd na de eerste dosis. De tweede dosis werd zeven dagen na de eerste injectie toegediend omdat uit eerdere studies gebleken is dat het meest uitgesproken versnelde bloedklaring (ABC) effect optrad bij immunocompetente muizen die dit doseringsschema ondergingen. Na de tweede injectie vertoonden gePEGyleerde en pHPMA-micellen een zeer snelle klaring van 10-30% van de geïnjecteerde dosis na 1 minuut in vergelijking met hun eerste dosis als gevolg van een nog onbekend fenomeen. En de resterende dosis werd iets sneller geëlimineerd dan de eerste geïnjecteerde dosis.

Over het algemeen werpt dit proefschrift licht op de synthese, karakterisering, in vitro stabiliteit en afgifte, en in vivo toepassingen van met biotine uitgeruste p(HPMAm)-b-p(HPMAm-Bz) micellen voor gerichte afgifte van geneesmiddelen. De gebiotinyleerde micellen kunnen niet alleen fungeren als solubilisatoren en actief getargete dragers van geneesmiddelen, maar ook als een platform om de afgifte en retentie van geneesmiddelen te kwantificeren. De verkregen resultaten laten zien dat de gebiotinyleerde polymere micellen die volledig gebaseerd zijn op een poly(HPMAm) ruggengraat, veelbelovende kandidaten zijn voor gerichte therapie en dus verdere farmaceutische ontwikkeling bemoedigen.

Curriculum vitae

Yan Wang was born in 1991 in Shandong, China. In 2010 she obtained her high school diploma and started her bachelor's study in Pharmacy at Shandong University. In 2014 she enrolled the master's program of Medicinal Chemistry at Shandong University. Her master's internship was performed at Shandong Chengchuang Pharmaceutical Technology Development Company under the supervision of Prof. dr. Zhaopeng Liu and Peifu Jiao. Her project aimed to synthesize drug conjugates for heart failure. In 2017 she started her PhD at the Department of Pharmaceutics at Utrecht University under the supervision of Prof. dr. Wim E. Hennink and Dr. C.F. van Nostrum. Her project was focused on investigating biotinylated polymeric micelles based on amphiphilic poly(*N*-2-hydroxypropyl methacrylamide)-block-poly(*N*-2-benzoyloxypropyl methacrylamide) (p(HPMAm)-b-p(HPMAm-Bz)) block copolymers for targeted drug delivery. The results of the research are described in this thesis.

List of publications

Publications in this thesis:

Y. Wang, M.H. Fens, N.C.H. Van Kronenburg, Y. Shi, T. Lammers, M. Heger, C.F. Van Nostrum, W.E. Hennink, Magnetic beads for the evaluation of drug release from biotinylated polymeric micelles in biological media, J. Control. Release. 349 (2022) 954–962.

Y. Wang, D.M.E. Thies-Weesie, E.D.C. Bosman, M.J. van Steenbergen, J. van den Dikkenberg, Y. Shi, T. Lammers, C.F. van Nostrum, W.E. Hennink, Tuning the size of all-HPMA polymeric micelles fabricated by solvent extraction, J. Control. Release. 343 (2022) 338–346.

Y. Wang, M.J. van Steenbergen, N. Beztsinna, Y. Shi, T. Lammers, C.F. van Nostrum, W.E. Hennink, Biotin-decorated all-HPMA polymeric micelles for paclitaxel delivery, J. Control. Release. 328 (2020) 970–984.

Y. Wang, M.H. Fens, A. Varela-Moreira, M. Bagheri, N.C.H. van Kronenburg, M. Estapé Senti, R.J. Kok, Y. Shi, T. Lammers, C.F. van Nostrum, W.E. Hennink, The effect of pHPMA as PEG alternative in polymeric micelles on circulation kinetics and possible accelerated blood clearance, in preparation.

Other publications:

C. Liang, X. Bai, C. Qi, Q. Sun, X. Han, T. Lan, H. Zhang, X. Zheng, R. Liang, J. Jiao, Z. Zheng, J. Fang, P. Lei, **Y. Wang**, D. Möckel, J.M. Metselaar, G. Storm, W.E. Hennink, F. Kiessling, H. Wei, T. Lammers, Y. Shi, B. Wei, Π Electron-Stabilized Polymeric Micelles Potentiate Docetaxel Therapy in Advanced-Stage Gastrointestinal Cancer, Biomaterials. 266 (2021) 120432.

Y. Wang, Z. Liu, PCSK9 inhibitors: novel therapeutic strategies for lowering LDL cholesterol, Mini-Reviews Med. Chem. 19 (2019) 165–176.

Acknowledgement

During my PhD, I met many nice and important people that contributed to finishing this thesis. I would like to thank everyone who provided assistance, encouragement, and guidance, and without whom I could not have succeeded.

My deep gratitude goes first to my promoter Wim. Dear Wim, I am grateful for your unwavering enthusiasm for the HPMA project. This work could not have been finished without your consistent support and guidance throughout the process. I am truly impressed by your knowledge of chemistry. You taught me to carefully describe the evidence from experiments, in which I have learned a kind of standard of integrity and honesty. Your instructive input and constructive criticism helped me lead to good publications. I will not forget my last experiment in the lab that we did together using a Ubbelohde viscometer. Your dedication to work inspires me to find/do a job that I love.

My sincere thanks go to my co-promoter Rene. Dear Rene, thanks for your insightful contributions to the project. It would be impossible to complete this work without your input. You gave me invaluable help with some analyses and calculations. Thanks for teaching me to use Wilhelmy plate in the lab. I am profoundly grateful that you introduced AF4 to our group which helped a lot in this thesis. Also, thanks for talking to me when I was very stressed approaching the end of my academic journey.

Special thanks go to Nataliia. Dear Nataliia, thanks for being my daily supervisor or mentor in the first year of my PhD. I am amazed by your knowledge of 3D cell culture although this has little to do with my research. You tried to help me as much as you can in biotin-related synthesis. Your kindness, patience, and suggestions were exactly what I needed at the beginning of my research.

From the bottom of my heart, I would like to thank Mies and Marcel. Dear Mies, you were involved in most of the projects in our group, especially the work of chapters 2 and 3 in this thesis. Thanks for your input in the progress meetings with my supervisors. I am grateful that you gave me instructions on every analytical machine that I used and helped me with troubleshooting. Your broad knowledge, good sense of humor, and hearty laughing were never to be forgotten. Dear Marcel, I was influenced by your 'cartoon' idea in scientific storytelling and amazed by your 'fishing' idea in chapter 4. Thanks for all your work in the animal experiments and your timely support in chapter 5. I am grateful for your essential contributions to the project. I will never forget the day we did the animal study, which was one of the most intense days during my PhD. Your sense of humor boosted my resilience though. Also, it is my honor to have you as one of my paranymphs. Thanks for your time and help to organize my promotion.

I would like to express my gratitude to our skilled technicians. Dear Joep, thanks for teaching me cell culture, and I enjoyed talking with you every time. Your insightful thoughts and good humor always enlightened the atmosphere. Dear Louis, Roel, Kim, Esmeralda, and Imro, thanks for taking care of the chemical order and I am grateful for your help and suggestions in the lab. Also, I would like to thank our secretary, dear Barbara, thanks for organizing appointments with my supervisors. I will always remember your kindness and patience.

I would like to say a big thank you to the girls. Dear Yanna, I was lucky to do my master's and PhD in the same group as you. You were someone I always respected because you were optimistic, diligent, and caring. Thanks for helping me settle down in the Netherlands and giving me suggestions in the lab. Dear Mahsa, thanks for being my lab buddy and helping me out of difficult times. I have learned a lot from you about PEGylated polymeric micelles. I admire your diligence, perseverance, and integrity. I am so happy that you are my other paranymph, which means a lot to me. Dear Xiangjie, you were always there for me whenever I needed someone the most. I began missing our Mandarin chats and your accompany in the lab, during lunch break, and sometimes at weekend. Thanks for teaching me to cook spareribs soup with Chinese yam I enjoy it a lot now and then. Dear Cristina, Blessing, and Martina, thanks for your accompany in our delta area in the lab, which brought lots of fun in an Italian way. And Cristina, I enjoyed your music list the most and talking with you.

The work presented in this thesis was accomplished with authors or collaborators from other departments or universities. Dear Twan, Yang, Xiangyang, and Maryam from RWTH Aachen University, thanks for your scientific advice in each main chapter of the thesis. I always learned something new after our meetings. Dear Dominique from the Department of Physical and Colloid Chemistry, thanks for your contribution to ultracentrifugation experiments in chapter 3. Dear Mariona from UMC Utrecht, thanks for helping with the ELISA experiments in chapter 5. Dear Hans from the Materials Chemistry and Catalysis group, I am happy to learn from you about scanning electron microscopy and it was always nice talking to you.

Dear AF4 team, Rene, Mies, Barbara, and Lucas, it was fantastic to work with you on AF4 application and had lots of discussions on the interpretation of the data. Dear Tina, Enrico, and Gert, I appreciate your insightful feedback on Tuesday morning's colloquia that helped me shape my mind as a researcher. Dear Johanna, thanks for teaching me how to use the dolomite microfluidics and results of that experiment are an important part of chapter 3. Dear Michal, I am honored to have your input in chapter 4. Your research on curcumin and knowledge in drug delivery is very impressive. Dear Robbert Jan, thanks for your contribution to PK analysis in chapter 5.